



Convolution Approach to the πNN System

By

Jordan Lee Wray
Bachelor of Science (Honours)

Thesis
Submitted to Flinders University
for the degree of

Doctor of Philosophy

College of Science and Engineering
January 2022

Contents

Abstract	v
Declaration	vi
Acknowledgements	vii
List of Figures	ix
List of Tables	xvii
1 Introduction	1
2 Time-ordered perturbation theory	17
2.1 Introduction	18
2.2 Time-ordered perturbation theory	18
2.3 Convolution approach for disconnected processes	19
2.4 Convolution approach for connected processes	21
2.4.1 Model Hamiltonian	21
2.4.2 The fully dressed NN OPE diagram	23
2.4.3 Fully dressed $\pi d \rightarrow NN$ Z -diagram	25
2.4.4 Rules for constructing fully dressed Z -diagrams	28
2.4.5 Dressed two-pion exchange with full dressing	29
3 The πNN convolution equations	32
3.1 Co-authorship statement	33
3.2 Introduction	33
3.3 Formalism for the πNN convolution equations	34
3.3.1 Green's functions	37
3.3.2 Sub-system NN and πN scattering	38
3.4 3-dimensional scattering equations	42
3.4.1 Faddeev-like equations	42

3.4.2	Convolution expressions for w_α	45
3.4.3	AGS-like equations	47
3.4.4	On-shell and off-shell amplitudes	50
3.4.5	Scattering equations	56
3.5	4-dimensional scattering equations	62
3.5.1	4-dimensional equations for separable potentials	69
4	Numerical techniques	73
4.1	Introduction	74
4.2	Numerical calculation of dressed one-pion exchange	75
4.2.1	Partial wave decomposition	75
4.2.2	4-dimensional NN Z -diagram	78
4.2.3	Calculation of the half off-shell OPE amplitude	79
4.2.4	One-pion exchange from the πNN convolution equations	81
4.2.5	Results	82
4.3	Numerical calculation of dressed two-pion exchange	85
4.3.1	Analytical form of dressed two-pion exchange	85
4.3.2	Numerical handling of the logarithmic singularities	88
4.3.3	Numerical handling of the poles	91
4.3.4	Numerical handling of the singularities in the z'' integral	93
4.3.5	Two-pion exchange from the πNN convolution equations	95
4.3.6	Two-pion exchange with different slopes	98
4.4	A brief review of solving 4-dimensional scattering equations	101
4.5	Spline interpolation	105
4.5.1	Introduction to splines	105
4.5.2	An overview of splines	107
4.5.3	Application to a one-dimensional equation	108
4.6	Application of splines to 2-dimensional scattering equations	115
4.6.1	Using Hermitian splines of Hüber et al.	115
4.6.2	The approach of Carbonell and Karmanov	121
5	Two-body input	127
5.1	Co-authorship statement	128
5.2	Introduction	128

5.3	The undressed inputs	129
5.3.1	The NN potentials	129
5.3.2	The πN potentials	131
5.4	Constructing πN input that incorporates nucleon dressing	132
5.4.1	Pion-nucleon equations	132
5.5	Solving the Dyson-Schwinger equations	135
5.5.1	Partial wave equations	135
5.5.2	Separable potential model	137
5.5.3	Numerical results	141
6	Numerical results	145
6.1	Co-authorship statement	146
6.2	Introduction	146
6.3	Numerical 4-dimensional πNN convolution equations	147
6.3.1	4-dimensional Z -diagram	150
6.3.2	Solving the scattering equations using splines	152
6.3.3	Singularities in the z'' integral	155
6.3.4	Numerical details	156
6.4	NN phase shifts	158
6.5	$\pi d \rightarrow \pi d$ observables	164
6.5.1	S -wave scattering length	164
6.5.2	Scattering cross section	168
6.5.3	Tensor observables	179
6.6	Pion production ($pp \rightarrow \pi^+ d$ observables)	188
7	Conclusions	198
	References	207
A	Pion-nucleon theory	220
A.1	Pion-nucleon model	221
A.2	The πN t -matrix	222
A.3	The dressed pion-nucleon vertex	223

B	Theory of one nucleon	225
B.1	The dressed one-nucleon propagator	226
B.2	Calculating the dressed one-nucleon propagator	227
B.3	Analytical Structure of $g(E)$	228
B.3.1	Calculating the dressed two-nucleon propagator	229
C	Theory of two nucleons	233
C.1	Time independent formulation	234
C.2	The t -matrix operator	235
C.3	Separable potential model of NN scattering	236
C.4	Separable potential model of the NN bound state	237
C.4.1	Finding the binding energy and normalisation constants using Reid Soft Core UPA	239
D	Dressed one-pion and two-exchange for NN	240
D.1	Dressed one-pion exchange from perturbation theory	241
D.2	Full derivation of the analytical form for dressed two-pion exchange	245
E	Unitary $NN - \pi NN$ equations	252
E.1	Numerical Unitary $NN - \pi NN$ equations	253
E.1.1	3-dimensional Z -diagram	254
E.2	Antisymmetry	255
F	Various numerical methods	261
F.1	Unitary pole expansion (UPE) method	262
F.1.1	Application to 1S_0 UPA in momentum space	262
F.1.2	Application to $^3S_1 - ^3D_1$ UPA in momentum space	264
F.2	Handling a double pole	266
F.2.1	The quadratures of Kolm and Rokhlin	268
F.3	Solving the NN scattering equations using Wick rotation	272
G	Three-body channels	275
H	Publications	292

Abstract


An outstanding problem in the theoretical formulation of the πNN system, where pion production and absorption is included, has been obtaining the simultaneous dressing of both nucleons in the framework of time-ordered perturbation theory. Previous descriptions of the πNN system, such as the “Unitary $NN - \pi NN$ ” model, used Hilbert space truncation to states of no more than one pion, which prevented the nucleons in two-nucleon states from obtaining full dressing. This, in turn, gave rise to a renormalisation problem, which has long been thought to be responsible for an inadequate description of several observables including the T_{20} tensor polarisation of πd elastic scattering and the differential cross section for $pp \rightarrow \pi^+ d$ scattering.

A solution to this problem has been proposed through the use of convolution integrals to sum all possible contributions occurring in disconnected processes, thereby taking into account simultaneous nucleon dressing in the two-nucleon propagator and in other processes where a nucleon is a spectator. These convolution integrals allow new equations to be derived where nucleons are fully dressed. Interestingly, the use of these convolution integrals leads to 4-dimensional πNN equations, while still being equivalent to a 3-dimensional description. The only approximation made in the derivation of these equations is neglecting connected three-body forces.

In this thesis, we develop the convolution approach to the coupled $NN - \pi NN$ system by deriving a set of equations that simultaneously describe πd elastic scattering, $pp \rightarrow \pi^+ d$ scattering and NN elastic scattering. We then proceed to solve these πNN convolution equations and make a comparison to previously formulated equations to determine whether this convolution approach is the long-sought-after solution to the problems of the “Unitary $NN - \pi NN$ ” model. Solving the 4-dimensional πNN convolution equations, however, is a difficult task, due to the presence of moving singularities in the integral equations. We are successfully able to solve our 4-dimensional convolution equations using cubic spline interpolation, however, we can only include one partial wave channel in intermediate states, due to the computational intensity of these 4-dimensional equations.

Declaration

I certify that this thesis does not incorporate without acknowledgment any material previously submitted for a degree or diploma in any university; and that to the best of my knowledge and belief it does not contain any material previously published or written by another person except where due reference is made in the text.

.....


Jordan Wray, Date: January 2022

Acknowledgements

To my supervisor, my mentor, and my friend, Dr Boris Blankleider. It's been a long journey, but we finally got there in the end. I want to thank you for your guidance and patience with me over so many years. I feel honoured that you saw potential in me and trusted me to contribute to your research. I will always be grateful to have been a small part of your academic endeavour.

To Mum and Dad, who have always put my needs and desires above their own. Thank you for the financial and emotional support you provided throughout my entire education. Thank you for always believing in me and always pushing me to do my best and achieve great things. I feel lucky every day to have such loving and supportive parents, and to have been given the opportunities you have provided me.

To my loving and supportive partner Elizabeth, who always knew the full extent of every high, and low, during my studies. You have been through this entire journey with me, and I do not know how I could have gotten to this point without your constant support and reassurance. This thesis is the end of one chapter for us and marks the beginning of a new chapter. I look forward to what the future holds for us.

I would like to acknowledge and give thanks to my associate supervisor Professor Sarah Harmer-Bassell, who I could always rely on for help and support with my HDR progression. You were always able to provide constant support and guidance when I got lost along my PhD journey, and knowing that you were always looking out for me was a constant reassurance.

I would also like to thank my previous associate supervisor Professor Jamie Quinton, who has been a constant support throughout my entire tertiary education. Your commitment to teaching and passion for physics has always been inspirational and was the reason I pursued physics at Flinders. I will always be grateful for the support I received from someone I admire so greatly.

Many interesting, engaging and, of course, educational discussions were had throughout my PhD in Boris' office, as our small (but mighty) theoretical physics group would present a series of physics lectures to each other. I always took something away from these sessions and always felt like I was part of a community. I would like to thank Robert McLeod, Sangeet Kumar and Roy Williams, for being part of this community.

I would also like to thank the Flinders University IDS team, in particular, the team working with the DeepThought HPC who, without their help, this work could not be possible

within a short time frame. This team has been incredibly helpful and supportive with providing everything I needed to carry out my calculations on the supercomputer.

I also wish to acknowledge that this research was supported through the Australian Government Research Training Program Scholarship.

List of Figures

1.1	Illustration of the πNN potentials V_α where $\alpha = \{1, 2, 3\}$ that are included in the work of Afnan and Thomas [29]. The solid lines represent the nucleons and the dashed lines represent the pions. The open circles represent all possible diagrams except for those that lead to πNN intermediate states.	5
1.2	Illustration of the πNN potentials V_α , where $\alpha \in \{1, 2, 3, 4, 5\}$, that are included in field-theoretical approaches of the “Unitary $NN - \pi NN$ ” model. The solid lines represent the nucleons and the dashed lines represent the pions. The smaller open circles represent the bare πNN vertices, the larger open circles represent all possible diagrams except for those that lead to πNN intermediate states and the dashed circles represent all possible diagrams except for those that lead to NN and πNN intermediate states.	7
1.3	Diagrammatic representation of the pole part of the $\pi N t$ -matrix used as input in the “Unitary $NN - \pi NN$ ” model. The solid dot represents the dressing of the nucleon, f represents the dressed πNN vertex and Z is the residue of the dressed one-nucleon propagator at the pole.	8
1.4	Diagrammatic representation of the NN OPE amplitude in the “Unitary $NN - \pi NN$ ” model, where Z_d is the residue of the different-time dressing NN propagator. The external legs of the NN OPE amplitude must be renormalised by Z_d in order to maintain unitarity.	8
1.5	The NN reducible and NN irreducible diagrams where one nucleon absorbs a pion and the other emits a pion. Diagram (b) is often referred to as the “Jennings” term.	9
1.6	Second order $\pi d \rightarrow \pi d$ diagram with two pions in flight at the same time. The addition of this diagram to πd elastic scattering drastically improves the reproducibility of the T_{20} observable.	10

1.7	Illustration of the πNN potentials V_α , where $\alpha \in \{1, 2, 3, 4, 5\}$, that are included in the work of Stingl and Stelbovics [44–46]. The solid lines represent the nucleons and the dashed lines represent the pions.	11
1.8	Illustration of the πNN potentials V_α , where $\alpha \in \{1, 2, 3, 4, 5\}$, that are included in the convolution approach of Kvinikhidze and Blankleider [49]. The solid lines represent the nucleons and the dashed lines represent the pions. The open circles represent all possible diagrams except for those that lead to πNN intermediate states.	13
2.1	Diagram representation of the integrand in Figure 2.32 for the fully dressed one-pion exchange between two nucleons.	25
2.2	Diagrammatic representation of the integrand in Equation 2.43 for the fully dressed $\pi d \rightarrow NN$ Z -diagram.	28
2.3	The time-ordered diagrams corresponding to two-pion exchange, where (a) is obtained from the first term in the sum of matrix elements in Equation 2.44 and (b) is obtained from the second term in Equation 2.44.	30
2.4	A convolution diagram representing two-pion exchange between two nucleons.	30
3.1	Coupled equations for a pion (dashed line) scattering off nucleon i (solid line): (a) The πN t -matrix expressed by Equation 3.32, (b) the “background” πN t -matrix as given by Equation 3.33a, (c) the dressed πNN vertex as given by Equation 3.34a, and (d) the dressed nucleon propagator as given by Equation 3.35 whose self-energy term Σ_i is expressed as in Equation 3.36a.	41
3.2	(a) Example of a connected πNN -irreducible contribution to the πNN potential V ; such contributions correspond to three-body forces and are neglected in this work. (b) A topologically similar contribution to that of (a), which however is included in our work as it is πNN reducible.	43
3.3	Examples of diagrams contributing to the NN -irreducible t -matrices w_α^0 . All possible diagrams of disconnectedness 3 contribute to w_3^0 , and this is indicated by the black circles.	59
4.1	The general Z -diagram with our “prime” notation convention, whose partial wave expansion is given Afnan and Thomas [29].	76

4.2	(a) Example of a dressing diagram that is included in the OPE of the πNN convolution equations (b) a dressing diagram involving a connected three-body force, which is not included in the OPE of the πNN convolution equations.	81
4.3	Diagram representation of the dressed one-pion exchange that with neglecting three-body forces can be represented by three individual diagrams. The black dots represent the dressing of each nucleon before and after the process of pion exchange.	83
4.4	${}^3S_1 \rightarrow {}^3S_1$ partial wave amplitudes for half off-shell NN one-pion exchange. The solid line represents the partial wave amplitude for the fully dressed one-pion exchange with full nucleon dressing, while the dashed line represents the partial wave amplitude for one-pion exchange from the πNN convolution equations, which neglects connected three-body forces. The dot dashed line represents the partial wave amplitude for one-pion exchange without any dressed nucleons.	84
4.5	Plot of the real and imaginary parts of the ${}^3S_1 \rightarrow {}^3S_1$ two-pion exchange partial wave amplitude of Equation 4.53 against the energy-like variable z'' at a fixed energy of $E = 2.2$ GeV. The function $I_p(z'')$ is Equation 4.32 as a function of the variable z'' , after the p'' integral has been performed.	94
4.6	Diagram representation of the dressed two-pion exchange that with neglecting three-body forces can be represented by three individual diagrams as in the πNN convolution equations.	95
4.7	${}^3S_1 \rightarrow {}^3S_1$ partial wave amplitudes for same slope fully on-shell NN two-pion exchange. The solid line represents the partial wave amplitude for the calculation with fully dressed nucleons, while the dashed line represents the partial wave amplitude from the πNN convolution equations, which neglects connected three-body forces.	97
4.8	Convolution diagram corresponding to different slope dressed two-nucleon exchange.	98
4.9	Diagram representation of the dressed two-pion exchange that with neglecting three-body forces can be represented by three individual diagrams as in the πNN convolution equations.	99

4.10	${}^3S_1 \rightarrow {}^3S_1$ partial wave amplitudes for different slope fully on-shell two-pion exchange. The solid line represents the partial wave amplitude for the calculation with fully dressed nucleons, while the dashed line represents the partial wave amplitude from the πNN convolution equations, which neglects connected three-body forces.	100
4.11	Diagrammatic representation of the Bethe-Salpeter equation for scattering states. The open circles represent all possible contributions, while the dashed circle represents all two-particle irreducible contributions. The Bethe-Salpeter equation for bound states is the same for scattering states, without the inhomogeneous term.	101
4.12	Diagrammatic representation of the Bethe-Salpeter equation for scattering states in the “ladder” approximation.	101
5.1	Illustration of the πN scattering equations: (a) The πN t -matrix expressed by Equation 5.9, (b) the “background” πN t -matrix as given by Equation 5.10a, (c) the dressed πNN vertex as given by Equation 5.11a, and (d) the dressed nucleon propagator as given by Equation 5.12 whose self-energy term Σ is expressed as in Equation 5.13a.	133
5.2	(a) Real and (b) imaginary parts of $g^R(E)(E - m_N)$ where $g^R(E) = g(E)/Z$ is the renormalised dressed nucleon propagator. The solid curves are for the Dyson propagator (resulting from the solution of the Dyson-Schwinger equations), while the dashed curves are for the non-Dyson propagator (resulting from the use of the one-pion-approximation).	142
5.3	(a) Real and (b) imaginary parts of $g^R(E)(E - m_N)$ where $g^R(E)$ is the renormalised dressed Dyson nucleon propagator, for the four models specified in Table 5.4. The solid curves represent the $M6$ model, the dashed curves represent the $M7$ model, the dot-dashed curves represent the $M8$ model and the dotted curves represent the $M9$ model.	142
6.1	The πd elastic scattering amplitude where $N\Delta$ is the only coupled channel. .	148
6.2	The $N\Delta \rightarrow \pi d$ scattering amplitude where $N\Delta$ is the only coupled channel. This amplitude is used in order to calculate the πd elastic scattering amplitude.	149
6.3	The πd elastic scattering amplitude where NN is the only coupled channel. .	149

6.4	The $NN \rightarrow \pi d$ scattering amplitude where NN is the only coupled channel. This amplitude is used in order to calculate the πd elastic scattering amplitude.	150
6.5	Comparison of the 4D NN phase shifts coupled to the NN channel with Dyson-dressing for different partial waves, calculated using the Wick rotation method of Levine et al. [54], compared with the 3D NN phase shifts, calculated using contour rotation. The dots represent the SW16 solution [175] obtained using the SAID database [176].	161
6.5	(cont.) Comparison of the 4D NN phase shifts coupled to the NN channel with Dyson-dressing for different partial waves, calculated using the Wick rotation method of Levine et al. [54], compared with the 3D NN phase shifts, calculated using contour rotation. The dots represent the SW16 solution [175] obtained using the SAID database [176].	162
6.6	Comparison of the 4D ${}^3P_1 NN$ phase shifts coupled to the P_{33} channel with Dyson-dressing, calculated using the spline interpolation method using 16 knots for p and z ($N_p = N_z = 16$), compared to the 3D NN phase shifts, calculated with contour rotation. The solid curve represents the phase shift with our 4D phase shifts with our $M7$ Dyson-dressing model, while the dashed curve represents the 3D phase shifts. The dots represent the SW16 solution [175] obtained using the SAID database [176].	163
6.7	The half off-shell $\pi d \rightarrow N\Delta$ Z -diagram.	166
6.8	Comparison of the 4D πd differential cross section when coupled to the P_{33} channel with the lab energy of the incident pion equal to 140 MeV. The three curves in this graph each represent a different number of spline knots used in the calculation: the dot-dashed curve represents 16 knots, the dashed curve represents 24 knots and the solid curve represents 32 knots.	173
6.9	Comparison of the 3D πd and 4D πd ($N_p = N_z = 32$) differential cross section when coupled to the P_{33} channel with the lab energy of the incident pion equal to 140 MeV, also compared with the experimental data points provided by Gabathuler et al. [187]. The solid curve represents the 4D differential cross section, while the dashed curve represents the 3D differential cross section. .	174

6.10	Comparison of the 4D πd differential cross section when coupled to the NN channel with the lab energy of the incident pion equal to 140 MeV. The three curves in this graph each represent a different number of spline knots used in the calculation: the dot-dashed curve represents 16 knots, the dashed curve represents 24 knots and the solid curve represents 32 knots.	176
6.11	Comparison of the 3D πd and 4D πd ($N_p = N_z = 32$) differential cross section when coupled to the NN channel with the lab energy of the incident pion equal to 140 MeV, also compared with the experimental data points provided by Gabathuler et al. [187]. The solid curve represents the 4D differential cross section, while the dashed curve represents the 3D differential cross section.	176
6.12	The 3D πd differential cross section with full coupling for the lab energy of the incident pion equal to 140 MeV, also compared with the experimental data points provided by Gabathuler et al. [187].	177
6.13	Comparison of the 4D πd polarisation observables when coupled to the P_{33} channel with the lab energy of the incident pion equal to 140 MeV. The three curves in this graph each represent a different number of spline knots used in the calculation: the dot-dashed curves represent 16 knots, the dashed curves represent 24 knots and the solid curves represent 32 knots.	183
6.14	Comparison of the 3D πd and 4D πd ($N_p = N_z = 32$) polarisation observables when coupled to the P_{33} channel with the lab energy of the incident pion equal to 140 MeV, also compared with experimental data points (T_{20} and τ_{21} from [192], T_{21} and T_{22} from [193], iT_{11} and τ_{22} from [190] and t_{20}^{lab} from [194]). The solid curves represent the 4D polarisation observables, while the dashed curves represent the 3D polarisation observables.	184
6.15	Comparison of the 4D πd polarisation observables when coupled to the NN channel with the lab energy of the incident pion equal to 140 MeV. The three curves in this graph each represent a different number of spline knots used in the calculation: the dot-dashed curves represent 16 knots, the dashed curves represent 24 knots and the solid curves represent 32 knots.	185

6.16	Comparison of the 3D πd and 4D πd ($N_p = N_z = 32$) polarisation observables when coupled to the NN channel with the lab energy of the incident pion equal to 140 MeV, also compared with experimental data points (T_{20} and τ_{21} from [192], T_{21} and T_{22} from [193], iT_{11} and τ_{22} from [190] and t_{20}^{lab} from [194]). The solid curves represent the 4D polarisation observables, while the dashed curves represent the 3D polarisation observables.	186
6.17	The 3D πd polarisation observables with full coupling for the lab energy of the incident pion equal to 140 MeV, also compared with experimental data points (T_{20} and τ_{21} from [192], T_{21} and T_{22} from [193], iT_{11} and τ_{22} from [190] and t_{20}^{lab} from [194]).	187
6.18	Comparison of the 4D $pp \rightarrow \pi d$ differential cross section with the lab energy of the incident proton equal to 560 MeV. The three curves in this graph each represent a different number of spline knots used in the calculation: the dot-dashed curve represents 16 knots, the dashed curve represents 24 knots and the solid curve represents 32 knots.	193
6.19	Comparison of the 3D and 4D ($N_p = N_z = 32$) $pp \rightarrow \pi d$ differential cross section with the lab energy of the incident proton equal to 560 MeV, also compared with the experimental data points provided by Hoftiezer et al. [195]. The solid curve represents the 4D differential cross section, while the dashed curve represents the 3D differential cross section.	193
6.20	The 3D differential cross section with full coupling for the lab energy of the incident proton equal to 560 MeV, also compared with the experimental data points provided by Hoftiezer et al. [195].	194
6.21	Comparison of the 4D $pp \rightarrow \pi d$ polarisation observables with the lab energy of the incident proton equal to 560 MeV. The three curves in this graph each represent a different number of spline knots used in the calculation: the dot-dashed curve represents 16 knots, the dashed curve represents 24 knots and the solid curve represents 32 knots.	195
6.22	Comparison of the 3D and 4D ($N_p = N_z = 32$) polarisation observables with the lab energy of the incident proton equal to 560 MeV, also compared with the experimental data points (A_{y0} from [196], A_{xx} , A_{yy} and A_{zz} from [197, 198] and A_{zx} from Hoftiezer et al. [199]). The solid curve represents the 4D observable, while the dashed curve represents the 3D observable.	196

6.23	The 3D $pp \rightarrow \pi d$ polarisation observables with full coupling for the lab energy of the incident proton equal to 560 MeV, also compared with the experimental data points (A_{y0} from [196], A_{xx} , A_{yy} and A_{zz} from [197, 198] and A_{zx} from Hoftiezer et al. [199]).	197
A.1	The $\pi N t$ represented diagrammatically as its pole and non-pole parts.	223
A.2	Diagram for v^b representing the sum of all one-particle irreducible πN graphs.	223
A.3	Diagram representation of the dressed vertex function $f(k, E)$, shown as a finite sum of Figure	223
A.4	Iteration of v^b	224
A.5	Diagram showing how a cut in the bubble of the iterated v^b can lead to factorising a f_0 term.	224
A.6	Diagrammatic representation of the dressing amplitude $\Sigma(E)$	224
B.1	The dressing of a single nucleon, shown as a perturbation expansion of diagrams, where the dashed lines represent the propagation of pions and the solid lines represent the propagation of the nucleon.	226
B.2	Real and imaginary parts of the dressed one-nucleon propagator $g(E)$	228
B.3	The contour enclosing the pole at $m + i\epsilon$ and that forms around the branch cut beginning at $m + m_\pi - i\epsilon$ present in the dressed one-nucleon propagator.	229
B.4	Real and Imaginary parts of the dressed two-nucleon propagator and two-nucleon propagator approximations. The solid line represents the dressed two-nucleon propagator $D_0(E)$, the long dash represents $G_{PT}(E)$, dot dashed represents $G^\pi(E)$ and the short dashed line represents $G_{DT}(E)$. To be consistent with the results of Blankleider and Kvinikhidze [48], these graphs are normalised by a factor of Z^2 so that each propagator has a unit residue.	232
D.1	Diagram representation of both time-ordering of one-pion exchange between two nucleons	241
D.2	Diagram representation of the one-pion exchange between two nucleons	244

List of Tables

3.1	Labelling schemes for denoting particle pairs.	35
4.1	Comparison of the on-shell $NN \rightarrow NN$ amplitude calculated using the contour rotation method and Hermitian spline interpolation for energies below pion production threshold. We use 100 knots in the interval $[0, \infty]$, constructed using Gaussian quadrature points.	112
4.2	Comparison of the on-shell $NN \rightarrow NN$ amplitude calculated using the contour rotation method and Hermitian spline interpolation for energies above pion production threshold. We use 100 knots in each sub-interval $[0, p_c], [p_c, \infty]$, constructed using Gaussian quadrature points.	114
5.1	Parameters for the form factors of the unitary pole approximation of the Reid Soft Core potential to the coupled ${}^3S_1 - {}^3D_1$ NN potential. The fits were performed by Bhatt et al. [133].	130
5.2	The parameters of the form factors of the uncoupled NN channels given by Mongan [134, 135].	131
5.3	The parameters of the form factors for the πN channel given by Thomas [22].	131
5.4	Parameters of four fits (labelled as models $M9$, $M8$, $M7$, and $M6$) to the P_{11} πN phase shifts through the solution of the Dyson-Schwinger equations of Equation 5.32. The first 9 parameters refer to the form factors of while m_0 is the bare nucleon mass and Z is the nucleon wave-function renormalisation constant.	143
5.5	Parameters of fits to the s - and p -wave πN phase shifts (other than P_{11}) for each of the four models ($M9$, $M8$, $M7$, and $M6$) for the dressed Dyson nucleon propagator $g(E)$ used in the coupled πN equations of Equation 5.19. The parameters refer to the form factors of Equation 5.35. The s -wave strengths are in fm^{-1} , for p -waves S_2 is dimensionless and S_1 is in fm^{-1}	144

6.1	Results of the πd extrapolation to determine the S -wave πd scattering length calculated using the spline interpolation method for different numbers of p and z spline knots, N_p and N_z respectively. These results include the extrapolated amplitude for $E_{lab} = 0$ calculated using a linear data fit and the corresponding S -wave scattering length for the respective knot number. The amplitudes are given in units of fm^{-1} , while the scattering length $a_{\pi d}$ is given in units of m_{π}^{-1} .	167
6.2	The partial wave channels considered in the calculation of πd scattering, in which we consider the same channels as Blankleider [178].	170
6.3	4D elastic πd scattering amplitudes when coupled to the P_{33} channel calculated using the spline interpolation method for different numbers of p and z spline knots, N_p and N_z respectively. The lab energy of the incident pion is equal to 140 MeV.	172
6.4	4D elastic πd scattering amplitudes when coupled to the NN channel calculated using the spline interpolation method for different numbers of p and z spline knots, N_p and N_z respectively. The lab energy of the incident pion is equal to 140 MeV.	175
6.5	The total and elastic πd scattering cross section for lab energy of the incident pion equal to 140 MeV, comparing the result from the Unitary equations and the results from the 4D equations for a different number of spline knots. The results from the 3D scattering equation with full coupling are also presented (we denote $3D_{FC}$ as the results with full couplings and $3D_{P_{33}}$ as the results with coupling only to P_{33}).	178
6.6	The partial wave channels considered in the calculation of pion production, in which we consider the same channels as Blankleider [178].	190
6.7	4D $pp \rightarrow \pi d$ scattering amplitudes calculated using the spline interpolation method for different numbers of p and z spline knots, N_p and N_z respectively. The lab energy of the incident proton equal is to 560 MeV.	192

Chapter 1

Introduction

Ever since Faddeev [1] developed his formulation for a system of three particles in quantum mechanics, the logical question quickly became “How can this be extended to include the creation and annihilation of particles?” The answer to this question is important for the study of the strong interaction, where particles are continuously created, annihilated, and exchanged. This thesis is devoted to the long-standing attempt to help answer this question by developing a description of the strongly interacting pion-nucleon-nucleon (πNN) system where coupling to NN channels is included. We do this using the quantum field theoretic framework of non-relativistic time-ordered perturbation theory (TOPT), which uses pions and nucleons as the degrees of freedom. To put this highly simplified framework for describing strong interactions into context, we will now give a brief overview of our current understanding of strong interactions, and summarise the various approaches that have been adopted over the years.

Currently, the generally accepted theory for strong interactions is Quantum Chromodynamics (QCD), a non-abelian gauge theory involving quarks and gluons as degrees of freedom. The main confirmation of QCD comes from consideration of processes at high energies and high momentum transfer [2, 3] where quarks exist in asymptotic freedom. This allows for calculations to be performed using perturbation theory, which is often referred to as perturbative QCD. In QCD, the effective coupling constant gives the strength of the interaction mediated by the exchange particles and is of the order $1/\ln(Q^2/\Lambda^2)$, where Q is the momentum transfer of the interaction process and Λ is the QCD scale parameter [4, 5]. This results in asymptotic freedom at high energies corresponding to $Q^2 \sim \Lambda^2$, and allows for high precision of theoretical calculations to be achieved [6]. However, at low-energy regions, the effective coupling constant is much greater, which leads to quark confinement and perturbation theory is no longer applicable [7].

Due to the non-perturbative nature in this low-energy region, a number of non-perturbative approaches have been developed. Lattice QCD, a subset of lattice gauge theory, was developed [8], in which 4-dimensional space-time is discretised onto a lattice, where quarks are placed at the lattice points and the gauge fields are replaced by the paths between the lattice points, often called “links” [4]. This discretisation allows for the application of various non-perturbative techniques and has allowed for QCD calculations to be performed in low-energy regions. While lattice QCD has allowed for a better fundamental understanding of QCD at low energies, it requires an immense amount of computing resources. Although it is believed that this issue of computational complexity could be resolved in the near future through

advances in quantum information technologies, lattice QCD possesses other inherent problems including the infamous “sign-problem,” and other issues relating to its formulation in Euclidean space-time [9].

A more phenomenological approach to low energy QCD is provided by quark or bag models, in which hadrons are considered to be “bags” of quarks, equivalent to confining the quarks in an infinite potential well. This idea was first proposed by Bogoliubov [10], which, despite being able to reproduce accurate nucleon properties, was later found to violate the conservation of energy and momentum. This led to, what is now known as, the MIT bag model [11], which was able to incorporate quark confinement into Bogoliubov’s bag model and overcame the violation of energy and momentum conservation. The MIT bag model gained great success, as it was able to describe certain nucleon properties such as charge radii, axial-vector charges, and the gyromagnetic ratios [12]. However, the MIT bag model lacked chiral symmetry, which is an important fundamental property of QCD and allows for a description of the long-ranged NN interaction [13]. It was later shown that chiral symmetry could be achieved by coupling the quarks in the bag directly to an elemental pion field at the bag surface [14]. While the original MIT bag model had success in describing certain nucleon properties, the coupling to an external pion field caused issues with the bag’s radius and it was no longer able to accurately predict these nucleon properties [15]. To overcome the issues with the external field, the cloudy bag model was developed [16], in which pions are no longer excluded from the bag’s interior and avoids the issues with the chiral bag model while still allowing the bag model to retain chiral symmetry.

Although quarks and gluons are believed to be the correct degrees of freedom for the description of the strong interaction, at low energies one can also consider using mesons and baryons as the degrees of freedom, thereby representing the strong interaction by various particle exchanges. In such descriptions, the long-ranged component of the strong interaction is mediated by the exchange of pions, the lightest of mesons, while the short-ranged component is governed by the exchange of heavier mesons such as ρ mesons. The traditional method of studying this strong interaction has been to consider all possible types of particle exchange in an effort to study the full interaction. Despite a long and largely successful history of analysing various nucleon processes, this traditional approach has the disadvantage of requiring many parameters for its description, and moreover, its connection to the underlying theory of strong interactions, QCD, is unclear. These observations led Weinberg [17, 18] to propose a new approach that uses the most general possible Lagrangian

involving pion and nucleon fields that is consistent with the chiral symmetry of QCD, to expand the nucleon-nucleon (NN) potential in powers of nucleon momenta. This approach, now known as effective field theory (EFT), has been developed over the years to the point where it now provides the standard way to analyse hadronic systems in a systematic and model independent way [19].

Amongst these various approaches to strong interactions, the framework chosen for the current work is that of the traditional approach using pion and nucleon degrees of freedom to describe the coupled $NN - \pi NN$ system. The major motivation for choosing this approach is to bring to fruition a quest, started more than 50 years ago, of describing the $NN - \pi NN$ system in a way that respects two- and three-body unitarity, and where practical equations describing this system are derived from quantum field theory (QFT) such that normalisation due to nucleon dressing is treated consistently. Also, despite the disadvantages of the traditional approach, discussed above, it may still be useful for describing processes at energies higher than what may be accessible by low-energy EFT. Moreover, by developing theoretical and numerical techniques that extend a quantum mechanical three-body (Faddeev) description to the realm of QFT where particle creation and absorption is included, we hope to contribute to a knowledge base that may prove to be useful in the wider context of nuclear and particle physics.

The traditional approach has been widely used in the investigation of the πNN system without pion absorption or creation [20–25], but ultimately a theoretically complete description of the πNN system and reproducibility of observables depends on the inclusion of pion absorption. Varma [26] was the earliest to study the πNN system using Faddeev theory while trying to include pion absorption. Varma utilised the approximation scheme of Lovelace [27], in which the Faddeev equations simplify when two-particle sub-systems are dominated by a finite number of low-energy bound states and was able to obtain NN scattering equations that preserve three-body unitarity. Varma incorporated pion absorption by assuming that the πN system has a bound state in the P_{11} channel with binding energy equal to the pion mass. This idea of assuming there is a πN bound state is known as the Bound-State πNN model. Thomas and Afnan [28] also applied the Faddeev equations to the πNN system, using the same model of pion absorption by assuming there is a πN bound state in the P_{11} channel. This idea was later extended to include pion production in NN scattering, pion absorption in πd scattering, and πd elastic scattering [29]. Their approach was to consider the πNN system as a pure three-body problem interacting via two-body

forces, in which the $\pi NN \rightarrow \pi NN$ potential V (for distinguishable nucleons), is given as a sum of three pair-wise terms

$$V = V_1 + V_2 + V_3 \quad (1.1)$$

as illustrated in Figure 1.1.

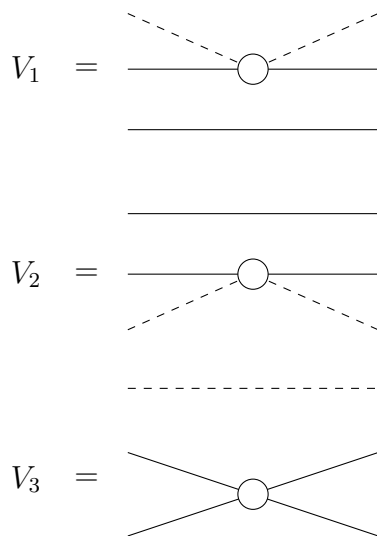


Figure 1.1: Illustration of the πNN potentials V_α where $\alpha = \{1, 2, 3\}$ that are included in the work of Afnan and Thomas [29]. The solid lines represent the nucleons and the dashed lines represent the pions. The open circles represent all possible diagrams except for those that lead to πNN intermediate states.

The πNN potential V_1 (formally identical to V_2) was constructed so that the corresponding sub-system πN t -matrix contains a bound state corresponding to the formation of a “bound-state nucleon,” denoted by N' , while an original nucleon N is a spectator. However, as only the nucleon that absorbed a pion, N' , is able to emit a pion, the two nucleons in the πNN system are not treated symmetrically. This inadequacy motivated the development of the “Coupled $NN - \pi NN$ ” model [30] also known as the “Unitary $NN - \pi NN$ ” model [31].

The “Unitary $NN - \pi NN$ ” model was a very successful field-theoretic model describing the πNN system, based on time-ordered perturbation theory, which takes into account pion absorption. Time-ordered perturbation theory is often referred to as “old-fashioned” time-ordered perturbation theory or simply “old-fashioned perturbation theory.” The essential

feature of the model is that it describes all the processes

$$\begin{aligned} \pi d &\rightarrow \pi d \\ \pi d &\rightarrow \pi NN \\ NN &\rightarrow \pi NN \\ NN &\rightarrow \pi d \\ NN &\rightarrow NN \end{aligned}$$

all within one set of coupled equations. This particular model relies on truncating the Hilbert space to only allow states of, at most, one pion, where whole classes of perturbation diagrams are summed into terms that are then described phenomenologically. This was commonly known as the “one-pion” approximation. The derivation of coupled $NN - \pi NN$ equations in this model has been done using various methods such as classification of diagrams according to their irreducibility [32, 33], non-relativistic reduction techniques [34] and Feshbach projection operators [35, 36]. These field-theoretical models introduced an explicit πNN vertex and allowed for the inclusion of non-pair wise πNN potentials, where one nucleon absorbs a pion and the other nucleon emits a pion. This potential together with the pair-like potentials then make up the full $\pi NN \rightarrow \pi NN$ potential V , given as

$$V = V_1 + V_2 + V_3 + V_4 + V_5, \tag{1.2}$$

where each contribution V_α , where $\alpha \in \{1, 2, 3, 4, 5\}$, is illustrated in Figure 1.2. Comparison with Figure 1.1 illustrates the basic difference between the Bound-State πNN model and the “Unitary $NN - \pi NN$ ” model.

While the models mentioned above have been partially successful in describing the πNN system and the coupling to NN , they lack a crucial piece of physics that could have a detrimental effect on the reproducibility of some scattering observables. The essential problem with the “Unitary $NN - \pi NN$ ” model is that the truncation of the Hilbert space to states of at most one pion, restricts the ability of the two nucleons in the system to obtain their full dressing, as this requires the inclusion of states where more than one pion is in flight at the same time [37]. As we can see from the πNN potentials in Figure 1.2, iteration of this potential would only lead to partially dressed nucleons, more specifically the nucleons would have different-time dressing. The failure to dress both nucleons at the same time results in a problem of nucleon wave-function renormalisation which can lead to an underestimation of pion production cross sections and other inaccuracies [38].

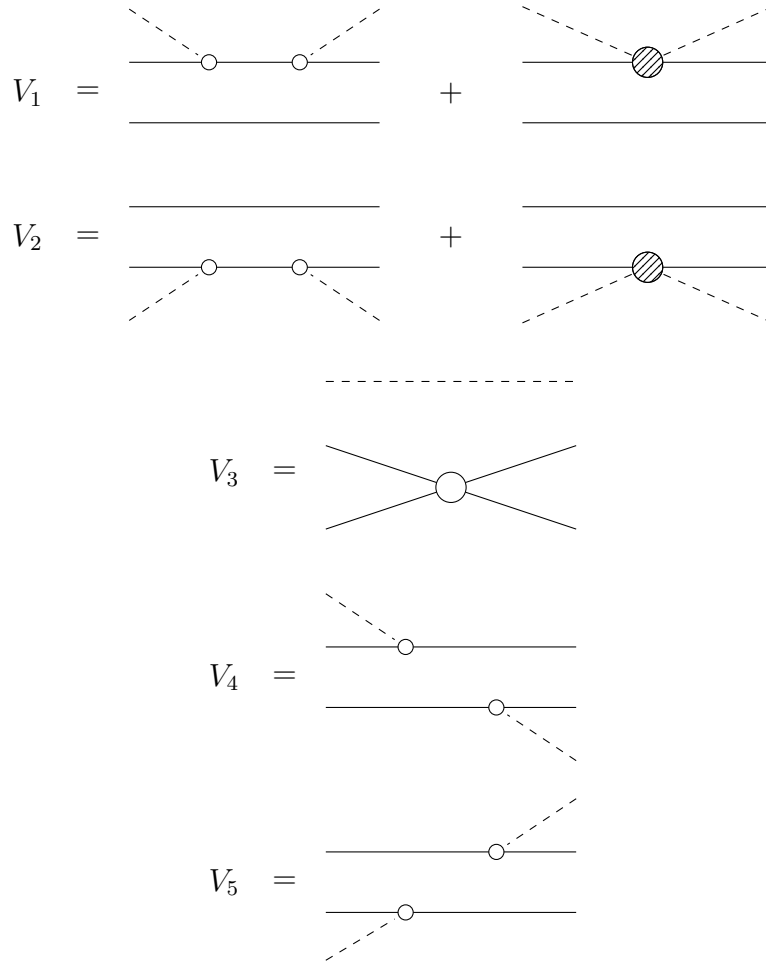


Figure 1.2: Illustration of the πNN potentials V_α , where $\alpha \in \{1, 2, 3, 4, 5\}$, that are included in field-theoretical approaches of the “Unitary $NN - \pi NN$ ” model. The solid lines represent the nucleons and the dashed lines represent the pions. The smaller open circles represent the bare πNN vertices, the larger open circles represent all possible diagrams except for those that lead to πNN intermediate states and the dashed circles represent all possible diagrams except for those that lead to NN and πNN intermediate states.

Theoretically calculated scattering cross sections of the $pp \rightarrow \pi^+d$ reaction in the “Unitary $NN - \pi NN$ ” model are significantly smaller than suggested by experimental data [39]. As just mentioned, a possible cause of these small cross sections is the renormalisation problem that results from the truncation of the Hilbert space to states of at most one pion. To see this, consider the pole part of the πN scattering t -matrix, which is illustrated in Figure 1.3

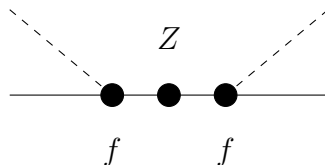


Figure 1.3: Diagrammatic representation of the pole part of the πN t -matrix used as input in the “Unitary $NN - \pi NN$ ” model. The solid dot represents the dressing of the nucleon, f represents the dressed πNN vertex and Z is the residue of the dressed one-nucleon propagator at the pole.

We define Z to be the residue of the dressed one-nucleon propagator. In the “Unitary $NN - \pi NN$ ” model, the nucleon in the pole part of the πN t -matrix can only be dressed when there are no other pions in flight. Thus, only the intermediate-state nucleon can be dressed. Thus, each πNN vertex effectively obtains a normalisation of \sqrt{Z} to account for the residue of the dressed one-nucleon propagator and the effective πNN coupling constant becomes $f_{\pi NN} = \sqrt{Z}f(m_N)$. A model is then fitted to the phase shifts and the experimental coupling constant, as such is done by Afnan and McLeod [40]. Now consider the NN one-pion exchange (OPE) amplitude given in Figure 1.4

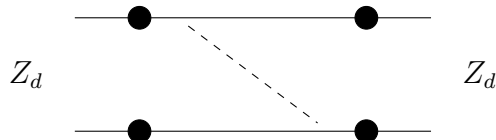


Figure 1.4: Diagrammatic representation of the NN OPE amplitude in the “Unitary $NN - \pi NN$ ” model, where Z_d is the residue of the different-time dressing NN propagator. The external legs of the NN OPE amplitude must be renormalised by Z_d in order to maintain unitarity.

Three-body unitarity is guaranteed through the iteration of the $\pi NN \rightarrow \pi NN$ potential V , which results in a different-time dressing NN propagator whose residue is Z_d . Calcula-

tions show that $Z_d \approx Z^2$, as one might expect from a fully dressed two-nucleon propagator. One can see that in the NN OPE, each πNN vertex is renormalised by a factor of $\sqrt{Z_d} \approx Z$. Thus, effectively, the πNN coupling constant in the NN OPE amplitude is \sqrt{Z} times than the physical one. As the typical range of Z is approximately between the values of 0.6 and 0.8, the value of \sqrt{Z} would be less than 1, thereby resulting in smaller amplitudes for processes, like $NN \rightarrow \pi d$, that strongly depends on the strength of the dressed πNN vertex.

Sauer [38] was first to suggest this truncation of the Hilbert space is responsible for the low cross sections, due to the problem of renormalisation, in which the effective πNN coupling constant is significantly lower than the one used to construct the πN input [31]. It seemed that no one knew how to solve this problem at the time and it was thought that there was no easy way of doing this without destroying the three-body unitarity. Ultimately, unitarity is obtained at the price of having to use an effective πNN coupling constant that is smaller than the experimental one.

Besides low $pp \rightarrow \pi^+ d$ cross sections, another inadequacy is that the spin polarisation observable T_{20} for πd elastic scattering at medium energies cannot be reproduced accurately in the “Unitary $NN - \pi NN$ ” model. Jennings [41] suggests that disconnected $\pi NN \rightarrow \pi NN$ diagrams where one nucleon absorbs a pion and the other emits it must contain both NN reducible and irreducible contributions. These diagrams are shown in Figure 1.5.

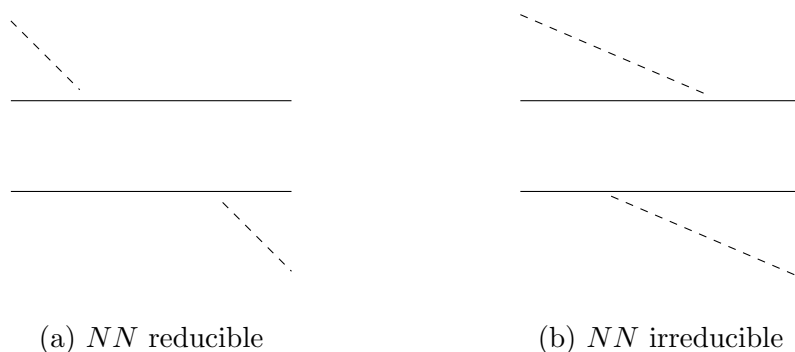


Figure 1.5: The NN reducible and NN irreducible diagrams where one nucleon absorbs a pion and the other emits a pion. Diagram (b) is often referred to as the “Jennings” term.

Jennings showed that the contribution of each diagram is of a similar size and opposite sign, thus there is a large cancellation between these diagrams which does not occur when only the NN reducible diagram is included. The NN irreducible diagram has often been referred to as the “Jennings” term in association with Jennings’ findings. Jennings and Rinat [42] investigated the addition of diagrams with two pions in flight at the same time to

the calculation of πd elastic scattering, particularly the diagram shown in Figure 1.6. They find that the discrepancy between the T_{20} experimental data and the predictions using the “Unitary $NN - \pi NN$ ” model is essentially removed. Similar results were found by Mizutani et al. [43] who conclude through a simple model of numerical calculations that the mechanism proposed by Jennings provides an improvement to the description of πd observables and in particular, the description of T_{20} . These findings demonstrate the need to include diagrams with more than one pion in flight at the same time and establishes further limitations of the “Unitary $NN - \pi NN$ ” model.

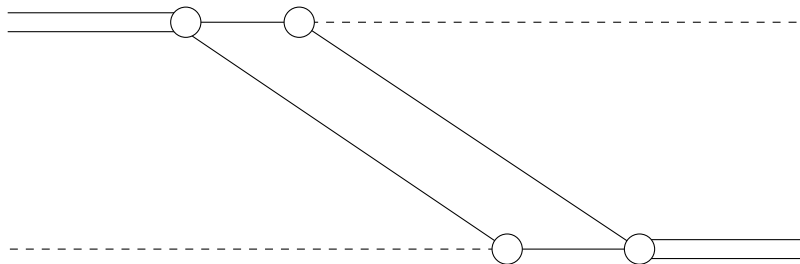


Figure 1.6: Second order $\pi d \rightarrow \pi d$ diagram with two pions in flight at the same time. The addition of this diagram to πd elastic scattering drastically improves the reproducibility of the T_{20} observable.

Completely independent of the work in the “Unitary $NN - \pi NN$ ” model was the work of Stingl and Stelbovics [44–46] who went beyond the “one-pion” approximation and derived a description of the coupled $NN - \pi NN$ system which included states of at most two pions. Their model is based on a $\pi NN \rightarrow \pi NN$ potential that is given by a sum of 5 terms as in Equation 1.2, however, unlike in the “Unitary $NN - \pi NN$ ” model, the potentials V_4 and V_5 include states with two pions. The individual potentials in the model of Stingl and Stelbovics are represented diagrammatically in Figure 1.7.

Unlike the “Unitary $NN - \pi NN$ ” model, where the πN and NN sub-systems consist of all possible perturbation diagrams, the model of Stingl and Stelbovics describes the πN potentials in πNN space (corresponding to the potentials V_1 and V_2) and the NN potential in πNN space (corresponding to V_3) in terms of the lowest order contributions generated by a πNN vertex, consistent with states of at most two pions. However, the model of Stingl and Stelbovics goes beyond the “Unitary $NN - \pi NN$ ” model by including the NN irreducible contributions of V_4 and V_5 , corresponding to the lowest order diagrams of V_4 and V_5 with two-pion intermediate states.

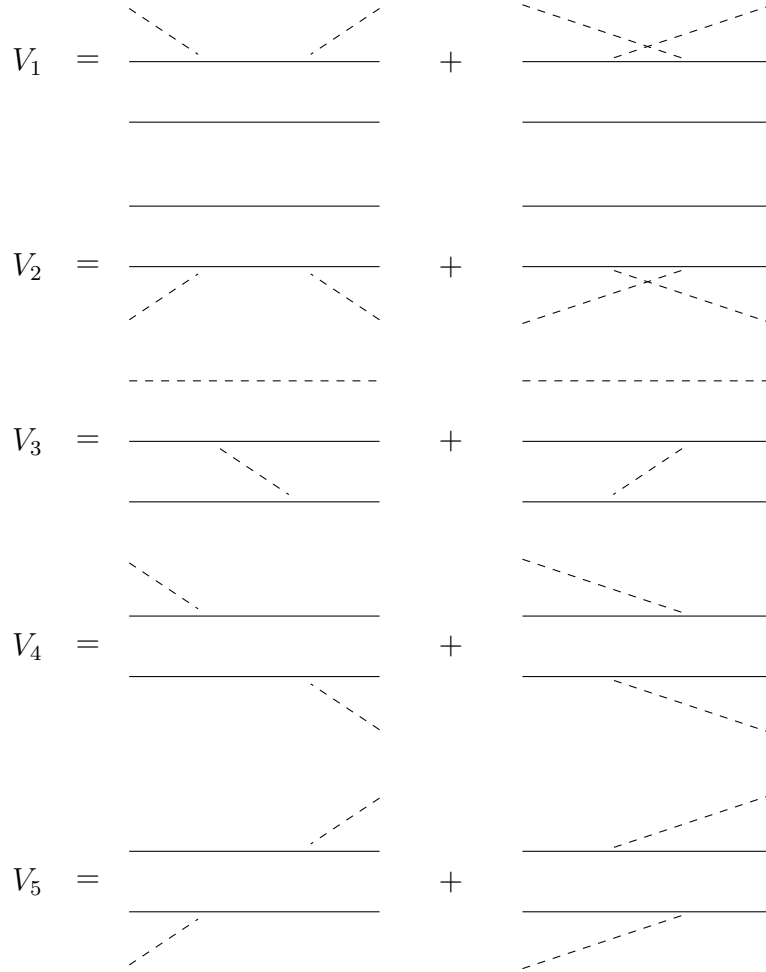


Figure 1.7: Illustration of the πNN potentials V_α , where $\alpha \in \{1, 2, 3, 4, 5\}$, that are included in the work of Stingl and Stelbovics [44–46]. The solid lines represent the nucleons and the dashed lines represent the pions.

Stingl and Stelbovics classify each of their πNN potentials into a class of disconnectedness with an appropriate momentum-conserving function δ_α where $\alpha = \{1, 2, 3, 4, 5\}$. These authors also partially dressed their πNN propagator by including the sum of fully disconnected πNN states where each nucleon has a pion bubble, which leads to different-time dressing of the nucleons. Afnan and Stelbovics [47] showed that the derived equations of Stingl and Stelbovics reduce to the equations of Afnan and Blankleider [33], provided that states of two-pions are neglected as in the “Unitary $NN - \pi NN$ ” model. While Stingl and Stelbovics formalise an approach to go beyond the “one-pion” approximation, the problem with the model of Stingl and Stelbovics is that it is a model that is difficult if not impossible to solve.

A theoretical solution to the problems of the “Unitary $NN - \pi NN$ ” model was found by

Kvinikhidze and Blankleider [48], as they were able to fully dress both nucleons at the same time, without having to compromise the three-body nature of the overall πNN equations. This approach involves the innovative use of convolution integrals, which they show can be used to sum all possible relative time-orderings of disconnected diagrams in TOPT. A convolution integral is a mathematical expression formed using two functions $a(E)$ and $b(E)$, being defined as

$$c(E) = a \otimes b = \left(-\frac{1}{2\pi i} \right) \int_{-\infty}^{\infty} dz a(E-z)b(z). \quad (1.3)$$

The summation of all different relative time-orderings through the use of convolution integrals allows two nucleons to be dressed at the same time, as previously the restriction of diagrams with at most one pion would not allow simultaneous dressing. In addition to two nucleons being able to be simultaneously dressed, three-body disconnected diagrams can be similarly described using convolution integrals. For example, the disconnected dressed pion-two-nucleon vertex, where a pion is absorbed (emitted) on one nucleon and the other nucleon is a spectator, can be described as a convolution of a $\pi N \rightarrow N$ ($N \rightarrow \pi N$) vertex and a dressed one-nucleon propagator, where all dressings can be retained even though more than one pion would be in flight at the same time. From this, Kvinikhidze and Blankleider [49] derived equations for $NN \rightarrow NN$ scattering. Theoretically, the renormalisation problems of the equations describing the πNN system can be overcome as the effective renormalisation of the dressed vertices in the πN t -matrix and NN OPE amplitude are consistent. The convolution approach also allows for the inclusion of time-ordered diagrams that were previously neglected in the “Unitary $NN - \pi NN$ ” model, specifically the $\pi d \rightarrow \pi d$ diagram in Figure 1.6. The only approximation used in the equations of [49] is neglecting connected three-body forces. The πNN potentials in the convolution approach are illustrated in Figure 1.8.

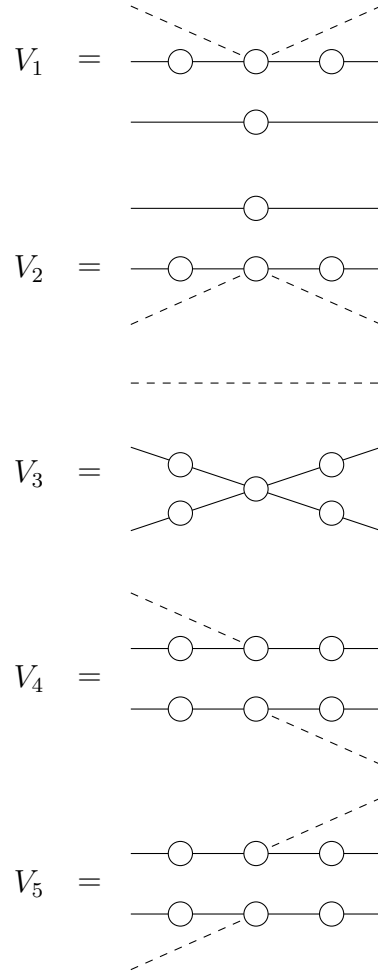


Figure 1.8: Illustration of the πNN potentials V_α , where $\alpha \in \{1, 2, 3, 4, 5\}$, that are included in the convolution approach of Kvinikhidze and Blankleider [49]. The solid lines represent the nucleons and the dashed lines represent the pions. The open circles represent all possible diagrams except for those that lead to πNN intermediate states.

In this thesis, we aim to continue the theoretical development of the coupled $NN - \pi NN$ system through the use of the convolution approach. We complete the established work of Kvinikhidze and Blankleider [49] by deriving a coupled set of equations describing the scattering processes for $NN \rightarrow NN$, $\pi d \rightarrow NN$, $NN \rightarrow \pi d$ and $\pi d \rightarrow \pi d$ using the convolution approach and the derived equations are shown in Equation 3.123. We refer to these derived equations as the 3-dimensional πNN convolution equations, which have the same form as the unitary $NN - \pi NN$ equations of Afnan and Blankleider [33], but unlike the equations of Afnan and Blankleider, all nucleons in the πNN convolution equations are fully dressed. The 3-dimensional πNN convolution equations solve the long-standing renormalisation problem inherent in the “Unitary $NN - \pi NN$ ” model that has been discussed. However, as can

be seen from Equation 3.114, these 3-dimensional πNN convolution equations involve non-pair-like interactions corresponding to disconnected three-body forces and therefore may be difficult to solve numerically. For this reason, an alternative formulation is also presented. Splitting the πN t -matrix into its pole and non-pole part, then convoluting each part individually leads to a 4-dimensional (4D) version of the πNN convolution equations, which only involve pair-like interactions. Now that we have convolution equations that involve pair-like interactions, we require two-body input that incorporates nucleon dressing for consistency. To achieve this, we create dressed πN input through the numerical solution of the Dyson-Schwinger equations.

With the derivation of the πNN convolution equations complete, we are then tasked with solving these equations numerically to determine their ability to reproduce experimental data. It is not clear how to solve the 3-dimensional form of the πNN convolution equations due to the non-pair-like interactions, therefore in this work, we focus on solving the 4-dimensional form of the πNN convolution equations as we have a known method to solve these equations. Solving 4-dimensional scattering equations is, on its own, a very interesting problem regardless of its connection to the πNN system, and may provide benefits to other areas of nuclear and particle physics. 4-dimensional equations typically describe relativistic processes, where the relativistic description of two interacting particles is most famously given by the Bethe-Salpeter equation [50]. The difficulty in solving these 4-dimensional scattering equations is in the moving singularities in the integrals of these equations. Common methods to avoid these moving singularities include Wick rotation [51–54], Padé approximants [55–62], Nakanishi integral representation with light-front projection [63–70] and spline interpolation [70–78]. However, Wick rotation can only be used for equations describing the scattering of two particles with equal mass, while Padé approximants rely on Wick rotation. Nakanishi integral representation with light-front projection suffers from being difficult to implement for scattering states and has only been achieved for simple cases, such as the zero-energy limit. As noted by Carbonell et al. [63–68], the Euclidean Bethe-Salpeter amplitude (i.e. the Wick-rotated solution to the Bethe-Salpeter equation) does not allow for the calculation of some observables, in particular, electromagnetic form factors due to the singularity structure in the form factor integral whose contributions are otherwise unknown. Thus, there is a necessity to calculate the Minkowski solution (i.e. solution without Wick rotation), by evaluating our integrals along the real axis. Therefore, we use the spline interpolation to solve our 4-dimensional πNN convolution equations, as

we are able to avoid the issues with other methods and calculate our integrals along the real axis. In the spline interpolation method, we represent the solution of our 4-dimensional equations as a sum over basis functions called splines. Carbonell and Karmanov [70, 72–76] present a method for calculating a 4-dimensional Bethe-Salpeter scattering amplitude using spline interpolation and successfully obtain results. The spline interpolation method allows us to account for the complex singularity structure in the integrals of our 4-dimensional equations. In this work, we adapt the method proposed by Carbonell and Karmanov to our 4-dimensional πNN convolution equations.

Through our investigation of splines and numerical methods, we are able to obtain results for our 4-dimensional πNN convolution equations and compare these results to the “Unitary $NN - \pi NN$ ” model using the Afnan and Blankleider [33] equations. We are particularly interested in the ability of our 4-dimensional equations to reproduce the $pp \rightarrow \pi^+ d$ differential cross section and the T_{20} polarisation observable for πd elastic scattering, but also various other scattering observables. We are also interested in the viability of the spline interpolation method in solving 4-dimensional equations in general. The spline interpolation method and proper handling of the complex singularities in our equations have proven to require high-performance computing (HPC) resources to perform calculations in a timely manner. The computational intensity of these calculations restricts our ability to perform numerical calculations with coupling to all channels and limits the number of partial waves included in our calculations. Due to the complex singularities, many spline interpolation points are required in order to obtain numerically stable results that converge with an increasing amount of interpolation points and due to the computational complexity of these calculations, we are limited by the number of interpolation points we can include. In terms of overall results, we were unable to make a full comparison between the πNN convolution equations and experimental data, due to the computational intensity of the spline interpolation method that restrict the inclusion of all coupled channels and many partial waves. We are unable to definitively conclude whether the πNN convolution equations resolve the discrepancies between the $pp \rightarrow \pi^+ d$ cross sections and the T_{20} polarisation observable with experiments, however, we believe we have provided the foundational work that would allow for the full calculation of the πNN convolution equations in the future.

The structure of this thesis is as follows: In Chapter 2, we discuss time-ordered perturbation theory. We show that temporarily introducing two types of nucleons and three types of pions lead to fully dressed disconnected and connected diagrams, as done in [39, 48], and

extend this idea to derive a fully dressed $\pi d \rightarrow NN$ diagram and fully dressed NN two-pion exchange. In Chapter 3, we extend the work of Kvinikhidze and Blankleider [49] by presenting a derivation of coupled scattering equations for the processes $NN \rightarrow NN$, $NN \rightarrow N\Delta$, $N\Delta \rightarrow N\Delta$, $NN \rightarrow \pi d$, $\pi d \rightarrow NN$, $\pi d \rightarrow N\Delta$ and $\pi d \rightarrow \pi d$ using the convolution approach. We show that the splitting of the πN t -matrix into its pole and non-pole parts leads to a 4-dimensional version of our coupled scattering equations, which is the focus of our numerical calculations. In Chapter 4, we discuss numerical techniques, with a particular emphasis on the numerical techniques for solving the 4-dimensional πNN convolution equations. Chapter 5 discusses the two-body πN and NN input that is used in the calculations of the πNN convolution equations. Chapter 6 involves the numerical results of the πNN convolution equations where we calculate scattering observables and compare the results of these calculations to the equations of the “Unitary $NN - \pi NN$ ” model. Finally, we finish with conclusions of the overall work and discuss further work that could be achieved.

Chapter 2

Time-ordered perturbation theory

2.1 Introduction

Time-ordered perturbation theory (TOPT) provides a convenient framework for describing processes involving particle creation and annihilation, in a non-relativistic 3-dimensional setting. However, as previously discussed, a major issue in using TOPT to formulate $NN - \pi NN$ equations has been the problem of incorporating full dressing of the nucleons. In this chapter, we describe how such full dressing can be achieved in both disconnected and connected perturbation diagrams of TOPT, as this will form the basis for the formulation and description of the $NN - \pi NN$ system in the following chapters.

It has previously been shown that one way to obtain full nucleon dressing is to start with the expression for a Feynman diagram of relativistic quantum field theory (RQFT), and then integrate out the 0th (energy) components of initial and final four-momenta. This follows the prescription of the so-called “equal time formalism” which can be shown to reduce RQFT to TOPT in theories where the dressed vacuum and bare vacuums are identical [39]. In this chapter, however, we would like to pursue a more general method for dressing nucleons that does not rely on any connection to RQFT. Formulated purely within TOPT, this method relies on the temporary introduction of two non-identical nucleons and three types of pions.

2.2 Time-ordered perturbation theory

Time-ordered perturbation theory (TOPT), also known as “old-fashioned perturbation theory”, is an expansion of the full Green’s function operator $1/(E^+ - H)$ of a particular system, where H is the Hamiltonian of the system given by $H = H_0 + H_I$, where H_0 is the free Hamiltonian and H_I is the interaction Hamiltonian. The expansion of the full Green’s function is performed around the free Green’s function operator $1/(E^+ - H_0)$ and results in the expansion

$$\frac{1}{E^+ - H} = \frac{1}{E^+ - H_0} + \frac{1}{E^+ - H_0} H_I \frac{1}{E^+ - H_0} + \frac{1}{E^+ - H_0} H_I \frac{1}{E^+ - H_0} H_I \frac{1}{E^+ - H_0} + \dots \quad (2.1)$$

We can then take matrix elements of the terms in the above expansion, which can be represented graphically as a sum of “perturbation diagrams”.

2.3 Convolution approach for disconnected processes

Kvinikhidze and Blankleider [48] showed that in TOPT the fully dressed two-nucleon propagator $D_0(E)$, which is the sum of all disconnected NN diagrams, can be expressed by a convolution of two dressed one-nucleon propagators $g(E)$ by temporarily considering the two nucleons as distinguishable particles.

Consider a TOPT of nucleons and pions described by a quantum-field theoretic Hamiltonian $H = H_0 + H_I$. We define the $NN \rightarrow NN$ Green's function operator D by

$$\langle \mathbf{p}'_1 \mathbf{p}'_2 | D(E) | \mathbf{p}_1 \mathbf{p}_2 \rangle = \langle \mathbf{p}'_1 \mathbf{p}'_2 | \frac{1}{E^+ - H} | \mathbf{p}_1 \mathbf{p}_2 \rangle. \quad (2.2)$$

The fully dressed two-nucleon propagator D_0 is defined as the fully disconnected part of the $NN \rightarrow NN$ Green's function operator which, after taking matrix elements of the operator between momenta states, gives the numerical form of the dressed two-nucleon propagator $D_0(E, \mathbf{p}_1, \mathbf{p}_2)$:

$$\langle \mathbf{p}'_1 \mathbf{p}'_2 | D_0(E) | \mathbf{p}_1 \mathbf{p}_2 \rangle = \langle \mathbf{p}'_1 \mathbf{p}'_2 | \frac{1}{E^+ - H} | \mathbf{p}_1 \mathbf{p}_2 \rangle_{disc} = \delta(\mathbf{p}'_1 - \mathbf{p}_1) \delta(\mathbf{p}'_2 - \mathbf{p}_2) D_0(E, \mathbf{p}_1, \mathbf{p}_2). \quad (2.3)$$

If we attempt to calculate $D_0(E, \mathbf{p}_1, \mathbf{p}_2)$ by performing the perturbation expansion of Equation 2.1, this would lead to complicated perturbation diagrams and detrimental simplifications are required for practical applications. However, we can obtain the fully dressed two-nucleon propagator by temporarily treating the two nucleons as two mutually non-identical particles, each with its own pion fields. The full Hamiltonian H can then be written as $H = H_1 + H_2$ and where H_1 and H_2 are of the same form as H but are defined in terms of their own nucleon and pion fields. This allows us to represent the operator $1/(E^+ - H)$ by a convolution integral

$$\frac{1}{E^+ - H} = \left(-\frac{1}{2\pi i} \right) \int_{-\infty}^{\infty} \frac{1}{z^+ - H_1} \frac{1}{E^+ - z - H_2} dz \quad (2.4)$$

because H_1 and H_2 commute due to acting on different Hilbert spaces and thus allows the use of Cauchy's Residue Theorem. Now, using the definition of the dressed one-nucleon propagator g_i and its numerical form $g_i(E, \mathbf{p}_i)$

$$\langle \mathbf{p}'_i | g_i(E) | \mathbf{p}_i \rangle = \langle \mathbf{p}'_i | \frac{1}{E^+ - H} | \mathbf{p}_i \rangle = \delta(\mathbf{p}'_i - \mathbf{p}_i) g_i(E, \mathbf{p}_i) \quad (2.5)$$

where $i = 1, 2$, the two-nucleon propagator $D_0(E, \mathbf{p}_1, \mathbf{p}_2)$ can be calculated by a convolution of two dressed one-nucleon propagators g_i

$$D_0(E, \mathbf{p}_1, \mathbf{p}_2) = \left(-\frac{1}{2\pi i} \right) \int_{-\infty}^{\infty} g_1(z, \mathbf{p}_1) g_2(E - z, \mathbf{p}_2) dz \quad (2.6)$$

The use of the convolution integrals suggests a connection to relativity, as it introduces a time-like energy variable and preserves the product-like nature of relativistic propagators. Indeed, it can also be derived from relativistic field theory in the equal-time approach [39, 79]. No approximation is required and the Hilbert space does not need to be truncated to obtain this result. Therefore, both nucleons are able to be dressed at the same time, potentially resolving the problem of inconsistent nucleon dressing the “Unitary $NN - \pi NN$ ” model.

This convolution approach can be used for other disconnected processes, by taking different matrix elements of Equation 2.4. For example, if we consider the disconnected pion-two-nucleon vertex operator \tilde{F}_1 , representing the process where a pion is created on nucleon 1 and nucleon 2 is a spectator (indicated by the subscript 1), this operator, as well as its numerical form $\tilde{F}_1(\mathbf{k}, \mathbf{p}'_1, \mathbf{p}_2)$, are defined as

$$\langle \mathbf{p}'_1 \mathbf{p}'_2 \mathbf{k} | \tilde{F}_1(E) | \mathbf{p}_1 \mathbf{p}_2 \rangle = \langle \mathbf{p}'_1 \mathbf{p}'_2 \mathbf{k} | \frac{1}{E^+ - H} | \mathbf{p}_1 \mathbf{p}_2 \rangle_{disc} = \delta(\mathbf{p}'_1 + \mathbf{k} - \mathbf{p}_1) \delta(\mathbf{p}'_2 - \mathbf{p}_2) \tilde{F}_1(\mathbf{k}, \mathbf{p}'_1, \mathbf{p}_2) \quad (2.7)$$

where \mathbf{k} is the momentum of the pion. We define the πNN vertex Green’s function \tilde{f}_i as

$$\langle \mathbf{p}'_i \mathbf{k} | \tilde{f}_i(E) | \mathbf{p}_i \rangle = \langle \mathbf{p}'_i \mathbf{k} | \frac{1}{E^+ - H} | \mathbf{p}_i \rangle = \delta(\mathbf{p}'_i + \mathbf{k} - \mathbf{p}_i) \tilde{f}_i(\mathbf{k}, \mathbf{p}_i, E) \quad (2.8)$$

where

$$\tilde{f}_i(E) = D_0(E) f_i(E) g_i(E) \quad (2.9)$$

and the subscript $i = 1, 2$ indicates the nucleon involved in the interaction. We can now represent $\tilde{F}_1(\mathbf{k}, \mathbf{p}'_1, \mathbf{p}_2)$ by a convolution integral by taking matrix elements of Equation 2.4 with a πNN state on the left and an NN state on the right:

$$\tilde{F}_1(\mathbf{k}, \mathbf{p}'_1, \mathbf{p}_2) = \left(-\frac{1}{2\pi i} \right) \int_{-\infty}^{\infty} \tilde{f}_1(\mathbf{k}, \mathbf{p}_1, z) g_2(E - z, \mathbf{p}_2) \quad (2.10)$$

We have shown that disconnected processes can be represented by convolution integrals, and no approximation or neglect of perturbation diagrams is necessary. An important aspect of this convolution approach for disconnected processes is that it is model independent, meaning that it is not necessary to define a specific model for the Hamiltonians in our TOPT.

2.4 Convolution approach for connected processes

2.4.1 Model Hamiltonian

We now want to investigate the same general approach, as above, for connected processes. Although it might be possible to formulate expressions for connected processes in a model independent way, as was just done for disconnected processes above, it is not clear how this would be done, at this stage. As a result, we will define a model Hamiltonian to carry out our investigation of connected processes. We will use the same interaction model as specified in [39, 48]. We assume a model Hamiltonian describing the interactions of pions and nucleons given by

$$\begin{aligned} H &= H_0 + H_I \\ &= H_0^N + H_0^\pi + H_I \end{aligned} \quad (2.11)$$

where

$$H_0^N = \int (E_N(\mathbf{p}) + m_0) a_N^\dagger(\mathbf{p}) a_N(\mathbf{p}) d\mathbf{p}, \quad (2.12a)$$

$$H_0^\pi = \int d\mathbf{k} \omega_k a_\pi^\dagger(\mathbf{k}) a_\pi(\mathbf{k}), \quad (2.12b)$$

$$H_I^\pi = \int d\mathbf{k} a_\pi^\dagger(\mathbf{k}) J_N(\mathbf{k}) + a_\pi(\mathbf{k}) J_N^\dagger(\mathbf{k}), \quad (2.12c)$$

$$J_N(\mathbf{k}) = \int d\mathbf{p} d\mathbf{p}' \delta(\mathbf{p} + \mathbf{k} - \mathbf{p}') \frac{1}{\sqrt{\omega_k}} F_0(\mathbf{p}, \mathbf{p}') a_N^\dagger(\mathbf{p}) a_N(\mathbf{p}'). \quad (2.12d)$$

Here, $a_\pi^\dagger(\mathbf{k})$ and $a_\pi(\mathbf{k})$ are creation and annihilation operators for a pion of momentum \mathbf{k} respectively, while $a_N^\dagger(\mathbf{p})$ and $a_N(\mathbf{p})$ are creation and annihilation operators for a nucleon of momentum \mathbf{p} respectively. In this model, we ignore antiparticles for the nucleons. We also have $E_N(\mathbf{p})$, which is the kinetic energy of a nucleon with momentum \mathbf{p} , m_0 is the bare mass of the nucleon and ω_k , which is the energy of a pion with momentum \mathbf{k} . We use semi-relativistic kinematics, so that $E_N(\mathbf{p}) = \mathbf{p}^2/2m_N$ and $\omega_k = (\mathbf{k}^2 + m_\pi^2)^{1/2}$, where m_N is the mass of the nucleon and m_π is the mass of a pion. These operators act on the vacuum state $|0\rangle$ to produce the respective free particle states

$$|\mathbf{p}\rangle = a_N^\dagger(\mathbf{p}) |0\rangle, \quad |\mathbf{k}\rangle = a_\pi^\dagger(\mathbf{k}) |0\rangle. \quad (2.13)$$

In this model, the bare vacuum and dressed vacuum are identical. The operator $J_N(\mathbf{k})$ describes the interaction of a nucleon and pion and includes a general form factor function

$F_0(\mathbf{p}, \mathbf{p}')$ to take into account the finite size of the nucleon. The operators a^\dagger and a obey the following (anti)commutator relations

$$[a_\pi(\mathbf{k}), a_\pi^\dagger(\mathbf{k}')] = \delta(\mathbf{k} - \mathbf{k}'), \quad (2.14a)$$

$$[a_\pi(\mathbf{k}), a_\pi(\mathbf{k}')] = 0, \quad (2.14b)$$

$$\{a_N(\mathbf{p}), a_N^\dagger(\mathbf{p}')\} = \delta(\mathbf{p} - \mathbf{p}'), \quad (2.14c)$$

$$\{a_N(\mathbf{p}), a_N(\mathbf{p}')\} = 0 \quad (2.14d)$$

so that

$$[a_\pi(\mathbf{k}), H_0^\pi] = \int \omega'_k [a_\pi(\mathbf{k}), a_\pi^\dagger(\mathbf{k}')] a_\pi(\mathbf{k}') d\mathbf{k}' = \omega_k a_\pi(\mathbf{k}) \quad (2.15)$$

and

$$\begin{aligned} [a_\pi(\mathbf{k}), H_I^\pi] &= \int J_N(\mathbf{k}') [a_\pi(\mathbf{k}), a_\pi^\dagger(\mathbf{k}')] d\mathbf{k}' + \int J_N^\dagger(\mathbf{k}') [a_\pi^\dagger(\mathbf{k}), a_\pi^\dagger(\mathbf{k}')] d\mathbf{k}' \\ &= \int J_N(\mathbf{k}') \delta(\mathbf{k} - \mathbf{k}') d\mathbf{k}' = J_N(\mathbf{k}). \end{aligned} \quad (2.16)$$

Thus

$$[a_\pi(\mathbf{k}), H_0^\pi] = \omega_k a_\pi(\mathbf{k}), \quad (2.17a)$$

$$[a_\pi(\mathbf{k}), H_I^\pi] = J_N(\mathbf{k}). \quad (2.17b)$$

Similarly

$$J_N(\mathbf{k}) |\mathbf{p}'\rangle = \frac{1}{\sqrt{\omega_\pi}} F_0(\mathbf{p}, \mathbf{p}') |\mathbf{p}\rangle, \quad (2.18a)$$

$$\langle \mathbf{p}' | J_N^\dagger(\mathbf{k}) = \langle \mathbf{p} | \frac{1}{\sqrt{\omega_\pi}} \bar{F}_0(\mathbf{p}', \mathbf{p}) \quad (2.18b)$$

where $\mathbf{p} + \mathbf{k} = \mathbf{p}'$. Thus

$$H_I |\mathbf{p}'\rangle = \int \delta(\mathbf{p} + \mathbf{k} - \mathbf{p}') \frac{1}{\sqrt{\omega_\pi}} F_0(\mathbf{p}, \mathbf{p}') |\mathbf{k} \mathbf{p}\rangle d\mathbf{k} d\mathbf{p}, \quad (2.19a)$$

$$\langle \mathbf{p}' | H_I = \int \delta(\mathbf{p} + \mathbf{k} - \mathbf{p}') \langle \mathbf{k} \mathbf{p} | \frac{1}{\sqrt{\omega_\pi}} \bar{F}_0(\mathbf{p}', \mathbf{p}) d\mathbf{k} d\mathbf{p}. \quad (2.19b)$$

Similar to the convolution approach for disconnected processes, we temporarily introduce two types of nucleons and three types of pions. We have two distinguishable nucleons N_1 and N_2 that are both dressed by their own respective pions π_1 and π_2 with a third pion π that can interact with both nucleons. Hamiltonians H_1 and H_2 , consisting of a free and interaction Hamiltonian, are defined for the $\pi_1 N_1$ and $\pi_2 N_2$ systems respectively.

$$H_1 = H_0(1) + H_I(1) \quad \longrightarrow \quad \pi_1 N_1, \quad (2.20a)$$

$$H_2 = H_0(2) + H_I(2) \quad \longrightarrow \quad \pi_2 N_2. \quad (2.20b)$$

We also define a similar Hamiltonian H^π describing a pion that can interact with both nucleons. This Hamiltonian consists of a free term and two interactions terms, corresponding to the interaction with each individual nucleon:

$$H^\pi = H_0^\pi + H_I^\pi(1) + H_I^\pi(2). \quad (2.21)$$

Therefore, the full Hamiltonian H can be written as a sum of Hamiltonians defined for the two types of nucleons and the three types of pions:

$$\begin{aligned} H &= H_1 + H_2 + H^\pi \\ &= H_0(1) + H_I(1) + H_0(2) + H_I(2) + H_0^\pi + H_I^\pi(1) + H_I^\pi(2). \end{aligned} \quad (2.22)$$

The explicit details for the Hamiltonians describing the $\pi_1 N_1$ and $\pi_2 N_2$ systems are not required. The interaction Hamiltonians $H_I^\pi(1)$ and $H_I^\pi(2)$ are defined by

$$H_I^\pi(1) = \int J_{N_1}(\mathbf{k}) a_\pi^\dagger(\mathbf{k}) d\mathbf{k} + \int J_{N_1}^\dagger(\mathbf{k}) a_\pi(\mathbf{k}) d\mathbf{k}, \quad (2.23a)$$

$$H_I^\pi(2) = \int J_{N_2}(\mathbf{k}) a_\pi^\dagger(\mathbf{k}) d\mathbf{k} + \int J_{N_2}^\dagger(\mathbf{k}) a_\pi(\mathbf{k}) d\mathbf{k}. \quad (2.23b)$$

This also defines creation and annihilation operators, $a_\pi^\dagger(\mathbf{k})$ and $a_\pi(\mathbf{k})$, for the pion that can interact with both nucleons.

We note that the following commutator relations are also true, when we have two distinguishable nucleons

$$[H_1, H_2] = [H_1, J_{N_2}] = [H_2, J_{N_1}] = 0. \quad (2.24)$$

2.4.2 The fully dressed NN OPE diagram

Our goal now is to obtain fully dressed connected diagrams that contain all possible nucleon dressing contributions. We consider the procedure of Blankleider and Kvinikhidze [39] and briefly present their derivation of the fully dressed NN one-pion exchange (OPE) Z -diagram ($NN \rightarrow NN$ Z -diagram) from TOPT.

Consider the operator $1/(E^+ - H)$, where the full Hamiltonian is given by $H = H_1 + H_2 + H^\pi$ as detailed above. Rather than the perturbation expansion in Equation 2.1, we will perform a perturbation expansion by expanding the Green's function operator around the interaction Hamiltonians $H_I^\pi(1)$ and $H_I^\pi(2)$. This leads to the perturbation expansion

$$\begin{aligned} \frac{1}{E^+ - H} &= \frac{1}{E^+ - H_1 - H_2 - H_0^\pi} \\ &+ \frac{1}{E^+ - H_1 - H_2 - H_0^\pi} [H_I^\pi(1) + H_I^\pi(2)] \frac{1}{E^+ - H_1 - H_2 - H_0^\pi} + \dots \end{aligned} \quad (2.25)$$

The NN OPE diagrams corresponds to the terms in the perturbation expansion, which contain two H_I^π in them. To save on notation, we do not write the free Green's functions $1/(E^+ - H_1 - H_2 - H_0^\pi)$ and only consider the interaction Hamiltonians. Taking the matrix elements of perturbation terms with two H_I^π gives us a sum of four terms

$$\begin{aligned} & \langle \mathbf{p}'_1 \mathbf{p}'_2 | H_I^\pi(1) H_I^\pi(1) | \mathbf{p}_1 \mathbf{p}_2 \rangle + \langle \mathbf{p}'_1 \mathbf{p}'_2 | H_I^\pi(1) H_I^\pi(2) | \mathbf{p}_1 \mathbf{p}_2 \rangle \\ & + \langle \mathbf{p}'_1 \mathbf{p}'_2 | H_I^\pi(2) H_I^\pi(1) | \mathbf{p}_1 \mathbf{p}_2 \rangle + \langle \mathbf{p}'_1 \mathbf{p}'_2 | H_I^\pi(2) H_I^\pi(2) | \mathbf{p}_1 \mathbf{p}_2 \rangle \end{aligned} \quad (2.26)$$

where \mathbf{p}_1 is the momentum of nucleon 1 and \mathbf{p}_2 is the momentum of nucleon 2. The second term in the above perturbation expansion leads to one-pion exchange where a pion is created on nucleon 2 then absorbed on nucleon 1. Through the definitions of $H_I^\pi(1)$ and $H_I^\pi(2)$, while also using the commutator relations of the previous section, we obtain the expression for fully dressed one-pion exchange

$$\begin{aligned} G_{12}^{OPE} = & \left(-\frac{1}{2\pi i} \right)^2 \delta(\mathbf{p}'_1 + \mathbf{p}'_2 - \mathbf{p}_1 - \mathbf{p}_2) \int dz dz' g(z', \mathbf{p}'_1) \bar{f}(\mathbf{p}'_1, \mathbf{p}_1, z', z) g(z, \mathbf{p}_1) \frac{1}{z'^+ - z - \omega_k} \\ & g(E - z', \mathbf{p}'_2) f(\mathbf{p}'_2, \mathbf{p}_2, E - z', E - z) g(E - z, \mathbf{p}_2). \end{aligned} \quad (2.27)$$

We present the explicit derivation of Equation 2.27 in Appendix D. From our perturbation expansion, we obtain two-energy vertices that differ from the usual one-energy vertices we obtain in TOPT. These two-energy vertices are defined by the matrix elements

$$\delta(\mathbf{p}' + \mathbf{k} - \mathbf{p}) g(z', \mathbf{p}') f(\mathbf{p}', \mathbf{p}, z', z) g(z, \mathbf{p}) = \langle \mathbf{p}' | \frac{1}{z'^+ - H} J_N(\mathbf{k}) \frac{1}{z^+ - H} | \mathbf{p} \rangle. \quad (2.28)$$

We define the dressed pion-nucleon vertex using the full Green's function

$$\delta(\mathbf{p}' - \mathbf{p} + \mathbf{k}) g(E - \omega_k, \mathbf{p}') f(\mathbf{k}, \mathbf{p}, E) g(E, \mathbf{p}) = \langle \mathbf{k} \mathbf{p}' | \frac{1}{E^+ - H} | \mathbf{p} \rangle. \quad (2.29)$$

As $\mathbf{p} + \mathbf{k} = \mathbf{p}'$, we can use a slightly different definition of the function f , where it depends on the initial and final momentum of the nucleon

$$\delta(\mathbf{p}' - \mathbf{p} + \mathbf{k}) g(E - \omega_k, \mathbf{p}') f(\mathbf{p}', \mathbf{p}, E) g(E, \mathbf{p}) = \langle \mathbf{k} \mathbf{p}' | \frac{1}{E^+ - H} | \mathbf{p} \rangle. \quad (2.30)$$

In this definition of the dressed pion-nucleon vertex, we are assuming the nucleons are dressed and the pions are not. One can show that

$$\begin{aligned} & \langle \mathbf{p}' | \frac{1}{z'^+ - H} J_N(\mathbf{k}) \frac{1}{z^+ - H} | \mathbf{p} \rangle \\ & = \langle \mathbf{k} \mathbf{p}' | \frac{1}{z^+ - H} | \mathbf{p} \rangle + (z - z' - \omega_k) \langle \mathbf{p}' | \frac{1}{z'^+ - H} a_\pi(\mathbf{k}) \frac{1}{z^+ - H} | \mathbf{p} \rangle. \end{aligned} \quad (2.31)$$

The left side of the equation defines the two-energy vertex and the first term of the right side defines the usual one-energy vertex. This shows that the two-energy vertex is equal to the usual one-energy vertex when initial and final energies are equal, namely $z = z' + \omega_k$. We are, therefore, motivated to approximate the two-energy vertex by the one-energy vertex $f(\mathbf{p}', \mathbf{p}, z', z) \approx f(\mathbf{p}', \mathbf{p}, z)$, which is exact when $z = z' + \omega_k$. Thus, we obtain our OPE Green's function with one-energy vertices

$$G_{12}^{OPE} = \left(-\frac{1}{2\pi i}\right)^2 \delta(\mathbf{p}'_1 + \mathbf{p}'_2 - \mathbf{p}_1 - \mathbf{p}_2) \int dz dz' g(z', \mathbf{p}'_1) \bar{f}(\mathbf{p}'_1, \mathbf{p}_1, z') g(z, \mathbf{p}_1) \frac{1}{z' + -z - \omega_k} g(E - z', \mathbf{p}'_2) f(\mathbf{p}'_2, \mathbf{p}_2, E - z) g(E - z, \mathbf{p}_2). \quad (2.32)$$

As a result, we obtain the Green's function for one-pion exchange between two nucleons, where all nucleons are fully dressed. This fully dressed NN OPE diagram is given in Figure 2.1. The dressed one-pion exchange potential V_{12}^{OPE} can therefore be calculated in the usual way of “chopping off” the external legs of the Green's function.

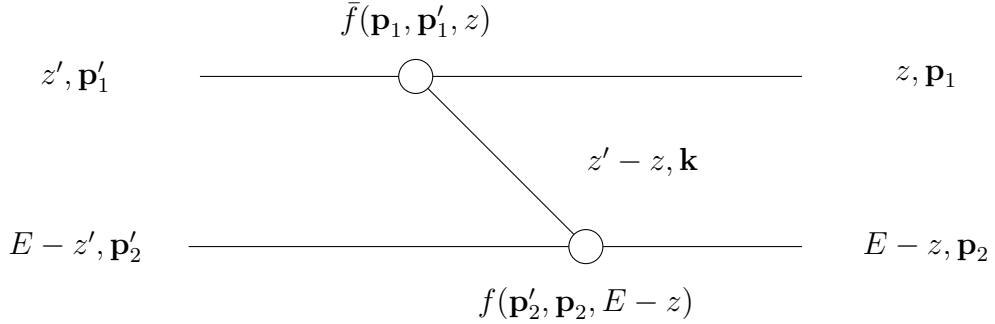


Figure 2.1: Diagram representation of the integrand in Figure 2.32 for the fully dressed one-pion exchange between two nucleons.

2.4.3 Fully dressed $\pi d \rightarrow NN$ Z -diagram

Since we have a derivation of the Z -diagram for NN OPE ($NN \rightarrow NN$), we can follow the same procedure to derive the Z -diagram for $\pi d \rightarrow NN$ where all nucleons are dressed. This differs from the derivation of the Z -diagram for $NN \rightarrow NN$ as we must introduce a t -matrix $T(E)$ to incorporate the deuteron. The same procedure is done for Z -diagrams involving $N\Delta$ states, so our derivation of the Z -diagram for $\pi d \rightarrow NN$ will allow us to determine the all remaining Z -diagrams. We use the same perturbation expansion given in Equation 2.25. As we need to incorporate a deuteron state into theory, we do this by

defining a sub-system NN t -matrix $T(E)$ in the obvious way using Equation 2.25:

$$\begin{aligned} \frac{1}{E^+ - H} &= \frac{1}{E^+ - H_1 - H_2 - H_0^\pi} \\ &+ \frac{1}{E^+ - H_1 - H_2 - H_0^\pi} T(E) \frac{1}{E^+ - H_1 - H_2 - H_0^\pi} \end{aligned} \quad (2.33)$$

where

$$T(E) = [H_I^\pi(1) + H_I^\pi(2)] + [H_I^\pi(1) + H_I^\pi(2)] \frac{1}{E^+ - H_1 - H_2 - H_0^\pi} [H_I^\pi(1) + H_I^\pi(2)] + \dots \quad (2.34)$$

Equation 2.33 is simply the usual definition of a t -matrix satisfying an equation of the form $G = G_0 + G_0 T G_0$. We want the Z -diagram where the initial state is πd and the pion remains in flight as the deuteron disintegrates into two nucleons, after which the pion is absorbed by nucleon N_1 . It is thus evident that the following expression will be useful:

$$\begin{aligned} a_\pi(\mathbf{k}) \frac{1}{E^+ - H} &= \left[\frac{1}{E^+ - H_1 - H_2 - H_0^\pi - \omega_k} \right. \\ &+ \left. \frac{1}{E^+ - H_1 - H_2 - H_0^\pi - \omega_k} [H_I^\pi(1) + H_I^\pi(2)] \frac{1}{E^+ - H_1 - H_2 - H_0^\pi - \omega_k} + \dots \right] a_\pi(\mathbf{k}) \\ &+ \dots \\ &= \frac{1}{E^+ - \omega_k - H} a_\pi(\mathbf{k}) + \text{terms where } a_\pi \text{ does not appear as the right-most operator.} \end{aligned} \quad (2.35)$$

We begin with the perturbation series for the $\pi NN \rightarrow NN$ Green's function in Equation 2.25, singling out the term where a pion is absorbed on nucleon 1, thus

$$\begin{aligned} \langle \mathbf{p}'_1 \mathbf{p}'_2 | \frac{1}{E^+ - H} | \mathbf{k} \mathbf{p}_1 \mathbf{p}_2 \rangle &= \\ &\langle \mathbf{p}'_1 \mathbf{p}'_2 | \frac{1}{E^+ - H_1 - H_2 - H_0^\pi} H_I^\pi(1) \frac{1}{E^+ - H} | \mathbf{k} \mathbf{p}_1 \mathbf{p}_2 \rangle + \dots \\ &= \int d\mathbf{k}' \langle \mathbf{p}'_1 \mathbf{p}'_2 | \frac{1}{E^+ - H_1 - H_2 - H_0^\pi} J_{N_1}^\dagger(\mathbf{k}') a_\pi(\mathbf{k}') \frac{1}{E^+ - H} | \mathbf{k} \mathbf{p}_1 \mathbf{p}_2 \rangle + \dots \\ &= \int d\mathbf{k}' \langle \mathbf{p}'_1 \mathbf{p}'_2 | \frac{1}{E^+ - H_1 - H_2} J_{N_1}^\dagger(\mathbf{k}') \frac{1}{E^+ - \omega_{\mathbf{k}'} - H} a_\pi(\mathbf{k}') a_\pi^\dagger(\mathbf{k}) | \mathbf{p}_1 \mathbf{p}_2 \rangle + \dots \\ &= \langle \mathbf{p}'_1 \mathbf{p}'_2 | \frac{1}{E^+ - H_1 - H_2} J_{N_1}^\dagger(\mathbf{k}) \frac{1}{E^+ - \omega_k - H} | \mathbf{p}_1 \mathbf{p}_2 \rangle + \dots \quad (2.36) \\ &= \langle \mathbf{p}'_1 \mathbf{p}'_2 | \frac{1}{E^+ - H_1 - H_2} J_{N_1}^\dagger(\mathbf{k}) \frac{1}{E^+ - \omega_k - H_1 - H_2 - H_0^\pi} \\ &\quad \times T(E - \omega_k) \frac{1}{E^+ - \omega_k - H_1 - H_2} | \mathbf{p}_1 \mathbf{p}_2 \rangle + \dots \\ &= \int d\mathbf{p}''_1 d\mathbf{p}''_2 \langle \mathbf{p}'_1 \mathbf{p}'_2 | \frac{1}{E^+ - H_1 - H_2} J_{N_1}^\dagger(\mathbf{k}) \frac{1}{E^+ - \omega_k - H_1 - H_2 - H_0^\pi} | \mathbf{p}''_1 \mathbf{p}''_2 \rangle \\ &\quad \times \langle \mathbf{p}''_1 \mathbf{p}''_2 | T(E - \omega_k) | \mathbf{p}_1 \mathbf{p}_2 \rangle D_0(E - \omega_k, \mathbf{p}_1, \mathbf{p}_2) + \dots \end{aligned}$$

where $D_0(E - \omega_k, \mathbf{p}_1, \mathbf{p}_2)$ is the dressed NN propagator and

$$T_{NN}(\mathbf{p}_1''\mathbf{p}_2'', \mathbf{p}_1\mathbf{p}_2; E) = \langle \mathbf{p}_1''\mathbf{p}_2'' | T(E) | \mathbf{p}_1\mathbf{p}_2 \rangle \quad (2.37)$$

is the t -matrix for NN scattering, and as such, has a pole at the deuteron mass, i.e.

$$T_{NN}(\mathbf{p}_1''\mathbf{p}_2'', \mathbf{p}_1\mathbf{p}_2; E) = \delta(\bar{\mathbf{p}}'' - \bar{\mathbf{p}}) \frac{\langle \mathbf{q}'' | \phi_d \rangle \langle \phi_d | \mathbf{q} \rangle}{E^+ - \frac{\bar{p}^2}{2(m_1+m_2)} - m_d} \quad (2.38)$$

where $\bar{\mathbf{p}} = \mathbf{p}_1 + \mathbf{p}_2$ is the total sub-system NN momentum and $\mathbf{q} = (m_1\mathbf{p}_2 - m_2\mathbf{p}_1)/(m_1 + m_2)$ is the NN relative momentum. Note that the on-shell energy expression is

$$E^{\text{on}} = \frac{\bar{p}^2}{2(m_1 + m_2)} + \frac{q^2}{2\mu_{12}} + m_1 + m_2. \quad (2.39)$$

So

$$\begin{aligned} \langle \mathbf{p}_1'\mathbf{p}_2' | \frac{1}{E^+ - H} | \mathbf{k} \mathbf{p}_1\mathbf{p}_2 \rangle = \\ \int d\mathbf{p}_1'' d\mathbf{p}_2'' \langle \mathbf{p}_1'\mathbf{p}_2' | \frac{1}{E^+ - H_1 - H_2} J_{N_1}^\dagger(\mathbf{k}) \frac{1}{E^+ - \omega_k - H_1 - H_2 - H_0^\pi} | \mathbf{p}_1''\mathbf{p}_2'' \rangle \\ \times \delta(\bar{\mathbf{p}}'' - \bar{\mathbf{p}}) \frac{\langle \mathbf{q}'' | \phi_d \rangle \langle \phi_d | \mathbf{q} \rangle}{E^+ - \omega_k - \frac{\bar{p}^2}{2(m_1+m_2)} - m_d} D_0(E - \omega_k, \mathbf{p}_1, \mathbf{p}_2) + \dots \end{aligned} \quad (2.40)$$

Taking the residue at the deuteron pole gives the Green's function for $\pi d \rightarrow NN$

$$\begin{aligned} G^{dN} &= \int d\mathbf{p}_1'' d\mathbf{p}_2'' \langle \mathbf{p}_1'\mathbf{p}_2' | \frac{1}{E^+ - H_1 - H_2} J_{N_1}^\dagger(\mathbf{k}) \frac{1}{E^+ - \omega_k - H_1 - H_2} | \mathbf{p}_1''\mathbf{p}_2'' \rangle \delta(\bar{\mathbf{p}}'' - \bar{\mathbf{p}}) \langle \mathbf{q}'' | \phi_d \rangle \\ &= \left(-\frac{1}{2\pi i} \right) \int_{-\infty}^{\infty} dz d\mathbf{p}_1'' d\mathbf{p}_2'' \langle \mathbf{p}_1' | \frac{1}{z^+ - H_1} J_{N_1}^\dagger(\mathbf{k}) \frac{1}{z^+ - \omega_k - H_1} | \mathbf{p}_1'' \rangle \\ &\quad \times \langle \mathbf{p}_2' | \frac{1}{E^+ - z - H_2} | \mathbf{p}_2'' \rangle \delta(\bar{\mathbf{p}}'' - \bar{\mathbf{p}}) \langle \mathbf{q}'' | \phi_d \rangle. \end{aligned} \quad (2.41)$$

Now, we again represent the two-energy vertices by usual one-energy vertices. So, we have

$$\begin{aligned} \langle \mathbf{p}_1' | \frac{1}{z^+ - H_1} J_{N_1}^\dagger(\mathbf{k}) \frac{1}{z^+ - \omega_k - H_1} | \mathbf{p}_1'' \rangle \\ = \delta(\mathbf{p}_1' - \mathbf{p}_1'' - \mathbf{k}) g(z, \mathbf{p}_1') \bar{f}(\mathbf{p}_1', \mathbf{p}_1'', z, z - \omega_k) g(z - \omega_k, \mathbf{p}_1'') \\ \approx \delta(\mathbf{p}_1' - \mathbf{p}_1'' - \mathbf{k}) g(z, \mathbf{p}_1') \bar{f}(\mathbf{k}, \mathbf{p}_1'', z) g(z - \omega_k, \mathbf{p}_1''). \end{aligned} \quad (2.42)$$

Therefore

$$\begin{aligned} G^{dN} &= \left(-\frac{1}{2\pi i} \right) \int_{-\infty}^{\infty} dz d\mathbf{p}_1'' d\mathbf{p}_2'' \delta(\mathbf{p}_1' - \mathbf{p}_1'' - \mathbf{k}) g(z, \mathbf{p}_1') \bar{f}(\mathbf{k}, \mathbf{p}_1'', z) g(z - \omega_k, \mathbf{p}_1'') \\ &\quad \times \delta(\mathbf{p}_2' - \mathbf{p}_2'') g(E - z, \mathbf{p}_2'') \delta(\bar{\mathbf{p}}'' - \bar{\mathbf{p}}) \langle \mathbf{q}'' | \phi_d \rangle \\ &= \left(-\frac{1}{2\pi i} \right) \delta(\bar{\mathbf{p}}' - \mathbf{k} - \bar{\mathbf{p}}) \int_{-\infty}^{\infty} dz g(z, \mathbf{p}_1') \bar{f}(\mathbf{k}, \mathbf{p}_1' - \mathbf{k}, z) g(z - \omega_k, \mathbf{p}_1' - \mathbf{k}) \\ &\quad \times g(E - z, \mathbf{p}_2') \langle \mathbf{q} | \phi_d \rangle \end{aligned} \quad (2.43)$$

where the Z -diagram would correspond to the Green's function with "chopped" nucleon legs. This Z -diagram is represented by the diagram shown in Figure 2.2.

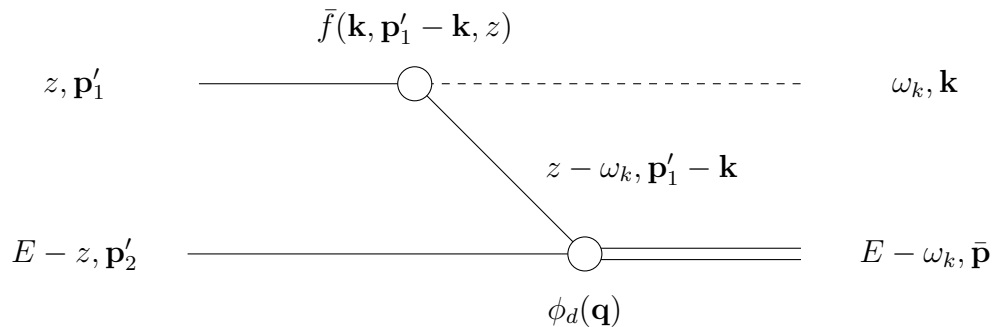


Figure 2.2: Diagrammatic representation of the integrand in Equation 2.43 for the fully dressed $\pi d \rightarrow NN$ Z -diagram.

2.4.4 Rules for constructing fully dressed Z -diagrams

From the derivation of the NN OPE and $\pi d \rightarrow NN$ fully dressed Z -diagrams, we suggest there are "Feynman rules" for constructing fully dressed 4-dimensional (4D) Z -diagrams that are analogous to the well-known covariant rules. Our rules for constructing fully dressed Z -diagrams are as follows:

1. Assign each external leg a 4-momentum. When we have a final or initial NN state, we assign nucleon 1 with the 4-momentum (z, \mathbf{p}_1) and nucleon 2 with 4-momentum $(E - z, \mathbf{p}_2)$. For πd final or initial states, we assign the pion with 4-momentum (ω_k, \mathbf{k}) and the deuteron with 4-momentum $(E - \omega_k, \bar{\mathbf{p}})$. For initial $N\Delta$ states, nucleon 1 is the spectator and we assign it the 4-momentum (z, \mathbf{p}_1) and the Δ particle we assign the 4-momentum $(E - z, \bar{\mathbf{p}})$. For final $N\Delta$ states, nucleon 2 is the spectator and we assign it the 4-momentum $(E - z, \mathbf{p}_2)$ and the Δ particle we assign the 4-momentum $(z, \bar{\mathbf{p}})$.
2. Assign a 4-momentum to the exchange particle using the conservation of momentum at the vertices
3. Allocate a dressed one-nucleon propagator for each nucleon and an undressed propagator for each pion. This includes the legs and the exchange particle
4. Allocate a function for each vertex. For a vertex involving a deuteron or Δ particle, assign $\langle \mathbf{q} | \phi_d \rangle$ or $\langle \mathbf{q} | \phi_\Delta \rangle$ respectively. For a $N \rightarrow \pi N$ ($\pi N \rightarrow N$) vertex, allocate the

dressed vertex function $f(\bar{f})$. The energy of this dressed vertex function is equal to the nucleon in the one particle state

5. Integrate over z and z' , remembering to include the factor $(-1/2\pi i)$ for each z variable

2.4.5 Dressed two-pion exchange with full dressing

We know that our rules for constructing fully dressed diagrams are correct for one particle exchange diagrams and now what we would like to investigate is if these rules can also be used for higher order diagrams. For now, we will only investigate a two-particle exchange diagram and determine the connection between our rules and time-ordered perturbation diagrams.

Let us now consider a second order NN diagram, corresponding to two-pion exchange (TPE) between two nucleons. In our perturbation expansion given in Equation 2.25, two-pion exchange corresponds to perturbation terms that contain four interaction Hamiltonians H_I^π . Again, to save on notation, we do not write the free Green's functions $1/(E^+ - H_1 - H_2 - H_0^\pi)$ and only consider the interaction Hamiltonians. The matrix elements of these terms are given by

$$\begin{aligned} & \langle \mathbf{p}'_1 \mathbf{p}'_2 | H_I^\pi(1) H_I^\pi(1) H_I^\pi(2) H_I^\pi(2) | \mathbf{p}_1 \mathbf{p}_2 \rangle + \langle \mathbf{p}'_1 \mathbf{p}'_2 | H_I^\pi(1) H_I^\pi(2) H_I^\pi(1) H_I^\pi(2) | \mathbf{p}_1 \mathbf{p}_2 \rangle \\ & + \langle \mathbf{p}'_1 \mathbf{p}'_2 | H_I^\pi(1) H_I^\pi(2) H_I^\pi(2) H_I^\pi(1) | \mathbf{p}_1 \mathbf{p}_2 \rangle + \langle \mathbf{p}'_1 \mathbf{p}'_2 | H_I^\pi(2) H_I^\pi(2) H_I^\pi(1) H_I^\pi(1) | \mathbf{p}_1 \mathbf{p}_2 \rangle \quad (2.44) \\ & + \langle \mathbf{p}'_1 \mathbf{p}'_2 | H_I^\pi(2) H_I^\pi(1) H_I^\pi(2) H_I^\pi(1) | \mathbf{p}_1 \mathbf{p}_2 \rangle + \langle \mathbf{p}'_1 \mathbf{p}'_2 | H_I^\pi(2) H_I^\pi(1) H_I^\pi(1) H_I^\pi(2) | \mathbf{p}_1 \mathbf{p}_2 \rangle. \end{aligned}$$

Each term corresponds to a variety of different time-ordered diagrams, similar to the term for one-pion exchange $\langle \mathbf{p}'_1 \mathbf{p}'_2 | H_I^\pi(1) H_I^\pi(2) | \mathbf{p}_1 \mathbf{p}_2 \rangle$. However, we are only interested in the diagrams that correspond to pion exchange between the two nucleons. Consider the first two terms of the above perturbation expansion, we can show that the first term will give us the two time-ordered diagrams in Figure 2.3 (a) and the second term will give us the two time-ordered diagrams in Figure 2.3 (b).

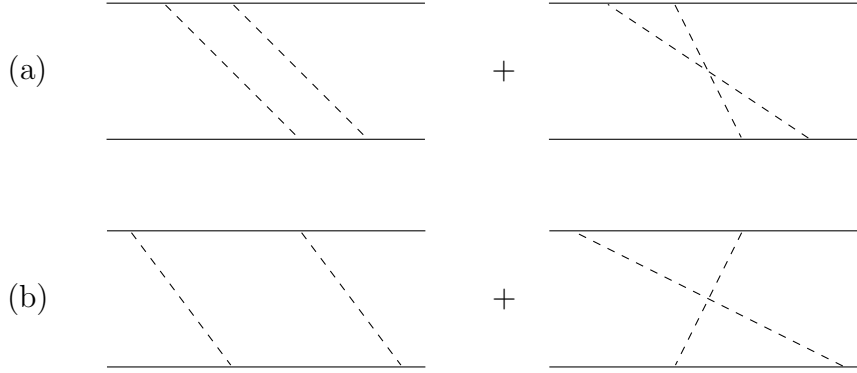


Figure 2.3: The time-ordered diagrams corresponding to two-pion exchange, where (a) is obtained from the first term in the sum of matrix elements in Equation 2.44 and (b) is obtained from the second term in Equation 2.44.

However, the connection of these diagrams with convolutions is not clear. So, let us construct a two-pion exchange diagram and use our rules of constructing fully dressed Z -diagrams to determine its mathematical expression. This will also help us determine the validity of our rules. The convolution diagram corresponding to two-pion exchange is drawn in Figure 2.4.

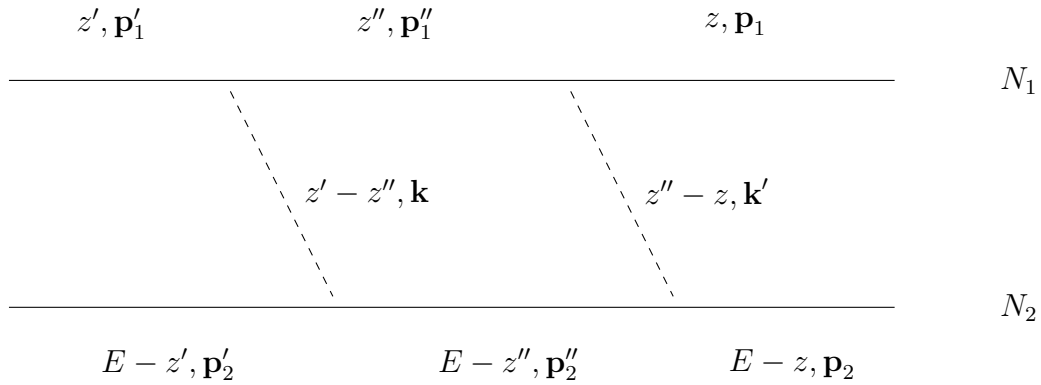


Figure 2.4: A convolution diagram representing two-pion exchange between two nucleons.

We can consider this diagram to be same slope or parallel two-pion exchange. We will need to extend our rules to include the intermediate state of two-pion exchange, which also applies to higher order diagrams:

6. Assign each intermediate particle with a 4-momenta, following the same convention as rule 1. Repeat all steps for the additional particles, integrating over each energy-like variable z, z', z'', \dots and intermediate momenta $\mathbf{p}'', \mathbf{p}''', \dots$

We can now consider our rules as rules for constructing fully dressed diagrams, not just for one-particle exchange Z -diagrams. From these rules, we can obtain an expression for the Green's function with one-energy vertices and without the momentum-conserving function δ

$$\begin{aligned}
 G_{12}^{TPE} &= \left(-\frac{1}{2\pi i}\right)^3 \int g(z', \mathbf{p}'_1) \bar{f}(\mathbf{p}'_1, \mathbf{p}''_1, z') \frac{1}{z'^+ - z'' - \omega_k} g(E - z', \mathbf{p}'_2) f(\mathbf{p}'_2, \mathbf{p}''_2, E - z'') \\
 &\quad g(z'', \mathbf{p}''_1) g(E - z'', \mathbf{p}''_2) \bar{f}(\mathbf{p}''_1, \mathbf{p}_1, z'') \frac{1}{z''^+ - z - \omega_{k'}} g(z, \mathbf{p}_1) f(\mathbf{p}_2, \mathbf{p}_2, E - z) \\
 &\quad g(E - z, \mathbf{p}_2) d\mathbf{p}''_1 d\mathbf{p}''_2 dz dz' dz''.
 \end{aligned} \tag{2.45}$$

If we use our definitions of our vertex and the dressed one-nucleon propagator, we can reduce this Green's function into an expression with the J_N and J_N^\dagger operators,

$$\begin{aligned}
 G_{12}^{TPE} &= \left(-\frac{1}{2\pi i}\right)^3 \int \langle \mathbf{p}'_1 \mathbf{p}'_2 | \frac{1}{z'^+ - H_1} J_{N_1}^\dagger(\mathbf{k}) \frac{1}{z''^+ - H_1} \frac{1}{z'^+ - z'' - \omega_k} \frac{1}{E^+ - z' - H_2} \\
 &\quad J_{N_2}(\mathbf{k}) \frac{1}{E^+ - z'' - H_2} J_{N_1}^\dagger(\mathbf{k}') \frac{1}{z''^+ - z - \omega_{k'}} J_{N_2}(\mathbf{k}') \frac{1}{z^+ - H_1} \\
 &\quad \frac{1}{E^+ - z - H_2} | \mathbf{p}_1 \mathbf{p}_2 \rangle d\mathbf{k} d\mathbf{k}' dz dz' dz''.
 \end{aligned} \tag{2.46}$$

Now, by using Cauchy's Residue Theorem to evaluate the z integrals, we obtain

$$\begin{aligned}
 G_{12}^{TPE} &= \int \langle \mathbf{p}'_1 \mathbf{p}'_2 | \frac{1}{E^+ - H_1 - H_2} J_{N_1}^\dagger(\mathbf{k}) \frac{1}{E^+ - H_1 - H_2 - \omega_k} J_{N_2}(\mathbf{k}) \frac{1}{E^+ - H_1 - H_2} \\
 &\quad J_{N_1}^\dagger(\mathbf{k}') \frac{1}{E^+ - H_1 - H_2 - \omega_{k'}} J_{N_2}(\mathbf{k}') \frac{1}{E^+ - H_1 - H_2} | \mathbf{p}_1 \mathbf{p}_2 \rangle d\mathbf{k} d\mathbf{k}' \\
 &\quad + \int \langle \mathbf{p}'_1 \mathbf{p}'_2 | \frac{1}{E^+ - H_1 - H_2} J_{N_1}^\dagger(\mathbf{k}) \frac{1}{E^+ - H_1 - H_2 - \omega_k} J_{N_2}(\mathbf{k}) \\
 &\quad \frac{1}{E^+ - H_1 - H_2 - \omega_k - \omega_{k'}} J_{N_1}^\dagger(\mathbf{k}') \frac{1}{E^+ - H_1 - H_2 - \omega_{k'}} J_{N_2}(\mathbf{k}') \frac{1}{E^+ - H_1 - H_2} | \mathbf{p}_1 \mathbf{p}_2 \rangle d\mathbf{k} d\mathbf{k}'.
 \end{aligned} \tag{2.47}$$

The first term corresponds to the first time-ordered diagram in Figure 2.3 (b), while the second term corresponds to the first time-ordered diagram in Figure 2.3 (a). What we have shown is that our rules for constructing fully dressed diagrams give us both time orderings of the diagram in Figure 2.4. We can similarly construct other convolution diagrams that will give us the remaining time-ordered diagrams that are obtained from the sum of matrix elements in Equation 2.44.

Chapter 3

The πNN convolution equations

3.1 Co-authorship statement

This chapter is adapted from a manuscript, soon to be submitted to a peer-reviewed journal. The reference for the manuscript is:

Blankleider, B., Khvinikidze, A. N., & Wray, J. L, (2021). Convolution approach to πNN . I. Theory. (to be submitted to *Physical Review C* upon completion)

The thesis author is listed as the third author in this manuscript. The relevant sections of this chapter that this manuscript is referred to is: Section 3.3 to the end of the chapter.

This publication constitutes the full development of a theory that was first introduced by B. Blankleider and A. N. Kvinikhidze in a conference proceeding published in: *Few-Body Syst. Suppl 7 (1994) 294*. The thesis author participated equally with B. Blankleider and A. N. Kvinikhidze in the development of this theory and the writing of the manuscript, and the alphabetical order of the authors reflects this. It is important that this publication is included in the body of the thesis (as Chapter 3), rather than in an Appendix, because the theory and its numerical implementation constitutes an inseparable one body of research work.

3.2 Introduction

Our goal in this chapter is to extend the work of Kvinikhidze and Blankleider [49] by presenting a derivation of fully coupled $NN - \pi NN$ equations for the processes $NN \rightarrow NN$, $NN \rightarrow \pi d$, $\pi d \rightarrow NN$ and $\pi d \rightarrow \pi d$ using the convolution approach.

The derivation starts with a three-body Lippmann-Schwinger equation for the process $\pi NN \rightarrow \pi NN$ where all connected three-body forces are neglected, and then through the use of a Faddeev-like rearrangement, we reformulate the disconnected πNN potentials in terms of disconnected t -matrices, which can then be determined through the use of convolution integrals. The resulting equations can then be represented in terms of Alt-Grassberger-Sandhas (AGS)-like amplitudes, which lead to coupled scattering equations for the processes $NN \rightarrow NN$, $NN \rightarrow N\Delta$, $N\Delta \rightarrow N\Delta$, $NN \rightarrow \pi d$, $\pi d \rightarrow NN$, $\pi d \rightarrow N\Delta$ and $\pi d \rightarrow \pi d$. We will refer to these newly derived equations as the πNN convolution equations. These convolution equations have the same form as the unitary $NN - \pi NN$ equations of Afnan

and Blankleider [33], however, unlike the equations of Afnan and Blankleider, all nucleons are fully dressed.

With all nucleons fully dressed, the πNN convolution equations solve the long-standing renormalisation problem inherent in the ‘‘Unitary $NN - \pi NN$ ’’ model. However, these convolution equations involve non-pair-like interactions and therefore may be difficult to solve numerically. For this reason, an alternative formulation is also presented. Splitting the πN t -matrix into its pole and non-pole part, then convoluting each part individually leads to a 4-dimensional (4D) version of the πNN convolution equations, which only involve pair-like interactions. Finally, we introduce a separable potential approximation to the two-body input potentials to obtain more easily calculable 4D equations.

3.3 Formalism for the πNN convolution equations

We consider a time-ordered perturbation theory (TOPT) described by a Hamiltonian H acting in the Fock space of two nucleons and any number of pions. The exact model for H need not be specified at this stage. Here we shall be concerned with the πNN system where coupling to NN states is taken into account, and for this purpose consider the Green’s function operator G describing the process $\pi NN \rightarrow \pi NN$, and acting in the space of two nucleons and one pion such that

$$\langle \mathbf{p}'_1 \mathbf{p}'_2 \mathbf{p}'_3 | G(E) | \mathbf{p}_1 \mathbf{p}_2 \mathbf{p}_3 \rangle = \langle \mathbf{p}'_1 \mathbf{p}'_2 \mathbf{p}'_3 | \frac{1}{E^+ - H} | \mathbf{p}_1 \mathbf{p}_2 \mathbf{p}_3 \rangle, \quad (3.1)$$

where \mathbf{p}_a (\mathbf{p}'_a) denote initial (final) momenta with $a = 1, 2$ labelling the two nucleons while $a = 3$ labels the pion. Similarly, we consider the Green’s function operator D describing the process $NN \rightarrow NN$, and acting in the space of two nucleons and zero pions such that

$$\langle \mathbf{p}'_1 \mathbf{p}'_2 | D(E) | \mathbf{p}_1 \mathbf{p}_2 \rangle = \langle \mathbf{p}'_1 \mathbf{p}'_2 | \frac{1}{E^+ - H} | \mathbf{p}_1 \mathbf{p}_2 \rangle. \quad (3.2)$$

In Equation 3.1 and 3.2, E is the total energy of the coupled $NN - \pi NN$ system. Note that we suppress spin-isospin labels in order to save on notation, and it is assumed that the nucleons are distinguishable since antisymmetrisation can be carried out at the end.

To label the particles of the πNN system in a general but systematic way, we shall use the alphabetically ordered set of labels $\{a, b, c\}$ to denote any cyclic permutation of $\{1, 2, 3\}$. Additionally, we shall use letters i and j to specifically label the nucleons, thus $i, j = 1$ or 2 . To label a pair of particles within a given three-body system it is common

to use the “spectator” notation whereby particle pairs $\{(23), (31), (12)\}$ are labelled by the numbers $\{1, 2, 3\}$, respectively. For the πNN system, however, it is also convenient to use a “nucleon participation” notation whereby the pairs $\{(23), (31), (12)\}$ are labelled by the numbers $\{2, 1, 3\}$, respectively. To distinguish these two ways of labelling particle pairs when the pairs are denoted by $\{(bc), (ca), (ab)\}$, we shall use $\{a, b, c\}$ (using Roman letters) for the “spectator” notation, and $\{\alpha, \beta, \gamma\}$ (using Greek letters) for “nucleon participation” notation. These labelling schemes are summarised in Table 3.1. In the case of the πNN system, the nucleon participation notation is convenient as it labels two-body operators that act in the space of a pion and nucleon i with subscript i .

Pair	(bc)	(ca)	(ab)	(23)	(31)	(12)
Spectator label	a	b	c	1	2	3
Participation label	α	β	γ	2	1	3

Table 3.1: Labelling schemes for denoting particle pairs.

Using the nucleon participation notation, the two-body Green’s function operator that acts in the (bc) sub-space of the πNN system is written as D_α and defined by

$$\langle \mathbf{p}'_b \mathbf{p}'_c | D_\alpha(e) | \mathbf{p}_b \mathbf{p}_c \rangle = \langle \mathbf{p}'_b \mathbf{p}'_c | \frac{1}{e^+ - H} | \mathbf{p}_b \mathbf{p}_c \rangle, \quad (3.3)$$

where e is the energy available to the (bc) system (i.e. the total energy E minus the energy of the spectator particle a). Similarly, the one-particle (π or N) Green’s function operator g_a acting in the space of particle a is defined by

$$\langle \mathbf{p}'_a | g_a(e) | \mathbf{p}_a \rangle = \langle \mathbf{p}'_a | \frac{1}{e^+ - H} | \mathbf{p}_a \rangle. \quad (3.4)$$

where e is the energy available to particle a .

Each of the above Green’s function operators corresponds to the sum of all possible time-ordered perturbation diagrams generated by the particular model under consideration. In reference to these diagrams, it is clear that one can write the $\pi NN \rightarrow \pi NN$ Green’s function operator as

$$G(E) = G_0(E) + G_0(E)T(E)G_0(E), \quad (3.5)$$

where $G_0(E)$ is the fully disconnected part of $G(E)$, and $T(E)$ is the $\pi NN \rightarrow \pi NN$ t -matrix operator defined by this equation. Furthermore, one can write

$$T(E) = V(E) + V(E)G_0(E)T(E), \quad (3.6)$$

where $V(E)$ corresponds to the sum of all possible πNN -irreducible graphs excluding those consisting of fully disconnected πNN states. It follows that

$$G(E) = G_0(E) + G_0(E)V(E)G(E). \quad (3.7)$$

The key feature of this work is that all possible particle dressings, consistent with the neglect of connected three-body forces, are retained. This means that the three particles making up the propagator G_0 are fully dressed. As was shown in [48], the way to achieve such full dressing in TOPT is through convolution integrals; and in particular, for the fully dressed πNN propagator $G_0(E)$, the convolution expression is

$$G_0(E) = \left(-\frac{1}{2\pi i}\right)^2 \int_{-\infty}^{\infty} dz_1 dz_2 g_1(E - z_1)g_2(z_1 - z_2)g_3(z_2). \quad (3.8)$$

Similarly expressions hold for the NN sector that is coupled to πNN space via pion absorption on a nucleon. Thus, one can express the $NN \rightarrow NN$ Green's function operator $D(E)$ in terms of the $NN \rightarrow NN$ t -matrix operator $T_{NN}(E)$ as

$$D(E) = D_0(E) + D_0(E)T_{NN}(E)D_0(E) \quad (3.9)$$

where $D_0(E)$ is the fully disconnected part of $D(E)$. One then has the Lippmann-Schwinger equation for NN scattering,

$$T_{NN}(E) = V_{NN}(E) + V_{NN}(E)D_0(E)T_{NN}(E) \quad (3.10)$$

where $V_{NN}(E)$ corresponds to the sum of all possible connected NN -irreducible graphs. Thus

$$D(E) = D_0(E) + D_0(E)V_{NN}(E)D(E). \quad (3.11)$$

The convolution expression for the fully dressed NN propagator $D_0(E)$ is [48]

$$D_0(E) = \left(-\frac{1}{2\pi i}\right) \int_{-\infty}^{\infty} dz g_1(E - z)g_2(z). \quad (3.12)$$

One similarly has for sub-system $\pi N \rightarrow \pi N$ and $NN \rightarrow NN$ scattering

$$D_\alpha(e) = D_{0\alpha}(e) + D_{0\alpha}(e)t_\alpha(e)D_{0\alpha}(e), \quad (3.13)$$

where $D_{0\alpha}(e)$ is the fully disconnected part of D_α and $t_\alpha(e)$ is the corresponding two-body t -matrix operator. One can further write

$$t_\alpha(e) = v_\alpha(e) + v_\alpha(e)D_{0\alpha}(e)t_\alpha(e) \quad (3.14)$$

where $v_\alpha(e)$ corresponds to the sum of all possible NN or πN - irreducible graphs excluding those consisting of fully disconnected states. It follows that

$$D_\alpha(e) = D_{0\alpha}(e) + D_{0\alpha}(e)v_\alpha(e)D_\alpha(e). \quad (3.15)$$

3.3.1 Green's functions

The formalism, so far, has been expressed in terms of operators in momentum space. To obtain numerical results we need to take matrix elements of these operators, and for this purpose it will be useful to define a number of different momentum variables. With free particle momenta denoted by \mathbf{p}'_a and \mathbf{p}_a as previously discussed, we define the total final and initial momenta of the πNN system as

$$\mathbf{P}' = \mathbf{p}'_1 + \mathbf{p}'_2 + \mathbf{p}'_3, \quad \mathbf{P} = \mathbf{p}_1 + \mathbf{p}_2 + \mathbf{p}_3, \quad (3.16)$$

and the total momenta of the two-body (bc) sub-systems as

$$\bar{\mathbf{p}}'_\alpha = \mathbf{p}'_b + \mathbf{p}'_c, \quad \bar{\mathbf{p}}_\alpha = \mathbf{p}_b + \mathbf{p}_c. \quad (3.17)$$

Similarly, the relative momenta of particles b and c are defined by

$$\mathbf{q}'_\alpha = \frac{m_b \mathbf{p}'_c - m_c \mathbf{p}'_b}{m_b + m_c}, \quad \mathbf{q}_\alpha = \frac{m_b \mathbf{p}_c - m_c \mathbf{p}_b}{m_b + m_c}, \quad (3.18)$$

so that \mathbf{q}_α corresponds to the momentum of particle c in the (bc) centre of mass (c.m.) system. Note the use of label α (rather than a) in Equation 3.17 and 3.18; that is, we are using the nucleon participation notation to label total and relative momenta of sub-system pairs. Thus, the state of two free sub-system particles b and c can be written in two equivalent ways:

$$|\mathbf{p}_b \mathbf{p}_c\rangle = |\mathbf{q}_\alpha \bar{\mathbf{p}}_\alpha\rangle. \quad (3.19)$$

Similarly, the state of three free particles can be written equivalently as

$$|\mathbf{p}_a \mathbf{p}_b \mathbf{p}_c\rangle = |\mathbf{p}_a \mathbf{q}_\alpha \bar{\mathbf{p}}_\alpha\rangle = |\mathbf{q}_\alpha \bar{\mathbf{p}}_\alpha \mathbf{P}\rangle. \quad (3.20)$$

If all particles are treated non-relativistically, then the on-shell energy of the three free particles can be expressed in terms of the above momentum variables (in units where $c = \hbar = 1$) as

$$E = \frac{p_a^2}{2m_a} + \frac{p_b^2}{2m_b} + \frac{p_c^2}{2m_c} + M, \quad (3.21a)$$

$$= \frac{p_a^2}{2m_a} + \frac{\bar{p}_\alpha^2}{2(m_b + m_c)} + \frac{q_\alpha^2}{2\mu_{bc}} + M, \quad (3.21b)$$

where $\mu_{bc} = m_b m_c / (m_b + m_c)$ and $M = m_a + m_b + m_c$.

With these definitions, the $3 \rightarrow 3$ Green's function G , the $2 \rightarrow 2$ Green's functions D_α and $D_{0\alpha}$, and the dressed pion or dressed nucleon propagator g_α are defined as follows:

$$\begin{aligned} \langle \mathbf{p}'_a \mathbf{p}'_b \mathbf{p}'_c | G(E) | \mathbf{p}_a \mathbf{p}_b \mathbf{p}_c \rangle &= \langle \mathbf{q}'_\alpha \bar{\mathbf{p}}'_\alpha \mathbf{P}' | G(E) | \mathbf{q}_\alpha \bar{\mathbf{p}}_\alpha \mathbf{P} \rangle \\ &= \delta(\mathbf{P}' - \mathbf{P}) G(E, \mathbf{q}'_\alpha \bar{\mathbf{p}}'_\alpha, \mathbf{q}_\alpha \bar{\mathbf{p}}_\alpha, \mathbf{P}), \end{aligned} \quad (3.22a)$$

$$\langle \mathbf{p}'_b \mathbf{p}'_c | D_\alpha(e) | \mathbf{p}_b \mathbf{p}_c \rangle = \delta(\bar{\mathbf{p}}'_\alpha - \bar{\mathbf{p}}_\alpha) D_\alpha(e, \mathbf{q}'_\alpha, \mathbf{q}_\alpha, \bar{\mathbf{p}}_\alpha), \quad (3.22b)$$

$$\langle \mathbf{p}'_b \mathbf{p}'_c | D_{0\alpha} | \mathbf{p}_b \mathbf{p}_c \rangle = \delta(\bar{\mathbf{p}}'_\alpha - \bar{\mathbf{p}}_\alpha) \delta(\mathbf{q}'_\alpha - \mathbf{q}_\alpha) D_{0\alpha}(e, \mathbf{q}_\alpha, \bar{\mathbf{p}}_\alpha), \quad (3.22c)$$

$$\langle \mathbf{p}'_a | g_\alpha(e) | \mathbf{p}_a \rangle = \delta(\mathbf{p}'_a - \mathbf{p}_a) g_\alpha(e, \mathbf{p}_a). \quad (3.22d)$$

In the above equations, we have used the same symbols for Green's function operators and corresponding Green's functions; this is not likely to cause confusion as the meaning of a symbol should be clear from the context and has the great advantage of keeping cumbersome notation to a minimum. In the same way, we save on notation by exploiting Galilean invariance to write

$$D_\alpha(e, \mathbf{q}'_\alpha, \mathbf{q}_\alpha, \bar{\mathbf{p}}_\alpha) = D_\alpha(e - \bar{E}_\alpha, \mathbf{q}'_\alpha, \mathbf{q}_\alpha, \mathbf{0}) \equiv D_\alpha(e - \bar{E}_\alpha, \mathbf{q}'_\alpha, \mathbf{q}_\alpha), \quad (3.23a)$$

$$D_{0\alpha}(e, \mathbf{q}_\alpha, \bar{\mathbf{p}}_\alpha) = D_{0\alpha}\left(e - \bar{E}_\alpha - \frac{q_\alpha^2}{2\mu_{bc}}, \mathbf{0}, \mathbf{0}\right) \equiv D_{0\alpha}\left(e - \bar{E}_\alpha - \frac{q_\alpha^2}{2\mu_{bc}}\right), \quad (3.23b)$$

$$g_\alpha(e, \mathbf{p}_a) = g_\alpha(e - E_a, \mathbf{0}) \equiv g_\alpha(e - E_a), \quad (3.23c)$$

where, assuming non-relativistic kinematics,

$$\bar{E}_\alpha = \frac{\bar{p}_\alpha^2}{2(m_b + m_c)}, \quad E_a = \frac{p_a^2}{2m_a}. \quad (3.24a)$$

Here we use non-relativistic kinematics for simplicity of presentation; however, in our calculations, presented in later chapters, we use relativistic kinematics for the pion, where $E_3 = (p_3^2 + m_3^2)^{1/2}$.

3.3.2 Sub-system NN and πN scattering

Special attention needs to be given to the description of the sub-system NN and πN scattering t -matrices, as these provide the input to the convolution $NN - \pi NN$ equations being derived in this work. This we do in the following subsection.

Sub-system NN scattering

In the πNN system, the interaction of the two nucleons while the pion is in flight, is described by Equation 3.14 with $\alpha = 3$:

$$t_3(e) = v_3(e) + v_3(e)D_{03}(e)t_3(e) \quad (3.25)$$

where $v_3(e)$ is an NN potential. It is to be understood that all quantities like $v_3(e)$, $t_3(e)$, etc., are operators in momentum space. As one of the main goals of the current work is to formulate a consistent description of nucleon dressing in the πNN system, it is essential that the two-nucleon propagator $D_{03}(e)$ also consist of two fully dressed nucleons. This is in contrast to previous works on the πNN system [33, 36, 80–83] where no explicit dressing was included in $D_{03}(e)$. Thus, in the current work $D_{03}(e)$ is expressed by the convolution integral

$$D_{03}(e) = \left(-\frac{1}{2\pi i} \right) \int_{-\infty}^{\infty} dz g_1(e-z) g_2(z) \quad (3.26)$$

where $g_1(e)$ and $g_2(e)$ are the dressed propagators of nucleons 1 and 2 respectively.

Because the NN system has a bound state, namely the deuteron (d), the sub-system NN t -matrix $\langle \mathbf{q}'_3 \bar{\mathbf{p}}'_3 | t_3(e) | \mathbf{q}_3 \bar{\mathbf{p}}_3 \rangle = \delta(\bar{\mathbf{p}}'_3 - \bar{\mathbf{p}}_3) t_3(e, \mathbf{q}'_3, \mathbf{q}_3, \bar{\mathbf{p}}_3)$ has a pole at energy $e = \bar{E}_3 + m_d$ corresponding to the formation a deuteron of mass m_d and kinetic energy $\bar{E}_3 = \bar{p}_3^2/2(m_1 + m_2)$. To preserve exact unitarity, we ignore the small difference between \bar{E}_3 and the precise expression $\bar{p}_3^2/2m_d$ for the deuteron's (non-relativistic) kinetic energy. Using Galilean invariance, we may write

$$t_3(e, \mathbf{q}'_3, \mathbf{q}_3, \bar{\mathbf{p}}_3) = t_3(e - \bar{E}_3, \mathbf{q}'_3, \mathbf{q}_3, \mathbf{0}) \equiv t_3(e - \bar{E}_3, \mathbf{q}'_3, \mathbf{q}_3). \quad (3.27)$$

Then, defining the NN “centre of mass” t -matrix operator $t_3^{\text{cm}}(e)$, which acts in the space of relative momenta, by

$$\langle \mathbf{q}'_3 | t_3^{\text{cm}}(e) | \mathbf{q}_3 \rangle \equiv t_3(e, \mathbf{q}'_3, \mathbf{q}_3), \quad (3.28)$$

one can expose the deuteron pole in the NN t -matrix by writing

$$t_3^{\text{cm}}(e) = \frac{|\phi_3\rangle\langle\phi_3|}{e^+ - \bar{m}_3} + t_3^b(e) \quad (3.29)$$

where $t_3^b(e)$ is a “background” term defined by this equation, $\bar{m}_3 \equiv m_d$ is the deuteron mass, and $|\phi_3\rangle$ is the deuteron bound state form factor which is related to the deuteron bound state wave-function $|\psi_3\rangle$ through

$$|\psi_3\rangle = D_{03}^{\text{cm}}(\bar{m}_3)|\phi_3\rangle. \quad (3.30)$$

In Equation 3.30, $D_{03}^{\text{cm}}(e)$ is the NN “centre of mass” free propagator which acts in the space of relative momenta such that

$$\begin{aligned} \langle \mathbf{q}'_3 \bar{\mathbf{p}}'_3 | D_{03}(e) | \mathbf{q}_3 \bar{\mathbf{p}}_3 \rangle &= \delta(\bar{\mathbf{p}}'_3 - \bar{\mathbf{p}}_3) D_{03}(e - \bar{E}_3, \mathbf{q}'_3, \mathbf{q}_3) \\ &\equiv \delta(\bar{\mathbf{p}}'_3 - \bar{\mathbf{p}}_3) \langle \mathbf{q}'_3 | D_{03}^{\text{cm}}(e - \bar{E}_3) | \mathbf{q}_3 \rangle. \end{aligned} \quad (3.31)$$

Sub-system πN scattering

The t -matrix $t_i(e)$ describing pion scattering off nucleon i can be expressed in terms of coupled equations as illustrated in Figure 3.1. First derived by Mizutani and Koltun using Feshbach projection operators [80], these equations have also been derived in the context of TOPT [33]. Here we give a brief derivation following the arguments used in [33]. Setting $\alpha = i$ in Equation 3.13, it is evident that the term $D_{0i}(e)t_i(e)D_{0i}(e)$ consists of all possible *connected* $\pi N \rightarrow \pi N$ diagrams with $t_i(e)$ being given by the same diagrams but with “chopped legs.” Then, defining the “background” πN t -matrix $t_i^b(e)$ as the sum of all diagrams of $t_i(e)$ that have one or more pions in every intermediate state, one can write

$$t_i(e) = f_i(e)g_i(e)\bar{f}_i(e) + t_i^b(e) \quad (3.32)$$

where $f_i(e)$ ($\bar{f}_i(e)$) is the “dressed vertex” consisting of all possible $N \rightarrow \pi N$ ($\pi N \rightarrow N$) chopped-leg diagrams with at least one pion in every intermediate state. Similarly, one can define $v_i(e)$ as the sum of all diagrams of $t_i(e)$ that have two or more pions in every intermediate state, in which case we can write Lippmann-Schwinger-like equations

$$t_i^b(e) = v_i(e) + v_i(e)D_{0i}(e)t_i^b(e), \quad (3.33a)$$

$$= v_i(E) + t_i^b D_{0i}(e)v_i(e) \quad (3.33b)$$

so that $v_i(E)$ plays the role of a $\pi N \rightarrow \pi N$ potential. Using a similar argument, one can obtain the equations

$$f_i(e) = f_{0i}(e) + t_i^b(e)D_{0i}(e)f_{0i}(e), \quad (3.34a)$$

$$\bar{f}_i(e) = \bar{f}_{0i}(e) + \bar{f}_{0i}(e)D_{0i}(e)t_i^b(e), \quad (3.34b)$$

where $f_{0i}(e)$ ($\bar{f}_{0i}(e)$) is the “bare vertex” consisting of all possible $N \rightarrow \pi N$ ($\pi N \rightarrow N$) chopped-leg diagrams with at least two pions in every intermediate state. Finally, one can similarly write

$$g_i(e) = g_{0i}(e) + g_{0i}(e)\Sigma_i(e)g_i(e) \quad (3.35)$$

where

$$\Sigma_i(e) = \bar{f}_{0i}(e)D_{0i}(e)f_i(e), \quad (3.36a)$$

$$= \bar{f}_i(e)D_{0i}(e)f_{0i}(e), \quad (3.36b)$$

is the nucleon “self-energy” or “dressing” term consisting of all diagrams of $g_i(e)$ with at least one pion in every intermediate state, but with chopped legs. The set of equations consisting of Equations 3.32-3.36 are illustrated in Figure 3.1, and provide an exact and useful way of expressing the πN t -matrix $t_i(e)$. Viewed as coupled equations for the dressed propagator $g_i(e)$, the equations corresponding to the diagrams of Figure 3.1(b), (c), and (d), are often referred to as the Dyson-Schwinger equations.

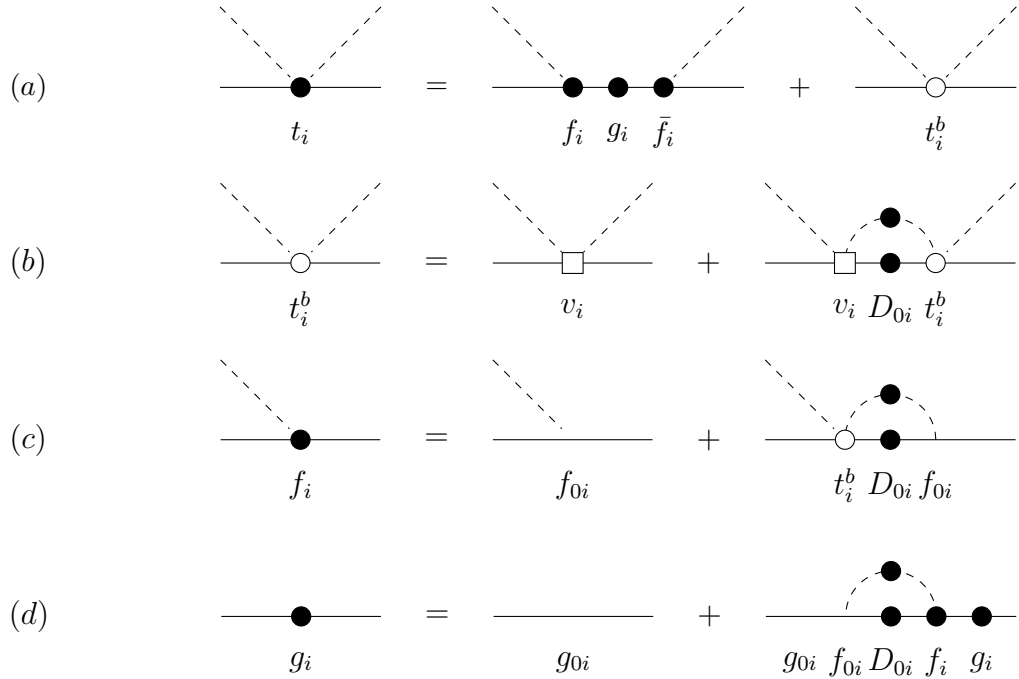


Figure 3.1: Coupled equations for a pion (dashed line) scattering off nucleon i (solid line): (a) The πN t -matrix expressed by Equation 3.32, (b) the “background” πN t -matrix as given by Equation 3.33a, (c) the dressed πNN vertex as given by Equation 3.34a, and (d) the dressed nucleon propagator as given by Equation 3.35 whose self-energy term Σ_i is expressed as in Equation 3.36a.

We note that $D_{0i}(e)$ is the fully dressed πN propagator, and just like Equation 3.26 for NN scattering, is given by a convolution expression

$$D_{0i}(e) = \left(-\frac{1}{2\pi i} \right) \int_{-\infty}^{\infty} dz g_i(e-z) g_3(z) \quad (3.37)$$

where $g_i(e)$ is the dressed propagator of nucleon i and $g_3(e)$ is the dressed propagator of the pion. For the case where explicit pion dressing is neglected, but nucleon dressing is retained, we have recently solved the above πN scattering equations while fitting to experimental πN data using parametrised forms for the potentials v_i and bare πNN vertex f_{0i} [84].

It is well known that πN scattering gives rise to the formation of resonances, the most prominent of which is the $\Delta(1232)$ resonance in the P_{33} partial wave. We shall take the $\Delta(1232)$ into account by demanding that the background πN t -matrix t_i^b contains a pole on the second sheet of the complex relative momentum plane corresponding to the formation of this resonance. We thus write, similarly to Equation 3.28 and Equation 3.29,

$$\begin{aligned} \langle \mathbf{q}'_i \bar{\mathbf{p}}'_i | t_i^b(e) | \mathbf{q}_i \bar{\mathbf{p}}_i \rangle &= \delta(\bar{\mathbf{p}}'_i - \bar{\mathbf{p}}_i) t_i^b(e - \bar{E}_i, \mathbf{q}'_i, \mathbf{q}_i) \\ &\equiv \delta(\bar{\mathbf{p}}'_i - \bar{\mathbf{p}}_i) \langle \mathbf{q}'_i | t_i^{b\text{cm}}(e - \bar{E}_i) | \mathbf{q}_i \rangle \end{aligned} \quad (3.38)$$

where

$$t_i^{b\text{cm}}(e) = \frac{|\phi_i\rangle\langle\phi_i|}{e^+ - \bar{m}_i} + t_i^{b'}(e) \quad (3.39)$$

with $|\phi_i\rangle$ being the resonance form factor and \bar{m}_i the (complex) resonance mass. It will also be useful to define the bound state wave-function $|\psi_i\rangle$ through

$$|\psi_i\rangle = D_{0i}^{\text{cm}}(\bar{m}_i) |\phi_i\rangle. \quad (3.40)$$

In Equation 3.40, $D_{0i}^{\text{cm}}(e)$ is the πN_i ‘‘centre of mass’’ free propagator which acts in the space of relative momenta such that

$$\begin{aligned} \langle \mathbf{q}'_i \bar{\mathbf{p}}'_i | D_{0i}(e) | \mathbf{q}_i \bar{\mathbf{p}}_i \rangle &= \delta(\bar{\mathbf{p}}'_i - \bar{\mathbf{p}}_i) D_{0i}(e - \bar{E}_i, \mathbf{q}'_i, \mathbf{q}_i) \\ &\equiv \delta(\bar{\mathbf{p}}'_i - \bar{\mathbf{p}}_i) \langle \mathbf{q}'_i | D_{0i}^{\text{cm}}(e - \bar{E}_i) | \mathbf{q}_i \rangle. \end{aligned} \quad (3.41)$$

3.4 3-dimensional scattering equations

3.4.1 Faddeev-like equations

Here we derive equations describing the πNN system. The starting point is Equation 3.6 which expresses the $\pi NN \rightarrow \pi NN$ t -matrix $T(E)$ in terms of the πNN -irreducible potential $V(E)$ and the fully dressed πNN propagator $G_0(E)$. Similarly to the case of fully dressed NN and πN propagators discussed above, the fully dressed πNN propagator in TOPT is given by the convolution expression in Equation 3.8.

Within the assumed formalism, we make just one approximation: we shall exclude connected contributions to the potential $V(E)$, one example of which is illustrated in Figure 3.2 (a). Such contributions correspond to three-body forces and will be considered elsewhere. We note, however, that the topologically similar but πNN reducible contribution of Figure 3.2 (b) is retained in this work.

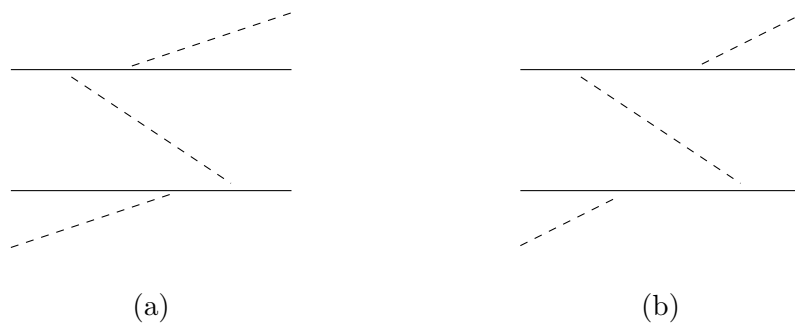


Figure 3.2: (a) Example of a connected πNN -irreducible contribution to the πNN potential V ; such contributions correspond to three-body forces and are neglected in this work. (b) A topologically similar contribution to that of (a), which however is included in our work as it is πNN reducible.

As discussed by Stingl and Stelbovics [44], all disconnected $\pi NN \rightarrow \pi NN$ diagrams contributing to $V(E)$, belong to one of five classes of disconnectedness, denoted by δ_α , characterised by an appropriate momentum-space δ function. According to this classification, $V(E)$ can be written as the sum

$$V(E) = \sum_{\alpha=1}^5 V_\alpha(E) \quad (3.42)$$

where V_α , illustrated in Figure 1.8, is the potential of disconnectedness δ_α .

To generate the corresponding $\pi NN \rightarrow \pi NN$ t -matrix $T(E)$ one cannot use Equation 3.6 directly, as its kernel is disconnected. To derive equations with a compact kernel we proceed by analogy with the case of Faddeev equations and eliminate the potentials $V_\alpha(E)$ in favour of completely summed contributions of disconnectedness δ_α . Let us, therefore, denote by \tilde{w}_α the set of all $\pi NN \rightarrow \pi NN$ diagrams, reducible and irreducible, belonging to the disconnectedness class δ_α . By their definition, the \tilde{w}_α are Green's function operators, so that the corresponding t -matrix operators w_α are defined as

$$\tilde{w}_\alpha = G_0 w_\alpha G_0. \quad (3.43)$$

Note that \tilde{w}_α and w_α are operators that act in πNN space. We now write the t -matrix operator $T(E)$ in Equation 3.6 in terms of its connected and disconnected parts. The connected part we denote by $T^c(E)$, while the disconnected part is, by the above definition, just the sum of the $w_\alpha(E)$.

Thus

$$\sum_{\alpha=1}^5 w_\alpha + T^c = \sum_{\alpha=1}^5 V_\alpha + \sum_{\alpha=1}^5 V_\alpha G_0 \left(\sum_{\beta=1}^5 w_\beta + T^c \right). \quad (3.44)$$

Equating terms with the same disconnectedness δ_α , it is easy to see that

$$w_1 = V_1 + V_1 G_0 w_1 + V_4 G_0 w_5 \quad (3.45a)$$

$$w_2 = V_2 + V_2 G_0 w_2 + V_5 G_0 w_4 \quad (3.45b)$$

$$w_3 = V_3 + V_3 G_0 w_3 \quad (3.45c)$$

$$w_4 = V_4 + V_4 G_0 w_2 + V_1 G_0 w_4 \quad (3.45d)$$

$$w_5 = V_5 + V_5 G_0 w_1 + V_2 G_0 w_5 \quad (3.45e)$$

These agree formally with Equations 2.15 of Stingl and Stelbovics [45], but have been obtained here in a much simpler way. We emphasise, however, that because we consider the general case, our definitions of the quantities w_α and V_α are different from those of Stingl and Stelbovics. Now that we have these equations for w_α , we follow Stingl and Stelbovics [45] and represent the full t -matrix by the sum

$$T = \sum_{\alpha=1}^5 T_\alpha \quad (3.46)$$

where each T_α is defined as the sum of the terms of T which begin with a disconnectedness δ_α . For example, the terms $V_1 G_0 w_2$ and $V_1 G_0 w_3 G_0 w_4$ both belong to T_1 . Each T_α consists of a disconnected part and a connected part, where the disconnected part is obviously w_α as this is the sum of all diagrams belonging to the disconnectedness δ_α . This leaves the connected part, which must be $w_\alpha G_0 T$ where T is given as the sum of T_α . However, some T_α terms are forbidden in this connected part as they contradict the definition of connected and the definition of T_α .

For example, if we have T_1 , this would be given by

$$T_1 = w_1 + w_1 G_0 (T_2 + T_3 + T_5). \quad (3.47)$$

As the term, $w_1 G_0 T_1$ would contain terms that are disconnected and the term $w_1 G_0 T_4$ would contradict the definition of T_1 as these terms would lead to terms that begin with

a disconnectedness of δ_4 . The same idea is applied to the case of three particles and leads to the traditional Faddeev equations. By implementing the same idea to the remaining T_α terms, one finds that T_α can be written as

$$T = \sum_{\alpha=1}^5 T_\alpha, \quad (3.48a)$$

$$T_\alpha = w_\alpha + \sum_{\beta=1}^5 w_\alpha \kappa_{\alpha\beta} G_0 T_\beta \quad (3.48b)$$

where

$$\kappa = \begin{pmatrix} 0 & 1 & 1 & 0 & 1 \\ 1 & 0 & 1 & 1 & 0 \\ 1 & 1 & 0 & 1 & 1 \\ 1 & 0 & 1 & 1 & 0 \\ 0 & 1 & 1 & 0 & 1 \end{pmatrix}. \quad (3.48c)$$

The first iteration of Equation 3.48b results in a compact kernel. Equations 3.48 are Faddeev-like equations that were first derived by Stingl and Stelbovics in the context of a simple field-theoretic model where all states containing more than two pions are neglected [44]. Here we have shown that these equations hold also in the general case of the full field theory. This would only be a theoretical achievement if the disconnected t -matrices w_α could not be calculated in practice. Remarkably, despite there being no practical way of calculating the disconnected potentials V_α , the corresponding t -matrices w_α are easily calculated using convolution expressions [48].

3.4.2 Convolution expressions for w_α

The fact that the amplitudes w_α contain all possible contributions of a particular disconnectedness is also the essential property needed to express these amplitudes directly in terms of dressed sub-system amplitudes (in our case the two-body t -matrices t_α , the πNN vertex f , and the dressed one-nucleon propagator g). As has been shown previously [48], this is done in terms of a convolution integrals which effectively sum all possible time-orderings of interactions taking place in the disconnected processes. As the convolution integrals are written for Green's function quantities, we shall utilise a "tilde" notation, as in Equation 3.43, to label amplitudes with additional initial and final-state propagators. Thus, for the

πN t -matrix ($\alpha = 1, 2$), and the sub-space NN t -matrix ($\alpha = 3$) we define

$$\tilde{t}_\alpha(e) = D_{0\alpha}(e)t_\alpha(e)D_{0\alpha}(e) \quad (3.49)$$

where $D_{0\alpha}(e)$ is the corresponding dressed πN or dressed NN propagator. We note further that \tilde{t}_α is the connected part of the corresponding full two-body Green's function; for example,

$$\langle \mathbf{p}'_i \mathbf{p}'_3 | \tilde{t}_i(e) | \mathbf{p}_i \mathbf{p}_3 \rangle = \langle \mathbf{p}'_i \mathbf{p}'_3 | \frac{1}{e^+ - H} | \mathbf{p}_i \mathbf{p}_3 \rangle_c. \quad (3.50)$$

Similarly, we write the πNN vertex Green's functions as

$$\tilde{f}_i(e) = D_{0i}(e)f_i(e)g_i(e), \quad (3.51a)$$

$$\tilde{\bar{f}}_i(e) = g_i(e)\bar{f}_i D_{0i}(e) \quad (3.51b)$$

where

$$\langle \mathbf{p}'_i \mathbf{p}'_3 | \tilde{f}_i(e) | \mathbf{p}_i \rangle = \langle \mathbf{p}'_i \mathbf{p}'_3 | \frac{1}{e^+ - H} | \mathbf{p}_i \rangle, \quad (3.52a)$$

$$\langle \mathbf{p}'_i | \tilde{\bar{f}}_i(e) | \mathbf{p}_i \mathbf{p}_3 \rangle = \langle \mathbf{p}'_i | \frac{1}{e^+ - H} | \mathbf{p}_i \mathbf{p}_3 \rangle. \quad (3.52b)$$

Using Galilean invariance, we note that

$$\begin{aligned} \langle \mathbf{p}'_i \mathbf{p}'_3 | \tilde{f}_i(e) | \mathbf{p}_i \rangle &= \langle \bar{\mathbf{p}}'_i \mathbf{q}'_i | \tilde{f}_i(e) | \mathbf{p}_i \rangle \\ &= \delta(\bar{\mathbf{p}}'_i - \mathbf{p}_i) D_{0i} \left(e - \bar{E}'_i - \frac{q_i'^2}{2\mu_{i3}} \right) f_i(e - E_i, \mathbf{q}'_i) g_i(e - E_i), \end{aligned} \quad (3.53)$$

$$\begin{aligned} \langle \mathbf{p}'_i | \tilde{\bar{f}}_i(e) | \mathbf{p}_i \mathbf{p}_3 \rangle &= \langle \mathbf{p}'_i | \tilde{\bar{f}}_i(e) | \bar{\mathbf{p}}_i \mathbf{q}_i \rangle \\ &= \delta(\mathbf{p}'_i - \bar{\mathbf{p}}_i) g_i(e - E'_i) \bar{f}_i(e - E'_i, \mathbf{q}_i) D_{0i} \left(e - \bar{E}_i - \frac{q_i^2}{2\mu_{i3}} \right), \end{aligned} \quad (3.54)$$

where E_i , \bar{E}_i , E'_i and \bar{E}'_i are defined as in Equation 3.24a. Because pion production or absorption on a nucleon is inherently a relativistic process, here Galilean invariance is violated; however, due to the mass of the pion being much smaller than that of a nucleon, we expect the consequences of this violation to be small.

In addition to these definitions, we shall write convolution integrals in a short-hand notation where

$$c = a \otimes b \quad (3.55)$$

means the convolution integral

$$c(e) = \left(-\frac{1}{2\pi i} \right) \int_{-\infty}^{\infty} dz a(e - z)b(z). \quad (3.56)$$

Using these definitions, the amplitudes w_α can be written in terms of convolution integrals as

$$\tilde{w}_1 = G_0 w_1 G_0 = \tilde{t}_1 \otimes g_2 \quad (3.57a)$$

$$\tilde{w}_2 = G_0 w_2 G_0 = \tilde{t}_2 \otimes g_1 \quad (3.57b)$$

$$\tilde{w}_3 = G_0 w_3 G_0 = \tilde{t}_3 \otimes g_3 \quad (3.57c)$$

$$\tilde{w}_4 = G_0 w_4 G_0 = \tilde{f}_1 \otimes \tilde{f}_2 \quad (3.57d)$$

$$\tilde{w}_5 = G_0 w_5 G_0 = \tilde{f}_2 \otimes \tilde{f}_1 \quad (3.57e)$$

3.4.3 AGS-like equations

The goal now is to turn Equations 3.48 into a form that can be more easily solved numerically. It is evident from Equation 3.48b that T_α is the sum of all diagrams that end (on the left) with a sub-process of disconnectedness δ_α . In order to group together diagrams that not only end with a sub-process of disconnectedness δ_α , but also start with a sub-process of disconnectedness δ_β , we follow Stingl and Stelbovics and define Alt-Grassberger-Sandhas (AGS)-like [85] amplitudes $U_{\alpha\beta}$ as satisfying

$$T_\alpha = w_\alpha + \sum_{\beta=1}^5 w_\alpha G_0 U_{\alpha\beta} G_0 w_\beta \quad (3.58)$$

so that

$$\sum_{\beta=1}^5 \kappa_{\alpha\beta} T_\beta \equiv \sum_{\beta=1}^5 U_{\alpha\beta} G_0 w_\beta \quad (3.59)$$

and therefore

$$\sum_{\beta=1}^5 U_{\alpha\beta} G_0 w_\beta = \sum_{\beta=1}^5 \kappa_{\alpha\beta} w_\beta + \sum_{\beta=1}^5 \sum_{\gamma=1}^5 \kappa_{\alpha\gamma} w_\gamma G_0 U_{\gamma\beta} G_0 w_\beta. \quad (3.60)$$

It then follows that

$$U_{\alpha\beta} = \kappa_{\alpha\beta} G_0^{-1} + \sum_{\gamma=1}^5 \kappa_{\alpha\gamma} w_\gamma G_0 U_{\gamma\beta} \quad (3.61)$$

with the full $\pi NN \rightarrow \pi NN$ t -matrix being given by

$$T = \sum_{\alpha=1}^5 w_\alpha + \sum_{\alpha,\beta=1}^5 w_\alpha G_0 U_{\alpha\beta} G_0 w_\beta. \quad (3.62)$$

The connected part of the full $\pi NN \rightarrow \pi NN$ t -matrix is thus

$$T_c = \sum_{\alpha, \beta=1}^5 w_\alpha G_0 U_{\alpha\beta} G_0 w_\beta. \quad (3.63)$$

Although Equation 3.61 is formally a set of 5×5 equations, it can be reduced to a set of 3×3 equations by making use of the fact that in the κ matrix of Equation 3.48c, rows 1 and 5 are identical, as are rows 2 and 4, columns 1 and 4, and columns 2 and 5. This means that

$$U_{\alpha 4} = U_{\alpha 1}; \quad U_{\alpha 5} = U_{\alpha 2}; \quad U_{4\beta} = U_{2\beta}; \quad U_{5\beta} = U_{1\beta}; \quad (3.64a)$$

$$\kappa_{\alpha 4} = \kappa_{\alpha 1}; \quad \kappa_{\alpha 5} = \kappa_{\alpha 2}; \quad (3.64b)$$

which can be used to write Equation 3.61 as

$$\begin{aligned} U_{\alpha\beta} &= \kappa_{\alpha\beta} G_0^{-1} + \kappa_{\alpha 1} w_1 G_0 U_{1\beta} + \kappa_{\alpha 2} w_2 G_0 U_{2\beta} + \kappa_{\alpha 3} w_3 G_0 U_{3\beta} + \kappa_{\alpha 4} w_4 G_0 U_{4\beta} + \kappa_{\alpha 5} w_5 G_0 U_{5\beta} \\ &= \kappa_{\alpha\beta} G_0^{-1} + (\kappa_{\alpha 1} w_1 + \kappa_{\alpha 2} w_5) G_0 U_{1\beta} + (\kappa_{\alpha 2} w_2 + \kappa_{\alpha 1} w_4) G_0 U_{2\beta} + \kappa_{\alpha 3} w_3 G_0 U_{3\beta} \end{aligned} \quad (3.65)$$

where α and β are now restricted to range over 1, 2, and 3, only. Within this restricted range, $\kappa_{\alpha\beta} = \bar{\delta}_{\alpha\beta}$ where $\bar{\delta}_{\alpha\beta} \equiv 1 - \delta_{\alpha\beta}$, so that Equation 3.65 becomes the set of 3×3 equations

$$U_{\alpha\beta} = \bar{\delta}_{\alpha\beta} G_0^{-1} + \sum_{\gamma=1}^3 W_{\alpha\gamma} G_0 U_{\gamma\beta} \quad (3.66)$$

where

$$W_{\alpha 1} = \bar{\delta}_{\alpha 1} w_1 + \bar{\delta}_{\alpha 2} w_5; \quad W_{\alpha 2} = \bar{\delta}_{\alpha 2} w_2 + \bar{\delta}_{\alpha 1} w_4; \quad W_{\alpha 3} = \bar{\delta}_{\alpha 3} w_3. \quad (3.67)$$

We note that Equation 3.67 specifies the elements of the matrix W :

$$W = \begin{pmatrix} w_5 & w_2 & w_3 \\ w_1 & w_4 & w_3 \\ w_1 + w_5 & w_2 + w_4 & 0 \end{pmatrix} = \begin{pmatrix} 0 & 1 & 1 \\ 1 & 0 & 1 \\ 1 & 1 & 0 \end{pmatrix} \begin{pmatrix} w_1 & w_4 & 0 \\ w_5 & w_2 & 0 \\ 0 & 0 & w_3 \end{pmatrix} \equiv \bar{I} w \quad (3.68)$$

where \bar{I} is the matrix with elements $\bar{I}_{\alpha\beta} = \bar{\delta}_{\alpha\beta}$, and

$$w = \begin{pmatrix} w_1 & w_4 & 0 \\ w_5 & w_2 & 0 \\ 0 & 0 & w_3 \end{pmatrix}. \quad (3.69)$$

With these definitions, Equation 3.66 can be written as the 3×3 matrix equation

$$U = \bar{I} G_0^{-1} + \bar{I} w G_0 U. \quad (3.70)$$

It is interesting that Equation 3.70 has the same matrix form as the AGS equations of standard quantum-mechanical three-body theory [85], with the only essential differences being that: (i) the matrix of three-body disconnected amplitudes, w , possesses off-diagonal elements (w_4 and w_5), (ii) every disconnected amplitude w_α includes all possible dressing terms, and (iii) the three-particle propagator G_0 is fully dressed. It is of course the quantum-field-theoretic nature of the πNN system that gives rise to these differences.

It is also interesting to note that Afnan and Stelbovics [47] have previously shown that the πNN equations of Afnan and Blankleider and Stingl and Stelbovics can both be written in the form of Equation 3.70, but with meanings of w and G_0 that differ from each other (and also from ours). In this way, Afnan and Stelbovics showed how the Stingl and Stelbovics approach reduces to the one of Afnan and Blankleider upon the neglect of two-pion states. Now we can see that the equations of Stingl and Stelbovics and Afnan and Blankleider are actually both special cases of Equation 3.70 whose w matrix has elements given by the convolution expressions of Equations 3.57. In particular, the equations of Stingl and Stelbovics result from our Equation 3.70 upon the neglect of all states with more than two pions, while the equations of Afnan and Blankleider result from our Equation 3.70 upon the neglect of all states with more than one pion; and further, the πNN three-body equations of Afnan and Thomas [29] result from our Equation 3.70 upon the neglect of the off-diagonal elements w_4 and w_5 , as well as all dressing.

One can similarly use the symmetries of $U_{\alpha\beta}$ to reduce the sums in Equation 3.62 to range from 1 to 3; in particular, one obtains

$$T = \sum_{\alpha,\beta=1}^3 \mathcal{T}_{\alpha\beta} \quad (3.71a)$$

where \mathcal{T} is the 3×3 matrix given by

$$\mathcal{T} = w + wG_0UG_0w. \quad (3.71b)$$

Multiplying the AGS-like Equation 3.70 on the left and right by wG_0 and G_0w , respectively, one obtains Faddeev-like equations for \mathcal{T} :

$$\mathcal{T} = w + w\bar{I}G_0\mathcal{T}. \quad (3.71c)$$

We note that Equations 3.71 were previously obtained by Afnan and Stelbovics in the context of the Stingl and Stelbovics model.

3.4.4 On-shell and off-shell amplitudes

Multiplying Equation 3.71a on the left and right by G_0 , one obtains the expression for the $\pi NN \rightarrow \pi NN$ Green's function $G - G_0$ whose connected part is given by

$$G_c = \sum_{\alpha, \beta=1}^3 (\tilde{w}U\tilde{w})_{\alpha\beta} \quad (3.72a)$$

$$= \sum_{\alpha, \beta=1}^3 \left[\begin{array}{c} \begin{pmatrix} \tilde{w}_1 & \tilde{w}_4 & 0 \\ \tilde{w}_5 & \tilde{w}_2 & 0 \\ 0 & 0 & \tilde{w}_3 \end{pmatrix} \begin{pmatrix} U_{11} & U_{12} & U_{13} \\ U_{21} & U_{22} & U_{23} \\ U_{31} & U_{32} & U_{33} \end{pmatrix} \begin{pmatrix} \tilde{w}_1 & \tilde{w}_4 & 0 \\ \tilde{w}_5 & \tilde{w}_2 & 0 \\ 0 & 0 & \tilde{w}_3 \end{pmatrix} \\ \alpha\beta \end{array} \right] \quad (3.72b)$$

Using this expression, the on-shell amplitudes for $\pi d \rightarrow \pi d$, $NN \rightarrow \pi d$ and $NN \rightarrow NN$ can now be obtained by taking residues at the appropriate poles in initial and final states.

$\pi d \rightarrow \pi d$

To obtain the expression for the πd elastic scattering amplitude, we single out the term involving U_{33} :

$$G_c(E) = \tilde{w}_3(E)U_{33}(E)\tilde{w}_3(E) + \dots, \quad (3.73)$$

and seek to expose the deuteron bound state poles in $\tilde{w}_3(E)$. To facilitate this, we consider the momentum matrix element of \tilde{w}_3 ,

$$\begin{aligned} \langle \mathbf{p}'_3 \bar{\mathbf{p}}'_3 \mathbf{q}'_3 | \tilde{w}_3(E) | \mathbf{p}_3 \bar{\mathbf{p}}_3 \mathbf{q}_3 \rangle &= \langle \mathbf{p}'_3 \bar{\mathbf{p}}'_3 \mathbf{q}'_3 | \tilde{t}_3 \otimes g_3 | \mathbf{p}_3 \bar{\mathbf{p}}_3 \mathbf{q}_3 \rangle \\ &= \left(-\frac{1}{2\pi i} \right) \int_{-\infty}^{\infty} dz \langle \mathbf{p}'_3 \bar{\mathbf{p}}'_3 \mathbf{q}'_3 | D_{03}(E-z) t_3(E-z) D_{03}(E-z) g_3(z) | \mathbf{p}_3 \bar{\mathbf{p}}_3 \mathbf{q}_3 \rangle \\ &= \left(-\frac{1}{2\pi i} \right) \delta(\mathbf{p}'_3 - \mathbf{p}_3) \delta(\bar{\mathbf{p}}'_3 - \bar{\mathbf{p}}_3) \int_{-\infty}^{\infty} dz D_{03} \left(E - z - \bar{E}_3 - \frac{q_3'^2}{2\mu_{12}} \right) \\ &\quad \times t_3(E - z - \bar{E}_3, \mathbf{q}'_3, \mathbf{q}_3) D_{03} \left(E - z - \bar{E}_3 - \frac{q_3^2}{2\mu_{12}} \right) g_3(z - E_3). \end{aligned} \quad (3.74)$$

This result can be used to expose the deuteron pole by recognising that:

- (i) The sub-system NN t -matrix $t_3(E - z - \bar{E}_3, \mathbf{q}'_3, \mathbf{q}_3)$ has a pole corresponding to the deuteron bound state, as previously specified by Equation 3.28 and Equation 3.29.
- (ii) The (numerical) dressed pion propagator $g_3(e)$ has a pole at the physical pion mass m_3 , and so can be written as

$$g_3(e) = \frac{Z_3}{e^+ - m_3} + g_3^b(e) \quad (3.75)$$

where Z_3 is the pion renormalisation constant. We shall assume that $g_3(e)$ has been renormalised so that $Z_3 = 1$.

With the pion propagator $g_3(e)$ expressed in the form given by Equation 3.75, the z integral in Equation 3.74 splits into two parts, one containing the pole part of g_3 , the other containing g_3^b . The z integral with the pole part of g_3 can be carried out by closing the contour in the lower half z plane, thus enabling us to write

$$\begin{aligned} \langle \mathbf{p}'_3 \bar{\mathbf{p}}'_3 \mathbf{q}'_3 | \tilde{w}_3(E) | \mathbf{p}_3 \bar{\mathbf{p}}_3 \mathbf{q}_3 \rangle &= \delta(\mathbf{p}'_3 - \mathbf{p}_3) \delta(\bar{\mathbf{p}}'_3 - \bar{\mathbf{p}}_3) \\ &\times \left[D_{03} \left(E - E_3 - m_3 - \bar{E}_3 - \frac{q_3'^2}{2\mu_{12}} \right) t_3(E - E_3 - m_3 - \bar{E}_3, \mathbf{q}'_3, \mathbf{q}_3) \right. \\ &\left. \times D_{03} \left(E - E_3 - m_3 - \bar{E}_3 - \frac{q_3^2}{2\mu_{12}} \right) + \dots \right] \end{aligned} \quad (3.76)$$

or using the definitions of Equation 3.29 and Equation 3.31,

$$\begin{aligned} \langle \mathbf{p}'_3 \bar{\mathbf{p}}'_3 \mathbf{q}'_3 | \tilde{w}_3(E) | \mathbf{p}_3 \bar{\mathbf{p}}_3 \mathbf{q}_3 \rangle &= \delta(\mathbf{p}'_3 - \mathbf{p}_3) \delta(\bar{\mathbf{p}}'_3 - \bar{\mathbf{p}}_3) \\ &\times [\langle \mathbf{q}'_3 | D_{03}^{\text{cm}}(e_3) t_3^{\text{cm}}(e_3) D_{03}^{\text{cm}}(e_3) | \mathbf{q}_3 \rangle + \dots], \end{aligned} \quad (3.77)$$

where $e_3 = E - E_3 - m_3 - \bar{E}_3$. Upon using Equation 3.29, one obtains that as E approaches the on-energy-shell limit $E \rightarrow E_3 + m_3 + \bar{E}_3 + m_d$,

$$\begin{aligned} \langle \mathbf{p}'_3 \bar{\mathbf{p}}'_3 \mathbf{q}'_3 | \tilde{w}_3(E) | \mathbf{p}_3 \bar{\mathbf{p}}_3 \mathbf{q}_3 \rangle &= \delta(\mathbf{p}'_3 - \mathbf{p}_3) \delta(\bar{\mathbf{p}}'_3 - \bar{\mathbf{p}}_3) \\ &\times \langle \mathbf{q}'_3 | \frac{|\psi_d\rangle \langle \psi_d|}{E^+ - E_3 - m_3 - \bar{E}_3 - m_d} | \mathbf{q}_3 \rangle \end{aligned} \quad (3.78)$$

and therefore

$$\tilde{w}_3(E) | \mathbf{p}_3 \bar{\mathbf{p}}_3 \mathbf{q}_3 \rangle = \frac{|\psi_d\rangle \langle \psi_d|}{E^+ - E_3 - m_3 - \bar{E}_3 - m_d} | \mathbf{p}_3 \bar{\mathbf{p}}_3 \mathbf{q}_3 \rangle. \quad (3.79)$$

Using this and the corresponding equation for $\langle \mathbf{p}_3 \bar{\mathbf{p}}_3 \mathbf{q}_3 | \tilde{w}_3(E)$, allows us to take left and right residues of Equation 3.73 to obtain the expression for the πd elastic scattering operator in $(\mathbf{p}_3, \bar{\mathbf{p}}_3)$ space:

$$T_{dd}(E) = \langle \psi_d | U_{33}(E) | \psi_d \rangle. \quad (3.80)$$

$NN \leftrightarrow \pi d, NN \rightarrow NN$

On-shell: The physical on-shell $NN \rightarrow \pi d$ scattering amplitude is obtained by writing Equation 3.72b as

$$G_c(E) = \tilde{w}_3(E) U_{31}(E) [\tilde{w}_1(E) + \tilde{w}_4(E)] \quad (3.81)$$

$$+ \tilde{w}_3(E) U_{32}(E) [\tilde{w}_2(E) + \tilde{w}_5(E)] + \dots \quad (3.82)$$

and taking initial- and final-state residues at the poles of the singled-out terms. To expose the initial-state two-nucleon pole terms it is sufficient to consider the momentum matrix elements of \tilde{w}_1 and \tilde{w}_4 as the matrix elements of \tilde{w}_2 and \tilde{w}_5 then follow by symmetry. Proceeding as for \tilde{w}_3 above, one has that

$$\begin{aligned}
 \langle \mathbf{p}'_2 \bar{\mathbf{p}}'_1 \mathbf{q}'_1 | \tilde{w}_1(E) | \mathbf{p}_2 \bar{\mathbf{p}}_1 \mathbf{q}_1 \rangle &= \langle \mathbf{p}'_2 \bar{\mathbf{p}}'_1 \mathbf{q}'_1 | \tilde{t}_1 \otimes g_2 | \mathbf{p}_2 \bar{\mathbf{p}}_1 \mathbf{q}_1 \rangle \\
 &= \left(-\frac{1}{2\pi i} \right) \int_{-\infty}^{\infty} dz \langle \mathbf{p}'_2 \bar{\mathbf{p}}'_1 \mathbf{q}'_1 | D_{01}(E-z) t_1(E-z) D_{01}(E-z) g_2(z) | \mathbf{p}_2 \bar{\mathbf{p}}_1 \mathbf{q}_1 \rangle \\
 &= \left(-\frac{1}{2\pi i} \right) \delta(\mathbf{p}'_2 - \mathbf{p}_2) \delta(\bar{\mathbf{p}}'_1 - \bar{\mathbf{p}}_1) \int_{-\infty}^{\infty} dz D_{01} \left(E - z - \bar{E}_1 - \frac{q_1'^2}{2\mu_{31}} \right) \\
 &\quad \times t_1(E - z - \bar{E}_1, \mathbf{q}'_1, \mathbf{q}_1) D_{01} \left(E - z - \bar{E}_1 - \frac{q_1^2}{2\mu_{31}} \right) g_2(z - E_2) \quad (3.83)
 \end{aligned}$$

where $t_1(e)$ can be written in terms of nucleon pole and background terms as in Equation 3.32, and where, similar to Equation 3.75, one can express the (numerical) dressed nucleon propagator $g_2(e)$ as

$$g_2(e) = \frac{Z_2}{e^+ - m_2} + g_2^b(e). \quad (3.84)$$

As for $g_3(e)$, we take $g_2(e)$ to be renormalised so that $Z_2 = 1$. Using the pole parts of $t_1(e)$ and $g_2(e)$, one can carry out the z integral to write Equation 3.83 as

$$\begin{aligned}
 \langle \mathbf{p}'_2 \bar{\mathbf{p}}'_1 \mathbf{q}'_1 | \tilde{w}_1(E) | \mathbf{p}_2 \bar{\mathbf{p}}_1 \mathbf{q}_1 \rangle &= \delta(\mathbf{p}'_2 - \mathbf{p}_2) \delta(\bar{\mathbf{p}}'_1 - \bar{\mathbf{p}}_1) \left[D_{01} \left(E - E_{N_2} - m_2 - \bar{E}_1 - \frac{q_1'^2}{2\mu_{31}} \right) \right. \\
 &\quad \times f_1(E - E_{N_2} - m_2 - E_{N_1}, \mathbf{q}'_1) g_1(E - E_{N_2} - m_2 - E_{N_1}) \\
 &\quad \left. \times \bar{f}_1(E - E_{N_2} - m_2 - E_{N_1}, \mathbf{q}_1) D_{01} \left(E - E_{N_2} - m_2 - \bar{E}_1 - \frac{q_1^2}{2\mu_{31}} \right) + \dots \right] \quad (3.85)
 \end{aligned}$$

where $E_{N_1} = \bar{p}_1^2/2m_1$ and $E_{N_2} = p_2^2/2m_1$. As E approaches the on-energy-shell limit $E \rightarrow E_{N_1} + m_1 + E_{N_2} + m_2$, we thus have that

$$\tilde{w}_1(E) | \mathbf{p}_2 \bar{\mathbf{p}}_1 \mathbf{q}_1 \rangle = \frac{D_{01}(E_{N_1} + m_1) f_1(E_{N_1} + m_1) \bar{f}_1(E_{N_1} + m_1) D_{01}(E_{N_1} + m_1)}{E^+ - E_{N_1} - m_1 - E_{N_2} - m_2} | \mathbf{p}_2 \bar{\mathbf{p}}_1 \mathbf{q}_1 \rangle. \quad (3.86)$$

Interchanging the 1 and 2 indices then gives

$$\tilde{w}_2(E) | \mathbf{p}_1 \bar{\mathbf{p}}_2 \mathbf{q}_2 \rangle = \frac{D_{02}(E_{N_2} + m_2) f_2(E_{N_2} + m_2) \bar{f}_2(E_{N_2} + m_2) D_{02}(E_{N_2} + m_2)}{E^+ - E_{N_1} - m_1 - E_{N_2} - m_2} | \mathbf{p}_1 \bar{\mathbf{p}}_2 \mathbf{q}_2 \rangle. \quad (3.87)$$

Similarly

$$\begin{aligned}
 \langle \mathbf{p}'_2 \bar{\mathbf{p}}'_1 \mathbf{q}'_1 | \tilde{w}_4(E) | \mathbf{p}_1 \bar{\mathbf{p}}_2 \mathbf{q}_2 \rangle &= \langle \mathbf{p}'_2 \bar{\mathbf{p}}'_1 \mathbf{q}'_1 | \tilde{f}_1 \otimes \tilde{f}_2(E) | \mathbf{p}_1 \bar{\mathbf{p}}_2 \mathbf{q}_2 \rangle \\
 &= \left(-\frac{1}{2\pi i} \right) \int_{-\infty}^{\infty} dz \langle \mathbf{p}'_2 \bar{\mathbf{p}}'_1 \mathbf{q}'_1 | D_{01}(E-z) f_1(E-z) g_1(E-z) \\
 &\quad \times g_2(z) \bar{f}_2(z) D_{02}(z) | \mathbf{p}_1 \bar{\mathbf{p}}_2 \mathbf{q}_2 \rangle \\
 &= \left(-\frac{1}{2\pi i} \right) \delta(\bar{\mathbf{p}}'_1 - \mathbf{p}_1) \delta(\mathbf{p}'_2 - \bar{\mathbf{p}}_2) \int_{-\infty}^{\infty} dz D_{01} \left(E - z - \bar{E}_1 - \frac{q_1'^2}{2\mu_{31}} \right) \\
 &\quad \times f_1(E - z - E_{N_1}, \mathbf{q}'_1) g_1(E - z - E_{N_1}) \\
 &\quad \times g_2(z - E_{N_2}) \bar{f}_2(z - E_{N_2}, \mathbf{q}_2) D_{02} \left(z - \bar{E}_2 - \frac{q_2^2}{2\mu_{23}} \right) \\
 &= \delta(\bar{\mathbf{p}}'_1 - \mathbf{p}_1) \delta(\mathbf{p}'_2 - \bar{\mathbf{p}}_2) D_{01} \left(E - E_{N_2} - m_2 - \bar{E}_1 - \frac{q_1'^2}{2\mu_{31}} \right) \\
 &\quad \times f_1(E - E_{N_2} - m_2 - E_{N_1}, \mathbf{q}'_1) g_1(E - E_{N_2} - m_2 - E_{N_1}) \\
 &\quad \times \bar{f}_2(m_2, \mathbf{q}_2) D_{02} \left(E_{N_2} + m_2 - \bar{E}_2 - \frac{q_2^2}{2\mu_{23}} \right). \tag{3.88}
 \end{aligned}$$

As E approaches the on-energy-shell limit $E \rightarrow E_{N_1} + m_1 + E_{N_2} + m_2$, we thus have that

$$\tilde{w}_4(E) | \mathbf{p}_1 \bar{\mathbf{p}}_2 \mathbf{q}_2 \rangle = \frac{D_{01}(E_{N_1} + m_1) f_1(E_{N_1} + m_1) \bar{f}_2(E_{N_2} + m_2) D_{02}(E_{N_2} + m_2)}{E^+ - E_{N_1} - m_1 - E_{N_2} - m_2} | \mathbf{p}_1 \bar{\mathbf{p}}_2 \mathbf{q}_2 \rangle. \tag{3.89}$$

Interchanging the 1 and 2 indices then gives

$$\tilde{w}_5(E) | \mathbf{p}_2 \bar{\mathbf{p}}_1 \mathbf{q}_1 \rangle = \frac{D_{02}(E_{N_2} + m_2) f_2(E_{N_2} + m_2) \bar{f}_1(E_{N_1} + m_1) D_{01}(E_{N_1} + m_1)}{E^+ - E_{N_1} - m_1 - E_{N_2} - m_2} | \mathbf{p}_2 \bar{\mathbf{p}}_1 \mathbf{q}_1 \rangle. \tag{3.90}$$

Recognising that $|\mathbf{p}_3 \bar{\mathbf{p}}_3 \mathbf{q}_3 \rangle = |\mathbf{p}_1 \bar{\mathbf{p}}_2 \mathbf{q}_2 \rangle = |\mathbf{p}_2 \bar{\mathbf{p}}_1 \mathbf{q}_1 \rangle = |\mathbf{p}_1 \mathbf{p}_2 \mathbf{p}_3 \rangle$, we can use the above relations in the momentum matrix element of Equation 3.82 to take residues at the πd and NN poles to obtain the expression for the on-shell $NN \rightarrow \pi d$ scattering operator

$$T_{dN}(E^{\text{on}}) = \sum_{j=1}^2 \langle \psi_3 | U_{3j} | D_{0j}(E_{N_j} + m_j) f_j(E_{N_j} + m_j), \tag{3.91}$$

where $E^{\text{on}} = E_{N_1} + m_1 + E_{N_2} + m_2$.

Off-shell: It will also be useful to define a $NN \rightarrow \pi d$ scattering operator with the initial two nucleons off shell. To do this, we introduce πNN vertex operators $F_i(E)$ and $\bar{F}_i(E)$ that

describe transitions between NN and πNN spaces, defined for $i \neq j$ as

$$\tilde{F}_i \equiv G_0 F_i D_0 = \tilde{f}_i \otimes g_j, \quad \tilde{\bar{F}}_i \equiv D_0 \bar{F}_i G_0 = \tilde{\bar{f}}_i \otimes g_j. \quad (3.92)$$

These operators have the property that, in the on-shell energy limit for NN scattering, $E \rightarrow E^{\text{on}} = E_{N_1} + m_1 + E_{N_2} + m_2$,

$$G_0 F_i(E^{\text{on}}) = D_{0i}(E_{N_i} + m_i) f_i(E_{N_j} + m_j). \quad (3.93)$$

To prove this, we first consider the momentum matrix element of $G_0 F_1 D_0$:

$$\begin{aligned} \langle \mathbf{p}'_2 \bar{\mathbf{p}}'_1 \mathbf{q}'_1 | \tilde{F}_1(E) | \mathbf{p}_1 \mathbf{p}_2 \rangle &= \langle \mathbf{p}'_2 \bar{\mathbf{p}}'_1 \mathbf{q}'_1 | \tilde{f}_1 \otimes g_2(E) | \mathbf{p}_1 \mathbf{p}_2 \rangle \\ &= \left(-\frac{1}{2\pi i} \right) \int_{-\infty}^{\infty} dz \langle \mathbf{p}'_2 \bar{\mathbf{p}}'_1 \mathbf{q}'_1 | D_{01}(E-z) f_1(E-z) g_1(E-z) g_2(z) | \mathbf{p}_1 \mathbf{p}_2 \rangle \\ &= \left(-\frac{1}{2\pi i} \right) \int_{-\infty}^{\infty} dz \langle \bar{\mathbf{p}}'_1 \mathbf{q}'_1 | D_{01}(E-z) f_1(E-z) g_1(E-z) | \mathbf{p}_1 \rangle \langle \mathbf{p}'_2 | g_2(z) | \mathbf{p}_2 \rangle \\ &= \left(-\frac{1}{2\pi i} \right) \delta(\bar{\mathbf{p}}'_1 - \mathbf{p}_1) \delta(\mathbf{p}'_2 - \mathbf{p}_2) \int_{-\infty}^{\infty} dz D_{01} \left(E - z - \bar{E}'_1 - \frac{q_1'^2}{2\mu_{31}} \right) \\ &\quad \times f_1(E - z - E_{N_1}, \mathbf{q}'_1) g_1(E - z - E_{N_1}) g_2(z - E_{N_2}), \\ &= \delta(\bar{\mathbf{p}}'_1 - \mathbf{p}_1) \delta(\mathbf{p}'_2 - \mathbf{p}_2) D_{01} \left(E - E_{N_2} - m_2 - \bar{E}'_1 - \frac{q_1'^2}{2\mu_{31}} \right) \\ &\quad \times f_1(E - E_{N_2} - m_2 - E_{N_1}, \mathbf{q}'_1) g_1(E - E_{N_2} - m_2 - E_{N_1}) + \dots \end{aligned} \quad (3.94)$$

where $E_{N_1} = E_1$, $E_{N_2} = E_2$, and the z integral was taken using the pole part of $g_2(z - E_{N_2})$.

It follows immediately that

$$\begin{aligned} \langle \mathbf{p}'_2 \bar{\mathbf{p}}'_1 \mathbf{q}'_1 | G_0 F_1(E) | \mathbf{p}_1 \mathbf{p}_2 \rangle &= \langle \mathbf{p}'_2 \bar{\mathbf{p}}'_1 \mathbf{q}'_1 | \tilde{f}_1 \otimes g_2 D_0^{-1}(E) | \mathbf{p}_1 \mathbf{p}_2 \rangle \\ &= \delta(\bar{\mathbf{p}}'_1 - \mathbf{p}_1) \delta(\mathbf{p}'_2 - \mathbf{p}_2) D_{01} \left(E - E_{N_2} - m_2 - \bar{E}'_1 - \frac{q_1'^2}{2\mu_{31}} \right) \\ &\quad \times f_1(E - E_{N_2} - m_2 - E_{N_1}, \mathbf{q}'_1) g_1(E - E_{N_2} - m_2 - E_{N_1}) D_0^{-1}(E - E_{N_1} - E_{N_2}) + \dots \end{aligned} \quad (3.95)$$

In the on-shell limit of $E = E_{N_1} + m_1 + E_{N_2} + m_2$ this gives the result

$$\langle \mathbf{p}'_2 \bar{\mathbf{p}}'_1 \mathbf{q}'_1 | G_0 F_1(E) | \mathbf{p}_1 \mathbf{p}_2 \rangle = \langle \mathbf{p}'_2 \bar{\mathbf{p}}'_1 \mathbf{q}'_1 | D_{01}(E_{N_1} + m_1) f_1(E_{N_1} + m_1) | \mathbf{p}_1 \mathbf{p}_2 \rangle. \quad (3.96)$$

This proves Equation 3.93 for the case $i = 1$ with the $i = 2$ case following by interchanging $1 \leftrightarrow 2$ in the above proof.

In view of Equation 3.91, we define the half-off shell $NN \rightarrow \pi d$ scattering operator as

$$T_{dN}(E) = \sum_{j=1}^2 \langle \psi_d | U_{3j} G_0 F_j, \quad (3.97a)$$

noting that this definition gives the correct on-shell limit. It's clear that one can similarly define the half-off shell $\pi d \rightarrow NN$ scattering operator as

$$T_{Nd}(E) = \sum_{i=1}^2 \bar{F}_i G_0 U_{i3} | \psi_d \rangle \quad (3.97b)$$

and the fully off-shell $NN \rightarrow NN$ scattering operator as

$$T_{NN}(E) = \sum_{i,j=1}^2 \bar{F}_i G_0 U_{ij} G_0 F_j. \quad (3.97c)$$

$N\Delta \leftrightarrow \pi d, N\Delta \leftrightarrow NN, N\Delta \rightarrow N\Delta$

The background πN t -matrix t_i^b contains a pole corresponding to the formation of the $\Delta(1232)$ resonances, as expressed by Equation 3.39. This fact allows us to define, at least formally (since the Δ mass is a complex number), the on-shell t -matrices involving $N\Delta$ states.

The on-shell $N_2\Delta_1 \rightarrow \pi d$ scattering amplitude is obtained by writing Equation 3.72b as

$$G_c(E) = \tilde{w}_3(E) U_{31}(E) \tilde{w}_1(E) + \dots \quad (3.98)$$

and taking initial- and final-state residues at the poles of the singled-out terms. To expose the initial-state $N_2\Delta_1$ pole term we consider the momentum matrix elements of \tilde{w}_1 . Proceeding as previously, one has that

$$\begin{aligned} \langle \mathbf{p}'_2 \mathbf{q}'_1 \bar{\mathbf{p}}'_1 | \tilde{w}_1(E) | \mathbf{p}_2 \mathbf{q}_1 \bar{\mathbf{p}}_1 \rangle &= \langle \mathbf{p}'_2 \mathbf{q}'_1 \bar{\mathbf{p}}'_1 | \tilde{t}_1 \otimes g_2(E) | \mathbf{p}_2 \mathbf{q}_1 \bar{\mathbf{p}}_1 \rangle \\ &= \left(-\frac{1}{2\pi i} \right) \int_{-\infty}^{\infty} dz \langle \mathbf{p}'_2 \mathbf{q}'_1 \bar{\mathbf{p}}'_1 | D_{01}(E-z) t_1(E-z) D_{01}(E-z) g_2(z) | \mathbf{p}_2 \mathbf{q}_1 \bar{\mathbf{p}}_1 \rangle \\ &= \left(-\frac{1}{2\pi i} \right) \delta(\mathbf{p}'_2 - \mathbf{p}_2) \delta(\bar{\mathbf{p}}'_1 - \bar{\mathbf{p}}_1) \int_{-\infty}^{\infty} dz D_{01} \left(E - z - \bar{E}_1 - \frac{q_1'^2}{2\mu_{31}} \right) \\ &\quad \times t_1^b \left(E - z - \bar{E}_1, \mathbf{q}'_1, \mathbf{q}_1 \right) D_{01} \left(E - z - \bar{E}_1 - \frac{q_1^2}{2\mu_{31}} \right) g_2(z - E_2) + \dots \end{aligned} \quad (3.99)$$

Using the pole parts of $t_1^b(e)$ and $g_2(e)$, one can carry out the z integral to write Equation 3.99 as

$$\begin{aligned} & \langle \mathbf{p}'_2 \mathbf{q}'_1 \bar{\mathbf{p}}'_1 | \tilde{w}_1(E) | \mathbf{p}_2 \mathbf{q}_1 \bar{\mathbf{p}}_1 \rangle \\ &= \delta(\mathbf{p}'_2 - \mathbf{p}_2) \delta(\bar{\mathbf{p}}'_1 - \bar{\mathbf{p}}_1) \left[D_{01} \left(E - E_{N_2} - m_2 - \bar{E}_1 - \frac{q_1'^2}{2\mu_{31}} \right) \right. \\ & \quad \left. \times \frac{\langle \mathbf{q}'_1 | \phi_1 \rangle \langle \phi_1 | \mathbf{q}_1 \rangle}{E^+ - E_{N_2} - m_2 - \bar{E}_1 - \bar{m}_1} D_{01} \left(E - E_{N_2} - m_2 - \bar{E}_1 - \frac{q_1^2}{2\mu_{31}} \right) + \dots \right]. \end{aligned} \quad (3.100)$$

As E approaches the on-energy-shell limit $E \rightarrow \bar{E}_1 + \bar{m}_1 + E_{N_2} + m_2$, we thus have that

$$\tilde{w}_1(E) | \mathbf{p}_2 \mathbf{q}_1 \bar{\mathbf{p}}_1 \rangle = \frac{D_{01}^{\text{cm}}(\bar{m}_1) | \phi_1 \rangle \langle \phi_1 | D_{01}^{\text{cm}}(\bar{m}_1)}{E^+ - \bar{E}_1 - \bar{m}_1 - E_{N_2} - m_2} | \mathbf{p}_2 \mathbf{q}_1 \bar{\mathbf{p}}_1 \rangle \quad (3.101)$$

Taking residues at the πd and $N_2 \Delta_1$ poles, one obtains the expression for the on-shell $N_2 \Delta_1 \rightarrow \pi d$ scattering operator

$$T_{d\Delta_1}(E) = \langle \psi_3 | U_{31} | \psi_1 \rangle, \quad (3.102)$$

where $E = \bar{E}_1 + \bar{m}_1 + E_{N_2} + m_2$. Similar derivations lead to the following full list of on-shell amplitude operators:

$$\begin{aligned} T_{NN} &= \sum_{ij} \bar{F}_i G_0 U_{ij} G_0 F_j, & T_{N\Delta_j} &= \sum_i \bar{F}_i G_0 U_{ij} | \psi_j \rangle, & T_{Nd} &= \sum_i \bar{F}_i G_0 U_{i3} | \psi_3 \rangle, \\ T_{\Delta_i N} &= \sum_j \langle \psi_i | U_{ij} G_0 F_j, & T_{\Delta_i \Delta_j} &= \langle \psi_i | U_{ij} | \psi_j \rangle, & T_{\Delta_i d} &= \langle \psi_i | U_{i3} | \psi_3 \rangle, \\ T_{dN} &= \sum_j \langle \psi_3 | U_{3j} G_0 F_j, & T_{d\Delta_j} &= \langle \psi_3 | U_{3j} | \psi_j \rangle, & T_{dd} &= \langle \psi_3 | U_{33} | \psi_3 \rangle. \end{aligned} \quad (3.103)$$

3.4.5 Scattering equations

Coupled Lippmann-Schwinger equations

$NN \rightarrow NN$

With the off-shell NN scattering amplitude T_{NN} defined by Equation 3.97c, we now seek to expose all the intermediate-state NN channels in the U_{ij} amplitudes, with the goal of deriving a closed scattering equation for T_{NN} . We note, however, that it is not entirely clear *a priori* whether this goal is achievable, nor whether in the process of iteration, the NN propagators will obtain their full dressing.

To help answer these questions, it will be convenient to use the matrix form of the AGS-like equations, Equation 3.70, and correspondingly introduce matrices of πNN vertex operators

$$F_N = \begin{pmatrix} F_1 \\ F_2 \\ 0 \end{pmatrix}, \quad \bar{F}_N = \begin{pmatrix} \bar{F}_1 & \bar{F}_2 & 0 \end{pmatrix}, \quad (3.104)$$

so that Equation 3.97c for T_{NN} can be written in matrix form as

$$T_{NN}(E) = \bar{F}_N G_0 U G_0 F_N. \quad (3.105)$$

The intermediate-state NN channels in the U amplitudes are hidden in the input terms w_α of Equation 3.70. To expose these, we first consider w_i ($i = 1, 2$) and recall that the corresponding Green's function \tilde{w}_i is defined as the set of all possible disconnected graphs for a pion scattering on nucleon i . This means that we can define a Green's function \tilde{w}_i^P to be the set of all two-nucleon reducible graphs belonging to \tilde{w}_i and write the corresponding amplitudes as

$$w_i = w_i^P + w_i^0 \quad (3.106)$$

where w_i^0 is two-nucleon irreducible. Since we consider all possible contributions, it is clear that one can write

$$w_i^P = F_i D_0 \bar{F}_i. \quad (3.107)$$

In the same way, we can separate out the two-nucleon reducible contributions from w_4 and w_5 , and write

$$w_4 = w_4^P + w_4^0, \quad w_5 = w_5^P + w_5^0 \quad (3.108)$$

where

$$w_4^P = F_1 D_0 \bar{F}_2, \quad w_5^P = F_2 D_0 \bar{F}_1. \quad (3.109)$$

With the further convention that $w_3^P = 0$ and $w_3^0 = w_3$, we can write generally

$$w_\alpha = w_\alpha^P + w_\alpha^0 \quad (3.110)$$

where w_α^P is the NN -reducible part of w_α . We can thus write the w matrix of Equation 3.69 as

$$w = w^P + w^0 \quad (3.111)$$

where

$$w = \begin{pmatrix} w_1 & w_4 & 0 \\ w_5 & w_2 & 0 \\ 0 & 0 & w_3 \end{pmatrix}, \quad w^P = \begin{pmatrix} w_1^P & w_4^P & 0 \\ w_5^P & w_2^P & 0 \\ 0 & 0 & 0 \end{pmatrix}, \quad w^0 = \begin{pmatrix} w_1^0 & w_4^0 & 0 \\ w_5^0 & w_2^0 & 0 \\ 0 & 0 & w_3 \end{pmatrix}. \quad (3.112)$$

In view of Equations 3.107 and 3.109, it is apparent that

$$w^P = F_N D_0 \bar{F}_N. \quad (3.113)$$

Each element of matrix w^P can be calculated directly from the fundamental inputs to the model, as can be w_3 . By contrast, apart from w_3 the elements of w^0 are not expressible in such a direct way, but rather, need to be determined by subtracting w^P from w . Examples of diagrams contributing to w^0 are given in Figure 3.3.

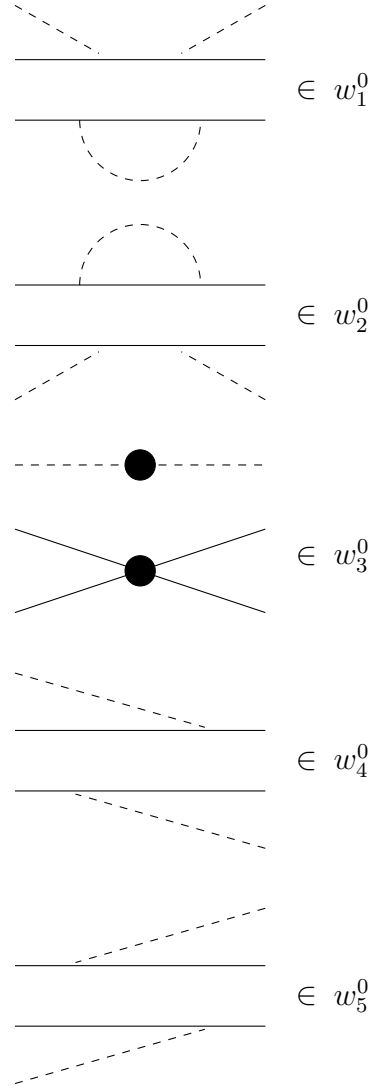


Figure 3.3: Examples of diagrams contributing to the NN -irreducible t -matrices w_α^0 . All possible diagrams of disconnectedness 3 contribute to w_3^0 , and this is indicated by the black circles.

As w^0 is the matrix of NN -irreducible parts of the input amplitudes, it is clear that the matrix U^0 , defined as the solution of the matrix AGS equation

$$U^0 = \bar{I}G_0^{-1} + \bar{I}w^0G_0U^0 \quad (3.114)$$

has elements $U_{\alpha\beta}^0$ which give the NN -irreducible parts of the full AGS amplitudes $U_{\alpha\beta}$. One can now combine Equations 3.70 and 3.114 to obtain

$$U = U^0 + U^0G_0w^PG_0U, \quad (3.115)$$

which expresses the full amplitude U in terms of its NN -irreducible part U^0 . Multiplying the above equation from the left and right by $\bar{F}G_0$ and G_0F , respectively, and then using

Equation 3.113, we derive the Lippmann-Schwinger equation for T_{NN} :

$$T_{NN}(E) = V_{NN}(E) + V_{NN}(E) D_0(E) T_{NN}(E) \quad (3.116)$$

where V_{NN} is the NN potential (sum of all NN -irreducible graphs) expressed as

$$V_{NN} = \bar{F}_N G_0 U^0 G_0 F_N. \quad (3.117)$$

This derivation shows explicitly that the NN propagator, which we did not have as an explicit input in the πNN AGS equations, Equation 3.70, is indeed the fully dressed propagator D_0 which is given in terms of the convolution integral of Equation 3.12. Although it may be clear that the amplitude U_{ij} is made up of fully dressed component amplitudes, it is noteworthy that the connection to the NN scattering amplitude is via the vertex functions F_i and \bar{F}_i which themselves have all possible dressings.

$NN \leftrightarrow \pi d$, and $\pi d \rightarrow \pi d$

Similarly, we can derive equations for the $NN \leftrightarrow \pi d$ and $\pi d \rightarrow \pi d$ amplitudes by defining column and row matrices

$$\Psi_d = \begin{pmatrix} 0 \\ 0 \\ |\psi_3\rangle \end{pmatrix}, \quad \bar{\Psi}_d = \left(0 \quad 0 \quad \langle \psi_3 | \right), \quad (3.118)$$

and using these to take matrix elements of Equation 3.115. Altogether, we thus arrive at the following set of coupled πNN equations:

$$T_{NN}(E) = V_{NN}(E) + V_{NN}(E) D_0(E) T_{NN}(E) \quad (3.119a)$$

$$T_{dN}(E) = V_{dN}(E) + V_{dN}(E) D_0(E) T_{NN}(E) \quad (3.119b)$$

$$T_{Nd}(E) = V_{Nd}(E) + V_{NN}(E) D_0(E) T_{Nd}(E) \quad (3.119c)$$

$$T_{dd}(E) = V_{dd}(E) + V_{dN}(E) D_0(E) T_{Nd}(E) \quad (3.119d)$$

where the potentials and t -matrices are defined as

$$V_{NN} = \bar{F}_N G_0 U^0 G_0 F_N, \quad T_{NN} = \bar{F}_N G_0 U G_0 F_N, \quad (3.120a)$$

$$V_{dN} = \bar{\Psi}_d U^0 G_0 F_N, \quad T_{dN} = \bar{\Psi}_d U G_0 F_N, \quad (3.120b)$$

$$V_{Nd} = \bar{F}_N G_0 U^0 \Psi_d, \quad T_{Nd} = \bar{F}_N G_0 U \Psi_d, \quad (3.120c)$$

$$V_{dd} = \bar{\Psi}_d U^0 \Psi_d, \quad T_{dd} = \bar{\Psi}_d U \Psi_d. \quad (3.120d)$$

These scattering equations have the feature that all intermediate-state NN propagators D_0 are fully dressed; moreover, the D_0 are defined by the convolution of two dressed nucleon propagators, as in Equation 3.12, and thus contain all possible contributions allowed by the underlying model of nucleon dressing. In this way, the long-standing normalisation problem suffered by the unitary πNN equations has been overcome.

3-dimensional $NN - \pi NN$ convolution equations

Using Equation 3.111 to write Equation 3.70 as

$$U = \bar{I}G_0^{-1} + \bar{I}F_N D_0 \bar{F}_N G_0 U + \bar{I}w^0 G_0 U, \quad (3.121)$$

leads directly to $NN - \pi NN$ equations that have the same form as those derived by Afnan and Blankleider [33], but now with all nucleon propagators fully dressed. Indeed, defining the amplitudes

$$T_{\lambda N} = \sum_{j=1}^2 U_{\lambda j} G_0 F_j, \quad (3.122a)$$

$$T_{N\mu} = \sum_{i=1}^2 \bar{F}_i G_0 U_{i\mu}, \quad (3.122b)$$

$$T_{\lambda\mu} = U_{\lambda\mu}, \quad (3.122c)$$

one can use Equation 3.104 and Equation 3.105 in Equation 3.121 to obtain the coupled equations

$$T_{NN} = Z_{NN} (1 + D_0 T_{NN}) + \sum_{i\lambda\mu} \bar{F}_i \bar{\delta}_{i\lambda} G_0 w_{\lambda\mu}^0 G_0 T_{\mu N}, \quad (3.123a)$$

$$T_{\lambda N} = \sum_j \bar{\delta}_{\lambda j} F_j (1 + D_0 T_{NN}) + \sum_{\mu\nu} \bar{\delta}_{\lambda\mu} w_{\mu\nu}^0 G_0 T_{\nu N}, \quad (3.123b)$$

$$T_{N\mu} = \sum_i \bar{F}_i \bar{\delta}_{i\mu} + Z_{NN} D_0 T_{N\mu} + \sum_{i\lambda\nu} \bar{F}_i \bar{\delta}_{i\lambda} G_0 w_{\lambda\nu}^0 G_0 T_{\nu\mu}, \quad (3.123c)$$

$$T_{\lambda\mu} = \bar{\delta}_{\lambda\mu} G_0^{-1} + \sum_i \bar{\delta}_{\lambda i} F_i D_0 T_{N\mu} + \sum_{\eta\nu} \bar{\delta}_{\lambda\eta} w_{\eta\nu}^0 G_0 T_{\nu\mu}. \quad (3.123d)$$

where Z_{NN} is the one-pion exchange term

$$Z_{NN} = \bar{F}_N G_0 F_N. \quad (3.124)$$

These equations may be viewed as the extension of the Afnan and Blankleider equations to include fully dressed nucleons. Note that the on-shell amplitude operators are given by

$$T_{NN}, \quad T_{N\Delta_j} = T_{Nj}|\psi_j\rangle, \quad T_{Nd} = T_{N3}|\psi_3\rangle, \quad (3.125a)$$

$$T_{\Delta_i N} = \langle\psi_i|T_{iN}, \quad T_{\Delta_i\Delta_j} = \langle\psi_i|T_{ij}|\psi_j\rangle, \quad T_{\Delta_i d} = \langle\psi_i|T_{i3}|\psi_3\rangle, \quad (3.125b)$$

$$T_{dN} = \langle\psi_3|T_{3N}, \quad T_{d\Delta_j} = \langle\psi_3|T_{3j}|\psi_j\rangle, \quad T_{dd} = \langle\psi_3|T_{33}|\psi_3\rangle. \quad (3.125c)$$

We note that in order to solve Equations 3.119 for the physical amplitudes, one first needs to construct the potentials as defined in Equations 3.120, and that means having to solve Equation 3.114 for the matrix of NN -irreducible amplitudes U^0 . Despite initial appearances, Equation 3.114 for U^0 differs markedly from the standard three-body AGS equation in that it involves input interactions, w_4^0 and w_5^0 , which are non-pair-like. Similarly, Equations 3.123 involve these non-pair-like terms. For this reason, we devote the next section to a formulation of πNN equations that involve only pair-like interactions, however, at the expense of introducing an extra dimension in the NN channels.

3.5 4-dimensional scattering equations

Here we introduce an alternative decomposition of w_α to that given in Equation 3.110. Namely, for $i \neq j$,

$$w_i = \bar{w}_i^P + \bar{w}_i^0 \quad (3.126)$$

where \bar{w}_i^P and \bar{w}_i^0 are formed, respectively, from the convolution of the pole and background parts of the πN t -matrix t_i , with the spectator dressed nucleon propagator g_j ; thus

$$G_0 \bar{w}_i^P G_0 = (D_{0i} f_i g_i \bar{f}_i D_{0i}) \otimes g_j, \quad (3.127a)$$

$$G_0 \bar{w}_i^0 G_0 = (D_{0i} t_i^b D_{0i}) \otimes g_j. \quad (3.127b)$$

By also defining

$$\bar{w}_3^P = 0, \quad \bar{w}_4^P = w_4, \quad \bar{w}_5^P = w_5, \quad (3.128a)$$

$$\bar{w}_3^0 = w_3, \quad \bar{w}_4^0 = 0, \quad \bar{w}_5^0 = 0, \quad (3.128b)$$

we can now write generally

$$w_\alpha = \bar{w}_\alpha^P + \bar{w}_\alpha^0. \quad (3.129)$$

Enumerating the above relations, we have for the pole parts \bar{w}_α^P

$$G_0 \bar{w}_1^P G_0 = (D_{01} f_1 g_1 \bar{f}_1 D_{01}) \otimes g_2 \quad (3.130a)$$

$$G_0 \bar{w}_2^P G_0 = (D_{02} f_2 g_2 \bar{f}_2 D_{02}) \otimes g_1 \quad (3.130b)$$

$$G_0 \bar{w}_3^P G_0 = 0 \quad (3.130c)$$

$$G_0 \bar{w}_4^P G_0 = (D_{01} f_1 g_1) \otimes (g_2 \bar{f}_2 D_{02}) \quad (3.130d)$$

$$G_0 \bar{w}_5^P G_0 = (D_{02} f_2 g_2) \otimes (g_1 \bar{f}_1 D_{01}) \quad (3.130e)$$

and for the background parts \bar{w}_α^0 ,

$$G_0 \bar{w}_1^0 G_0 = (D_{01} t_1^b D_{01}) \otimes g_2 \quad (3.131a)$$

$$G_0 \bar{w}_2^0 G_0 = (D_{02} t_2^b D_{02}) \otimes g_1 \quad (3.131b)$$

$$G_0 \bar{w}_3^0 G_0 = (D_{03} t_3 D_{03}) \otimes g_3 \quad (3.131c)$$

$$G_0 \bar{w}_4^0 G_0 = 0 \quad (3.131d)$$

$$G_0 \bar{w}_5^0 G_0 = 0. \quad (3.131e)$$

By analogy with Equation 3.112, we now write the above quantities in matrix form by defining

$$w = \bar{w}^P + \bar{w}^0 \quad (3.132)$$

where

$$w = \begin{pmatrix} w_1 & w_4 & 0 \\ w_5 & w_2 & 0 \\ 0 & 0 & w_3 \end{pmatrix}, \quad \bar{w}^P = \begin{pmatrix} \bar{w}_1^P & \bar{w}_4^P & 0 \\ \bar{w}_5^P & \bar{w}_2^P & 0 \\ 0 & 0 & 0 \end{pmatrix}, \quad \bar{w}^0 = \begin{pmatrix} \bar{w}_1^0 & 0 & 0 \\ 0 & \bar{w}_2^0 & 0 \\ 0 & 0 & \bar{w}_3^0 \end{pmatrix}. \quad (3.133)$$

In order to help focus on the two-nucleon contributions to the convolution relations of Equations 3.130, it is useful to introduce a short-hand notation illustrated generally by

$$(ab)_{\alpha z} = a_\alpha(z) b_\alpha(z), \quad (3.134a)$$

$$(ab)_{\alpha \bar{z}} = a_\alpha(E - z) b_\alpha(E - z). \quad (3.134b)$$

Using this notation, we write Equations 3.130 showing the convolution integrals explicitly,

$$G_0 \bar{w}_1^P G_0 = \left(-\frac{1}{2\pi i} \right) \int_{-\infty}^{\infty} dz (D_0 f)_{1\bar{z}} g_1(E-z) g_2(z) (\bar{f} D_0)_{1\bar{z}} \quad (3.135a)$$

$$G_0 \bar{w}_2^P G_0 = \left(-\frac{1}{2\pi i} \right) \int_{-\infty}^{\infty} dz (D_0 f)_{2z} g_1(E-z) g_2(z) (\bar{f} D_0)_{2z} \quad (3.135b)$$

$$G_0 \bar{w}_3^P G_0 = 0 \quad (3.135c)$$

$$G_0 \bar{w}_4^P G_0 = \left(-\frac{1}{2\pi i} \right) \int_{-\infty}^{\infty} dz (D_0 f)_{1\bar{z}} g_1(E-z) g_2(z) (\bar{f} D_0)_{2z} \quad (3.135d)$$

$$G_0 \bar{w}_5^P G_0 = \left(-\frac{1}{2\pi i} \right) \int_{-\infty}^{\infty} dz (D_0 f)_{2z} g_1(E-z) g_2(z) (\bar{f} D_0)_{1\bar{z}}. \quad (3.135e)$$

Thus the Green's function corresponding to the matrix \bar{w}^P can be written as

$$G_0 \bar{w}^P G_0 = \left(-\frac{1}{2\pi i} \right) \int_{-\infty}^{\infty} dz \Psi_N(z) g(E-z) g(z) \bar{\Psi}_N(z) \quad (3.136)$$

where $\Psi_N(z)$ and $\bar{\Psi}_N(z)$ are column and row matrices defined by

$$\Psi_N(z) = \begin{bmatrix} (D_0 f)_{1\bar{z}} \\ (D_0 f)_{2z} \\ 0 \end{bmatrix}, \quad \bar{\Psi}_N(z) = \begin{bmatrix} (\bar{f} D_0)_{1\bar{z}} & (\bar{f} D_0)_{2z} & 0 \end{bmatrix}. \quad (3.137)$$

Note that $\Psi_N(z)$ and $\bar{\Psi}_N(z)$ depend on energy E , but we do not show this explicitly to save on notation. Also, in Equation 3.136, we have dropped the particle labels on the propagators g as these propagators are identical functions.

With the decomposition of the w matrix as in Equation 3.132, the AGS equations, Equation 3.70, can themselves be expressed, by analogy with Equation 3.114 and Equation 3.115, as

$$\bar{U}^0 = \bar{I} G_0^{-1} + \bar{I} \bar{w}^0 G_0 \bar{U}^0 \quad (3.138)$$

and

$$U = \bar{U}^0 + \bar{U}^0 G_0 \bar{w}^P G_0 U. \quad (3.139)$$

Using Equation 3.136 in Equation 3.139 and multiplying on the left and right by $\bar{\Psi}_N(z')$ and $\Psi_N(z)$, respectively, one obtains a 4D integral equation for NN scattering:

$$\begin{aligned} T_{NN}(z', z; E) &= V_{NN}(z', z; E) \\ &+ \left(-\frac{1}{2\pi i} \right) \int_{-\infty}^{\infty} dz'' V_{NN}(z', z''; E) g(E-z'') g(z'') T_{NN}(z'', z; E) \end{aligned} \quad (3.140)$$

where the NN potential $V_{NN}(z', z; E)$ and t -matrix $T_{NN}(z', z; E)$ are defined as

$$V_{NN}(z', z; E) = \bar{\Psi}_N(z') \bar{U}^0(E) \Psi_N(z), \quad (3.141)$$

$$T_{NN}(z', z; E) = \bar{\Psi}_N(z') U(E) \Psi_N(z). \quad (3.142)$$

Equation 3.140 is an operator equation in the space of momenta of the two nucleons. As such, the “4D” label given to this equation refers to the fact that once momentum matrix elements of this equation are taken, a numerical 4-dimensional integral equation results. Equation 3.140 is analogous to the Bethe-Salpeter equation of covariant QFT with the z variable playing the role of the 0th component of a 4-momentum. Indeed, taking the 3-momentum matrix element of Equation 3.140 results in the equation

$$\begin{aligned} T_{NN}(p', p; P) &= V_{NN}(p', p; P) \\ &+ \left(-\frac{1}{2\pi i} \right) \int d^4p V_{NN}(p', p''; P) g(E - z'', \mathbf{P} - \mathbf{p}'') g(z'', \mathbf{p}'') T_{NN}(p'', p; P) \end{aligned} \quad (3.143)$$

where p , p' , p'' , and P are 4-momenta defined by $p = (z, \mathbf{p})$, $p' = (z', \mathbf{p}')$, $p'' = (z'', \mathbf{p}'')$, and $P = (E, \mathbf{P})$ where \mathbf{P} is the total momentum of the two nucleon system. Moreover, for on-shell values of p and p' , one has that $E - z = E_{N_1} + m_1$, $z = E_{N_2} + m_2$, $E - z' = E'_{N_1} + m_1$, and $z' = E'_{N_2} + m_2$, so that

$$\begin{aligned} \Psi_N(z) &= \begin{bmatrix} (D_0 f)_{1\bar{z}} \\ (D_0 f)_{2z} \\ 0 \end{bmatrix} = \begin{bmatrix} D_{01}(E_{N_1} + m_1) f_1(E_{N_1} + m_1) \\ D_{02}(E_{N_2} + m_2) f_2(E_{N_2} + m_2) \\ 0 \end{bmatrix} \quad (\text{on-shell}) \\ &= \begin{bmatrix} G_0 F_1(E) \\ G_0 F_2(E) \\ 0 \end{bmatrix} = G_0 F_N(E) \end{aligned} \quad (3.144)$$

where Equation 3.93 and Equation 3.104 have been used. Similarly,

$$\bar{\Psi}_N(z) = \bar{F}_N G_0(E) \quad (\text{on-shell}) \quad (3.145)$$

This shows that for z and z' on-shell, the 4D NN t -matrix of Equation 3.142 coincides with the physical NN t -matrix previously specified in Equation 3.105.

Similarly, using Equation 3.136 in Equation 3.139 and multiplying on the left and right

by $\bar{\Psi}_d$ and Ψ_d , respectively, leads to the set of equations

$$T_{NN}(z', z; E) = V_{NN}(z', z; E) + \left(-\frac{1}{2\pi i}\right) \int_{-\infty}^{\infty} dz'' V_{NN}(z', z''; E) g(E - z'') g(z'') T_{NN}(z'', z; E) \quad (3.146a)$$

$$T_{dN}(z; E) = V_{dN}(z; E) + \left(-\frac{1}{2\pi i}\right) \int_{-\infty}^{\infty} dz'' V_{dN}(z''; E) g(E - z'') g(z'') T_{NN}(z'', z; E) \quad (3.146b)$$

$$T_{Nd}(z'; E) = V_{Nd}(z'; E) + \left(-\frac{1}{2\pi i}\right) \int_{-\infty}^{\infty} dz'' V_{NN}(z', z''; E) g(E - z'') g(z'') T_{Nd}(z''; E) \quad (3.146c)$$

$$T_{dd}(E) = V_{dd}(E) + \left(-\frac{1}{2\pi i}\right) \int_{-\infty}^{\infty} dz'' V_{dN}(z''; E) g(E - z'') g(z'') T_{Nd}(z''; E) \quad (3.146d)$$

where

$$V_{NN}(z', z; E) = \bar{\Psi}_N(z') \bar{U}^0 \Psi_N(z), \quad T_{NN}(z', z; E) = \bar{\Psi}_N(z') U \Psi_N(z), \quad (3.147a)$$

$$V_{dN}(z; E) = \bar{\Psi}_d \bar{U}^0 \Psi_N(z), \quad T_{dN}(z; E) = \bar{\Psi}_d U \Psi_N(z), \quad (3.147b)$$

$$V_{Nd}(z'; E) = \bar{\Psi}_N(z') \bar{U}^0 \Psi_d, \quad T_{Nd}(z'; E) = \bar{\Psi}_N(z') U \Psi_d, \quad (3.147c)$$

$$V_{dd}(E) = \bar{\Psi}_d \bar{U}^0 \Psi_d, \quad T_{dd}(E) = \bar{\Psi}_d U \Psi_d. \quad (3.147d)$$

Equations 3.146 and 3.147 are 4D equations that have an identical structure to that of the 3D equations of Equation 3.119 and Equation 3.120. However, the 4D equations utilise potentials that require the solution of an AGS equation, Equation 3.138, involving only pair-interactions, while the potentials of the 3D equations require the solution of an AGS-like equation, Equation 3.114, whose kernel contains complicated disconnected three-body forces. This suggests that the 4D equations, despite their extra dimension, would be easier to solve numerically than the otherwise equivalent 3D equations.

4-dimensional $NN - \pi NN$ convolution equations

As was done for the derivation of the 3D $NN - \pi NN$ convolution equations, Equation 3.123, we begin with Equation 3.70, but now use the decomposition of w specified by Equation 3.132, so that

$$U = \bar{I}G_0^{-1} + \bar{I}G_0^{-1} (G_0 \bar{w}^P G_0) U + \bar{I}G_0^{-1} (G_0 \bar{w}^0 G_0) U. \quad (3.148)$$

Then using Equations 3.131 and Equation 3.136, we obtain the root equation from which the 4D $NN - \pi NN$ convolution equations follow,

$$\begin{aligned}
 U_{\lambda\mu} = & \bar{\delta}_{\lambda\mu} G_0^{-1} + \left(-\frac{1}{2\pi i} \right) \sum_{ij} \bar{\delta}_{\lambda i} G_0^{-1} \int_{-\infty}^{\infty} dz'' \Psi_{Ni}(z'') g(E - z'') g(z'') \bar{\Psi}_{Nj}(z'') U_{j\mu} \\
 & + \left(-\frac{1}{2\pi i} \right) \sum_{\alpha} \bar{\delta}_{\lambda\alpha} G_0^{-1} \int_{-\infty}^{\infty} dz'' D_{0\alpha}(E - z'') t_{\alpha}^b(E - z'') D_{0\alpha}(E - z'') g_{\alpha}(z'') U_{\alpha\mu}. \quad (3.149)
 \end{aligned}$$

To derive 4D equations that have the same form as the 3D $NN - \pi NN$ convolution equations, Equations 3.123, we define matrices

$$\Phi_N(z) = G_0^{-1}(E) \Psi_N(z) = G_0^{-1}(E) \begin{bmatrix} (D_0 f)_{1\bar{z}} \\ (D_0 f)_{2z} \\ 0 \end{bmatrix}, \quad (3.150a)$$

$$\bar{\Phi}_N(z) = \bar{\Psi}_N(z) G_0^{-1}(E) = \begin{bmatrix} (\bar{f} D_0)_{1\bar{z}} & (\bar{f} D_0)_{2z} & 0 \end{bmatrix} G_0^{-1}(E), \quad (3.150b)$$

whose i 'th element corresponds to a πNN vertex function where the pion is produced or annihilated on nucleon i . We also define the amplitudes

$$T_{\lambda N}(z) = \sum_j U_{\lambda j} \Psi_{Nj}(z), \quad (3.151)$$

$$T_{N\mu}(z') = \sum_i \bar{\Psi}_{Ni}(z') U_{i\mu}, \quad (3.152)$$

$$T_{\lambda\mu} = U_{\lambda\mu}, \quad (3.153)$$

which for on-shell values of z , z' , and E , coincide with the corresponding amplitudes in Equations 3.122, used for the 3D formulation. Then, multiplying Equation 3.149 on the left by $\bar{\Psi}_{N\lambda}(z')$ and on the right by $\Psi_{N\mu}(z)$, and summing over λ and μ , as appropriate, one

obtains the set of coupled equations

$$\begin{aligned}
 T_{NN}(z', z) &= Z_{NN}(z', z) + \left(-\frac{1}{2\pi i}\right) \int_{-\infty}^{\infty} dz'' Z_{NN}(z', z'')g(E - z'')g(z'')T_{NN}(z'', z) \\
 &+ \left(-\frac{1}{2\pi i}\right) \sum_{i\alpha} \bar{\Phi}_{Ni}(z')\bar{\delta}_{i\alpha} \int_{-\infty}^{\infty} dz'' D_{0\alpha}(E - z'')t_{\alpha}^b(E - z'')D_{0\alpha}(E - z'')g_{\alpha}(z'')T_{\alpha N}(z),
 \end{aligned} \tag{3.154a}$$

$$\begin{aligned}
 T_{\lambda N}(z) &= \sum_j \bar{\delta}_{\lambda j} \bar{\Phi}_{Nj}(z) \\
 &+ \left(-\frac{1}{2\pi i}\right) \sum_i \bar{\delta}_{\lambda i} \int_{-\infty}^{\infty} dz'' \bar{\Phi}_{Ni}(z'')g(E - z'')g(z'')T_{NN}(z'', z) \\
 &+ \left(-\frac{1}{2\pi i}\right) \sum_{\alpha} \bar{\delta}_{\lambda\alpha} G_0^{-1} \int_{-\infty}^{\infty} dz'' D_{0\alpha}(E - z'')t_{\alpha}^b(E - z'')D_{0\alpha}(E - z'')g_{\alpha}(z'')T_{\alpha N}(z),
 \end{aligned} \tag{3.154b}$$

$$\begin{aligned}
 T_{N\mu}(z') &= \sum_i \bar{\delta}_{i\mu} \bar{\Phi}_{Ni}(z') + \left(-\frac{1}{2\pi i}\right) \int_{-\infty}^{\infty} dz'' Z_{NN}(z', z'')g(E - z'')g(z'')T_{N\mu}(z'') \\
 &+ \left(-\frac{1}{2\pi i}\right) \sum_{i\alpha} \bar{\delta}_{i\alpha} \bar{\Phi}_{Ni}(z') \int_{-\infty}^{\infty} dz'' D_{0\alpha}(E - z'')t_{\alpha}^b(E - z'')D_{0\alpha}(E - z'')g_{\alpha}(z'')T_{\alpha\mu},
 \end{aligned} \tag{3.154c}$$

$$\begin{aligned}
 T_{\lambda\mu} &= \bar{\delta}_{\lambda\mu} G_0^{-1} + \left(-\frac{1}{2\pi i}\right) \sum_i \bar{\delta}_{\lambda i} G_0^{-1} \int_{-\infty}^{\infty} dz'' \bar{\Psi}_{Ni}(z'')g(E - z'')g(z'')T_{N\mu}(z'') \\
 &+ \left(-\frac{1}{2\pi i}\right) \sum_{\alpha} \bar{\delta}_{\lambda\alpha} G_0^{-1} \int_{-\infty}^{\infty} dz'' D_{0\alpha}(E - z'')t_{\alpha}^b(E - z'')D_{0\alpha}(E - z'')g_{\alpha}(z'')T_{\alpha\mu},
 \end{aligned} \tag{3.154d}$$

where

$$Z_{NN}(z', z) = \sum_{ij} \bar{\Psi}_{Ni}(z')\bar{\delta}_{ij}G_0^{-1}(E)\Psi_{Nj}(z). \tag{3.155}$$

These are the 4D $NN - \pi NN$ convolution equations (4D πNN convolution equations) whose structure is formally similar to that of the 3D $NN - \pi NN$ convolution equations (3D πNN convolution equations), Equations 3.123; however, Equations 3.154 involve only pair-wise interactions and thus may be more practical for numerical solution.

3.5.1 4-dimensional equations for separable potentials

Despite the 4D convolution equations, Equations 3.154, appearing easier to solve than the corresponding 3D ones, Equations 3.123, solving 4-dimensional three-body equations is still a formidable numerical task. To reduce the complexity of their solution, one can use a separable potential approximation for the input πN and NN interactions, which would effectively reduce the problem down to a two-body problem, albeit still 4-dimensional.

To use the separable approximation, we first need to perform a partial wave expansion of the background two-body t -matrices t_α^b . To do this we introduce the two-body partial wave basis states $|\omega_{l_\alpha s_\alpha}^{j_\alpha t_\alpha}\rangle$ defined for the (bc) particle pair by

$$\begin{aligned} |\omega_{l_\alpha s_\alpha}^{j_\alpha t_\alpha}\rangle |m_{j_\alpha} m_{t_\alpha}\rangle &= \sum_{\substack{m_{\sigma_b}, m_{\sigma_c}, m_{\tau_b}, m_{\tau_c} \\ m_{l_\alpha}, m_{s_\alpha}}} \int d\hat{p}_\alpha \langle l_\alpha m_{l_\alpha} s_\alpha m_{s_\alpha} | j_\alpha m_{j_\alpha} \rangle \langle \sigma_b m_{\sigma_b} \sigma_c m_{\sigma_c} | s_\alpha m_{s_\alpha} \rangle \\ &\times \langle \tau_b m_{\tau_b} \tau_c m_{\tau_c} | t_\alpha m_{t_\alpha} \rangle Y_{l_\alpha m_{l_\alpha}}(\hat{p}_\alpha) |\sigma_b m_{\sigma_b} \sigma_c m_{\sigma_c}, \tau_b m_{\tau_b} \tau_c m_{\tau_c}, \hat{p}_\alpha\rangle \end{aligned} \quad (3.156)$$

where l_α is the relative orbital angular momentum quantum number, s_α is the sum of the particle spins (σ_b and σ_c), j_α is the total angular momentum of the pair, and t_α is sum of the particle isospins (τ_b and τ_c). Because of rotational invariance, the states $|m_{j_\alpha} m_{t_\alpha}\rangle$ do not appear in final expressions and so may effectively be dropped at this stage. To save on notation we shall write $|\omega_{l_\alpha s_\alpha}^{j_\alpha t_\alpha}\rangle = |\omega_{n_\alpha}\rangle$ where $n_\alpha = \{l_\alpha, s_\alpha, j_\alpha, t_\alpha\}$. The partial wave expansion of $t_\alpha^b(e)$ may thus be expressed as

$$t_\alpha^b(e) = \sum_{n'_\alpha n_\alpha} |\omega_{n'_\alpha}\rangle t_{n'_\alpha, n_\alpha}^b(e) \langle \omega_{n_\alpha} | \quad (3.157)$$

where now the partial wave t -matrix $t_{n'_\alpha, n_\alpha}^b(e)$ is assumed to be of separable form

$$t_{n'_\alpha, n_\alpha}^b(e) = |h_{n'_\alpha}\rangle \tau_{n'_\alpha, n_\alpha}(e) \langle h_{n_\alpha} | \quad (3.158)$$

where $|h_{n_\alpha}\rangle$ and $\langle h_{n_\alpha} |$ are energy-independent form factor states in radial relative momentum (p_α) space. One can thus write

$$t_\alpha^b(e) = \sum_{n'_\alpha n_\alpha} |\eta_{n'_\alpha}\rangle \tau_{n'_\alpha, n_\alpha}(e) \langle \eta_{n_\alpha} | \quad (3.159)$$

where

$$|\eta_{n_\alpha}\rangle \equiv |\omega_{n'_\alpha}\rangle |h_{n'_\alpha}\rangle, \quad \langle \eta_{n_\alpha} | \equiv \langle \omega_{n'_\alpha} | \langle h_{n'_\alpha} |. \quad (3.160)$$

We minimise notation further by writing Equation 3.159 in matrix form as

$$t_\alpha^b(e) \equiv |\eta_\alpha\rangle \tau_\alpha(e) \langle \eta_\alpha| \quad (3.161)$$

where $|\eta_\alpha\rangle$ is a row matrix, $\tau_\alpha(e)$ is a square matrix, and $\langle \eta_\alpha|$ is a column matrix.

To help identify the type of quasiparticle implied by a separable interaction, we shall label sub-system πN_i channels by subscript Δ_i and sub-system NN channels by subscript d ; for example, the quasiparticle propagator matrix τ_α will be written such that $\tau_i \equiv \tau_{\Delta_i}$ for $i = 1, 2$, and $\tau_3 \equiv \tau_d$. Then, substituting Equation 3.161 into Equations 3.154 suggests defining the amplitudes

$$\begin{aligned} X_{NN}(z', z) &= T_{NN}(z', z), \\ X_{\Delta_i N}(z', z) &= \langle \eta_i | D_{0i}(E - z') T_{iN}(z), \\ X_{dN}(z', z) &= \langle \eta_3 | D_{03}(E - z') T_{3N}(z), \\ X_{N\Delta_j}(z', z) &= T_{Nj}(z') D_{0j}(E - z) | \eta_j \rangle, \\ X_{Nd}(z', z) &= T_{N3}(z') D_{03}(E - z) | \eta_3 \rangle, \\ X_{\Delta_i \Delta_j}(z', z) &= \langle \eta_i | D_{0i}(E - z') T_{ij} D_{0j}(E - z) | \eta_j \rangle, \\ X_{\Delta_i d}(z', z) &= \langle \eta_i | D_{0i}(E - z') T_{i3} D_{03}(E - z) | \eta_3 \rangle, \\ X_{dd}(z', z) &= \langle \eta_3 | D_{03}(E - z') T_{33} D_{03}(E - z) | \eta_3 \rangle, \end{aligned} \quad (3.162)$$

with Equations 3.154 then being written as

$$\begin{aligned}
 X_{NN}(z', z) &= Z_{NN}(z', z) + \left(-\frac{1}{2\pi i}\right) \int_{-\infty}^{\infty} dz'' Z_{NN}(z', z'') g_N(E - z'') g_N(z'') X_{NN}(z'', z) \\
 &+ \left(-\frac{1}{2\pi i}\right) \sum_j \int_{-\infty}^{\infty} dz'' Z_{N\Delta_j}(z', z'') \tau_{\Delta_j}(E - z'') g_N(z'') X_{\Delta_j N}(z'', z) \\
 &+ \left(-\frac{1}{2\pi i}\right) \int_{-\infty}^{\infty} dz'' Z_{Nd}(z', z'') \tau_d(E - z'') g_\pi(z'') X_{dN}(z'', z), \tag{3.163a}
 \end{aligned}$$

$$\begin{aligned}
 X_{\Delta_i N}(z', z) &= Z_{\Delta_i N}(z', z) + \left(-\frac{1}{2\pi i}\right) \int_{-\infty}^{\infty} dz'' Z_{\Delta_i N}(z', z'') g_N(E - z'') g_N(z'') X_{NN}(z'', z) \\
 &+ \left(-\frac{1}{2\pi i}\right) \sum_j \int_{-\infty}^{\infty} dz'' Z_{\Delta_i \Delta_j}(z', z'') \tau_{\Delta_j}(E - z'') g_N(z'') X_{\Delta_j N}(z'', z) \\
 &+ \left(-\frac{1}{2\pi i}\right) \int_{-\infty}^{\infty} dz'' Z_{\Delta_i d}(z', z'') \tau_d(E - z'') g_\pi(z'') X_{dN}(z'', z), \tag{3.163b}
 \end{aligned}$$

$$\begin{aligned}
 X_{dN}(z', z) &= Z_{dN}(z', z) + \left(-\frac{1}{2\pi i}\right) \int_{-\infty}^{\infty} dz'' Z_{dN}(z', z'') g_N(E - z'') g_N(z'') X_{NN}(z'', z) \\
 &+ \left(-\frac{1}{2\pi i}\right) \sum_j \int_{-\infty}^{\infty} dz'' Z_{d\Delta_j}(z', z'') \tau_{\Delta_j}(E - z'') g_N(z'') X_{\Delta_j N}(z'', z), \tag{3.163c}
 \end{aligned}$$

$$\begin{aligned}
 X_{Nd}(z', z) &= Z_{Nd}(z', z) + \left(-\frac{1}{2\pi i}\right) \int_{-\infty}^{\infty} dz'' Z_{NN}(z', z'') g_N(E - z'') g_N(z'') X_{Nd}(z'', z) \\
 &+ \left(-\frac{1}{2\pi i}\right) \sum_j \int_{-\infty}^{\infty} dz'' Z_{N\Delta_j}(z', z'') \tau_{\Delta_j}(E - z'') g_N(z'') X_{\Delta_j d}(z'', z), \\
 &+ \left(-\frac{1}{2\pi i}\right) \int_{-\infty}^{\infty} dz'' Z_{Nd}(z', z'') \tau_d(E - z'') g_\pi(z'') X_{dd}(z'', z), \tag{3.163d}
 \end{aligned}$$

$$\begin{aligned}
 X_{\Delta_i d}(z', z) &= Z_{\Delta_i d}(z', z) + \left(-\frac{1}{2\pi i}\right) \int_{-\infty}^{\infty} dz'' Z_{\Delta_i N}(z', z'') g_N(E - z'') g_N(z'') X_{Nd}(z'', z) \\
 &+ \left(-\frac{1}{2\pi i}\right) \sum_j \int_{-\infty}^{\infty} dz'' Z_{\Delta_i \Delta_j}(z', z'') \tau_{\Delta_j}(E - z'') g_N(z'') X_{\Delta_j d}(z'', z), \\
 &+ \left(-\frac{1}{2\pi i}\right) \int_{-\infty}^{\infty} dz'' Z_{\Delta_i d}(z', z'') \tau_d(E - z'') g_\pi(z'') X_{dd}(z'', z), \tag{3.163e}
 \end{aligned}$$

$$\begin{aligned}
 X_{dd}(z', z) &= \left(-\frac{1}{2\pi i}\right) \int_{-\infty}^{\infty} dz'' Z_{dN}(z', z'') g_N(E - z'') g_N(z'') X_{Nd}(z'', z) \\
 &+ \left(-\frac{1}{2\pi i}\right) \sum_j \int_{-\infty}^{\infty} dz'' Z_{d\Delta_j}(z', z'') \tau_{\Delta_j}(E - z'') g_N(z'') X_{\Delta_j d}(z'', z). \tag{3.163f}
 \end{aligned}$$

where

$$Z_{NN}(z', z) = \sum_{ij} \bar{\Phi}_{Ni}(z') \bar{\delta}_{ij}(E) G_0(E) \Phi_{Nj}(z) \quad (3.164a)$$

$$Z_{\Delta_i N}(z', z) = \sum_j \langle \eta_i | D_{0i}(E - z') \bar{\delta}_{ij} \Phi_{Nj}(z) \rangle \quad (3.164b)$$

$$Z_{dN}(z', z) = \sum_j \langle \eta_3 | D_{03}(E - z') \Phi_{Nj}(z) \rangle \quad (3.164c)$$

$$Z_{\Delta_i d}(z', z) = \langle \eta_i | D_{0i}(E - z') \bar{\delta}_{ij} G_0^{-1}(E) D_{03}(E - z) | \eta_3 \rangle \quad (3.164d)$$

$$Z_{\Delta_i \Delta_j}(z', z) = \langle \eta_i | D_{0i}(E - z') \bar{\delta}_{ij} G_0^{-1}(E) D_{0j}(E - z) | \eta_j \rangle. \quad (3.164e)$$

These kernels can be written out in more detail by using the definition of Ψ_N and $\bar{\Psi}_N$ given in Equation 3.137. Thus the kernel for NN scattering, $Z_{NN}(z', z)$, is a sum of two terms:

$$\begin{aligned} Z_{NN}(z', z) &= \bar{f}_1(E - z') D_{01}(E - z') G_0^{-1}(E) D_{02}(z) f_2(z) \\ &\quad + \bar{f}_2(z') D_{02}(z') G_0^{-1}(E) D_{01}(E - z) f_1(E - z) \end{aligned} \quad (3.165)$$

and corresponds to the two time orderings of the NN one-pion-exchange potential (OPE).

Chapter 4

Numerical techniques

4.1 Introduction

This chapter is devoted to the development of various numerical techniques used to solve our 4-dimensional πNN convolution equations.

In the derivation of the πNN convolution equations, it was crucial that connected three-body forces were neglected. However, the neglect of connected three-body forces results in missing diagrams in the πNN convolution equations that leads to connected diagrams not being fully dressed, such as the one-pion exchange (OPE) diagram. We would now like to determine the effect that neglecting these connected three-body forces has on the πNN convolution equations and determine whether this missing dressing is essential. To determine this, we numerically calculate one- and two-pion exchange amplitudes and compare these to a numerical calculation of the amplitudes from the πNN convolution equations. We suspect the contribution of these connected three-body forces on the πNN convolution equations to be minimal, but it is worth exploring [86].

As discussed in the previous chapter, the 4-dimensional πNN convolution equations of Equations 3.154 appear easier to solve than the 3-dimensional version in Equations 3.123. Here, we focus on solving a simplified 4-dimensional $NN \rightarrow NN$ equation to provide a framework to solve our 4-dimensional equations and to develop our numerical techniques. This simplified 4-dimensional $NN \rightarrow NN$ equation is the same $NN \rightarrow NN$ equation given in Equation 3.163, however we only include NN intermediate channels and only calculate the ${}^3S_1 - {}^3D_1$ partial waves for $J^\pi = 1^+$ and $T = 0$. Additionally, we use a simplified NN Born term (Z -diagram) by approximating some kinematic elements of the Z -diagram.

Due to the moving singularities in the kernel of our 4-dimensional πNN convolution equations, these equations are still difficult to solve numerically. The approach we take in solving these equations is the spline interpolation method, which allows us to handle these moving singularities accurately and solve the equations through discretisation and matrix inversion. The spline interpolation method seems to be the only practically viable method for solving general 4-dimensional scattering equations [74].

We test the accuracy of this spline interpolation method by applying it to a 3-dimensional $NN \rightarrow NN$ equation from the “Unitary $NN - \pi NN$ ” model. We compare the calculation of the 3-dimensional equation using spline interpolation to the conventional method for solving these equations, namely contour rotation, to determine the accuracy and validity of this method.

4.2 Numerical calculation of dressed one-pion exchange

4.2.1 Partial wave decomposition

We now want to introduce a partial wave decomposition of the 4-dimensional πNN convolution equations, to reduce the number of dimensions to 2. As the extra dimension z , does not play a role in the integration of the angles, the partial wave decomposition of our 4-dimensional equations will be the same as for the 3-dimensional equations of Afnan and Thomas [29]. Therefore, we can follow the procedure of Afnan and Thomas, who provide a general expression for the partial wave Born amplitude (Z -diagram) in a quasiparticle model.

We introduce new notation that differs from the notation used by Afnan and Thomas, in order to avoid confusion with the spectator/nucleon participation notation in Table 3.1. We refer to this notation as “prime” notation, as it consists of a cyclic permutation of primes $(0, 1, 2) = (, ', '')$, where no primes refer to the initial state, one prime refers to the final state and two primes refers to the exchange particle (or the intermediate state). We assign the initial and final spectator the momentum \mathbf{p} and \mathbf{p}' respectively, and thus the initial and final quasiparticles will be assign the momentum $-\mathbf{p}$ and $-\mathbf{p}'$ respectively, as we are in the centre of mass system. However, if the final quasiparticle is a nucleon, then we assign it the momentum \mathbf{p}' (essentially we make the replacement $-\mathbf{p}' \rightarrow \mathbf{p}'$). The exchange particle is assigned the momentum \mathbf{p}'' , though we tend to replace by a combination of \mathbf{p} and \mathbf{p}' through momentum conservation at the vertices so we can use the double prime label when we integrate over intermediate momenta. The initial quasiparticle is labelled with total spin (isospin) \mathbf{j} (\mathbf{t}) and the final quasiparticle is labelled with total spin (isospin) \mathbf{j}' (\mathbf{t}'), while the initial spectator is labelled with spin (isospin) \mathbf{s} ($\boldsymbol{\tau}$) and the final spectator is labelled with spin (isospin) \mathbf{s}' ($\boldsymbol{\tau}'$).

The coupling scheme used is that in which the quasiparticle spin angular momentum j is coupled to the spectator particles spin s to obtain the total spin S

$$\begin{aligned}\mathbf{S}' &= \mathbf{j}' + \mathbf{s}', \\ \mathbf{S} &= \mathbf{j} + \mathbf{s}.\end{aligned}\tag{4.1}$$

This is commonly known as LS coupling. We find the quasiparticle’s spin in the following

way

$$\begin{aligned}
 \mathbf{S}' &= \mathbf{s}'' + \mathbf{s}, \\
 \mathbf{S} &= \mathbf{s}' + \mathbf{s}'', \\
 \mathbf{j}' &= \mathbf{l}' + \mathbf{S}', \\
 \mathbf{j} &= \mathbf{l} + \mathbf{S}.
 \end{aligned}
 \tag{4.2}$$

The orbital angular momentum L is specified by the partial wave being studied. The orbital angular momentum is then coupled to the total spin S to give the total angular momentum

$$\mathbf{J} = \mathbf{L} + \mathbf{S} = \mathbf{L}' + \mathbf{S}'.
 \tag{4.3}$$

Similarly, the isospin of the quasiparticle t is coupled to the spectator isospin τ to give the total isospin

$$\begin{aligned}
 \mathbf{T} &= \mathbf{t}' + \boldsymbol{\tau}', \\
 \mathbf{T} &= \mathbf{t} + \boldsymbol{\tau},
 \end{aligned}
 \tag{4.4}$$

where the isospin of the quasiparticles are given by

$$\begin{aligned}
 \mathbf{t} &= \boldsymbol{\tau}' + \boldsymbol{\tau}'', \\
 \mathbf{t}' &= \boldsymbol{\tau}'' + \boldsymbol{\tau}.
 \end{aligned}
 \tag{4.5}$$

For a two nucleon system, the total isospin T can either be 1 or 0. The total symmetry factor for the system is $(-1)^{L+S+T}$ which must be -1 , as the total wave-function has to be antisymmetric. This allows us to determine the total isospin T for each partial wave. Here, we use spectroscopic notation $\{^{2S+1}L_J\}$ to denote the partial waves for the scattering process and are interested in the ${}^3S_1 - {}^3D_1$ coupled channel.

The general Z -diagram with this labelling convention is given in Figure 4.1.

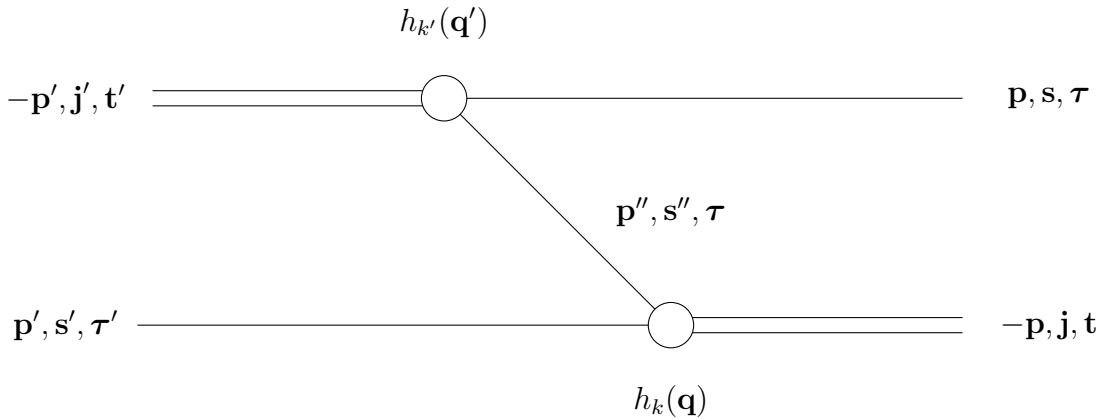


Figure 4.1: The general Z -diagram with our “prime” notation convention, whose partial wave expansion is given Afnan and Thomas [29].

The general partial wave Born amplitude corresponding to the diagram shown in Figure 4.1 can be determined by the following:

$$Z_{K',K}^{JT}(p', p; E) = \sum_{l',l,L} p'' p' \Gamma_{k',k}^L(p', p; E) \sum_{a=0}^{l'} \sum_{b=0}^l A_{K',K}^{L,a,b} \left(\frac{p'}{p} \right)^{a-b} \quad (4.6)$$

where

$$\Gamma_{k',k}^L(p', p; E) = \frac{1}{2} \int_{-1}^1 \frac{q'^{-l'} h_{k'}(q') h_k(q) q^{-l}}{E - p'^2/(2m') - p^2/2m - (p'')^2/(2m'')} P_L(x) dx \quad (4.7)$$

and

$$\mathbf{q}' = \rho' \mathbf{p}' - \mathbf{p}; \quad \mathbf{q} = \rho \mathbf{p} - \mathbf{p}' \text{ if the final quasiparticle is a nucleon,} \quad (4.8a)$$

$$\mathbf{q}' = -\rho' \mathbf{p}' - \mathbf{p}; \quad \mathbf{q} = \rho \mathbf{p} + \mathbf{p}' \text{ otherwise,} \quad (4.8b)$$

$$\rho' = \frac{m}{m + m''}; \quad \rho = \frac{m'}{m' + m''}, \quad (4.8c)$$

$$x = \hat{p}' \cdot \hat{p}. \quad (4.8d)$$

Here, m is the mass of the initial spectator, m' is the mass of the final spectator and m'' is the mass of the exchange particle. The subscript K is short-hand for the quantum numbers of the three-body system other than J and T , i.e. $K = \{tjSL\}$, while the subscript k refers to the quantum number of the two-body sub-system. In this equation, $P_L(x)$ is the Legendre polynomial of order L , while $h_{k'}$ is the form factor for the two-body channel k' corresponding to relative orbital angular momentum l' and equivalent for h_k . The coefficient $A_{K',K}^{L,a,b}$ can be determined using the procedure of Stingl and Rinat [87], given as

$$A_{K',K}^{L,a,b} = (-1)^{R} \hat{t} \hat{t}' \hat{l} \hat{l}' \hat{L}' \hat{L} \hat{S}' \hat{S} \hat{j}' \hat{j} \hat{S}' \hat{S} \hat{L} \hat{L} \rho'^a \rho^b \left[\frac{(2l' + 1)!(2l + 1)!}{(2a)!(2l - 2b)!(2l' - 2a)!(2b)!} \right] \\ \left\{ \begin{matrix} \tau & \tau'' & t' \\ \tau' & T & t \end{matrix} \right\} \sum_f \sum_{\Omega'} (\hat{f} \hat{\Omega} \hat{\Omega}')^2 \left\{ \begin{matrix} S' & S & f \\ L & L' & J \end{matrix} \right\} \left\{ \begin{matrix} s' & S' & S & s \\ j' & f & j & s_\gamma \\ S' & l' & l & S \end{matrix} \right\} \\ \left(\begin{matrix} \Omega' & L & L \\ 0 & 0 & 0 \end{matrix} \right) \left(\begin{matrix} \Omega & L & L' \\ 0 & 0 & 0 \end{matrix} \right) \left(\begin{matrix} l' - a & b & \Omega' \\ 0 & 0 & 0 \end{matrix} \right) \left(\begin{matrix} a & l - b & \Omega \\ 0 & 0 & 0 \end{matrix} \right) \left\{ \begin{matrix} L' & L & f \\ \Omega' & \Omega & L \end{matrix} \right\} \\ \left\{ \begin{matrix} l' & l & f \\ a & l - b & \Omega \\ l' & b & \Omega' \end{matrix} \right\} \quad (4.9)$$

where $\hat{a} \equiv (2a + 1)^{1/2}$ and the phase R is given by

$$R = -J + L' + L + S' + S + j' + j - s' + S + l' + \tau'' + \tau' - t + 2T + L. \quad (4.10)$$

The coefficient in the above expression also includes a $12j$ Wigner coefficient which is given by Ord-Smith [88].

4.2.2 4-dimensional NN Z -diagram

In order to determine the effect of neglecting connected three-body forces on the πNN convolution equations, we perform a numerical calculation of the fully dressed one-pion exchange (OPE) diagram found in Chapter 2 and compare it to the numerical calculation of the OPE diagram found in the πNN convolution equations. We now detail the numerical version of the fully dressed OPE diagram in Equation 2.32. In the following calculations, we will consider the ${}^3S_1 - {}^3D_1$ processes for $J^\pi = 1^+$ and $T = 0$. Using Galilean invariance on the dressed one-nucleon propagators

$$g(E, \mathbf{p}) = g\left(E - \frac{\mathbf{p}^2}{2m_N}, \mathbf{0}\right) = g(E - E_p) \quad (4.11)$$

where $E_p = \frac{\mathbf{p}^2}{2m_N}$. Using Galilean invariance, and assuming $m_\pi \ll m_N$, the dressed pion-nucleon vertices become

$$f(\mathbf{p}', \mathbf{p}, E) \approx f\left(\mathbf{p}' - \mathbf{p}, \mathbf{0}, E - \frac{\mathbf{p}^2}{2m_N}\right) = f(\mathbf{k}, E - E_p). \quad (4.12)$$

Therefore, the Green's function in Equation 2.32, without the momentum-conserving function δ , becomes

$$G_{12}^{OPE} = \left(-\frac{1}{2\pi i}\right)^2 \int dz dz' g(z' - E_{p_1}) \bar{f}(\mathbf{k}, z' - E_{p_1}) g(z - E_{p_1}) \frac{1}{z'^+ - z - \omega_k} g(E - z' - E_{p_2}) f(\mathbf{k}, E - z - E_{p_2}) g(E - z - E_{p_2}). \quad (4.13)$$

The variables k' and k denote the two-body partial wave channel of the πN . Because of parity conservation, pion creation (annihilation) on a nucleon only occurs in the P_{11} channel, so we can drop the references to k' and k and change our notation $\Gamma_{k',k}^L \rightarrow \Gamma_L$. Because we are considering the P_{11} partial wave for πN , the relative orbital angular momentum (l' and l) are both equal to 1. We approximate the quantities ρ' and ρ by assuming the mass of the nucleon is much greater than the mass of the pion. Thus, we have

$$\rho' = \rho = \frac{m_N}{m_N + m_\pi} \approx 1 \quad (4.14)$$

which allows the relative momentum to be exactly equal to the pion's momentum i.e. $\mathbf{q}' = \mathbf{k}$ and $\mathbf{q} = -\mathbf{k}$. Our corresponding Z -diagram, which we denote as $Z_{L'S'LS}^{OPE}$, becomes a function

of the extra z variable due to the convolution. Thus, our 4-dimensional Z -diagram $Z_{L'S'LS}^{OPE}$ is given by

$$Z_{L'S'LS}^{OPE}(z', p', z, p; E) = \sum_L p' p \Gamma_L(z', p', z, p; E) \sum_{a=0}^1 \sum_{b=0}^1 A_{L'S'LS}^{L,a,b} \left(\frac{p'}{p}\right)^{a-b} \quad (4.15)$$

where

$$\Gamma_L(z', p', z, p; E) = \frac{1}{2} \int_{-1}^1 k^{-1} \tilde{V}_{12}^{OPE}(z', p', z, p; E) k^{-1} P_L(x) dx \quad (4.16)$$

and \tilde{V}_{12}^{OPE} is the OPE Green's function with "chopped" nucleon legs

$$\tilde{V}_{12}^{OPE}(z', p', z, p; E) = \frac{\bar{f}(k, z' - E_{p_1}) f(k, E - z - E_{p_2})}{z'^+ - z - \omega_k}. \quad (4.17)$$

Here, we also have $k = |\mathbf{p}' - \mathbf{p}| = \sqrt{p'^2 + p^2 - 2p'p x}$. We note that this is a simplified calculation of the Z -diagram. When we come to calculating our different scattering processes in the πNN system, we will be more precise with the calculation of ρ' (ρ) and \mathbf{q}' (\mathbf{q}). For now, we only need a simple model to determine the effect of neglecting connected three-body forces, whereas we need to be more precise in our numerical calculations of the πNN equations, as we are interested in reproducing experimental data.

4.2.3 Calculation of the half off-shell OPE amplitude

When calculating the potential V_{12}^{OPE} , we "chop" the external legs using D_0 . When we consider the initial and/or the final process to be on-shell, the one-nucleon propagators corresponding to the external legs will be cancelled out by the corresponding D_0 . Thus, choosing the initial state to be on-shell i.e. $\mathbf{p} \rightarrow \mathbf{p}_0$, V_{12}^{OPE} becomes

$$V_{12}^{OPE} = \left(-\frac{1}{2\pi i}\right) \frac{1}{D_0(E - 2E_p)} \int dz' \frac{f(k, z' - E_p) f(k, m_N)}{z'^+ - E/2 - \omega_k} g(z' - E_p) g(E - z' - E_p). \quad (4.18)$$

Now, we need to calculate the z' integral. One can see that there are two poles below the real z' axis, but only one above the real z' axis. So, we choose to close the contour above the real z' axis, enclosing the pole belonging to the second dressed one-nucleon propagator in the equation above. We can use the dispersion relation of the dressed one-nucleon propagator to expose the pole, which is given by

$$g(E) = \frac{Z}{E^+ - m_N} - \frac{1}{\pi} \int_{m_N + m_\pi}^{\infty} d\omega \frac{\text{Im } g(\omega)}{E^+ - \omega} = \frac{Z}{E^+ - m_N} + g_c(E) \quad (4.19)$$

Using Cauchy's Residue Theorem to calculate the z' integral, V_{12}^{OPE} becomes

$$\begin{aligned}
 V_{12}^{OPE} &= f(k, m_N) \frac{1}{D_0(E - 2E_p)} \frac{Zg(E - 2E_p - m_N)f(k, E - 2E_p - m_N)}{E/2 - E_p - m - \omega_k} \\
 &\quad - \frac{1}{\pi} f(k, m_N) \frac{1}{D_0(E - 2E_p)} \int_{m_N + m_\pi}^{\infty} \frac{\text{Im } g(\omega)g(E - 2E_p - \omega)f(k, E - 2E_p - \omega)}{E/2 - E_p - \omega - \omega_k} d\omega.
 \end{aligned} \tag{4.20}$$

The first term is of no concern, however, the second term still contains the integral over ω , so we have to proceed with caution. There will be logarithmic singularities in ω after partial wave decomposition, due to the term in the denominator. However, this depends on our choice of the off-shell momentum p . So, if we choose a momentum that satisfies a particular condition, there will be no logarithmic singularities in the integral. This condition is

$$E/2 - E_p - \sqrt{m_\pi^2 + p^2 + p_0^2 \pm 2pp_0} < m_N + m_\pi. \tag{4.21}$$

In the absence of logarithmic singularities, the only singularity to consider is the pole due to the dressed one-nucleon propagator, which only occurs when $E - 2E_p - m_N > m_N + m_\pi$. If there is no pole present, we proceed with the integral over ω using Gaussian quadratures. If the pole is present, we use a subtraction method to handle the singularity. Denoting the pole as ω_0 , the omega integral becomes

$$\begin{aligned}
 &\int_{m_\pi + m}^{\infty} \frac{\text{Im } g(\omega)g(E - 2E_p - \omega)f(k, E - 2E_p - \omega)}{E/2 - E_p - \omega - \omega_k} d\omega \\
 &= \int_a^b \frac{\text{Im } g(\omega)g(E - 2E_p - \omega)f(k, E - 2E_p - \omega)}{E/2 - E_p - \omega - \omega_k} d\omega \\
 &\quad + \int_b^{\infty} \frac{\text{Im } g(\omega)g(E - 2E_p - \omega)f(k, E - 2E_p - \omega)}{E/2 - E_p - \omega - \omega_k} d\omega
 \end{aligned} \tag{4.22}$$

where $a = m_N + m_\pi$ and $a < \omega_0 < b$. The integral from a to b contains no pole, so there is no issue calculating this integral. Use the dispersion relation of $g(E)$ again, the integral from a to b becomes

$$\begin{aligned}
 &\int_a^b \frac{\text{Im } g(\omega)g(E - 2E_p - \omega)f(k, E - 2E_p - \omega)}{E/2 - E_p - \omega - \omega_k} d\omega \\
 &= \int_a^b \frac{Z \text{Im } g(\omega)f(k, E - 2E_p - \omega)}{(E/2 - E_p - \omega - \omega_k)(E^+ - 2E_p - \omega)} d\omega \\
 &\quad + \int_a^b \frac{\text{Im } g(\omega)g_c(E - 2E_p - \omega)f(k, E - 2E_p - \omega)}{E/2 - E_p - \omega - \omega_k} d\omega \\
 &= \int_a^b \frac{h(\omega)}{\omega_0 - \omega} d\omega + \int_a^b \frac{\text{Im } g(\omega)g_c(E - 2E_p - \omega)f(k, E - 2E_p - \omega)}{E/2 - E_p - \omega - \omega_k} d\omega
 \end{aligned} \tag{4.23}$$

where

$$h(\omega) = \frac{Z \operatorname{Im} g(\omega) f(k, E - 2E_p - \omega)}{E/2 - E_p - \omega - \omega_k}. \quad (4.24)$$

Now, applying the subtraction method

$$\begin{aligned} \int_a^b \frac{\operatorname{Im} g(\omega) g(E - 2E_p - \omega) f(k, E - 2E_p - \omega)}{E/2 - E_p - \omega - \omega_k} d\omega &= \int_a^b \frac{h(\omega) - h(\omega_0)}{\omega_0 - \omega} d\omega \\ &+ h(\omega_0) \int_a^b \frac{1}{\omega_0 - \omega} d\omega + \int_a^b \frac{\operatorname{Im} g(\omega) g_c(E - 2E_p - \omega) f(k, E - 2E_p - \omega)}{E/2 - E_p - \omega - \omega_k} d\omega. \end{aligned} \quad (4.25)$$

Finally,

$$\begin{aligned} &\int_{m_N + m_\pi}^\infty \frac{\operatorname{Im} g(\omega) g(E - 2E_p - \omega) f(k, E - 2E_p - \omega)}{E/2 - E_p - \omega - \omega_k} d\omega \\ &= \int_a^b \frac{\operatorname{Im} g(\omega) g(E - 2E_p - \omega) f(k, E - 2E_p - \omega)}{E/2 - E_p - \omega - \omega_k} d\omega + \int_a^b \frac{h(\omega) - h(\omega_0)}{\omega_0 - \omega} d\omega \\ &\quad + h(\omega_0) \left(\log \left(1 - \frac{a}{\omega_0} \right) - \log \left(1 - \frac{b}{\omega_0} \right) \right) \\ &\quad + \int_a^b \frac{\operatorname{Im} g(\omega) g_c(E - 2E_p - \omega) f(k, E - 2E_p - \omega)}{E/2 - E_p - \omega - \omega_k} d\omega. \end{aligned} \quad (4.26)$$

4.2.4 One-pion exchange from the πNN convolution equations

As detailed in Chapter 2, the fully dressed NN OPE contains all dressing contributions. However, the dressed OPE used in the πNN convolution equations is not fully dressed, as we neglect connected three-body forces. In Figure 4.2, we provide an example of a contribution that is included in the OPE from the πNN convolution equations and an example of a contribution that is missing in the OPE from the πNN convolution equations. The comparison of the fully dressed OPE and the one from the πNN convolution equations

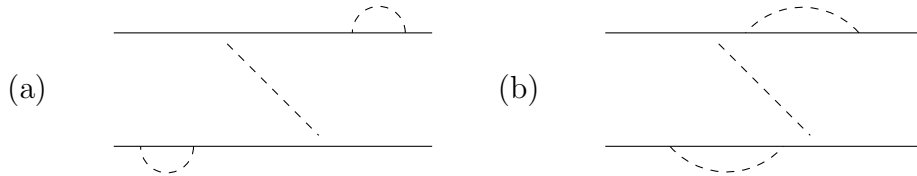


Figure 4.2: (a) Example of a dressing diagram that is included in the OPE of the πNN convolution equations (b) a dressing diagram involving a connected three-body force, which is not included in the OPE of the πNN convolution equations.

gives us an indication of the effect that neglecting these connected three-body forces, which is the approximation used to derive the πNN convolution equations.

We can calculate the OPE amplitude from the πNN convolution equations using the OPE term defined by Equation 3.124. This OPE term in Equation 3.124 can be written as sum of the two OPE time-orderings

$$Z_{NN} = V_{12}^{OPE} + V_{21}^{OPE}. \quad (4.27)$$

We consider the first time-ordering (negative slope), which is given by

$$V_{12}^{OPE} = \bar{F}_1 G_0 F_2. \quad (4.28)$$

This is shown diagrammatically in Figure 4.3. Here, contributing diagrams that exhibit a connected three-body force are neglected, and thereby becomes an approximation to the fully dressed OPE amplitude. Note that in the potential given above, each term \bar{F}_1 , G_0 and F_2 each represent an individual convolution integral. Therefore, the OPE amplitude can be written as

$$V_{12}^{OPE} = D_0^{-1}(\tilde{f}_1 \otimes g_2)(G_0^{-1})(\tilde{f}_2 \otimes g_2)D_0^{-1} \quad (4.29)$$

where G_0 is the πNN propagator and represents a convolution over three individual particle propagators. We, thus, obtain a Green's function that is a product of three convolution integrals. Using our ‘‘prime’’ notation, this expression is

$$G_{12}^{OPE}(\mathbf{p}', \mathbf{p}, E) = \left(-\frac{1}{2\pi i}\right) \left[\int dz g(z, \mathbf{p}') \bar{f}(\mathbf{p}', \mathbf{p}, E) g(z - \omega_k, \mathbf{p}) g(E - z, \mathbf{p}') \right] \left[\int dz g(z, \mathbf{p}) g(E - \omega_k - z, -\mathbf{p}') \right]^{-1} \left[\int dz g(z - \omega_k, -\mathbf{p}') f(-\mathbf{p}', -\mathbf{p}, E) g(z, -\mathbf{p}) g(E - z, \mathbf{p}) \right]. \quad (4.30)$$

4.2.5 Results

The results are given in Figure 4.4. In our numerical calculation, we use the $M1$ πN interaction of Afnan and McLeod [40] for our dressed pion-nucleon vertices $f(k, E)$. While πNN convolution equations use two-body input that is constructed with dressed nucleons, the input of Afnan and McLeod is much easier to calculate and reduces overall computation time, despite being constructed with undressed nucleons. We plot the half off-shell partial wave amplitude as a function of centre of mass energy E for the partial wave ${}^3S_1 \rightarrow {}^3S_1$

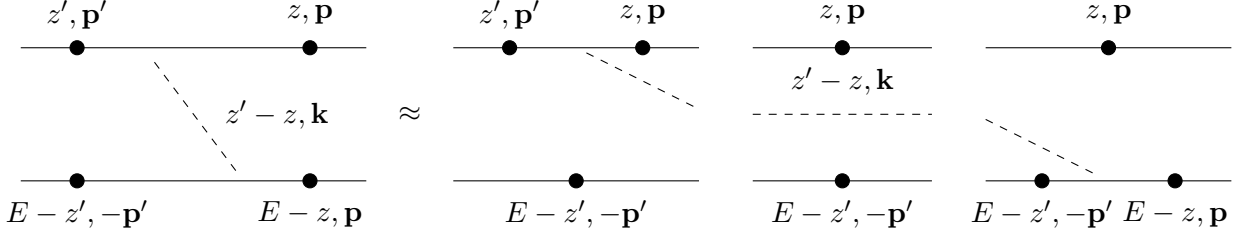


Figure 4.3: Diagram representation of the dressed one-pion exchange that with neglecting three-body forces can be represented by three individual diagrams. The black dots represent the dressing of each nucleon before and after the process of pion exchange.

using no dressing, full dressing and dressing neglecting connected three-body forces. The undressed OPE potential is simply given by

$$V_{12}^{OPE}(p', p; E) = \frac{1}{E^+ - E_{p'} - E_p - 2m_N - \omega_k}. \quad (4.31)$$

For this calculation, we put the final momentum on-shell $\mathbf{p}' \rightarrow \mathbf{p}_0$ where $E = p_0^2/m_N + 2m_N$. The half off-shell amplitude then depends on two variables, the energy E and the off-shell momentum \mathbf{p} , which we choose as $p = 0.1p_0$.

Analysing the results of Figure 4.4, we initially notice the impact that dressing has on the OPE amplitude. One then notices the similarity between full dressing and dressing neglecting connected three-body forces, as they are essentially overlapping plots. This suggests the effect of neglecting connected three-body forces one the OPE amplitude is negligible, justifying its use as an approximation to derive the πNN convolution equations.

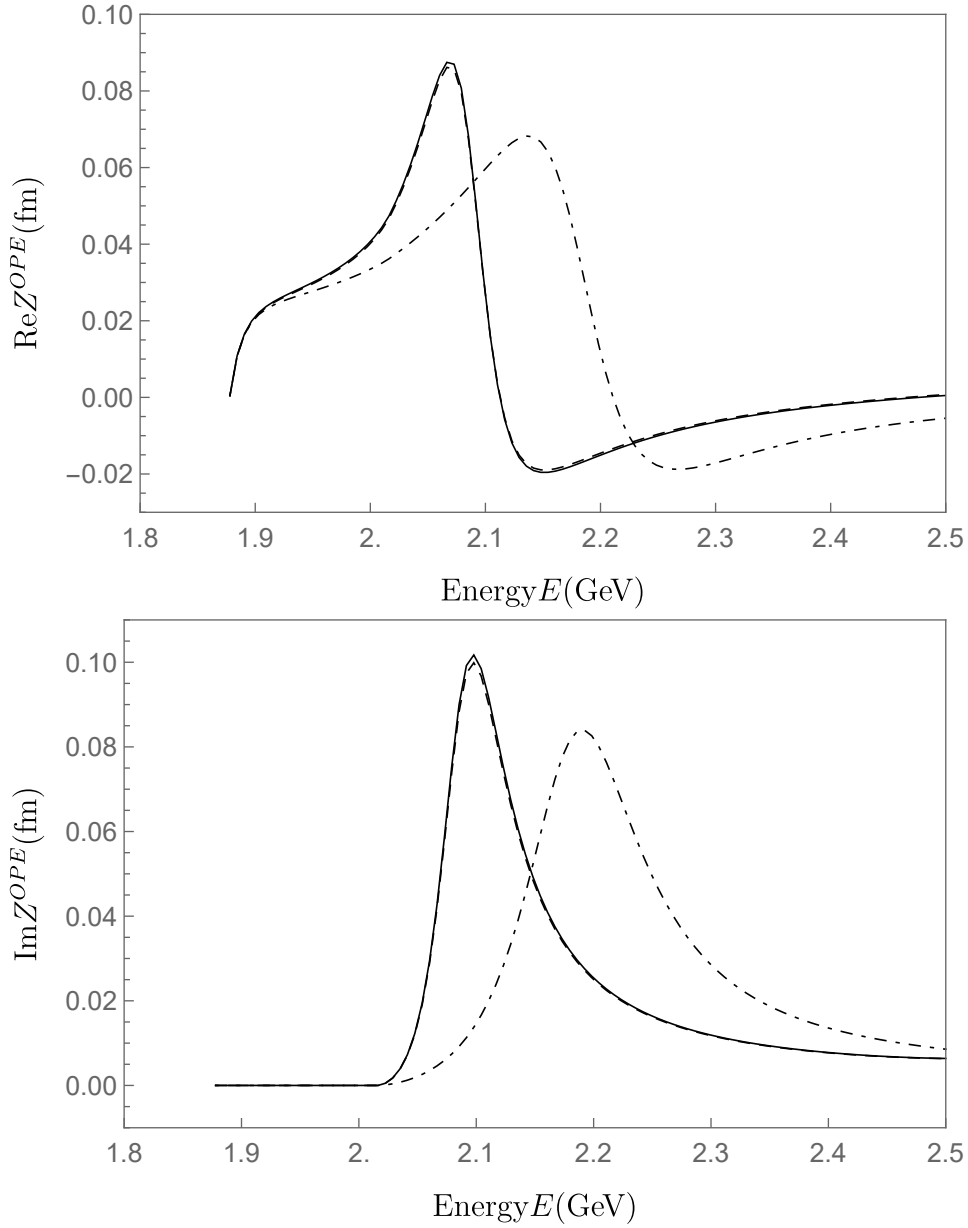


Figure 4.4: ${}^3S_1 \rightarrow {}^3S_1$ partial wave amplitudes for half off-shell NN one-pion exchange. The solid line represents the partial wave amplitude for the fully dressed one-pion exchange with full nucleon dressing, while the dashed line represents the partial wave amplitude for one-pion exchange from the πNN convolution equations, which neglects connected three-body forces. The dot dashed line represents the partial wave amplitude for one-pion exchange without any dressed nucleons.

4.3 Numerical calculation of dressed two-pion exchange

Now, we want to perform a numerical calculation of the dressed two-pion exchange (TPE) amplitude using the two-pion exchange Green's function in Equation 2.45 and compare it to the TPE amplitude of the πNN convolution equations. The numerical calculation of the TPE amplitude is more difficult than the OPE amplitude of the previous section, due to the extra z'' integral that we now have to evaluate. We find that there are two methods for evaluating this z'' integral; an analytical method by evaluating the integral by taking residues at the poles or evaluating the integral numerically.

4.3.1 Analytical form of dressed two-pion exchange

After partial wave decomposition, the expression for fully dressed TPE in Equation 2.45, with our earlier defined "prime" notation, becomes

$$Z^{TPE}(z', p', z, p; E) = \sum_{L''S''} \int Z_{L'S'L''S''}^{OPE}(z', p', z'', p''; E) g(z'' - E_{p''}) g(E - z'' - E_{p''}) Z_{L''S''LS}^{OPE}(z'', p'', z, p; E) p''^2 dp'' dz'' \quad (4.32)$$

where the Z -diagram $Z_{L'S'L''S''}^{OPE}(z', p', z, p; E)$ is the same Z -diagram used in the calculation of the one-pion exchange amplitude, given in Equation 4.15.

We concern ourselves primarily with how to perform the z'' integral. For simplicity, we focus only on terms that contain z'' and ignore everything else, which can easily be added back in later. This leaves us with

$$\left(-\frac{1}{2\pi i}\right) \int_0^\infty dp'' (p'')^2 \int_{-\infty}^\infty dz'' \frac{f(k, m_N) f(k, E - z'' - E_{p''})}{E/2 + i\epsilon - z'' - \omega_k} g(z'' - E_{p''}) g(E - z'' - E_{p''}) \frac{f(k', z'' - E_{p''}) f(k', m_N)}{z'' + i\epsilon - E/2 - \omega_{k'}}. \quad (4.33)$$

Notice that $f(k, m_N)$ and $f(k', m_N)$ do not contain z'' , so we take them out of the z'' integral,

$$\left(-\frac{1}{2\pi i}\right) \int_0^\infty dp'' (p'')^2 f(k, m_N) f(k', m_N) \int_{-\infty}^\infty dz'' \frac{f(k, E - z'' - E_{p''})}{E/2 + i\epsilon - z'' - \omega_k} g(z'' - E_{p''}) g(E - z'' - E_{p''}) \frac{f(k', z'' - E_{p''})}{z'' + i\epsilon - E/2 - \omega_{k'}}. \quad (4.34)$$

We now perform the z'' integral using Cauchy's Residue Theorem by taking the residues of the poles. We choose to take the residue of the poles below the real z'' axis. As can be seen from the above equation, there are 3 possible poles below the real z'' axis; one due to the nucleon propagator, one due to the dressed vertex function and the last one due to the pion propagator. To expose the poles in the nucleon propagator and dressed vertex, we use the analytical structure of both functions. We use a reduced form to save on notation and also choose the $+i\epsilon$ for convenience to our calculation, as they need not equal. Our analytical structure in reduced form becomes

$$\begin{aligned} f(k, E) &= f_0(k) + \frac{X(\omega_1)}{E + 3i\epsilon - \omega_1}, \\ g(E) &= \frac{Z}{E + 2i\epsilon - m_N} + \frac{Y(\omega_2)}{E + 2i\epsilon - \omega_2}. \end{aligned} \quad (4.35)$$

Putting these equation into our integral for the functions that contain the poles and expanding, we would then proceed with calculating the residue at each of the poles. The full derivation of this expression and calculation of the z'' integral is given in Appendix D. The final expression after performing the z'' integral is given as

$$\begin{aligned} &\int_0^\infty dp'' (p'')^2 f(k, m_N) f(k', m_N) \\ &\frac{f(k, E/2 - E_{p''} + i\epsilon - \omega_{k'}) g(E/2 - E_{p''} + i\epsilon - \omega_{k'})}{2i\epsilon - \omega_k - \omega_{k'}} \\ &\quad \times g(E/2 - E_{p''} + \omega_{k'}) f(k', E/2 - E_{p''} + \omega_{k'}) \\ &+ \frac{Z f(k, E - 2E_{p''} + 2i\epsilon - m_N) g(E - 2E_{p''} + 2i\epsilon - m_N)}{(E/2 - E_{p''} + 3i\epsilon - m_N - \omega_k) (-E/2 + E_{p''} - i\epsilon + m_N - \omega_{k'})} f(k', m_N) \\ &+ \frac{f(k, E - 2E_{p''} + 3i\epsilon - \omega_1) g(E - 2E_{p''} + 3i\epsilon - \omega_1) X(\omega_1)}{(E/2 - E_{p''} + 4i\epsilon - \omega_1 - \omega_k) (-E/2 + E_{p''} - 2i\epsilon + \omega_1 - \omega_{k'})} g^*(\omega_1) \\ &+ \frac{f(k, E - 2E_{p''} + 2i\epsilon - \omega_2) g(E - 2E_{p''} + 2i\epsilon - \omega_2) Y(\omega_2)}{(E/2 - E_{p''} + 3i\epsilon - \omega_2 - \omega_k) (-E/2 + E_{p''} - i\epsilon + \omega_2 - \omega_{k'})} f(k', \omega_2). \end{aligned} \quad (4.36)$$

While we have gone through a rather "lengthy" derivation to evaluate the z'' integral, we mention particular issues that arise with calculating the z'' integral analytically:

1. Just to obtain the expression above required much algebra and there seems to be no obvious and systematic way to obtain this expression without going through the tedious derivation. While we now have the expression for TPE, the same procedure would need to be repeated for higher pion exchange with the task being foreseeably much more difficult.
2. Our overall goal is to solve the scattering equations derived in the previous chapter. One could solve the equation numerically by iterating the equation and calculating each

term individually, until the amplitude converges. However, per point 1, the second-order term is difficult enough to calculate. One cannot simply perform the z'' integral in the scattering equations by hand using Cauchy's Residue Theorem, as the analytic structure of the πNN convolution equations is not clear and it is unknown whether the equations contain poles in the contour of integration. We would also have to repeat this process when we consider the scattering processes other than $NN \rightarrow NN$.

3. Evaluation of the z'' integral is not the end of the calculation, the p'' integral and the ω integrals still need to be calculated. Because of the singularities in the p'' integral, we have to be a bit careful about how we handle this numerically. We can use a standard contour rotation of the p'' integral to avoid these singularities. This is no problem for the first, second and fourth term in Equation 4.36. However, a problem arises with the third term, which we have confirmed numerically cannot be calculated using contour rotation. The problem is the technique of contour rotation is a consequence of Cauchy's integral theorem, which requires the function to be analytic in the complex plane and the third term is not analytic because of the $X(\omega)$. For a function $f(z)$ of a complex value $z = x + iy$ to be analytic, it must satisfy the Cauchy-Riemann equations, which for a complex-valued function represented as $f(z) = f(x, y) = u(x, y) + iv(x, y)$ where $u(x, y)$ and $v(x, y)$ are real-valued functions, must satisfy:

$$\begin{aligned} \frac{\partial u}{\partial x} &= \frac{\partial v}{\partial y}, \\ \frac{\partial u}{\partial y} &= -\frac{\partial v}{\partial x}. \end{aligned} \tag{4.37}$$

Now, the $X(\omega)$ is not analytic as it does not satisfy the Cauchy-Riemann equations. As $X(\omega) = \text{Im } f(q, \omega)$, this function is real and hence $v(x, y) = 0$. The only way for this function to satisfy the Cauchy-Riemann equations is if $\text{Im } f(q, \omega)$ is constant for both x and y . This is not possible as it would imply that $\text{Im } f(q, \omega)$ is not dependent on the complex variable p'' , which it clearly is as it is explicitly dependent on q , which contains the complex value p'' . Therefore, this function is not analytic and hence, contour rotation cannot be used to evaluate the integral over the third term in Equation 4.36.

We have determined that the p'' integral in Equation 4.36 cannot be calculated using conventional methods, such as contour rotation, due to the term 3 not being analytic. We could, however, calculate the other terms using contour rotation and calculate the term 3

being integration along the real p'' momentum axis. But, if we were to go through this effort, we could just as easily calculate the p'' integral in Equation 4.32 along the real axis, and then calculate the z'' integral numerically rather than analytically. The opportunity to calculate the z'' integral numerically avoids the problems that were mentioned previously concerning the difficulties in the analytic evaluation of the z'' integral. For our calculation of the two-pion exchange amplitude, we choose this method of evaluating the integrals along the real axis. As a result, we must consider the numerical singularities in the integrals that are commonly avoided when using contour rotation.

4.3.2 Numerical handling of the logarithmic singularities

Our expression for the full convolution of TPE contains two Z^{OPE} terms, which each contain the function Γ_L given below

$$\Gamma_L(z', p', z, p; E) = \frac{1}{2} \int_{-1}^1 \frac{k^{-1} f(k, z' - E_{p'}) f(k, E - z - E_p) k^{-1}}{z'^+ - z - \sqrt{k^2 + m_\pi^2}} P_L(x) dx. \quad (4.38)$$

When we integrate over the angle x in Γ_L , logarithmic singularities at the end points (when $x = \pm 1$) arise from the pion propagator term as integration results in a logarithmic function.

To see this explicitly, consider the x integral in Γ_L ,

$$\frac{f(x)}{b + i\epsilon + \sqrt{a - cx}} \quad (4.39)$$

where

$$\begin{aligned} f(x) &= \frac{1}{2} k^{-1} f(k, z' - E_{p'}) f(k, E - z - E_p) k^{-1} P_L(x), \\ b &= z' - z, \\ a &= m_\pi^2 + p'^2 + p^2, \\ c &= 2p'p. \end{aligned} \quad (4.40)$$

We suppress the integral over x to save notation. Now, we exploit the square-root in the denominator to expose the pole

$$\frac{f(x)}{b + i\epsilon + \sqrt{a - cx}} \frac{b + i\epsilon - \sqrt{a - cx}}{b + i\epsilon - \sqrt{a - cx}} = \frac{f(x)(b + i\epsilon - \sqrt{a - cx})}{(b + i\epsilon)^2 - (a - cx)} = \frac{f(x)(b + i\epsilon - \sqrt{a - cx})}{b^2 - 2b\epsilon i - \epsilon^2 - a + cx}. \quad (4.41)$$

Therefore,

$$\frac{h(x)}{b^2 - 2b\epsilon i - \epsilon^2 - a + cx} = \frac{1}{c} \frac{h(x)}{x - x_0 + i\epsilon'} \quad (4.42)$$

where

$$\begin{aligned} h(x) &= f(x)(b + i\epsilon - \sqrt{a - cx}), \\ x_0 &= \frac{1}{c}(a - b^2), \\ \epsilon' &= 2b\epsilon/c. \end{aligned} \quad (4.43)$$

It is important that we have this new definition of ϵ , as a change in sign may occur because the values of b and c vary. It is vital that we have the correct sign for the $i\epsilon$, as this we change the analytic nature of the function. Since ϵ is already small, we can simply neglect ϵ^2 . Now, we want to use a pole subtraction but we need to be careful about how we use this pole subtraction. We could simply write

$$\frac{1}{c} \int_{-1}^1 \frac{h(x)}{x - x_0 + i\epsilon'} dx = \frac{1}{c} \left(\int_{-1}^1 \frac{h(x) - h(x_0)}{x - x_0 + i\epsilon'} dx + h(x_0) \int_{-1}^1 \frac{1}{x - x_0 + i\epsilon'} dx \right) \quad (4.44)$$

and therefore

$$\begin{aligned} &\frac{1}{c} \int_{-1}^1 \frac{h(x)}{x - x_0 + i\epsilon'} dx \\ &= \frac{1}{c} \left(\int_{-1}^1 \frac{h(x) - h(x_0)}{x - x_0 + i\epsilon'} dx + h(x_0) (\log(1 - x_0 + i\epsilon') - \log(-1 - x_0 + i\epsilon')) \right). \end{aligned} \quad (4.45)$$

One can now see that evaluating the x integral introduces logarithmic singularities in the Z^{OPE} term, which occur when $x_0 = \pm 1$.

If the poles x_0 is outside of the integral limits, then the pole subtraction should not be necessary. In practice, it is numerically advantageous to always use a pole subtraction as there can be a large numerical error when x_0 is close to -1 or 1 . Though, this issue could be avoided by using the pole subtraction method when the x_0 is within a larger interval (say $x_0 \in [-2, 2]$). However, there is a possible error in using the pole subtraction method when the pole is outside of the integral limits as it can cause the input of the dressed vertex function $f(k, E)$ to be complex. As these vertex functions are essentially $1/(k^2 + \beta^2)$, it is possible for there to be a pole if k is complex.

To avoid a possible pole in the dressed vertex function, we adapt the method described by Liu et al. [89] who suggest replacing the function $h(x_0)$ by the function $\hat{h}(x_0)$ which has the condition

$$\hat{h}(x_0) = \begin{cases} h(x_0) & \text{if } |x_0| \leq 1 \\ h\left(\frac{x_0}{|x_0|}\right) & \text{if } |x_0| > 1 \end{cases}. \quad (4.46)$$

Our pole subtraction then becomes

$$\begin{aligned} & \frac{1}{c} \int_{-1}^1 \frac{h(x)}{x - x_0 + i\epsilon'} dx \\ &= \frac{1}{c} \left(\int_{-1}^1 \frac{h(x) - \hat{h}(x_0)}{x - x_0 + i\epsilon'} dx + \hat{h}(x_0) (\log(1 - x_0 + i\epsilon') - \log(-1 - x_0 + i\epsilon')) \right). \end{aligned} \quad (4.47)$$

This should avoid the possibility of a pole in the dressed vertex function while allowing us to use the pole subtraction all the time. Our pole subtraction is slightly different to the one detailed by Liu et al. [89], as the authors have not accounted for the possibility that $i\epsilon$ can change sign as a result of the rearrangement to expose the x integral pole, as ϵ is now a function of z', z, p' and p .

These logarithmic singularities can be found by solving

$$z' - z - \sqrt{m_\pi^2 + p'^2 + p^2 \pm 2pp'} = 0. \quad (4.48)$$

These logarithmic singularities are not as detrimental as pole singularities, so the momentum integral can still be calculated with “brute force,” by using many quadrature points. However, one would require an enormous amount of quadrature points to obtain sufficient accuracy, so it is better practice to account for these logarithmic singularities. Since these singularities are discontinuities along the p axis, instead of using quadrature points along the entire integration interval, we should split the integration interval at each logarithmic singularity and calculate each interval using quadrature points. In practice, this method reduces the overall amount of quadrature points needed to accurately calculate the p integral.

Standard Gauss-Legendre quadrature points will suffice in when handling the logarithmic singularities by splitting the interval. But if one wants greater accuracy of the p integral, one can use the modified Gaussian quadratures of Pachucki et al. [90] who have created quadrature points specifically to integrate intervals with an end-point logarithmic singularity. The authors provide the *Mathematica* code used to calculate these modified quadrature points (which we refer to as Gauss-Log points) for the interval $[0, 1]$, which are used to calculate integrals with a logarithmic singularity at 0. These quadratures can be transformed to any finite interval and modified to account for when the end-point singularity is on the left side or right side of the interval. We can do this by using a linear transform to map $[0, 1] \rightarrow [a, b]$ if the interval we are integrating has a logarithmic singularity at a and we map $[0, 1] \rightarrow [b, a]$ if the interval we are integrating has a logarithmic singularity at b . If we denote the Gauss-log quadrature points as $\{x_i^{log}\}$ and the associated weights as $\{w_i^{log}\}$, the

transformation for a logarithmic singularity on the left is given by

$$\begin{aligned}\bar{x}^{log} &= (b - a)x^{log} + a, \\ \bar{w}^{log} &= (b - a)w^{log},\end{aligned}\tag{4.49}$$

where we use the bar notation to denote the quadrature points and weight on the interval $[a, b]$. The transformation for a logarithmic singularity on the right is given by

$$\begin{aligned}\bar{x}^{log} &= \text{Reverse}((a - b)x^{log} + b), \\ \bar{w}^{log} &= (b - a)w^{log},\end{aligned}\tag{4.50}$$

where ‘‘Reverse’’ denotes the process of reversing the order of the quadrature points.

These Gauss-Log quadrature points only work when there is only one end-point singularity on the integration interval, so intervals with a singularity at both ends will have to be subdivided in order for the Gauss-Log quadrature point to be effective.

When we evaluate the p'' integral, we adapt the method describe by Matsuyama [91], where a change of variables is adopted to handle the logarithmic singularity. If we integrate a function $f(p)$ in the interval $[a, b]$ and a logarithmic singularity denoted by p_{log} exists in this interval, our integral becomes

$$\int_a^b f(p)dp = \int_{-t_1}^0 f(p_{log} + t^3)3t^2 dt + \int_0^{t_2} f(p_{log} + t^3)3t^2 dt\tag{4.51}$$

where $t_1 = (p_{log} - a)^{1/3}$ and $t_2 = (b - p_{log})^{1/3}$. We calculate the integrals in the above method using the Gauss-log quadrature points described before. If we are integrating in an interval, which has two or more logarithmic singularities within it, we split the full interval half-way between adjacent singularities and perform the above method to handle them. We denote this method as the ‘‘change of variable’’ method.

4.3.3 Numerical handling of the poles

The first method in trying to calculate a full convolution is an analytic method, using Cauchy’s Residue Theorem to determine the residue of the amplitude at the poles. This is a tedious task requiring much algebra in order to obtain an amplitude that is suitable for numerical evaluation. Another difficulty is that the intermediate momentum must be integrated over for convolution diagrams of higher order than OPE, where the amplitude contains singularities. A technique to avoid these singularities is the method of rotating the quadratures off the real axis by a small angle, which is a consequence of Cauchy’s Residue

Theorem. However, because of its relation to Cauchy's Residue Theorem, we can only use this rotation of quadratures technique when we have analytic functions. In most situations, this is the case anyway, though often we encounter functions that are either real or purely imaginary. In this case, the function is not analytic as it does not satisfy the Cauchy-Riemann equations. This cannot be guaranteed for all functions that may appear in this calculation, therefore integration must be carried out on the real axis.

Though, because of the $+i\epsilon$ protecting the pole in the dressed one-nucleon propagator, one can use the Sokhotski-Plemelj theorem stating for a complex function $f(x)$, that is defined and continuous on the real axis:

$$\int_a^b \frac{f(x)}{x - x_0 + i\epsilon} dx = PV \int_a^b \frac{f(x)}{x - x_0} dx - i\pi f(x_0) \quad (4.52)$$

where PV refers to the Cauchy principal value integral. Following the procedure of Noble [92], the principal value integral can be calculated numerically using Gaussian quadratures by making quadrature intervals of equal length around the pole.

Kolm and Rokhlin [93] present a different approach to Noble to evaluate these principal value integrals. The authors use a modified version of the quadrature weights, which can be used rather than creating quadrature intervals of equal length around the pole. Further, Kolm and Rokhlin present a numerical method to calculate integrals with a pole of order 2, which cannot be achieved by Noble's method. Though, we tend to the method specified by Noble, as we do not have to change the functional form of our numerical equations as we would using the quadratures of Kolm and Rokhlin. This makes it easier to implement the method of Noble into our equations.

One can also use a subtraction method, similar to the subtraction method used to handle the x integral. Though, since the integration interval is $[0, \infty)$, we would not use the adapted method of Liu mentioned above. Handling the poles using either the Sokhotski-Plemelj theorem or pole subtraction method should be equivalent, however, using the Sokhotski-Plemelj theorem is a bit more involved as we would need to calculate the principal value integral. While this is not such a difficult procedure as we would simply choose quadrature points within equal intervals around the pole, it becomes more difficult when we also have to consider the logarithmic singularities as now we have to be more careful about how we choose our quadrature points. Because of this, the pole subtraction method can be often favoured as we only need to choose the quadrature points based on the logarithmic singularities, rather than worrying about the pole.

4.3.4 Numerical handling of the singularities in the z'' integral

We have mentioned above about the difficulties in calculating the z'' integral analytically using Cauchy's Residue Theorem. Here, we discuss how to calculate the z'' integral numerically, which becomes advantageous in calculations in later chapters.

We want to calculate the z'' integral numerical using quadrature points, however we suspect there might be singularities like in the p'' integral. However, looking at the functional form at the Z -diagrams in Equation 4.32, the singularities in the z'' integral are not obvious, in comparison to the pole and logarithmic singularities in the p'' integral. To determine if there are any singularities in the z'' integral and their position, we can plot the p'' integral of Equation 4.32 as a function of z'' . We represent this function by $I_p(z'')$, which is given explicitly by Equation 4.53

$$\begin{aligned}
 I_p(z'') &= \sum_{L''S''} \int Z_{L'S'L''S''}^{OPE}(z', p', z'', p''; E) g(z'' - E_{p''}) g(E - z'' - E_{p''}) Z_{L''S''LS}^{OPE}(z'', p'', z, p; E) p''^2 dp''.
 \end{aligned}
 \tag{4.53}$$

We plot the p'' integral as a function of z'' in Figure 4.5 at a fixed energy of $E = 2.2$ GeV, while using the $M1$ πN interaction of Afnan and McLeod [40] for our dressed pion-nucleon vertices $f(k, E)$.

As we can see from the plot of the p'' integral as a function of z'' , there are two distinct structures corresponding to sharp spikes. One of these structures seems to occur just below $z'' = 5$ and the other seems to occur just above $z'' = 6$. After some investigation, we determine that the main peak in the real part of the plot occurs at $z'' = E/2 = 5.57445$ and that the sharp spikes occur at $z'' = E/2 - m_\pi = 4.87866$ and $z'' = E/2 + m_\pi = 6.27024$. These singularities in the z'' integral must occur due to the presence of the logarithmic singularities in the p'' integral, as the points $z'' = E/2 \pm m_\pi$ correspond to the boundaries of logarithmic singularity on-set in the p'' integral. So, now that we know there are singularities in the z'' and we know the location of these singularities, we can calculate the z'' integral using Gaussian quadrature points. We construct these quadrature points on the interval $[-\infty, \infty]$, while splitting the interval at $z'' = E/2 - m_\pi$ and $z'' = E/2 + m_\pi$. Therefore, our integration intervals are $[-\infty, E/2 - m_\pi]$, $[E/2 - m_\pi, E/2 + m_\pi]$ and $[E/2 + m_\pi, \infty]$ and we population each interval with quadrature points to calculate the full z'' integral.

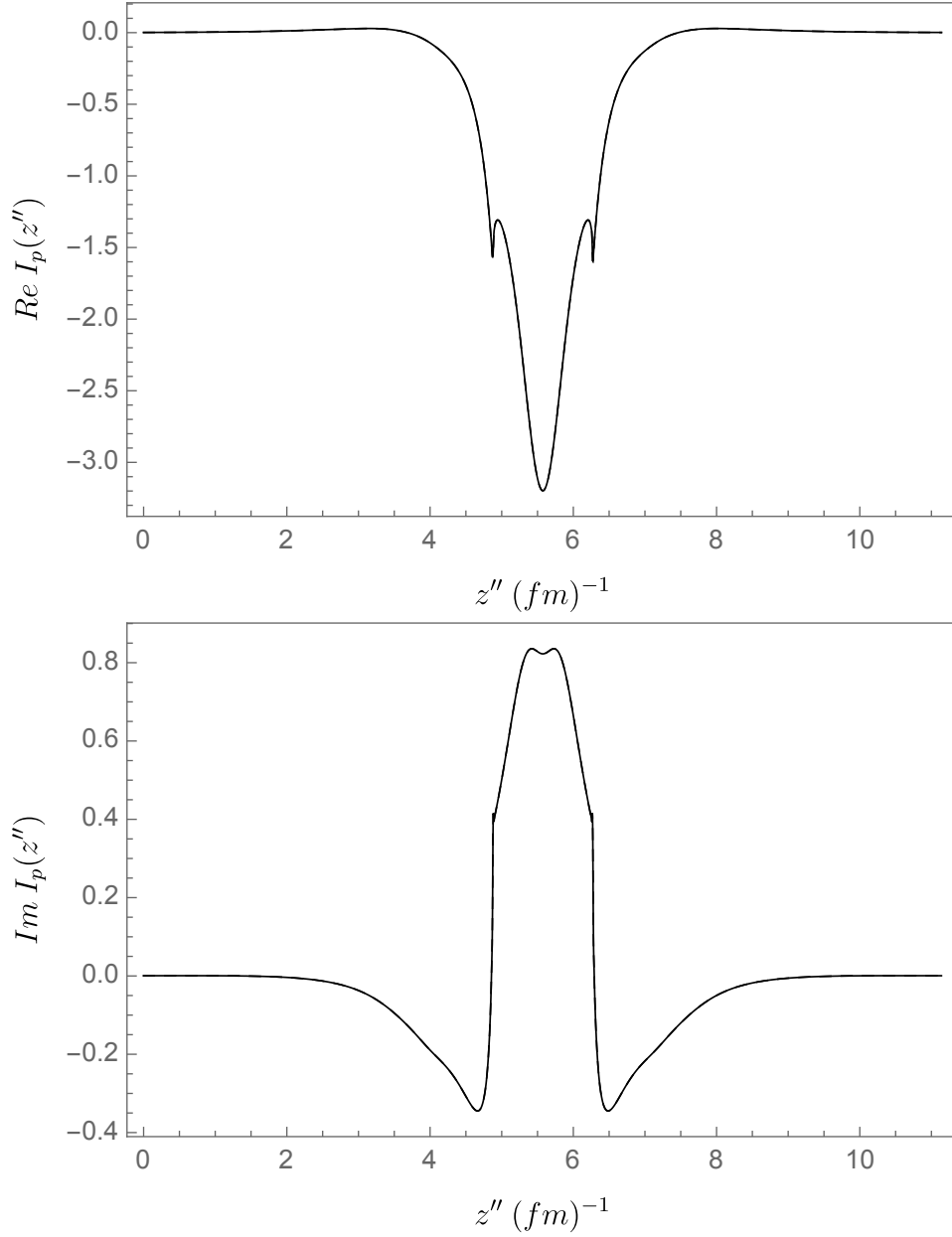


Figure 4.5: Plot of the real and imaginary parts of the ${}^3S_1 \rightarrow {}^3S_1$ two-pion exchange partial wave amplitude of Equation 4.53 against the energy-like variable z'' at a fixed energy of $E = 2.2$ GeV. The function $I_p(z'')$ is Equation 4.32 as a function of the variable z'' , after the p'' integral has been performed.

4.3.5 Two-pion exchange from the πNN convolution equations

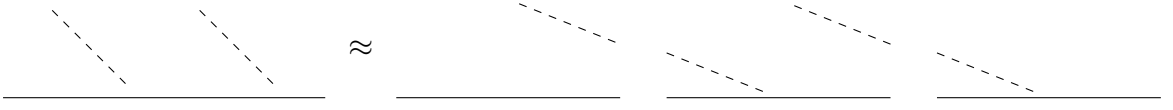


Figure 4.6: Diagram representation of the dressed two-pion exchange that with neglecting three-body forces can be represented by three individual diagrams as in the πNN convolution equations.

Similarly to the case of one-pion exchange, two-pion exchange can be determined from the πNN convolution equations and is given as

$$V_{12}^{TPE} = \bar{F}_1 w_5 F_2 \quad (4.54)$$

which is given diagrammatically in Figure 4.6. This corresponds to the convolutions

$$V_{12}^{TPE} = D_0^{-1}(\tilde{f}_1 \otimes g_2)G_0^{-1}(\tilde{f}_2 \otimes \tilde{f}_1)G_0^{-1}(\tilde{f}_2 \otimes g_1)D_0^{-1}. \quad (4.55)$$

We, thus, obtain the Green's function

$$\begin{aligned} G_{12}^{TPE}(\mathbf{p}', \mathbf{p}, E) &= \left(-\frac{1}{2\pi i} \right) \int d\mathbf{p}'' \\ &\left[\int dz' g(z', \mathbf{p}') \bar{f}(\mathbf{p}', \mathbf{p}'', E) g(z' - \omega_k, \mathbf{p}'') g(E - z', -\mathbf{p}) \right] \\ &\left[\int dz' g(z' - \omega_k, \mathbf{p}'') g(E - z', -\mathbf{p}') \right]^{-1} \\ &\left[\int dz'' g(z'', \mathbf{p}'') \bar{f}(\mathbf{p}'', \mathbf{p}, E) g(z'' - \omega_{k'}, \mathbf{p}) g(E - z'' - \omega_k, -\mathbf{p}') f(-\mathbf{p}', -\mathbf{p}'', E) g(E - z'', -\mathbf{p}'') \right] \\ &\left[\int dz g(z, \mathbf{p}) g(E - z - \omega_{k'}, -\mathbf{p}'') \right]^{-1} \\ &\left[\int dz g(z, \mathbf{p}) g(E - z - \omega_{k'}, -\mathbf{p}'') f(-\mathbf{p}'', -\mathbf{p}, E) g(E - z, -\mathbf{p}) \right]. \end{aligned} \quad (4.56)$$

But, as we are only consider fully on-shell TPE, the external legs in this Green's function will be cancelled out by the external two-nucleon propagators. Therefore, by “chopping off” these external legs and setting the z variables on-shell ($z' = z = E/2$), our expression for

the TPE amplitude becomes

$$\begin{aligned}
 V_{12}^{TPE}(\mathbf{p}', \mathbf{p}, E) &= \left(-\frac{1}{2\pi i} \right) \int d\mathbf{p}'' \\
 &\bar{f}(\mathbf{p}', \mathbf{p}'', E)g(E/2 - \omega_k, \mathbf{p}'')D_0^{-1}(E - \omega_k, \mathbf{p}', \mathbf{p}'') \\
 &\left[\int dz'' g(z'', \mathbf{p}'')\bar{f}(\mathbf{p}'', \mathbf{p}, E)g(z'' - \omega_{k'}, \mathbf{p})g(E - z'' - \omega_k, -\mathbf{p}')f(-\mathbf{p}', -\mathbf{p}'', E)g(E - z'', -\mathbf{p}'') \right] \\
 &D_0^{-1}(E - \omega_{k'}, \mathbf{p}'', \mathbf{p})g(E/2 - \omega_{k'}, -\mathbf{p}'')f(-\mathbf{p}'', -\mathbf{p}, E).
 \end{aligned} \tag{4.57}$$

Now, presented in a “ready-to-calculate” form where we put both sides on-shell ($p' = p = p_0$)

$$\begin{aligned}
 V_{12}^{TPE}(E) &= \left(-\frac{1}{2\pi i} \right) \int dp' \\
 &\bar{f}(k, m_N)g(E/2 - E_{p''} - \omega_k)D_0^{-1}(E/2 + m_N - E_{p''} - \omega_k) \\
 &\left[\int dz'' g(z'' - E_{p''})\bar{f}(k', z'' - E_{p''})g(z'' - E/2 + m_N - \omega_{k'}) \right. \\
 &\quad \left. g(E/2 - z'' + m_N - \omega_k)f(k, z'' - E_{p''})g(E - z'' - E_{p''}) \right] \\
 &D_0^{-1}(E/2 + m_N - \omega_{k'} - E_{p''})g(E/2 - E_{p''} - \omega_{k'})f(k', m_N).
 \end{aligned} \tag{4.58}$$

The results for parallel (same slope) two-pion exchange is given in Figure 4.7. Again, we use the $M1$ πN interaction of Afnan and McLeod [40] for our dressed pion-nucleon vertices $f(k, E)$. Comparing the full calculation with all nucleons fully dressed to the calculation neglecting connected three-body forces obtained from the πNN convolution equations, we see a similar shape across the energy range. The amplitudes start at the minimal energy essentially overlapping and begin to diverge slightly as the energy increases, however, this difference in the amplitudes at higher energies is minimal. From the trend seen in Figure 4.7, it is expected that connected three-body forces have more of an effect on the amplitude for higher pion exchanges. The effect of connected three-body forces on the two-pion exchange amplitude tends to be more significant at higher energies, but these energies are beyond the energies we will use in our three-body πNN calculations, so we do not expect that neglecting these connected three-body forces will have a significant effect on our three-body πNN calculations.

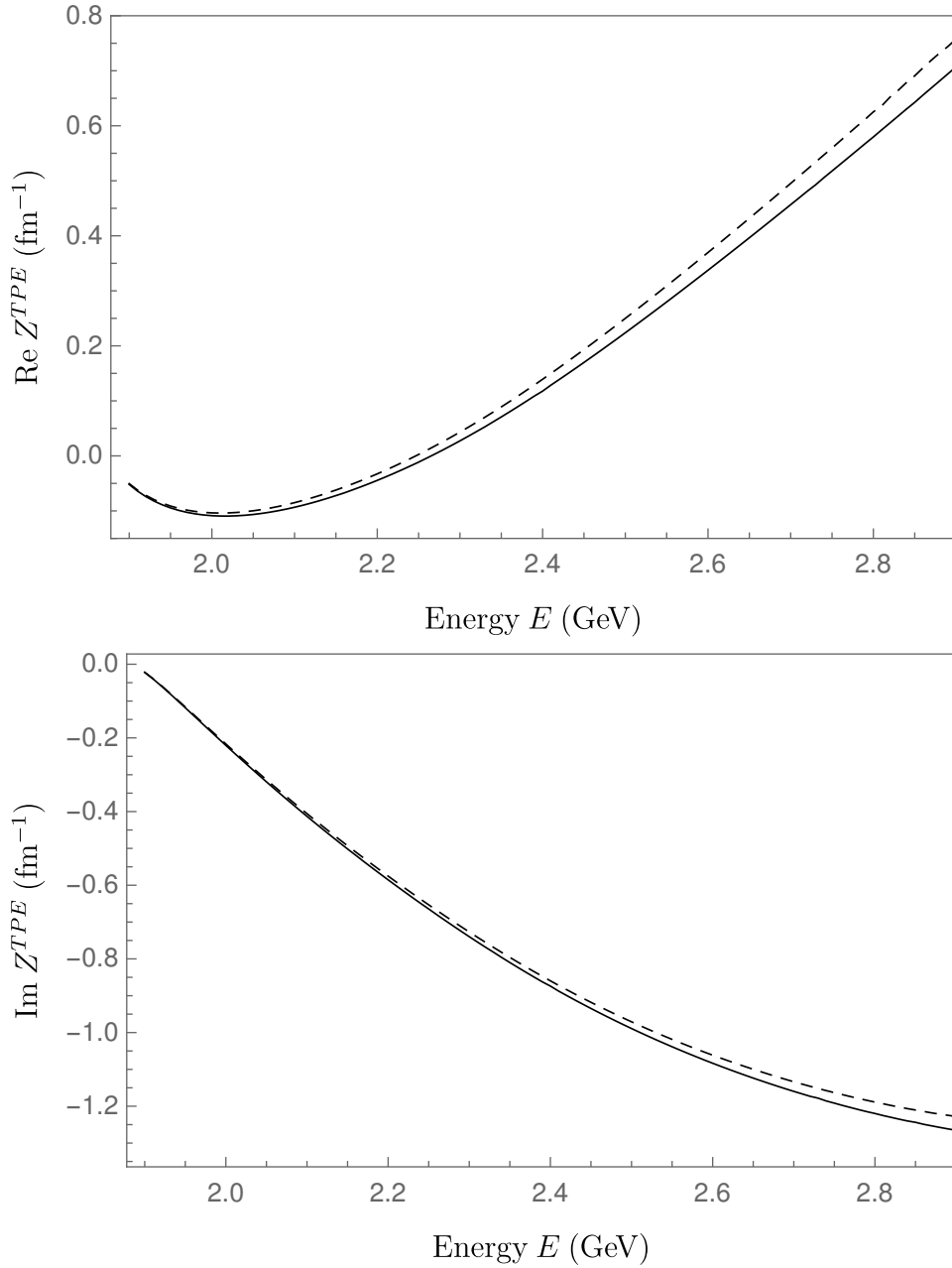


Figure 4.7: ${}^3S_1 \rightarrow {}^3S_1$ partial wave amplitudes for same slope fully on-shell NN two-pion exchange. The solid line represents the partial wave amplitude for the calculation with fully dressed nucleons, while the dashed line represents the partial wave amplitude from the πNN convolution equations, which neglects connected three-body forces.

4.3.6 Two-pion exchange with different slopes

We repeat the same procedure for different slope two-nucleon exchange to determine if the effect of neglecting connected three-body forces is minimal for a different time-ordering.

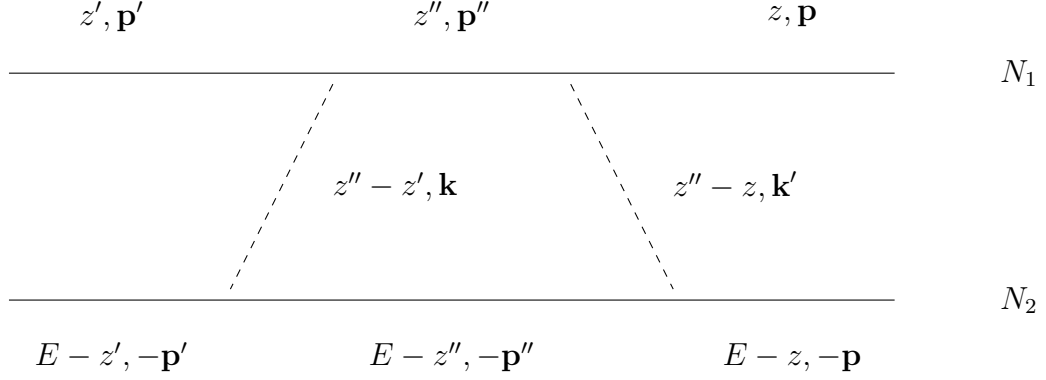


Figure 4.8: Convolution diagram corresponding to different slope dressed two-nucleon exchange.

The diagram for different slope two-nucleon exchange is given in Figure 4.8, while the diagram representing the product of convolutions representation for different slope two-nucleon exchange is given in Figure 4.9. The equation for different slope two-nucleon exchange with full nucleon dressing and after partial wave decomposition is given as

$$\left(-\frac{1}{2\pi i}\right) \int_0^\infty dp'' (p'')^2 f(k, m_N) f(k', m_N) \int_{-\infty}^\infty dz'' \frac{f(k, z'' - E_{p''})}{z'' + i\epsilon - E/2 - \omega_k} g(z'' - E_{p''}) g(E - z'' - E_{p''}) \frac{f(k', z'' - E_{p''})}{z'' + i\epsilon - E/2 - \omega_{k'}}. \quad (4.59)$$

Again, we ignore everything including the terms corresponding to the partial wave decomposition to illustrate the functional form of the amplitude. The equation for different slope two-nucleon exchange from the πNN convolution equations is given as

$$V_{12}^{TPE} = \bar{F}_2 w_1^P F_2. \quad (4.60)$$

Explicitly showing the convolutions, we obtain

$$V_{12}^{TPE} = D_0^{-1} (\tilde{f}_2 \otimes g_1) G_0^{-1} ((g_{\pi N} f g \bar{f} g_{\pi N})_1 \otimes g_2) G_0^{-1} (\tilde{f}_2 \otimes g_1) D_0^{-1}. \quad (4.61)$$

Now explicitly showing the energy and momentum variables as well as the convolution inte-

grals

$$\begin{aligned}
 V_{12}^{TPE}(\mathbf{p}', \mathbf{p}, E) &= \left(-\frac{1}{2\pi i} \right) \int d\mathbf{p}'' \\
 &\bar{f}(-\mathbf{p}', -\mathbf{p}'', E)g(E/2 - \omega_k, \mathbf{p}'')D_0^{-1}(E - \omega_k, \mathbf{p}', \mathbf{p}'') \\
 &\left[\int dz''g(z'' - \omega_k, \mathbf{p}')f(\mathbf{p}', \mathbf{p}'', E)g(z'', \mathbf{p}'')\bar{f}(-\mathbf{p}', -\mathbf{p}'', E)g(z'' - \omega_{k'}, \mathbf{p})g(E - z'', -\mathbf{p}'') \right] \\
 &D_0^{-1}(E - \omega_{k'}, \mathbf{p}'', \mathbf{p})g(E/2 - \omega_{k'}, \mathbf{p}'')f(-\mathbf{p}'', -\mathbf{p}, E).
 \end{aligned} \tag{4.62}$$

The results for different slope two-nucleon exchange is given in Figure 4.10. Again, we see a similar trend to the two-pion exchange amplitude for parallel slopes, in which the two graphs essentially overlap, over to diverge at higher energies. In conjunction with our results comparing the one-pion exchange amplitude with and without connected three-body forces, we have sufficient evidence to suggest that these connected three-body forces will have a neglectable effect on the overall πNN convolution equations.

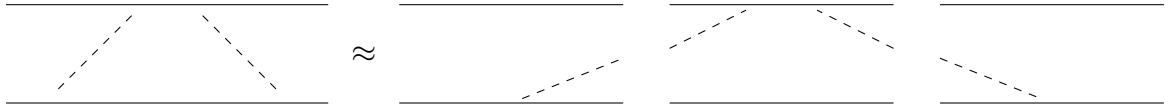


Figure 4.9: Diagram representation of the dressed two-pion exchange that with neglecting three-body forces can be represented by three individual diagrams as in the πNN convolution equations.

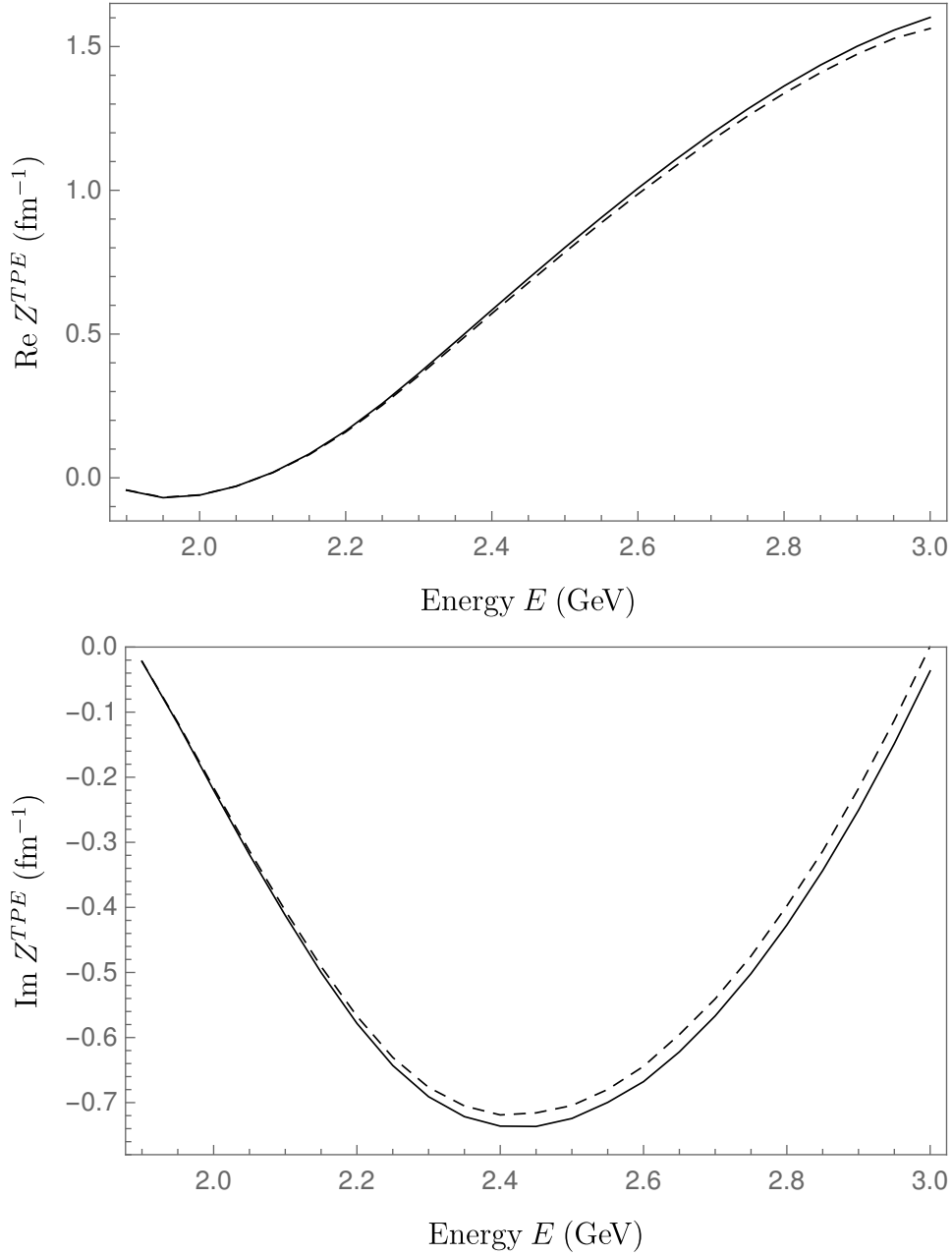


Figure 4.10: ${}^3S_1 \rightarrow {}^3S_1$ partial wave amplitudes for different slope fully on-shell two-pion exchange. The solid line represents the partial wave amplitude for the calculation with fully dressed nucleons, while the dashed line represents the partial wave amplitude from the πNN convolution equations, which neglects connected three-body forces.

4.4 A brief review of solving 4-dimensional scattering equations

While we have a set of coupled 4-dimensional equations that are non-relativistic, 4-dimensional equations typically describe relativistic processes, where the relativistic description of two interacting particles is most famously given by the Bethe-Salpeter equation [50], given diagrammatically in Figure 4.11

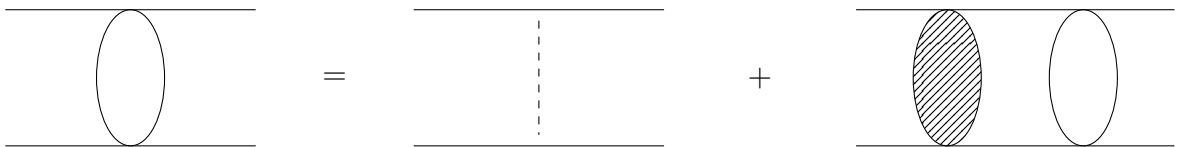


Figure 4.11: Diagrammatic representation of the Bethe-Salpeter equation for scattering states. The open circles represent all possible contributions, while the dashed circle represents all two-particle irreducible contributions. The Bethe-Salpeter equation for bound states is the same for scattering states, without the inhomogeneous term.

Salpeter and Bethe [50] discuss that the kernel of the Bethe-Salpeter equation, which involves all two-particle irreducible processes, can be simplified by only considering the simplest two-particle irreducible process, namely one particle exchange. This approximation leads to the inclusion of only reducible graphs and is known as the “ladder” approximation or “ladder” model, and is given by the diagram in Figure 4.12

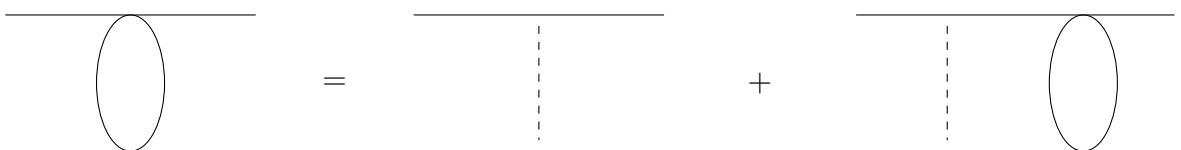


Figure 4.12: Diagrammatic representation of the Bethe-Salpeter equation for scattering states in the “ladder” approximation.

A partial wave decomposition is performed to reduce the Bethe-Salpeter equation from a 4-dimensional equation to a 2-dimensional equation. However, solving the partial wave Bethe-Salpeter equation in the ladder approximation is still difficult, due to the 4 singularities in the equation kernel that result from the poles of the two-particle propagator. In addition to these 4 pole singularities, the partial wave decomposition also introduces logarithmic singularities in the kernel of the Bethe-Salpeter equation. If the precise location of

these singularities is known, one can create quadrature points that incorporate the location of the singularities, thereby discretising and solving the equation using matrix inversion. However, as the pole singularities and logarithmic singularities are dependent on both equation variables, the singularities are not a fixed location, rather the location of the singularities in one variable moves with respect to the other variable and discretisation using quadrature points becomes difficult.

The seminal papers by Wick [51] and Cutkosky [52] showed that bound state solutions could be obtained by analytically continuing the “relative” time variable ω to the imaginary time axes, thereby avoiding all the singularities in the kernel. This famously become known as Wick rotation. For bound states, Wick rotation can be easily implemented as two pole singularities lie above the negative $\text{Re} [\omega]$ axis in the 4th quadrant and the remaining 2 singularities lie below the positive $\text{Re} [\omega]$ axis in the second quadrant. However, Wick rotation is more difficult to implement in scattering states as there is a pole singularity in each quadrant of the complex ω plane and “pinches” the ω integration contour, which prevents a simple analytical continuation and the residues of the poles must be included. The most detrimental case is where two of the poles will “pinch” the integration contour, in which two poles overlap at the imaginary ω axis. This occurs when the integrated momentum is equal to the on-shell momentum p_0 . In order to obtain a non-singular Bethe-Salpeter equation for scattering states, Levine et al. [53, 54] adapted the factorisation method of Noyes [94], in which they factor the off-shell contribution to the half off-shell Bethe-Salpeter amplitude

$$T(\omega, p, \omega_0, p_0) = f(\omega, p)T(\omega_0, p_0, \omega_0, p_0) = f(\omega, p)T^{on} \quad (4.63)$$

where $T^{on} = T(p_0, \omega_0, p_0, \omega_0)$ is the fully on-shell Bethe-Salpeter amplitude. Inserting this factorisation into the Bethe-Salpeter equation, one can obtain an integral equation for the function $f(p, \omega)$ in order to determine the Bethe-Salpeter amplitude. This factorisation introduces a zero into the potential of the equation’s kernel at the on-shell momentum, thereby handling the “pinching” of the integration contour that occurs when the integrated momentum is equal to the on-shell momentum [94, 95].

The methods of Levine et al. only describe a system of two particles with equal masses, whereas, in the πNN system, we have scattering processes for two particles of unequal mass i.e. πd elastic scattering. In the study of the πN system with a covariant formulation, Lahiff and Afnan [96, 97] found that they could perform a Wick rotation without any additional manipulation or factorisation, provided that the cutoff masses in the form factors are not too

small. Though, it is not clear that their approach could be applied to πd elastic scattering or $NN \rightarrow \pi d$ scattering.

The Wick rotation method requires the inversion of large matrices, which, at the time, was very computationally intensive. This led to the use of Padé approximants as an alternative method to solving the Bethe-Salpeter equation, as it was the only feasible method to avoid matrix inversion [57]. Padé approximants allow for faster convergence of a series by approximating the series by a ratio of polynomials. For $m \geq 1$ and $n \geq 1$, the $[m/n]$ Padé approximant is given by the rational function $R(x)$

$$R(x) = \frac{\sum_{j=0}^m a_j x^j}{1 + \sum_{k=1}^n b_k x^k}. \quad (4.64)$$

To solve the Bethe-Salpeter equation using Padé approximants, a Taylor expansion is used on this rational function $R(x)$ and the coefficients of the expansion are equated with the iterated Bethe-Salpeter equation by setting $x = 1$. The use of Padé approximants is also valid if the sum of iterated terms of the Bethe-Salpeter were divergent, which makes it a powerful numerical tool. To perform a $[m/n]$ Padé approximation, we would need to calculate $m+n$ terms in the iterated Bethe-Salpeter equation explicitly. Nuttall [55] found that a $[1/1]$ Padé approximant was a sufficient approximation for scalar particles of equal mass. However, Nieland and Tjon [56] found that when solving the Bethe-Salpeter equation for πN scattering using Padé approximants, a $[1/1]$ Padé approximant provided a bad approximation and much more convergent approximations required a $[3/3]$ or higher Padé approximants.

In the case of our 4-dimensional equations, we would struggle to numerically calculate terms due to the compounding singularities. While it may not be an issue for NN scattering, as suggested by Nuttall's findings, our 4-dimensional equations for πd elastic scattering and $NN \rightarrow \pi d$ scattering would require higher order Padé approximants. However, the iterations of the Bethe-Salpeter equation can be calculated using Wick rotation, as opposed to calculating the integrals along the real axis which was done in the previous chapter. This hybrid Wick rotation and Padé approximant method have had a rich history in the calculation of the Bethe-Salpeter equation for NN scattering in intermediate energies and including heavier meson exchanges [57–62]. Despite Padé approximants being a well established method for solving the Bethe-Salpeter equation, at the current time, matrix inversion is no longer as computationally intensive.

The 4-dimensional Bethe-Salpeter equation can be reduced to a 3-dimensional equation using various reduction techniques that often allow the equation to be more easily solved.

There is no unique method of reducing the Bethe-Salpeter equation and we mention a few notable methods here. The Gross Spectator model was first introduced by Gross [98] and is based on the idea that one of the particles, typically a non-interacting spectator, is restricted to being on its mass shell. The Blankenbecler-Sugar reduction [99] is based on replacing the free Green's function in the Bethe-Salpeter equation by a function that is only singular when both external legs are on-shell. Lastly, the equal time approach is based on the idea of two particles beginning their propagation at equal times and ending their propagation at equal time. The idea was introduced early by Logunov and Tavkhelide [79], with the approach used by several authors over the years [39, 86, 100–106].

While Wick rotation tends to be an effective and efficient method for solving the Bethe-Salpeter equation, there has been recent investigations into calculating the Bethe-Salpeter equation along the real axis. Carbonell et al. [63–68] find that the Euclidean Bethe-Salpeter amplitude (i.e. the Wick-rotated solution to the Bethe-Salpeter equation) provides the same binding energy as the Minkowski solution (i.e. solution without Wick rotation). However, Euclidean Bethe-Salpeter amplitude does not allow for the calculation of some observables, in particular, electromagnetic form factors due to the unknown singularity structure. The Euclidean Bethe-Salpeter amplitude can only be used to calculate the form factors approximately, which is called the static approximation. Carbonell et al. suggest that the off-shell Bethe-Salpeter scattering amplitude is important for many different physical aspects, such as the transition electromagnetic form factors or solving three-body Bethe-Salpeter-Faddeev equations [70]. The authors proceed to calculate the Minkowski solution to the homogeneous Bethe-Salpeter equation using an approach based on the Nakanishi integral representation [71], in which the bound state solution is represented by an integral over a non-singular Nakanishi weight function. The Bethe-Salpeter equation is then transformed using light-front projection [69], which allows the equation to become non-singular. Solving the Bethe-Salpeter equation using a Nakanishi integral representation and light-front projection has also been extended to the case of scattering by Frederico et al. [77, 78], however, only a simple solution could be obtained (the solution in the zero-energy limit) despite a rather lengthy derivation. Therefore, these methods are not ideal for solving the inhomogeneous Bethe-Salpeter equation for scattering states, especially for realistic scattering equations.

While the Nakanishi integral representation and light-front projection method of solving the Bethe-Salpeter equation for scattering states may be unviable for realistic scattering equations, a more straightforward method has been proposed. Carbonell and Karmanov

[70, 72–76] detail a method to calculate the Bethe-Salpeter equation for scattering states, by transforming the equation into a form that does not contain the original pole singularities through the use of the Sokhotski-Plemelj theorem. The authors proceed to solve the resulting equation using splines and handle the singularities in the solution by factoring out the inhomogeneous term from the solution, which we discussed in more detail later in the chapter.

We adapt the method of Carbonell and Karmanov for solving our 4-dimensional πNN convolution equations by using splines and a factorisation method, however, we handle the pole singularities numerically rather than using the Sokhotski-Plemelj theorem. We discuss the method of Carbonell and Karmanov, as well as its application to our 4-dimensional NN convolution equation in greater detail later in the chapter.

4.5 Spline interpolation

4.5.1 Introduction to splines

Let us introduce the concept of splines by applying the concept to NN scattering equations.

Firstly, we have the $NN \rightarrow NN$ Lippmann-Schwinger equation, which is 3-dimensional (3D), given by

$$T(p', p; E) = Z(p', p; E) + \int_0^\infty Z(p', p''; E) D_0(E - E_{p''}) T(p'', p; E) p''^2 dp'' \quad (4.65)$$

where $E_{p''} = p''/(2m_N)$, while our 4-dimensional (4D) $NN \rightarrow NN$ equation is

$$T(z', p', z, p; E) = Z(z', p', z, p; E) + \left(-\frac{1}{2\pi i}\right) \int_{-\infty}^\infty \int_0^\infty Z(z', p', z'', p''; E) g(E - z'') g(z'') T(z'', p'', z, p; E) p''^2 dp'' dz''. \quad (4.66)$$

As these equations have moving singularities in the kernel, discretisation using quadrature points cannot be used to solve the equations. Methods to avoid these singularities, such as contour rotation and Wick rotation, rely on a thorough understanding of the analytic properties of the equation as these methods analytically continue the integrand into the complex plane. As a result, it can be advantageous to solve Equation 4.65 and 4.66 by calculating the integrals along the real axis, which can be done using the method of spline interpolation. The idea of this spline interpolation method is to approximate the unknown

solution $T(p', p; E)$ by the sum

$$T(p', p; E) = \sum_i S_i(p') T(p_i, p; E) \quad (4.67)$$

where $S_i(p)$ are known functions called splines. These splines are piecewise cubic polynomials defined on a set of points $\{p_i\}$ called knots along the interval of integration. The idea of splines is to have a set of functions which allows the approximation in Equation 4.67 to agree with the function at the knots ($T(p_j, p; E) = \sum_i S_i(p_j) T(p_i, p; E)$). Essentially the spline functions act as a Kronecker delta at the knots ($S_i(p_j) = \delta_{ij}$). Not only can they agree on the function value at each knot, but we can use certain spline functions so that the first derivative and higher order derivatives also agree at the knots. Since, we are interested in calculating the fully on-shell amplitude, we let $p = p_0$ where p_0 is the on-shell NN momentum. By using the approximation of Equation 4.67 in our Lippmann-Schwinger equation and calculating this equation at each knot $\{p_i\}$, we obtain a discretised Lippmann-Schwinger equation, given as

$$T(p_i, p_0; E) = Z(p_i, p_0; E) + \sum_{i'} T(p_{i'}, p_0; E) \int_0^\infty Z(p_i, p''; E) D_0(E - E_{p''}) S_{i'}(p'') p''^2 dp''. \quad (4.68)$$

Now, the collection of points $T(p_i, p_0; E)$ are independent of the p'' integral and this integral can now be calculated as accurately as possible, while accounting for the logarithmic singularities in $Z(p_i, p''; E)$ and the pole in the two-nucleon propagator $D_0(E - E_{p''})$. This discretisation allows us to perform a matrix inversion and solve for the points $T(p_i, p_0; E)$, despite the presence of singularities in the integral. This can be extended to the 4D NN equation by having a spline interpolation for both the p and z integral, which we label as $S_{p_i}(p)$ and $S_{z_j}(z)$ respectively.

However, there is a difficulty in using this spline approximation to solve these equations. As has been reported in literature, the half off-shell solution of Equation 4.65, given as $T(p, p_0; E)$, contains a singularity in the off-shell momentum variable p . In the literature, these singularities in the half off-shell solution are known as a square-root type singularity, which results from the logarithmic singularities of the kernel in Equation 4.65. This makes it difficult to use the spline interpolation method, as the approximation in Equation 4.67 relies on the unknown function being a continuously smooth function with respect to p . We now present a brief review of spline interpolation and discuss the attempts to overcome the square-root type singularity present in the half off-shell solution.

4.5.2 An overview of splines

Different functions can be used to construct the interpolating spline functions $S_i(p)$ and according to Matsuyama et al. [107], the choice of splines should be decided based on the function that is to be interpolated. Larson and Hetherington [108] were early investigators of alternative approaches for solving three-body equations without contour rotation, who noted the presence of this square-root type singularity and used Lagrange polynomials as a basis for their interpolation. This is considered to be polynomial interpolation rather than spline interpolation, as splines are typically piecewise cubic polynomials whereas the order of the interpolating polynomial in polynomial interpolation is typically dependent on the number of interpolation points. Deltuva et al. [109] investigated nucleon-deuteron scattering while using Chebyshev polynomials to interpolate their two-baryon transition matrix and deuteron wave-function. Their justification for using Chebyshev polynomials comes from the so-called *Moral Principle 1* described by Boyd [110]. There are also certain benefits with using Chebyshev interpolation including ease of implementation due to the simplicity of the polynomials, but also the choice of knots becomes trivial as one simply chooses the zeros of the Chebyshev polynomials as the knots. The only major disadvantage of Chebyshev interpolation is suggested by Liu [111], in which the kernel of the equation and the inhomogeneous term must be continuous in order to obtain convergence. However, discontinuous integral kernels can be calculated by splitting the integration interval at the discontinuities and populating the intervals with Gaussian quadrature points. The issue with using Chebyshev polynomials is that for higher orders, the Chebyshev polynomial becomes highly oscillatory, which makes it difficult to integrate using Gauss-Legendre quadrature points.

Matsuyama et al. [107] also suggest that spline interpolation is numerically better than polynomial interpolation for the three-body problem as a change in a small region may cause a global effect when using polynomial interpolation. Therefore, it is better practice to use spline interpolation as the splines depend locally on the knots. They also suggest that spline interpolation is known to be less oscillating compared to polynomial interpolation.

There has been much work devoted to using B-splines to solve three-body equations particularly by Alaylioglu et al. [112] and by Huizing and Bakker [113]. Alaylioglu et al. explain that if simple knots are used to construct the B-splines (i.e. $t_{-2} \leq t_{-1} \leq \dots \leq t_{N+2} \leq t_{N+3}$), then one obtains C_2 continuity everywhere. However, this continuity is lost where

multiple knots are introduced and, therefore a triple knot should be placed at the location of the square-root singularity to ensure the interpolation has a C_0 continuity (C_1 discontinuity) at the location of the singularity, which thereby models the behaviour of the square-root singularity. Matsuyama [91] has previously used the modified spline interpolation of Glöckle [114], which have been given the name “natural” splines, and have continuous first and second derivatives at the chosen grid points. Matsuyama suggests one should distribute the knots in such a way as to properly represent the behaviour of the square-root singularity, however, Huizing and Bakker showed numerical errors using these “natural” splines. Matsuyama et al. [107] also suggest these splines are not suitable for such an interpolation and suggest using the Hermitean splines of Hüber et al. [115] in which only the first derivatives are continuous at the knots. These Hermitean splines are also a local spline in the sense that the spline function $S_i(p)$ depends on four knot points $\{p_{i-1}, p_i, p_{i+1}, p_{i+2}\}$, as opposed to the “natural” splines which are a global spline since they depend on all the knots. To overcome the square-root singularity, Matsuyama et al. suggests dividing the whole integration region $[0, \infty]$ into two regions $[0, p_c]$ and $[p_c, \infty]$ where p_c is the location of the square-root singularity and using separate Hermitean splines in each region.

4.5.3 Application to a one-dimensional equation

We now use the spline interpolation method on the $NN \rightarrow NN$ Lippmann-Schwinger equation and compare it to the calculation using contour rotation, in order to determine the accuracy of spline interpolation. Our $NN \rightarrow NN$ Lippmann-Schwinger equation in Equation 4.65, with partial wave indices is given by

$$T_{K',K}(p', p; E) = Z_{K',K}(p', p; E) + \sum_{K_\gamma} \int_0^\infty Z_{K',K_\gamma}(p', p''; E) D_0(E - E_{p''}) T_{K_\gamma, K}(p'', p; E) p''^2 dp'' \quad (4.69)$$

where

$$Z_{K',K}(p', p; E) = \sum_L p' p \Gamma_L(p', p; E) \sum_{a=0}^1 \sum_{b=0}^1 A_{K',K}^{L,a,b} \left(\frac{p'}{p} \right)^{a-b} \quad (4.70)$$

and the function Γ is given as

$$\Gamma_L(p', p; E) = \frac{1}{2} \int_{-1}^1 \frac{k^{-1} f(k, m_N) f(k, m_N) k^{-1}}{E^+ - \frac{p'^2}{2m_N} - \frac{p^2}{2m_N} - 2m_N - \sqrt{m_\pi^2 + p'^2 + p^2} - 2p'px} P_L(x) dx. \quad (4.71)$$

Here, f is the dressed πNN vertex function and all other symbols are defined in Chapter 2 and earlier in this chapter. While we use Equation 4.69 in our calculations, for the proposes

of illustrating the numerical techniques of spline interpolation, we drop the partial wave indices in the subsequent use of Equation 4.69 and we will simply use Equation 4.65.

For the spline interpolation method, we will use the Hermitean splines of Hüber et al. [115] and use the suggestion of Matsuyama et al. [107] to account for the square-root singularity in the solution. While we refer to these equations as 3-dimensional, they reduce to one-dimension through the partial wave decomposition of Afnan and Thomas [29], which we have discussed earlier in the chapter. So, our equation is a partial wave equation, but we suppress any partial wave indices to save on notation.

As previously mentioned, the Hermitean splines of Hüber et al. are local splines and depend only on the neighbouring knots and provide a set of spline function $\{S_0^i, S_1^i, S_2^i, S_3^i\}$ where

$$f_i(x) = \sum_{j=0}^3 S_j^i(x) f(x_j). \quad (4.72)$$

We seek a spline interpolation of the form

$$f(x) = \sum_{i=1}^n \mathcal{S}_i(x) f(x_i) \quad (4.73)$$

where $\mathcal{S}_i(x)$ is an alternate spline function to the Hermitean splines of Hüber et al., n is the number of interpolating points (knots) given by x_1, x_2, \dots, x_n . For the interval $[x_{i-1}, x_{i+1}]$, the function interpolation in that interval is given by

$$\begin{aligned} f(x) &= \sum_{j=0}^3 S_j^i(x) f(x_{i-1+j}) \\ &= S_0^i(x) f(x_{i-1}) + S_1^i(x) f(x_i) + S_2^i(x) f(x_{i+1}) + S_3^i(x) f(x_{i+2}). \end{aligned} \quad (4.74)$$

Comparing this with our desired spline interpolation

$$f(x) = \dots + \mathcal{S}_{i-1}(x) f(x_{i-1}) + \mathcal{S}_i(x) f(x_i) + \mathcal{S}_{i+1}(x) f(x_{i+1}) + \mathcal{S}_{i+2}(x) f(x_{i+2}) + \dots \quad (4.75)$$

one can see that we can write our spline functions as

$$\begin{aligned} \mathcal{S}_{i-1} &= S_0^i & \text{for } x_{i-1} \leq x \leq x_{i+1}, \\ \mathcal{S}_i &= S_1^i & \text{for } x_{i-1} \leq x \leq x_{i+1}, \\ \mathcal{S}_{i+1} &= S_2^i & \text{for } x_{i-1} \leq x \leq x_{i+1}, \\ \mathcal{S}_{i+2} &= S_3^i & \text{for } x_{i-1} \leq x \leq x_{i+1}. \end{aligned} \quad (4.76)$$

Therefore, by swapping the index i , we obtain

$$\begin{aligned}
 \mathcal{S}_i &= S_0^{i+1} & \text{for } x_{i+1} \leq x \leq x_{i+2}, \\
 \mathcal{S}_i &= S_1^i & \text{for } x_{i-1} \leq x \leq x_{i+1}, \\
 \mathcal{S}_i &= S_2^{i-1} & \text{for } x_{i-1} \leq x \leq x_i, \\
 \mathcal{S}_i &= S_3^{i-2} & \text{for } x_{i-2} \leq x \leq x_{i-1}, \\
 \mathcal{S}_i &= 0 & \text{otherwise.}
 \end{aligned} \tag{4.77}$$

Notice now that these new spline functions \mathcal{S}_i interpolate over the interval $[x_{i-2}, x_{i+2}]$. We proceed with these splines in an attempt to solve Equation 4.65.

The main effort is put into calculating the kernel of the Lippmann-Schwinger equation, in which we need to properly handle the poles and logarithmic singularities. A property of splines is that each spline is only non-zero on a finite interval, for example, the Hermitean splines of Hüber et al. are only non-zero on the interval $[x_{i-1}, x_{i+2}]$ and zero everywhere else. This allows us to reduce the integration intervals to greatly improve computation time. Generally, for a spline with the spline index i , which is interpolating the variable x , would only be non-zero on the interval $[x_{i_{\min}}, x_{i_{\max}}]$, thus the kernel of Equation 4.65 becomes

$$K_{ij}(p', p; E) = \int_{p_{i_{\min}}}^{p_{i_{\max}}} Z(p', p''; E) D_0(E - E_{p''}) S_{p_i}(p) p''^2 dp''. \tag{4.78}$$

In this way, the full integral becomes only an integral over the region in which the spline is non-zero, which would also increase the accuracy of the overall integral as we take into account the structure of the spline itself. The integrand of Equation 4.78 exhibits a pole singularity and logarithmic singularities, which arise due to converting the amplitude to a partial wave. The pole singularity corresponds to the on-shell momentum p_0 and can be handled by the subtraction method. Rearranging the kernel equation

$$\begin{aligned}
 K_{ij}(p', p; E) &= \int_{p_{i_{\min}}}^{p_{i_{\max}}} Z(p', p''; E) D_0(E - E_{p''}) S_{p_i}(p'') p''^2 dp'' \\
 &= \int_{p_{i_{\min}}}^{p_{i_{\max}}} \frac{Z(p', p''; E) S_{p_i}(p'') p''^2}{E^+ - \frac{p''^2}{m_N} - 2m_N} dp'' = \int_{p_{i_{\min}}}^{p_{i_{\max}}} \frac{m_N Z(p', p''; E) S_{p_i}(p'') p''^2}{(p_0 + p'')(p_0 - p'')} dp'' \\
 &= \int_{p_{i_{\min}}}^{p_{i_{\max}}} \frac{h(p'')}{p_0 - p''} dp''
 \end{aligned} \tag{4.79}$$

where

$$h(p'') = \frac{m_N Z(p', p''; E) S_{p_i}(p'') p''^2}{p_0 + p''}. \tag{4.80}$$

Now, we apply the subtraction method

$$\begin{aligned}
 K_{ij}(p', p; E) &= \int_{p_{i_{\min}}}^{p_{i_{\max}}} \frac{h(p'')}{p_0 - p''} dp'' \\
 &= \int_{p_{i_{\min}}}^{p_{i_{\max}}} \frac{h(p'') - h(p_0)}{p_0 - p''} dp'' + h(p_0) \int_{p_{i_{\min}}}^{p_{i_{\max}}} \frac{1}{p_0 - p''} dp'' \\
 &= \int_{p_{i_{\min}}}^{p_{i_{\max}}} \frac{h(p'') - h(p_0)}{p_0 - p''} dp'' + h(p_0) \log \left(\frac{p_{i_{\min}} - p_0}{p_0 - p_{i_{\max}}} \right).
 \end{aligned} \tag{4.81}$$

As the integral is over each individual spline region, the subtraction method is only needed when $p_{i_{\min}} < p_0 < p_{i_{\max}}$. If the pole lies outside the integral region, we can simply carry out the integral without any modification. The logarithmic singularities can be determined by solving the equation

$$E^+ - \frac{p^2}{2m_N} - \frac{p'^2}{2m_N} - 2m_N - \sqrt{m_\pi^2 + (p - p')^2} = 0. \tag{4.82}$$

We split the interval of integration at the location of these logarithmic singularities and proceed with the numerical integration using Gaussian quadrature points in each interval.

We can then use matrix inversion to solve Equation 4.65 by converting it into a matrix equation using the set of knots. Specifically,

$$\tilde{T}_i = \tilde{Z}_i + \tilde{K}_{ij} \tilde{T}_j \tag{4.83}$$

where

$$\begin{aligned}
 \tilde{Z}_i &= Z(p_i, p_0; E), \\
 \tilde{K}_i &= K(p_i, p_0; E), \\
 \tilde{T}_i &= T(p_i, p_0; E).
 \end{aligned} \tag{4.84}$$

Here, the set of points $\{p_i\}$ correspond to the knots of $S_i(p)$. We specify the indices of the matrices for clarification, where i would correspond to the knots and i' would correspond to the spline index. So, the solution becomes

$$\tilde{T}_i = (\delta_i - \tilde{K}_{ij})^{-1} \tilde{Z}_i \tag{4.85}$$

and in matrix form

$$\tilde{T} = (\tilde{I} - \tilde{K})^{-1} \tilde{Z} \tag{4.86}$$

where \tilde{I} is the identity matrix. The matrix \tilde{T} gives the off-shell amplitude, but only at the values of the specified knots. However, we can use the splines to interpolate any value of p

Energy (MeV)	Method	Partial Wave Amplitude		
			3S_1	3D_1
$2m_N + 0.001$	Contour	3S_1	$0.0776803 - 0.00311859i$	$0.000417875 - 0.0000167257i$
		3D_1	$0.000417875 - 0.0000167257i$	$-5.577 \times 10^{-6} - 9.05077 \times 10^{-8}i$
	Spline	3S_1	$0.0776586 - 0.00311429i$	$0.000418118 - 0.0000167658i$
		3D_1	$0.000418118 - 0.0000167658i$	$-5.57964 \times 10^{-6} - 9.0289 \times 10^{-8}i$
$2m_N + 0.25m_\pi$	Contour	3S_1	$0.0458811 - 0.0353082i$	$0.0407862 - 0.0133179i$
		3D_1	$0.0407862 - 0.0133179i$	$-0.0144786 - 0.0155977i$
	Spline	3S_1	$0.0458756 - 0.0353073i$	$0.0407944 - 0.0133166i$
		3D_1	$0.0407944 - 0.0133166i$	$-0.0144856 - 0.0156033i$
$2m_N + m_\pi$	Contour	3S_1	$-0.0173664 - 0.0620648i$	$0.0123891 - 0.0160232i$
		3D_1	$0.0123891 - 0.0160232i$	$-0.0288525 - 0.0472092i$
	Spline	3S_1	$-0.0173607 - 0.0620492i$	$0.0124041 - 0.0160077i$
		3D_1	$0.0124041 - 0.0160077i$	$-0.0288553 - 0.0472093i$

Table 4.1: Comparison of the on-shell $NN \rightarrow NN$ amplitude calculated using the contour rotation method and Hermitian spline interpolation for energies below pion production threshold. We use 100 knots in the interval $[0, \infty]$, constructed using Gaussian quadrature points.

as long as these values lie within the whole interval which the splines are defined on. To do this, we use the equation

$$T(p, p_0; E) = \sum_i S_{p_i}(p) \tilde{T}_i. \quad (4.87)$$

If the solution is smooth and does not exhibit any singularities, then we can simply construct knots using Gaussian quadrature points on the interval $[0, \infty]$. However, an issue arises if the solution exhibits a singularity in the off-shell momentum. For energies below $E = 2m_N + m_\pi$ we find that there is no singularity in the solution and there is no difficulty in obtaining a numerically stable answer with respect to the spline knots. We present the results of the spline interpolation method in comparison to the result of contour rotation for energies below $E = 2m_N + m_\pi$ in Table 4.1.

For energies greater than $E = 2m_N + m_\pi$, we find a single square-root singularity and its location can be determined as follows: our OPE driving term contains a denominator of

the form

$$E^+ - \frac{p^2}{2m_N} - \frac{p'^2}{2m_N} - 2m_N - \sqrt{m_\pi^2 + (p - p')^2} \quad (4.88)$$

and the logarithmic singularities that occur in the p'' integral are found by solving the roots of this equation. There is some critical momentum p_c for which there are no solutions for this equations and no logarithmic singularities occur, corresponding to the on-set of the logarithmic singularities. This value of p_c corresponds exactly to the square-root type singularity in the half off-shell amplitude and can be found by simultaneously solving the above equation with it's first derivative with respect to p . Now that we know the location of this square-root singularity, we will need to choose our knots to incorporate this singularity in the solution. Matsuyama et al. [107] suggests to divide the whole integration $[0, \infty]$ into two regions $[0, p_c]$ and $[p_c, \infty]$ where p_c is the location of the square-root singularity. We construct the knots by populating each interval with Gaussian quadrature points and compare the results with the method of contour rotation. We present a comparison of these results in Table 4.2. We see from the results in Table 4.1 and 4.2 that the spline interpolation method provides an accurate alternative to contour rotation. While contour rotation may be easier to implement and computationally less intensive, the fact that splines can be used as an alternative to contour rotation gives us hope that we can use them to calculate our 4-dimensional equations, where contour rotation cannot be used.

Energy (MeV)	Method	Partial Wave Amplitude		
			3S_1	3D_1
$2m_N + 1.1m_\pi$	Contour	3S_1	$-0.0244948 - 0.0563061i$	$0.00660919 - 0.0116121i$
		3D_1	$0.00660919 - 0.0116121i$	$-0.0307488 - 0.0453217i$
	Spline	3S_1	$-0.0244953 - 0.0563064i$	$0.00661011 - 0.0116094i$
		3D_1	$0.00661016 - 0.0116094i$	$-0.0307492 - 0.0453261i$
$2m_N + 1.5m_\pi$	Contour	3S_1	$-0.0351513 + 0.000352941i$	$-0.00436341 + 0.027995i$
		3D_1	$-0.00436341 + 0.027995i$	$-0.0311666 - 0.0203163i$
	Spline	3S_1	$-0.0351516 + 0.000348961i$	$-0.00436306 + 0.0279952i$
		3D_1	$-0.00436293 + 0.0279953i$	$-0.0311675 - 0.0203209i$
$2m_N + 2m_\pi$	Contour	3S_1	$0.00767697 + 0.210377i$	$0.0220606 + 0.173076i$
		3D_1	$0.0220606 + 0.173076i$	$-0.00575005 + 0.0799615i$
	Spline	3S_1	$0.00764185 + 0.210273i$	$0.0220353 + 0.173005i$
		3D_1	$0.0220354 + 0.173005i$	$-0.00576792 + 0.0799114i$

Table 4.2: Comparison of the on-shell $NN \rightarrow NN$ amplitude calculated using the contour rotation method and Hermitian spline interpolation for energies above pion production threshold. We use 100 knots in each sub-interval $[0, p_c]$, $[p_c, \infty]$, constructed using Gaussian quadrature points.

4.6 Application of splines to 2-dimensional scattering equations

We now attempt to solve our 4-dimensional $NN \rightarrow NN$ equation using spline interpolation. Here, we solve for the half off-shell scattering amplitude by letting the initial momentum p and energy-like variable z be on-shell ($p = p_0 = \sqrt{m_N(E - 2m_N)}$, $z = z_0 = E/2$).

4.6.1 Using Hermitian splines of Hüber et al.

The main effort in the calculation of our 4-dimensional NN equation using splines is the calculation of the kernel, in which we need to properly handle the poles and logarithmic singularities. As mentioned previously, a property of splines is that each spline is only non-zero on a finite interval, for example the Hermitean splines of Hüber et al. are only non-zero on the interval $[x_{i-1}, x_{i+2}]$ and zero everywhere else. This allows us to reduce the integration intervals to greatly improve computation time and increases the accuracy of the overall integral as we take into account the structure of the spline itself. Generally, a spline with the index i , which is interpolating the variable x , would only be non-zero on the interval $[x_{i_{\min}}, x_{i_{\max}}]$, thus the kernel of our 4-dimensional NN equation becomes

$$\begin{aligned}
 K_{ij}(z', p', z, p; E) &= \left(-\frac{1}{2\pi i} \right) \int_{z_{j_{\min}}}^{z_{j_{\max}}} \int_{p_{i_{\min}}}^{p_{i_{\max}}} Z(z', p', z'', p''; E) g(E - z'') g(z'') S_{p_i}(p) S_{z_j}(z) p''^2 dp'' dz''.
 \end{aligned}
 \tag{4.89}$$

We then proceed to calculate Equation 4.89 using the methods we have previously developed, namely using a subtraction method to handle the nucleon poles and splitting the interval where a logarithmic singularity occurs for the p'' integral. We then, calculate the integral over $[p_{i_{\min}}, p_{i_{\max}}]$ depending on the singularities that are within the interval. If there are no singularities present within the interval, we simply use Gaussian quadrature points to numerically calculate the integral. If the logarithmic singularities appear within the interval, we split the interval where the singularity occurs and use Gauss-log quadrature points discussed in the previous chapter to calculate the integral. This requires knowing the precise location of the logarithmic singularities, which is also discussed below. If a pole singularity occurs, then we are required to use the subtraction method as shown below.

To handle the pole singularities caused by the dressed propagators, we can either use the Sokhotski-Plemelj theorem or a subtraction method. Here, we choose to use a subtraction method, but we will have to consider the cases where there is only one pole present or if both poles are present. We have the integral

$$\int_{p_{\min}}^{p_{\max}} dp f(p) g_1(z - E_p) g_2(E - z - E_p) \quad (4.90)$$

where $f(p)$ is a function of the momentum p which we are integrating over and contains both the Z term and the spline. If there is one pole present, say, due to the propagator g_1 , then we split the propagator up as follows

$$\begin{aligned} & \int_{p_{\min}}^{p_{\max}} dp f(p) g_1(z - E_p) g_2(E - z - E_p) \\ &= \int_{p_{\min}}^{p_{\max}} dp \left(\frac{Z f(p) g_2(E - z - E_p)}{E_{p_1} - E_p + i\epsilon} + f(p) g_{1c}(z - E_p) g_2(E - z - E_p) \right) \end{aligned} \quad (4.91)$$

where $E_{p_1} = z - m$ and g_{1c} is the cut term of the dressed propagator and contains no pole. The second term of the integral is not a problem, so we only need to worry about the first term. Applying the subtraction method

$$\begin{aligned} & \int_{p_{\min}}^{p_{\max}} dp f(p) g_1(z - E_p) g_2(E - z - E_p) \\ &= \int_{p_{\min}}^{p_{\max}} dp \frac{Z f(p) g_2(E - z - E_p) - Z f(p_1) g_2(E - z - E_{p_1})}{E_{p_1} - E_p + i\epsilon} \\ &+ Z f(p_1) g_2(E - z - E_{p_1}) \int_{p_{\min}}^{p_{\max}} dp \frac{1}{E_{p_1} - E_p + i\epsilon} \\ &+ \int_{p_{\min}}^{p_{\max}} dp f(p) g_{1c}(z - E_p) g_2(E - z - E_p). \end{aligned} \quad (4.92)$$

The final expression we obtain is

$$\begin{aligned} & \int_{p_{\min}}^{p_{\max}} dp f(p) g_1(z - E_p) g_2(E - z - E_p) \\ &= \int_{p_{\min}}^{p_{\max}} dp \frac{Z f(p) g_2(E - z - E_p) - Z f(p_1) g_2(E - z - E_{p_1})}{E_{p_1} - E_p + i\epsilon} \\ &+ Z f(p_1) g_2(E - z - E_{p_1}) \frac{m_N}{p_1} (\log_1^+ - \log_1^-) \\ &+ \int_{p_{\min}}^{p_{\max}} dp f(p) g_{1c}(z - E_p) g_2(E - z - E_p) \end{aligned} \quad (4.93)$$

where

$$\log_1^+ = \log(p_1 + p_{\max} + i\epsilon) - \log(p_1 + p_{\min} + i\epsilon), \quad (4.94a)$$

$$\log_1^- = \log(p_1 - p_{\max} + i\epsilon) - \log(p_1 - p_{\min} + i\epsilon). \quad (4.94b)$$

and we used

$$\begin{aligned}
 \int_{p_{\min}}^{p_{\max}} dp \frac{1}{E_{p_1} - E_p + i\epsilon} &= \int_{p_{\min}}^{p_{\max}} dp \frac{2m_N}{p_1^2 - p^2 + i\epsilon} = \int_{p_{\min}}^{p_{\max}} dp \frac{2m_N}{(p_1 + p)(p_1 - p) + i\epsilon} \\
 &= \frac{m_N}{p_1} \int_{p_{\min}}^{p_{\max}} dp \left[\frac{1}{(p_1 + p) + i\epsilon} + \frac{1}{(p_1 - p) + i\epsilon} \right] \\
 &= \frac{m_N}{p_1} (\log_1^+ - \log_1^-).
 \end{aligned} \tag{4.95}$$

Similarly, if the pole is due to the propagator g_2 . Now, if both poles contribute,

$$\begin{aligned}
 &\int_{p_{\min}}^{p_{\max}} dp f(p) g_1(z - E_p) g_2(E - z - E_p) \\
 &= \int_{p_{\min}}^{p_{\max}} dp f(p) g_{1c}(z - E_p) g_{2c}(E - z - E_p) + \int_{p_{\min}}^{p_{\max}} dp \frac{f(p) Z g_{2c}(E - z - E_p)}{E_{p_1} - E_p + i\epsilon} \\
 &+ \int_{p_{\min}}^{p_{\max}} dp \frac{f(p) g_{1c}(z - E_p) Z}{E_{p_2} - E_p + i\epsilon} + \int_{p_{\min}}^{p_{\max}} dp \frac{f(p) Z^2}{(E_{p_1} - E_p + i\epsilon)(E_{p_2} - E_p + i\epsilon)}.
 \end{aligned} \tag{4.96}$$

The last term of this expansion we split up using partial fractions, which we can then combine with the other terms of the same denominator,

$$\begin{aligned}
 &= \int_{p_{\min}}^{p_{\max}} dp f(p) g_{1c}(z - E_p) g_{2c}(E - z - E_p) \\
 &+ \int_{p_{\min}}^{p_{\max}} dp \frac{f(p) Z g_{2c}(E - z - E_p)}{E_{p_1} - E_p + i\epsilon} + \int_{p_{\min}}^{p_{\max}} dp \frac{f(p) g_{1c}(z - E_p) Z}{E_{p_2} - E_p + i\epsilon} \\
 &+ \int_{p_{\min}}^{p_{\max}} dp \frac{f(p) Z^2}{E_{p_2} - E_{p_1}} \left(\frac{1}{E_{p_1} - E_p + i\epsilon} - \frac{1}{E_{p_2} - E_p + i\epsilon} \right) \\
 &= \int_{p_{\min}}^{p_{\max}} dp f(p) g_{1c}(z - E_p) g_{2c}(E - z - E_p) \\
 &+ \int_{p_{\min}}^{p_{\max}} dp \frac{f(p) Z \left(g_{2c}(E - z - E_p) + \frac{Z}{E_{p_2} - E_{p_1}} \right)}{E_{p_1} - E_p + i\epsilon} + \int_{p_{\min}}^{p_{\max}} dp \frac{f(p) Z \left(g_{1c}(z - E_p) - \frac{Z}{E_{p_2} - E_{p_1}} \right)}{E_{p_2} - E_p + i\epsilon}.
 \end{aligned} \tag{4.97}$$

We now apply the subtraction method

$$\begin{aligned}
 &= \int_{p_{\min}}^{p_{\max}} dp f(p) g_{1c}(z - E_p) g_{2c}(E - z - E_p) \\
 &+ \int_{p_{\min}}^{p_{\max}} dp \frac{f(p) Z \left(g_{2c}(E - z - E_p) + \frac{Z}{E_{p_2} - E_{p_1}} \right) - f(p_1) Z \left(g_{2c}(E - z - E_{p_1}) + \frac{Z}{E_{p_2} - E_{p_1}} \right)}{E_{p_1} - E_p + i\epsilon} \\
 &+ \int_{p_{\min}}^{p_{\max}} dp \frac{f(p) Z \left(g_{1c}(z - E_p) - \frac{Z}{E_{p_2} - E_{p_1}} \right) - f(p_2) Z \left(g_{1c}(z - E_{p_2}) - \frac{Z}{E_{p_2} - E_{p_1}} \right)}{E_{p_2} - E_p + i\epsilon} \\
 &+ f(p_1) Z \left(g_{2c}(E - z - E_{p_1}) + \frac{Z}{E_{p_2} - E_{p_1}} \right) \int_{p_{\min}}^{p_{\max}} dp \frac{1}{E_{p_1} - E_p + i\epsilon} \\
 &+ f(p_2) Z \left(g_{1c}(z - E_{p_2}) - \frac{Z}{E_{p_2} - E_{p_1}} \right) \int_{p_{\min}}^{p_{\max}} dp \frac{1}{E_{p_2} - E_p + i\epsilon}.
 \end{aligned} \tag{4.98}$$

The final expression that we obtain is

$$\begin{aligned}
 &= \int_{p_{\min}}^{p_{\max}} dp f(p) g_{1c}(z - E_p) g_{2c}(E - z - E_p) \\
 &+ \int_{p_{\min}}^{p_{\max}} dp \frac{f(p) Z \left(g_{2c}(E - z - E_p) + \frac{Z}{E_{p_2} - E_{p_1}} \right) - f(p_1) Z \left(g_{2c}(E - z - E_{p_1}) + \frac{Z}{E_{p_2} - E_{p_1}} \right)}{E_{p_1} - E_p + i\epsilon} \\
 &+ \int_{p_{\min}}^{p_{\max}} dp \frac{f(p) Z \left(g_{1c}(z - E_p) - \frac{Z}{E_{p_2} - E_{p_1}} \right) - f(p_2) Z \left(g_{1c}(z - E_{p_2}) - \frac{Z}{E_{p_2} - E_{p_1}} \right)}{E_{p_2} - E_p + i\epsilon} \\
 &+ f(p_1) Z \left(g_{2c}(E - z - E_{p_1}) + \frac{Z}{E_{p_2} - E_{p_1}} \right) \frac{m_N}{p_1} (\log_1^+ - \log_1^-) \\
 &+ f(p_2) Z \left(g_{1c}(z - E_{p_2}) - \frac{Z}{E_{p_2} - E_{p_1}} \right) \frac{m_N}{p_2} (\log_2^+ - \log_2^-).
 \end{aligned} \tag{4.99}$$

where \log_2^+ and \log_2^- are similarly defined by Equation 4.94. The logarithmic singularities are easily obtained by solving the equation

$$z' - z'' - \sqrt{m_\pi^2 + (p' \pm p'')^2} = 0. \tag{4.100}$$

We also need to take into account singularities or discontinuities that occur in the z'' integral. To find the location of these singularities or discontinuities, we can consider Equation 4.89 as a function of z'' after the p'' integral is calculated and plot this function against z'' to visually see the discontinuities.

In our investigation of kernel singularities, we often refer to the singularities as strong singularities and minor singularities based on their effect in the numerical calculation of the kernel. It is critical that we properly account for strong singularities when calculating the kernel integrals, as it is detrimental to the numerical accuracy if not handled properly. Minor singularities in the kernel integral, on the other hand, can be handled by simple “brute force” i.e. many quadratures points, and are not as detrimental to numerical accuracy as strong singularities. However, for more numerical accuracy, it is advantageous for the minor singularities to be accounted for as well.

The strongest singularities have been determined and mimic the square-root singularities that were seen when considering the NN Lippmann-Schwinger equation, where the singularity occurs at the value of z'' for which there are no more logarithmic singularities in the p'' integral i.e. the on-set of the logarithmic singularities. Therefore, the singularity in z'' can be found by simultaneously solving the equation of the logarithmic singularities with

it's first derivative with respect to p''

$$\begin{aligned} \frac{p' \pm p''}{\sqrt{m_\pi^2 + (p' \pm p'')^2}} &= 0, \\ z' - z'' - \sqrt{m_\pi^2 + (p' \pm p'')^2} &= 0. \end{aligned} \quad (4.101)$$

Solving these equations simultaneously gives the location of the square-root like singularity

$$z'' = z' - m_\pi. \quad (4.102)$$

This supports the splitting of the z'' integral for the case of the fully on-shell dressed two-pion exchange (TPE) amplitude that was calculated earlier, as when $z' = E/2$ and $p' = p_0$ the singularity corresponds to a value of $z'' = E/2 - m_\pi$. We have an extra singularity in the case of the dressed TPE amplitude as we have two Z^{OPE} terms as opposed to one in Equation 4.89. For dressed TPE amplitude, the denominator of one Z^{OPE} term is $z' - z'' - \sqrt{m_\pi^2 + (p' \pm p'')^2}$ while the other is $z'' - z' - \sqrt{m_\pi^2 + (p' \pm p'')^2}$, so this extra singularity is found by interchanging z' and z'' in Equation 4.101 and we find corresponds to a value of $z'' = E/2 + m_\pi$.

Other strong singularities can be seen at the nucleon mass $z'' = m_N$ and at the total energy minus the nucleon mass $z'' = E - m_N$. These values come from the poles due to the propagators and correspond to the minimum/maximum value for a pole singularity to exist in the p'' integral. More explicitly, if $z'' < m_N$, only the pole which is a solution of $E - z'' - p''^2/2m_N - m_N = 0$ exists, whereas if $z'' > E - m_N$, then only the pole which is a solution of $z'' - p''^2/2m_N - m_N = 0$ exists. If $m_N < z'' < E - m_N$, then both poles exist, so the values for $z'' = m_N$ and $z'' = E - m_N$ are in essence, the boundaries of poles existence in the p'' integral. The analytical structure of the z'' integrand changes rapidly when the pole structure in the p'' integral changes, which manifests as a discontinuity.

There are also minor singularities in the z'' variable and have been determined to be when a logarithmic singularity and a pole occur at the same location in the p'' integration.

We, therefore, solve the simultaneous equations

$$\begin{aligned} z' - z'' - \sqrt{m_\pi^2 + (p' \pm p'')^2} &= 0, \\ z'' - \frac{p''^2}{2m_N} - m_N &= 0, \end{aligned} \quad (4.103)$$

and we solve

$$\begin{aligned} z' - z'' - \sqrt{m_\pi^2 + (p' \pm p'')^2} &= 0, \\ E - z'' - \frac{p''^2}{2m_N} - m_N &= 0, \end{aligned} \quad (4.104)$$

which to obtain values for p'' and z'' . We denote these as ‘minor’ singularities, as we believe they do not contribute to the convergence of the z'' integral, as greatly as the singularities mentioned previously. It may be that the contribution of these singularities may be minimised or even neglected if the p'' integral is calculated with high accuracy by using many Gauss-Legendre quadrature points, which may be the reason we did not encounter these singularities when calculating the fully on-shell dressed TPE amplitude. Nevertheless, we treat them in the same way as the other singularities, in case their contribution is greater than initially anticipated.

We then proceed with the integration over z'' in a similar way to the p'' integral. If there are no singularities present within the interval, we simply use Gaussian quadrature points to numerically calculate the integral. However, if there are singularities present, we split the interval where the singularity occurs and used Gaussian quadrature points in each interval (we do not use Gauss-log quadrature points for the z'' integral, as the singularities are not explicitly logarithmic singularities like in the p'' integral).

We can then use matrix inversion to solve Equation 4.66 by converting it into a matrix equation using the set of knots. Specifically,

$$\tilde{T}_{ij} = \tilde{Z}_{ij} + \tilde{K}_{ijj'}\tilde{T}_{ij'} \quad (4.105)$$

where

$$\begin{aligned} \tilde{Z}_{ij} &= Z(z_j, p_i, z_0, p_0; E), \\ \tilde{K}_{ij} &= K(z_j, p_i, z_0, p_0; E), \\ \tilde{T}_{ij} &= T(z_j, p_i, z_0, p_0; E). \end{aligned} \quad (4.106)$$

Here, the set of points $\{z_j\}$ correspond to the knots of S_{z_j} , while the points $\{p_i\}$ correspond to the knots of S_{p_i} . We specify the indices of the matrices for clarification, where i, j would correspond to the knots and i', j' would correspond to the spline index. So, the solution becomes

$$\tilde{T}_{ij} = (\delta_{ii'}\delta_{jj'} - \tilde{K}_{ijj'})^{-1}\tilde{Z}_{ij} \quad (4.107)$$

and in matrix form

$$\tilde{T} = (\tilde{I} - \tilde{K})^{-1}\tilde{Z} \quad (4.108)$$

where \tilde{I} is the identity matrix. The matrix \tilde{T} gives the off-shell amplitude, but only at the values of the specified knots. However, we can use the splines to interpolate any value of p

and z as long as these values lie within the whole interval which the splines are defined on. To do this, we use the equation

$$T(z, p, z_0, p_0; E) = \sum_{ij} S_{p_i}(p) S_{z_j}(z) \tilde{T}_{ij}. \quad (4.109)$$

We proceed with the calculation without any modification to the knots, in an attempt to see if there are any singularities present in the solution. We try to find the singularities in the p variable by having a relatively low number of z knots and a high number of p knots. We then plot the calculated off-shell amplitude for a fixed z knot against the p knots. What we find is that when the z knot is below a value of $E/2$, there are no visible singularities and the amplitude is smooth. When the z knot is between $E/2$ and $E - m_N$, there seems to be a single singularity. Finally, when the z knot is greater than $E - m_N$, there seem to be multiple singularities. The singularities for $z > E - m_N$ correspond to the same singularities found in the inhomogeneous term of our 4-dimensional NN equation $Z(z, p, z_0, p_0; E)$ in the p variable. This makes sense, as the inhomogeneous term is part of the solution and its singularities only occur when $z > E - m_N$. These singularities are found by solving

$$z - z_0 - \sqrt{m_\pi^2 + (p \pm p_0)^2} = 0. \quad (4.110)$$

So, unfortunately, it seems like the solution of our 4-dimensional NN equation has singularities in it, similar to the square-root singularities that we encountered for our 3-dimensional Lippmann-Schwinger. The issue with the 4-dimensional (numerically 2-dimensional after partial wave decomposition) is that these singularities could exist for both p and z variables. So there is no systematic method to choose knots, which avoid the singularities in both variables. This is a big problem and we need to explore a method that can overcome these singularities in the solution.

4.6.2 The approach of Carbonell and Karmanov

We now examine the method for solving the Bethe-Salpeter for scattering states proposed by Carbonell and Karmanov [70, 72–76]. While the Bethe-Salpeter equation is fully relativistic, the problem that they present directly correlates to ours, as the authors describe the problem as difficulty in computing the off-shell scattering amplitude due to the singular nature of the kernel. They also suggest that the singularities are integrable in the mathematical sense, due to $i\epsilon$ in the denominators of propagators, but their integration is quite a delicate

task and requires the use of appropriate analytical as well as numerical methods. In order to handle the 4 pole singularities of the Bethe-Salpeter equation, Carbonell and Karmanov use the Sokhotski-Plemelj theorem. With the Sokhotski-Plemelj theorem and a subtraction method, they obtain a full expression of the off-shell Bethe-Salpeter equation for scattering states, which does not contain the pole singularities due to the propagators. Carbonell and Karmanov also suggest that the logarithmic singularities can be integrated over numerically using a “brute force” method of using an excessive number of Gaussian quadrature points. However, it is an advantage to determine the precise location of these singularities to improve precision, as one can use a change of variable to carry out the integration.

The authors outline their use of splines in earlier work [116], saying they use Hermitean splines of Payne [117], which differ from the explicit splines that are used by Hüber et al. The property of Hermitean splines is that they agree with the function at each knot and they also agree with the first derivative at each knot. We denote the function interpolation denoted as $f_i(x)$ on the interval $[x_{i-1}, x_{i+1}]$, which is given by

$$f_i(x) = f(x_i)\phi_1(x) + f(x_i)\phi_2(x) + f'(x_i)\phi_3(x) + f'(x_i)\phi_4(x) \quad (4.111)$$

where ϕ_1, ϕ_3 interpolate the region $[x_{i-1}, x_i]$ and ϕ_2, ϕ_4 interpolate the region $[x_i, x_{i+1}]$. This is true for both cases, but Hüber et al. approximate the derivatives by using a quadratic polynomial. The reason is that the spline interpolation becomes dependent only on the function itself and independent of its derivative, meaning that the coefficients that are solved for are simply the value of the function at the knots. However, approximating the derivatives adds an extra level of approximation which may lead to inaccuracy. Carbonell and Karmanov explain how to apply these Hermitean splines without approximating the derivative of the unknown function, which require an alternative method of “collocation”. We will apply this method to our case of the 4-dimensional NN equation of Equation 4.66.

We approximate the half off-shell amplitude by the spline interpolation

$$T(z, p, z_0, p_0; E) = \sum_{ij} \tilde{a}_{ij} S_{p_i}(p) S_{z_j}(z) \quad (4.112)$$

where \tilde{a}_{ij} are unknown coefficients that we solve for. The splines are defined on the intervals $[0, p_{\max}]$ and $[z_{\min}, z_{\max}]$, which we divide at the points $\{p_i\}$ and $\{z_j\}$ into N_p and N_z intervals respectively. The set of knots $\{p_i\}$ and $\{z_j\}$ correspond to the knots for which the set of splines are defined on. Here, we have $i = 0, N_p$ and $j = 0, N_z$ where $p_0 = 0, p_{N_p} = p_{\max}$ and $z_0 = z_{\min}, z_{N_z} = z_{\max}$ (let us not confused p_0 and z_0 here with the on-shell values for p and

z). The spline function are given as

$$S_{p_i}(p) = \begin{cases} \phi_p(\frac{i}{2}, p) & \text{if } i \text{ is even} \\ \xi_p(\frac{i-1}{2}, p) & \text{if } i \text{ is odd} \end{cases} \quad (4.113)$$

$$S_{z_j}(z) = \begin{cases} \phi_z(\frac{j}{2}, z) & \text{if } j \text{ is even} \\ \xi_z(\frac{j-1}{2}, z) & \text{if } j \text{ is odd} \end{cases} \quad (4.114)$$

where, for a general variable x

$$\phi_{x_i}(x) = \begin{cases} 3 \left(\frac{x-x_{i-1}}{x_i-x_{i-1}} \right)^2 - 2 \left(\frac{x-x_{i-1}}{x_i-x_{i-1}} \right)^3 & \text{if } x \in [x_{i-1}, x_i] \\ 3 \left(\frac{x_{i+1}-x}{x_{i+1}-x_i} \right)^2 - 2 \left(\frac{x_{i+1}-x}{x_{i+1}-x_i} \right)^3 & \text{if } x \in [x_i, x_{i+1}] \\ 0 & \text{otherwise} \end{cases} \quad (4.115)$$

$$\xi_{x_i}(x) = \begin{cases} \left[- \left(\frac{x-x_{i-1}}{x_i-x_{i-1}} \right)^2 + \left(\frac{x-x_{i-1}}{x_i-x_{i-1}} \right)^3 \right] (x_i - x_{i-1}) & \text{if } x \in [x_{i-1}, x_i] \\ \left[\left(\frac{x_{i+1}-x}{x_{i+1}-x_i} \right)^2 - \left(\frac{x_{i+1}-x}{x_{i+1}-x_i} \right)^3 \right] (x_{i+1} - x_i) & \text{if } x \in [x_i, x_{i+1}] \\ 0 & \text{otherwise} \end{cases} \cdot \quad (4.116)$$

Here, ϕ_{x_i} correspond to ϕ_1 and ϕ_2 in Equation 4.111, while ξ_{x_i} correspond to ϕ_3 and ϕ_4 . As we essentially have 2 splines for every knot (ϕ_{x_i} corresponding to the value of the function at the knot and ξ_{x_i} corresponding to the first derivative at the knot), we will need to run our spline indices over $i = 0, 2N_p + 1$ and $j = 0, 2N_z + 1$. We will choose two sets of points $\{\bar{p}_i\}$ and $\{\bar{z}_j\}$ called collocation points within the intervals $[0, p_{\max}]$ and $[z_{\min}, z_{\max}]$, for which we have $2N_p + 2$ points in $[0, p_{\max}]$ and $2N_z + 2$ points in $[z_{\min}, z_{\max}]$. These will be the points, for which we collect the unknown spline coefficients \tilde{a}_{ij} , rather than using the knots for the case of Hüber et al. and Matsuyama. Now, inserting our spline interpolation of Equation 4.112 into Equation 4.66

$$\sum_{i'j'} \tilde{U}_{ij,i'j'} \tilde{a}_{i'j'} = \tilde{Z}_{ij} + \sum_{i'j'} \tilde{K}_{ij,i'j'} \tilde{a}_{i'j'} \quad (4.117)$$

where

$$\begin{aligned} \tilde{Z}_{ij} &= Z(\bar{z}_j, \bar{p}_i, z_0, p_0; E), \\ \tilde{K}_{ij} &= K(\bar{z}_j, \bar{p}_i, z_0, p_0; E), \\ \tilde{U}_{ij,i'j'} &= S_{p_{i'}}(\bar{p}_i) S_{z_{j'}}(\bar{z}_j). \end{aligned} \quad (4.118)$$

and $K(z', p', z'', p''; E)$ is the same kernel in Equation 4.89 using the splines defined above. Again, we use the tilde notation with subscript indices to denote the matrix elements where

ij correspond to the collocation points and $i'j'$ correspond to the spline indices. We then proceed to solve for the coefficients \tilde{a}_{ij} by solving matrix equation

$$\tilde{a} = (\tilde{U} - \tilde{K})\tilde{Z}. \quad (4.119)$$

Once the spline coefficients are known, any value of p and z within the interval $[0, p_{\max}]$ and $[z_{\min}, z_{\max}]$ can be determined using Equation 4.112.

We are now ready to calculate the off-shell amplitude using the procedure outlined by Carbonell and Karmanov, however they suggest that the amplitude has many non-analyticities due to the inhomogeneous term and due to the interaction kernel. This is similar to what was found earlier using the splines of Hüber et al., as we saw singularities in the solution corresponding to the singularities present in the inhomogeneous term. They suggest because of these singularities, it is difficult to represent the off-shell amplitude on a basis of non-singular functions, namely the splines in which we approximate the amplitude with. They suggest to factor out the inhomogeneous term by making the replacement

$$T(z, p, z_0, p_0; E) = Z(z, p, z_0, p_0; E)\chi(z, p; E)t(z, p, z_0, p_0; E) \quad (4.120)$$

where t will now be a smoother function and χ is an arbitrary but suitable scalar function introduced to provide a convenient inhomogeneous term. Upon this factorisation, our 4-dimensional NN equation will become

$$\begin{aligned} Z(z, p, z_0, p_0; E)\chi(z, p; E)t(z, p, z_0, p_0; E) &= Z(z, p, z_0, p_0; E) \\ &+ \left(-\frac{1}{2\pi i}\right) \int_{-\infty}^{\infty} \int_0^{\infty} Z(z, p, z'', p''; E)g(E - z'')g(z'')Z(z'', p'', z_0, p_0; E) \\ &\times \chi(z'', p''; E)t(z'', p'', z_0, p_0; E)p''^2 dp'' dz''. \end{aligned} \quad (4.121)$$

Now, taking the inverse of $Z(z, p, z_0, p_0; E)\chi(z, p; E)$,

$$\begin{aligned} t(z, p, z_0, p_0; E) &= \frac{1}{\chi(z, p; E)}Z(z, p, z_0, p_0; E)^{-1}Z(z, p, z_0, p_0; E) \\ &+ \left(-\frac{1}{2\pi i}\right) \frac{1}{\chi(z, p; E)}Z(z, p, z_0, p_0; E)^{-1} \int_{-\infty}^{\infty} \int_0^{\infty} Z(z, p, z'', p''; E)g(E - z'')g(z'') \\ &\times Z(z'', p'', z_0, p_0; E)\chi(z'', p''; E)t(z'', p'', z_0, p_0; E)p''^2 dp'' dz''. \end{aligned} \quad (4.122)$$

Our final expression is

$$t(z, p, z_0, p_0; E) = \frac{1}{\chi(z, p; E)}I + \int_{-\infty}^{\infty} \int_0^{\infty} K_F(z, p, z'', p''; E)t(z'', p'', z_0, p_0; E)p''^2 dp'' dz''. \quad (4.123)$$

where

$$\begin{aligned}
 K_F(z, p, z'', p''; E) = & \left(-\frac{1}{2\pi i} \right) \frac{1}{\chi(z, p; E)} Z(z, p, z_0, p_0; E)^{-1} Z(z, p, z'', p''; E) \\
 & \times g(E - z'')g(z'')Z(z'', p'', z_0, p_0; E)\chi(z'', p''; E).
 \end{aligned}
 \tag{4.124}$$

We now use the spline interpolation method on the smooth function t . We refer to this method as Carbonell-Karmanov (CK) factorisation.

While the CK factorisation has theoretically removed the singularities in the solution, in practice, this factorisation is numerically unviable. This is because the kernel function in Equation 4.124 becomes much larger than the original kernel of Equation 4.89, due to the inverse Z -diagram. As the inverse Z -diagram contains a term of the form $1/p$, the kernel function approaches infinity when the p knots as calculated close to zero.

To overcome this, instead of performing the CK factorisation, we could factor out a scalar function from the solution which has the same functional form as a Z -diagram (we will call this scalar function Z_l), instead of factoring out the whole Z -diagram. As we keep the same functional form, this scalar function will contain the same singularities as a Z -diagram, but we avoid this problem of having an inverse Z -diagram in the kernel function. However, it can be shown that the function $Z_l^{-1}Z$ still possesses the singularities of Z . This would most likely be because the magnitude of the singularities in Z_l and Z are not equal, so the singularities do not exactly cancel each other out. Therefore, a factorisation of Z_l from the solution would not result in a smooth function and the spline interpolation would still be difficult. Thus, we must factor out the whole Z -diagram from the solution, in order to eliminate the singularities in the solution. The only other way to avoid the issue with using an inverse Z -diagram would be to truncate the interval $[0, p_{\max}]$, so the 0 is not one of the p knots. We suggest choosing knots on the interval $[0.1, p_{\max}]$. In practice, this truncation provides ensures the kernel of Equation 4.124 is not extremely large at the first few p knots, while also not being a sufficient truncation in which would impact the interpolation of the interval $[0, \infty]$.

This factorisation introduces new singularities in the kernel function as the inhomogeneous term must be integrated in the kernel. Though, as they are the same singularities, we already know their location. In the p'' integral, the singularities introduced by the inhomogeneous term are obtained by solving the equation

$$z'' - z_0 - \sqrt{m_\pi^2 + (p'' \pm p_0)^2} = 0. \quad (4.125)$$

Similarly, in the z'' , we find a square-root like singularity when

$$z'' = z_0 - m_\pi. \quad (4.126)$$

We also find minor singularities, due to the interaction of the pole singularities and logarithmic singularities in the p'' integral. We find these singularities in the z'' integral by solving the simultaneous equations

$$\begin{aligned} z'' - z_0 - \sqrt{m_\pi^2 + (p'' \pm p_0)^2} &= 0, \\ z'' - \frac{p''^2}{2m_N} - m_N &= 0, \end{aligned} \quad (4.127)$$

and we solve

$$\begin{aligned} z'' - z_0 - \sqrt{m_\pi^2 + (p'' \pm p_0)^2} &= 0, \\ E - z'' - \frac{p''^2}{2m_N} - m_N &= 0. \end{aligned} \quad (4.128)$$

Chapter 5

Two-body input

5.1 Co-authorship statement

This chapter is adapted from a manuscript, that has been published in a peer-reviewed journal. The reference for this publication is:

Blankleider, B., Wray, J. L., & Khvinikidze, A. N, (2021). Dyson–Schwinger approach to pion–nucleon scattering using time-ordered perturbation theory. *AIP Advances*, 11(2), 1-11. [025204]. <https://doi.org/10.1063/5.0034753>

The thesis author is listed as the second author in this manuscript. The relevant sections of this chapter that this manuscript is referred to is: Section 5.4 to the end of the chapter.

The content of this manuscript relates to the πN scattering in the framework of time-ordered perturbation theory, where all nucleons are fully dressed. The essential goal of this thesis is to formulate the πNN system where all nucleons are fully dressed, where the equations derived from this formulation, namely the πNN convolution equations, rely on πN t -matrices with fully dressed nucleons as input. Therefore, it is essential to include a description of πN scattering with fully dressed nucleons in this thesis. The primary content and research ideas were formulated and discussed between the first author and the thesis author (second author). The thesis author was responsible for producing the results, including writing the computer code to conduct the calculations, producing the table of values, and producing the graphs. The thesis author has also significantly contributed to the editing of the manuscript.

5.2 Introduction

As solving 4-dimensional three-body equations is a difficult numerical task, we can use a separable potential approximation to the two-body processes, which will reduce the problem of solving 4-dimensional equations to, effectively, a two-body problem. In this case, the general 4-dimensional form of the πNN convolution equations given in Equations 3.154 can be reduced, after partial wave decomposition, to the 2-dimensional form given in Equation 3.163. A notable aspect of these equations is that the input separable two-body t -matrices have dressed nucleons in the intermediate states. Therefore, two-body t -matrices with dressed nucleons would need to be constructed as the previously constructed πN and NN

separable t -matrices readily available in the literature all use undressed nucleons in the intermediate states.

We create dressed πN input by numerically solving the Dyson-Schwinger equations given in Equation 5.10a, Equation 5.11a, and Equation 5.12.

The importance of accurate NN potentials as input in few-body problems led to the development of accurate NN potentials, such as the Bonn [118, 119], Argonne [120, 121], Nijmegen [122, 123], Paris [124, 125] and the Reid [126] potentials. Of course, it is advantageous to have a separable approximation to these accurate NN potentials, such as the separable approximations constructed in [127–132]. However, for our purposes, these potentials are constructed using undressed nucleon propagators, whereas we require input that is constructed using dressed nucleon propagators. Due to the lack of accurate NN potentials that incorporate nucleon dressing in the literature, and no other way to construct a realistic separable NN potential that incorporates dressing, we will use NN input that is constructed using undressed nucleon propagators, such as the input given by Bhatt et al. [133] and Mongan [134, 135].

In the absence of NN input that incorporates nucleon dressing, we will only use our Dyson-dressed πN inputs in calculations of the πNN convolution equations, where we only have πN two-body processes. For example, we use Dyson-dressed πN inputs in calculations of NN elastic scattering where NN is the only intermediate channel. For calculations containing both πN and NN two-body processes, we use two-body inputs constructed using undressed nucleon propagators, such as the NN input mentioned previously and πN input given by Afnan and McLeod [40] and Thomas [22]. We refer to this input as “undressed input” and specify this input below.

5.3 The undressed inputs

5.3.1 The NN potentials

For the coupled ${}^3S_1 - {}^3D_1$ channel, we will use a unitary pole approximation (UPA) of the Reid Soft Core potential. The form factor of the UPA is given by Equation 5.1

$$h_l^{\text{UPA}}(k) = \sum_i C_{il} \frac{k^l}{(k^2 + \beta_i^2)^{\frac{l+2}{2}}} \quad (5.1)$$

where l is the orbital angular momentum ($l = 0$ corresponding to the 3S_1 and $l = 2$ corresponding to the 3D_1). The parameters for the UPA are given in Table 5.1. The ${}^3S_1 - {}^3D_1$ channel is the only coupled two-body channel that we consider in our calculations.

i	β_i (fm $^{-1}$)	C_{i0} (fm $^{-1}$)	C_{i2} (fm $^{-1}$)
1	0.7	1.76363×10^{-2}	-5.89573×10^{-3}
2	1.4	-1.53401×10^0	2.21753×10^{-1}
3	2.1	4.26244×10^1	-1.24662×10^1
4	2.8	-3.42140×10^2	7.79072×10^1
5	3.5	1.22668×10^3	-2.26824×10^2
6	4.2	-1.59317×10^3	2.20502×10^2
7	5.6	9.22828×10^2	-5.00828×10^1
8	8.4	-3.19981×10^2	-2.04641×10^1
9	12.6	6.54176×10^1	1.18944×10^1

Table 5.1: Parameters for the form factors of the unitary pole approximation of the Reid Soft Core potential to the coupled ${}^3S_1 - {}^3D_1$ NN potential. The fits were performed by Bhatt et al. [133].

For the πN channels other than the coupled ${}^3S_1 - {}^3D_1$ channel, the form factor is given by

$$h_{li}(k) = \frac{C_{li} k^l}{(k^2 + \beta_{li}^2)^\gamma} \quad (5.2)$$

and the parameters are given in Table 5.2

NN channel	γ	C_{l1} (fm $^{1+l-2\gamma}$)	β_{l1} (fm $^{-1}$)	λ_{l1}	C_{l2} (fm $^{1+l-2\gamma}$)	β_{l2} (fm $^{-1}$)	λ_{l2}
1S_0	1	21.49867	6.157	+1	1.945558	1.786	-1
1P_1	3/2	35.59382	2.951	+1			
3P_0	2	94.60838	5.000	+1	1.922066	1.462	-1
3P_1	2	14.25889	2.661	+1			
3P_2	2	8.72049	2.720	-1			
1D_2	2	1.50135	1.944	-1			
3D_2	2	1.46647	1.468	-1			
3D_3	2	35.15246	6.558	+1	0.549284	1.451	-1

Table 5.2: The parameters of the form factors of the uncoupled NN channels given by Mongan [134, 135].

5.3.2 The πN potentials

When the two body process involves pion creation or annihilation, the form factor is the dressed vertex function ($f(k, E)$ for creation and $\bar{f}(k, E)$ for annihilation). The form factor for s -wave πN input is given by

$$h(k) = \frac{S_1}{\alpha_1^2 + k^2} + \frac{S_2}{\alpha_2^2 + k^2}, \quad (5.3a)$$

while the form factor for p -wave πN input is given by

$$h(k) = \frac{S_1 k}{(\alpha_1^2 + k^2)^2} + \frac{S_2 k^3}{(\alpha_2^2 + k^2)^2}. \quad (5.3b)$$

The parameters for the πN input are given in Table 5.3.

πN channel	S_1	α_1 (fm $^{-1}$)	S_2	α_2 (fm $^{-1}$)	λ
S_{11}	1.7826	3.188	0.0894	0.8225	-1
S_{31}	6.0786	3.382	-0.1661	1.107	+1
P_{33}	0.5403	1.475	1.0583	3.400	-1
P_{31}	4.290	2.059			+1
P_{13}	1.557	1.244	3.659	1.945	+1

Table 5.3: The parameters of the form factors for the πN channel given by Thomas [22].

The πN scattering length is given as

$$a_{\pi N} \sim -\pi\mu T_{\pi N}(k_0, k_0) \quad \text{as } k_0 \rightarrow 0 \quad (5.4)$$

for s -waves and

$$a_{\pi N} \sim -\pi\mu \frac{T_{\pi N}(k_0, k_0)}{k_0^2} \quad \text{as } k_0 \rightarrow 0 \quad (5.5)$$

for p -waves, where μ is the reduced mass of the πN system and k_0 is the on-shell πN momentum.

5.4 Constructing πN input that incorporates nucleon dressing

5.4.1 Pion-nucleon equations

With the model describing the interactions of pions and nucleon given in Chapter 2, we can define the Green's function G that shall be used to describe pion-nucleon scattering, as

$$\delta(\mathbf{k} + \mathbf{p} - \mathbf{k}' - \mathbf{p}') G(\mathbf{p}', \mathbf{k}, \mathbf{p}, E) = \langle \mathbf{k}' \mathbf{p}' | \frac{1}{E^+ - H} | \mathbf{k} \mathbf{p} \rangle. \quad (5.6)$$

As the Green's function $G(\mathbf{p}', \mathbf{k}, \mathbf{p}, E)$ describing πN scattering can be equated to a complete sum of perturbation diagrams, this provides the opportunity to rearrange this sum so as to express it completely in terms of useful quantities like potentials, t -matrices, and other Green's functions, thereby generating scattering equations of a similar nature to those found in Quantum Mechanics (e.g. the Lippmann-Schwinger equation). Such a rearrangement leads to a set of coupled equations for πN scattering illustrated in Figure 5.1.

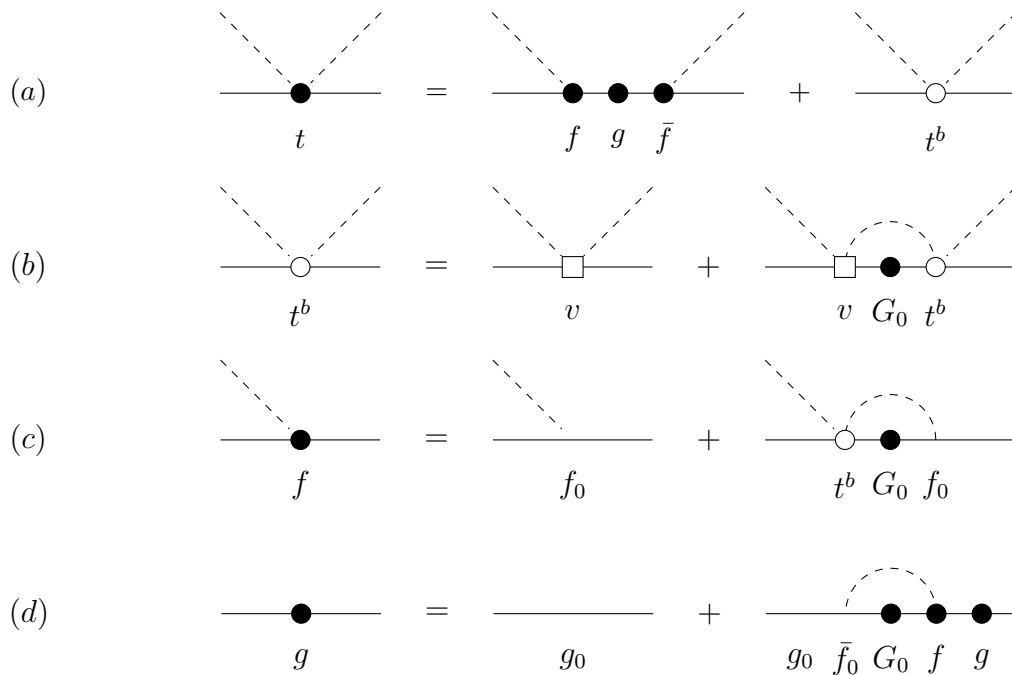


Figure 5.1: Illustration of the πN scattering equations: (a) The πN t -matrix expressed by Equation 5.9, (b) the “background” πN t -matrix as given by Equation 5.10a, (c) the dressed πNN vertex as given by Equation 5.11a, and (d) the dressed nucleon propagator as given by Equation 5.12 whose self-energy term Σ is expressed as in Equation 5.13a.

First derived by Mizutani and Koltun using Feshbach projection operators [80], these equations were later derived in the same context of TOPT as used here [33] and also in the context of relativistic quantum field theory (RQFT) [136]. Here we shall give a brief derivation following the arguments used in [33].

We start by writing the Green’s function $G(\mathbf{p}', \mathbf{k}, \mathbf{p}, E)$ in operator form as

$$G(E) = G_0(E) + G_0(E)t(E)G_0(E) \quad (5.7)$$

where $G_0(E)$ is the “dressed πN propagator” consisting of all the disconnected diagrams of $G(E)$, and $t(E)$ is the $\pi N \rightarrow \pi N$ t -matrix which is defined by this equation. Note that each quantity in Equation 5.7 is an operator acting in subspace $\mathcal{H}_{\pi N}$, with $G(E)$ being specifically defined such that

$$\langle \mathbf{k}' \mathbf{p}' | G(E) | \mathbf{k} \mathbf{p} \rangle = \langle \mathbf{k}' \mathbf{p}' | \frac{1}{E^+ - H} | \mathbf{k} \mathbf{p} \rangle. \quad (5.8)$$

It is evident that the term $G_0(E)t(E)G_0(E)$ in Equation 5.7 consists of all possible *connected* $\pi N \rightarrow \pi N$ diagrams and that $t(E)$ consists of the same diagrams but with no attached initial- and final-state πN propagators, colloquially referred to as diagrams with “chopped legs”.

Further progress can be made by defining a “background” πN t -matrix $t^b(E)$ as the sum of all diagrams of $t(E)$ that have one or more pions in every intermediate state, as one can then write

$$t(E) = f(E)g(E)\bar{f}(E) + t^b(E) \quad (5.9)$$

where $f(E)$ ($\bar{f}(E)$) is the “dressed vertex” consisting of all possible $N \rightarrow \pi N$ ($\pi N \rightarrow N$) chopped-leg diagrams with at least one pion in every intermediate state. Similarly, one can define t -matrix $t^{(2)}(E)$ as the sum of all diagrams of $t(E)$ that have two or more pions in every intermediate state, in which case we can write Lippmann-Schwinger-like equations

$$t^b(E) = v(E) + v(E)G_0(E)t^b(E), \quad (5.10a)$$

$$= v(E) + t^b G_0(E)v(E) \quad (5.10b)$$

where $v(E) \equiv t^{(2)}(E)$ plays the role of a $\pi N \rightarrow \pi N$ potential. Using a similar argument, one can obtain the equations

$$f(E) = f_0(E) + t^b(E)G_0(E)f_0(E), \quad (5.11a)$$

$$\bar{f}(E) = \bar{f}_0(E) + \bar{f}_0(E)G_0(E)t^b(E), \quad (5.11b)$$

where $f_0(E) \equiv f^{(2)}(E)$ ($\bar{f}_0(E) \equiv \bar{f}^{(2)}(E)$) is the “bare vertex” consisting of all possible $N \rightarrow \pi N$ ($\pi N \rightarrow N$) chopped-leg diagrams with at least two pions in every intermediate state. Finally, one can similarly write

$$g(E) = g_0(E) + g_0(E)\Sigma(E)g(E) \quad (5.12)$$

where

$$\Sigma(E) = \bar{f}_0(E)G_0(E)f(E), \quad (5.13a)$$

$$= \bar{f}(E)G_0(E)f_0(E), \quad (5.13b)$$

is the nucleon “self-energy” or “dressing” term consisting of all diagrams of $g(E)$ with at least one pion in every intermediate state, but with chopped legs. The set of equations consisting of Equations 5.9-5.13 are illustrated in Figure 5.1, and provide an exact and useful way of expressing the πN t -matrix $t(E)$.

In the context of RQFT, Equation 5.12 (illustrated in Figure 5.1 (d)) is known as the Dyson equation, while the coupled set of equations Equation 5.10a, Equation 5.11a, and Equation 5.12, illustrated in Figure 5.1 (b)-(d), are known as the Dyson-Schwinger (DS)

equations, and that is how we shall refer to the TOPT versions of these equations here. A feature of the Dyson equation is the fact that the dressed nucleon propagator g is expressed in terms of the self-energy term Σ which itself is expressed in terms of g via the πN propagator $G_0(E)$. Such self-referencing also occurs for the background t -matrix t^b and the dressed vertex f in the Dyson-Schwinger equations, a feature that makes these equations embody a lot of physics even in the case where the bare vertex f_0 and background potential v are modelled phenomenologically, as will be the case in the next section.

5.5 Solving the Dyson-Schwinger equations

Here we shall follow an often used procedure where the bare πNN vertex f_0 and the “background” πN potential v are modelled by energy-independent parametrized phenomenological functions; however, unlike in all such previous models [33, 36, 80–83], we shall not be using the approximation where the exact πN propagator $G_0(E, \mathbf{k}, \mathbf{p})$, defined as

$$\delta(\mathbf{k}' - \mathbf{k})\delta(\mathbf{p}' - \mathbf{p})G_0(E, \mathbf{k}, \mathbf{p}) = \langle \mathbf{k}' \mathbf{p}' | \frac{1}{E^+ - H} | \mathbf{k} \mathbf{p} \rangle_{disc}, \quad (5.14)$$

is modelled by the pole term $1/[E^+ - E_N(p) - m - \omega_\pi(k)]$; rather, we shall retain its full exact form, which in the model specified by the Hamiltonian defined in Equations 2.12, is given by

$$G_0(E, \mathbf{k}, \mathbf{p}) = g[E - E_N(p) - \omega_\pi(k)]. \quad (5.15)$$

As mentioned above, it is this exact form for G_0 which gives the Dyson-Schwinger equations the property of retaining a rich amount of physics despite what may be lost by taking phenomenological forms for f_0 and v .

5.5.1 Partial wave equations

It is convenient to solve the Dyson-Schwinger set of equations, given in operator form in Equations 5.10-5.13, in the centre of mass (c.m.) of the πN system, so that $\mathbf{k} + \mathbf{p} = \mathbf{k}' + \mathbf{p}' = \mathbf{0}$, in which case Equation 5.15 can be expressed as

$$G_0(E, \mathbf{k}) = g(E - \omega_k) \quad (5.16)$$

where

$$\omega_k = E_N(k) + \omega_\pi(k). \quad (5.17)$$

In order to reduce the dimension of these equations from 3 to 1, we shall work in the partial wave representation using the basis states

$$|l s j t, m_j m_t, k\rangle = \sum_{\substack{m_{t_1} m_{t_2} \\ m_l m_s}} (l m_l s m_s | j m_j) (t_1 m_{t_1} t_2 m_{t_2} | t m_t) \int d\hat{k} Y_{l m_l}(\hat{k}) |t_1 m_{t_1} t_2 m_{t_2}, \mathbf{k}\rangle \quad (5.18)$$

where $t_1 = 1$ is the isospin of the pion, $t_2 = 1/2$ is the isospin of the nucleon, $s = 1/2$ is the spin of the nucleon, l specifies the πN relative orbital angular momentum, t is the total isospin, and j is the total angular momentum. By construction, the model Hamiltonian of Equation 2.12 is invariant under rotations, which implies that all matrix elements using the above partial wave basis states will not depend on the magnetic quantum numbers m_j and m_t . Similarly, the model Hamiltonian is chosen to be invariant under space inversion, thus ensuring parity is conserved in our model which in turn, leads to πN partial wave matrix elements that preserve the value of l . We shall refer to the partial wave specified by the quantum numbers $\{l j t\}$ using the usual (for πN scattering) spectroscopic notation of the form “ $L_{(2t)(2j)}$ ”. Because the nucleon has quantum numbers $t = j = 1/2$ and the pion has intrinsic parity of -1 , it follows that the first term on the right hand side (RHS) of Equation 5.9, the so-called *nucleon pole term*, contributes only in the P_{11} partial wave. Likewise, the background πN t -matrix t^b appearing in the expression for the dressed πNN vertices of Equations 5.11 is the one in the P_{11} partial wave. Thus, restricting the discussion to πN scattering in the P_{11} partial wave, we can write the numerical form of the partial wave equations corresponding to Figure 5.1 as

$$t(k', k, E) = f(k, E)g(E)\bar{f}(k, E) + t^b(k', k, E) \quad (5.19a)$$

$$t^b(k', k, E) = v(k', k) + \int_0^\infty dq q^2 v(k', q)g(E - \omega_q)t^b(q, k, E) \quad (5.19b)$$

$$f(k, E) = f_0(k) + \int_0^\infty dq q^2 t^b(k, q, E)g(E - \omega_q)f_0(q) \quad (5.19c)$$

$$g(E) = \frac{1}{E^+ - m_0 - \Sigma(E)} \quad (5.19d)$$

$$\Sigma(E) = \int_0^\infty dq q^2 f_0(q)g(E - \omega_q)f(q, E) \quad (5.19e)$$

where partial wave labels have been omitted to save on notation. For scattering in partial waves other than P_{11} , essentially the same equations would apply, the only differences being that the pole term in Equation 5.19a would not appear, and one would need to distinguish the t^b appearing in Equation 5.19a from the P_{11} partial wave t^b appearing in Equation 5.19c.

In order to help solve these equations numerically, it is useful to know the analytic structure of the dressed nucleon propagator $g(E)$. As a basic requirement of theory, $g(E)$ must have a pole at the physical nucleon mass m . To ensure this, the bare mass is set to the value $m_0 = m - \Sigma(m)$ so that

$$g(E) = \frac{1}{E^+ - m - \Sigma(E) + \Sigma(m)} \quad (5.20)$$

and therefore

$$g(E) \underset{E \rightarrow m}{\sim} \frac{Z}{E^+ - m} \quad (5.21)$$

where Z is the wave function renormalization constant given by

$$Z = \frac{1}{1 - \Sigma'(m)} \quad (5.22)$$

where the prime indicates a derivative with respect to E . To evaluate $\Sigma'(m)$, one can use the identity

$$\Sigma'(E) = \int_0^\infty dq q^2 \bar{f}(q, E) g'(E - \omega_q) f(q, E). \quad (5.23)$$

which can be easily proved using the operator form of Equations 5.19. In this work we do not consider nucleon resonances in the P_{11} channel as these lie beyond the energies that we consider. Thus, in our model, there are no further poles in the complex energy plane.

Besides a nucleon pole, it can be shown that $g(E)$ also contains a cut starting at $E = m + m_\pi$ and extending to $+\infty$, and that this analytic structure implies the following ‘‘dispersion relation’’ [48]

$$g(E) = \frac{Z}{E^+ - m} - \frac{1}{\pi} \int_{m+m_\pi}^\infty \frac{\text{Im}g(\omega)}{E^+ - \omega} d\omega. \quad (5.24)$$

As we shall see, this relationship between $g(E)$ and its imaginary part will prove very useful in the numerical solution of the Dyson-Schwinger equations. This expression for $g(E)$ is also convenient for the evaluation of Equation 5.23 as

$$g'(E) = -\frac{Z}{(E^+ - m)^2} + \frac{1}{\pi} \int_{m+m_\pi}^\infty \frac{\text{Im}g(\omega)}{(E^+ - \omega)^2} d\omega. \quad (5.25)$$

5.5.2 Separable potential model

To keep this model as simple as possible, we choose a separable form for the partial wave potential v :

$$v(k', k) = h(k') \lambda h(k), \quad (5.26)$$

where $h(k)$ is a phenomenological form factor and λ specifies the sign of the potential (for the P_{11} partial wave under consideration here, $\lambda = -1$). The use of separable potentials to describe the strong interactions of a pion and a nucleon has a long and rich history. In 1967, Varma [26] used such potentials to perform the first three-body calculation of the πNN system; since then, they have been used extensively to investigate effects of pion absorption [33, 36, 80–82], pion-nucleus scattering [137–140], three-body forces [141, 142], pion photoproduction [143, 144], dibaryons [145, 146], and also to facilitate solutions of relativistic equations [147–150]. The motivation for their widespread use is their convenience, often leading to significant simplifications in both analytic and numerical work. Although short-range interactions are naturally separable at energies close to resonance poles, they can also be well approximated through the use of low-rank separable potentials at energies away from scattering poles, as long as the underlying realistic potential is energy independent [151–157]. For πN scattering at the considered energies ($0 < T_\pi < 390$ MeV), much of the low-energy energy dependence of the underlying interaction is due to the nucleon pole term, which only contributes to the P_{11} partial wave. As we treat the pole term separately, it is reasonable to assume that the P_{11} background term and the rest of the partial wave interactions can be reasonably modelled with separable potentials [158]. Nevertheless, the neglect of residual energy dependence and the lack of crossing symmetry in our model [159] suggests that the separable potentials developed in this work would be most useful as input to calculations that do not rely critically on the accuracy of the off-shell behaviour of the πN interaction.

In the case of a separable potential, Equation 5.19b can be solved algebraically, giving also a separable form for the background πN t -matrix:

$$t^b(k', k, E) = h(k') \tau(E) h(k) \quad (5.27)$$

where

$$\tau(E) = \left[1 - \lambda \int_0^\infty dq q^2 h(q) g(E - \omega_q) h(q) \right]^{-1} \lambda. \quad (5.28)$$

Defining the four dressing terms

$$\Sigma_{ij}(E) = \int_0^\infty dq q^2 \phi_i(q) g(E - \omega_q) \phi_j(q), \quad (i, j = 1, 2) \quad (5.29)$$

where $\phi_1(q) \equiv f_0(q)$ and $\phi_2(q) \equiv h(q)$, the Dyson-Schwinger equations can be conveniently

expressed as the set of three equations

$$g(E) = \frac{1}{E^+ - m - \Sigma(E) + \Sigma(m)} \quad (5.30a)$$

$$\Sigma(E) = \Sigma_{11}(E) + \Sigma_{12}(E)\tau(E)\Sigma_{21}(E) \quad (5.30b)$$

$$\tau(E) = [1 - \lambda\Sigma_{22}(E)]^{-1} \lambda, \quad (5.30c)$$

which determine the dressed nucleon propagator $g(E)$, together with the additional two equations

$$t(k', k, E) = f(k, E)g(E)\bar{f}(k, E) + h(k')\tau(E)h(k) \quad (5.31a)$$

$$f(k, E) = f_0(k) + h(k)\tau(E)\Sigma_{21}(E), \quad (5.31b)$$

that determine the consequent dressed πNN vertex f and πN t -matrix t .

Numerical procedure

In our approach, modelling πN scattering with Equations 5.19 begins by choosing parametrised analytic functions for the form factors $f_0(k)$ and $h(k)$. These form factors need to fulfil the requirement of providing a momentum cutoff that ensures finite values for the integrals defining the Σ functions of Equation 5.13, and they must behave linearly with k in the limit of low momenta in order to be consistent with the $l = 1$ nature of a P_{11} partial wave amplitude. We shall follow a previous work where separable potentials were used to model πN scattering, and choose the following analytic forms [83]

$$f_0(k) = \frac{k C_0}{\sqrt{\omega_\pi(k)}} \frac{1}{(k^2 + \Lambda^2)^{n_0}}, \quad (5.32a)$$

$$h(k) = \frac{k C_1}{\sqrt{\omega_\pi(k)}} \left[\frac{1}{(k^2 + \beta_1^2)^{n_1}} + \frac{C_2 k^{2n_2}}{(k^2 + \beta_2^2)^{n_3}} \right], \quad (5.32b)$$

where $C_0, C_1, C_2, \beta_1, \beta_2, \Lambda$ are free parameters, and the powers n_0, n_1, n_2, n_3 are integers that can be chosen to change the functional form of the form factors.

For any given set of parameters, the first task is to solve the Dyson-Schwinger equations in the form of Equations 5.30 for the dressed nucleon propagator $g(E)$. We do this by following an iterative procedure where an approximation to $g(E)$ is used in Equation 5.29 to calculate all the functions $\Sigma_{ij}(E)$, which are then used to calculate a new (and hopefully more accurate) version of $g(E)$ using Equations 5.30. The process is repeated until convergence

for $g(E)$ is achieved. By construction, the resulting propagator $g(E)$ satisfied the Dyson-Schwinger equations and can be then used to generate the dressed vertex f and the πN t -matrix t using Equations 5.31.

Technical Aspects

To carry out the integral in Equation 5.29 numerically, we use Gaussian quadratures, and to avoid the singularity coming from the pole of $g(E)$, we rotate the integration contour from the positive real axis, into the 4th quadrant of the complex q plane. However, a practical problem remains in carrying out these integrals because in order to generate a propagator $g(E)$ at any iteration, one needs to know the previous iteration's propagators $g(E - \omega_{q_i})$ for each of the rotated quadrature points q_i . Thus the number of energies at which one needs to know g quickly escalates as the iteration proceeds. To get around this problem, we make use of the fact that the dressed nucleon propagator $g(E)$, at each step of the iteration, satisfies the dispersion relation of Equation B.20. This allows us to evaluate Equation 5.29 as

$$\begin{aligned} \Sigma_{ij}(E) = & \int_0^\infty dq q^2 \frac{Z\phi_i(q)\phi_j(q)}{E^+ - \omega_q - m_N} \\ & - \frac{1}{\pi} \int_{m_N+m_\pi}^\infty \text{Im}g(\omega) \int_0^\infty dq q^2 \frac{\phi_i(q)\phi_j(q)}{E^+ - \omega_q - \omega} d\omega \end{aligned} \quad (5.33)$$

which requires knowledge of $g(E)$ only at a number of fixed values of E corresponding to the Gaussian integration points ω_i used to evaluate the ω integral in Equation 5.33. The iterative process thus proceeds according to the following steps:

1. For any given set of form factor parameters, begin the iteration by generating the “non-Dyson” dressed nucleon propagator $g^{(0)}(E)$ defined by Equations 5.30 but where the nucleon in the πN propagator used in the dressing terms Σ_{ij} , is not explicitly dressed; that is, by using

$$\Sigma_{ij}(E) \rightarrow \int_0^\infty dq q^2 \frac{\phi_i(q)\phi_j(q)}{E^+ - \omega_q - m_N}. \quad (5.34)$$

It is just this $g^{(0)}(E)$ that has been used in previous works [40, 83] to model πN scattering.

2. Having constructed the “0th iteration” of $g(E)$ as above, we now use this g in Equation 5.33 to generate new dressing terms $\Sigma_{ij}(E)$.
3. Using these newly constructed $\Sigma_{ij}(E)$'s in Equations 5.30 generates the next iteration of the dressed nucleon propagator $g(E)$.

5.5.3 Numerical results

After constructing the dressed nucleon propagator $g(E)$ as prescribed by the 3 steps outlined above, we now repeat steps 2 and 3 over and over, thus generating successive iterations of $g(E)$, denoted as $g^{(1)}(E), g^{(2)}(E), g^{(3)}(E), \dots$ until the values of $g^{(r)}(E)$ converge according to the criterion $|[g^{(r)}(\omega_i) - g^{(r-1)}(\omega_i)]/g^{(r)}(\omega_i)| < \epsilon$ for all ω integration points ω_i , where ϵ is some chosen tolerance value. We have found that the iterated dressed propagators $g^{(r)}(E)$ converge for all considered models using a convergence tolerance of $\epsilon = 10^{-4}$, and that correspondingly, the resulting numerical values of the converged $g(E)$ functions are stable to at least 5 significant figures with respect to variations in the number of quadrature points used for all integrals, and in the contour rotation angle used for all the q momentum integrals. We note that the convergence of $g(E)$ also provides a self-consistency check that no resonance poles have been generated by the assumed separable potentials.

With the Dyson-Schwinger equations of Equations 5.19 solved in this way, it is interesting to compare the resulting fully dressed ‘‘Dyson’’ nucleon propagator $g(E)$ with the ‘‘non-Dyson’’ one where the coupled equations of Figure 5.1 are solved in the ‘‘one-pion’’ approximation where nucleon dressing in πN states is neglected. We present this comparison in Figure 5.2 for the case where the parameters of the input bare πNN vertex and background πN potential are those of model $M1$ in [83]. For ease of comparison, we have plotted the corresponding real and imaginary values of $(E - m_N)g(E)/Z$, being the renormalised nucleon propagators with the nucleon pole term factored out. As can be seen, there is a substantial difference between the two propagators, suggesting the importance of retaining nucleon dressing in πN states.

To obtain a variety of models of nucleon dressing, we have carried out fits to the WI08 P_{11} πN phase shifts [160] (for pion laboratory energies up to 390 MeV) by using the functional forms of Equations 5.32 for a range of cutoff values Λ for the bare πNN vertex function $f_0(k)$. Each such fit was constrained to reproduce the πNN coupling constant $f_{\pi NN}^2 = 0.079$ in the way described in [83]. The parameters of four such fits are given in Table 5.4 with the corresponding values of $(E - m_N)g(E)/Z$ plotted in Figure 5.3. Unsurprisingly, the large number of parameters in this model allows one to fit πN data equally well for a wide range of cutoff parameters Λ . Although this flexibility of the model can be viewed as one of its weaknesses, it does allow one to accommodate the wide variety of πNN vertex cutoffs, in the range $300 < \Lambda < 2200$ MeV, used in the literature [161–171].

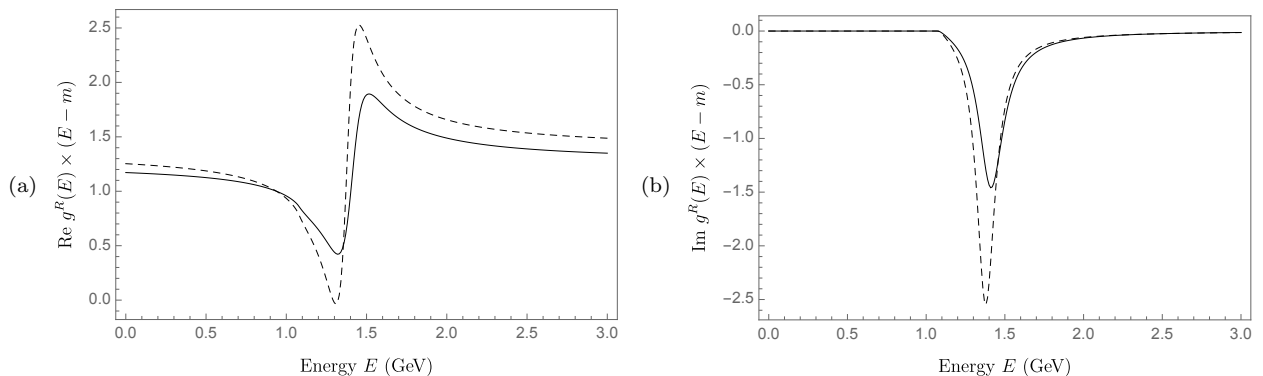


Figure 5.2: (a) Real and (b) imaginary parts of $g^R(E)(E - m_N)$ where $g^R(E) = g(E)/Z$ is the renormalised dressed nucleon propagator. The solid curves are for the Dyson propagator (resulting from the solution of the Dyson-Schwinger equations), while the dashed curves are for the non-Dyson propagator (resulting from the use of the one-pion-approximation).

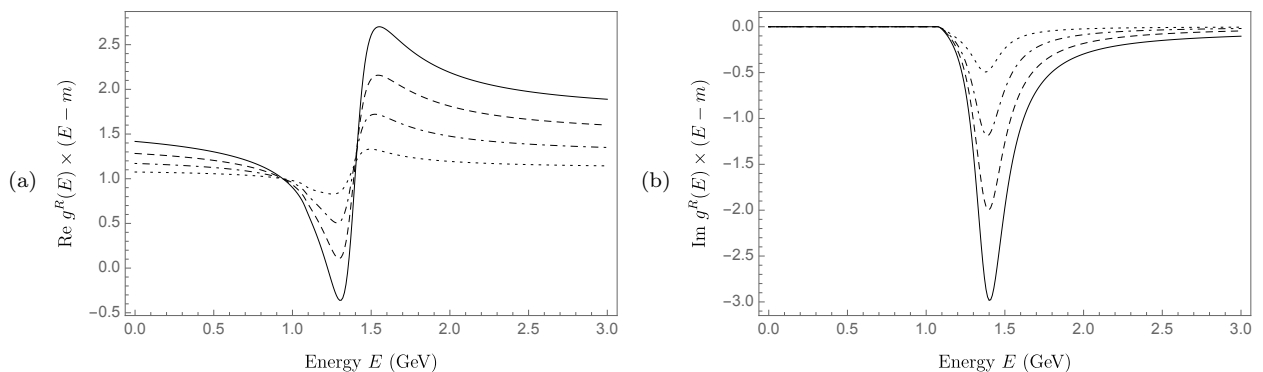


Figure 5.3: (a) Real and (b) imaginary parts of $g^R(E)(E - m_N)$ where $g^R(E)$ is the renormalised dressed Dyson nucleon propagator, for the four models specified in Table 5.4. The solid curves represent the $M6$ model, the dashed curves represent the $M7$ model, the dot-dashed curves represent the $M8$ model and the dotted curves represent the $M9$ model.

Finally we show that Equations 5.19, which use the fully dressed Dyson propagators, are able to be used to fit all s - and p -wave πN phase shifts for pion lab kinetic energies in the range $0 < T_{lab} < 390$ MeV. To demonstrate this explicitly, we have chosen the $M7$ model of Table 5.4 whose cutoff parameter is $\Lambda = 800$ MeV, a value suggested by an investigation of Quantum Chromodynamic sum rules [172]. For the non- P_{11} partial wave πN potentials, we use the separable forms of Thomas [22] whose form factors are parametrised as

$$h(k) = \frac{S_1}{\alpha_1^2 + k^2} + \frac{S_2}{\alpha_2^2 + k^2}, \quad (5.35a)$$

for s -waves and

$$h(k) = \frac{S_1 k}{(\alpha_1^2 + k^2)^2} + \frac{S_2 k^3}{(\alpha_2^2 + k^2)^2}, \quad (5.35b)$$

for p -waves. These form factors were used by Thomas to describe pion-deuteron scattering in a calculation using semi-relativistic kinematics [22].

Potential	Λ (fm ⁻¹)	β_1 (fm ⁻¹)	β_2 (fm ⁻¹)	C_0	C_1	C_2	m_0 (fm ⁻¹)	Z
<i>M9</i>	1.71991	1.14162	1.88154	0.64225	0.23808	8.9632	5.00289	0.90054
<i>M8</i>	2.72329	1.26878	1.78328	1.1778	0.32923	6.2150	5.33579	0.79369
<i>M7</i>	4.04994	1.4176	1.77246	1.7827	0.42271	4.8618	5.69286	0.69481
<i>M6</i>	10.8023	1.62718	1.8684	4.7174	0.58264	3.5638	6.29540	0.60027

Table 5.4: Parameters of four fits (labelled as models *M9*, *M8*, *M7*, and *M6*) to the P_{11} πN phase shifts through the solution of the Dyson-Schwinger equations of Equation 5.32. The first 9 parameters refer to the form factors of while m_0 is the bare nucleon mass and Z is the nucleon wave-function renormalisation constant.

Our partial wave phase shift fits using the *M7* model for the Dyson propagator $g(E)$ are shown in with the corresponding parameters listed (under the rows labelled *M7*) in Table 5.5. Equally good fits to all the phase shifts can be obtained using the other models for $g(E)$ (*M9*, *M8* and *M6*) with the corresponding parameters being given in Table 5.4 for the P_{11} and Table 5.5 for the other partial waves. It should be noted, however, that equally good fits can also be obtained using non-Dyson propagators. Thus, even though we are able to demonstrate the importance of nucleon dressing, the large number of parameters in our model does not allow us to identify any features of the phase-shift data that may prefer the “Dyson” over the “non-Dyson” dressed nucleon propagators.

πN	λ	P_{11}	S_1	α_1	S_2	α_2
Partial wave		model		(fm ⁻¹)		(fm ⁻¹)
S_{11}	-1	$M9$	-11.557	10.057	-0.12483	0.85466
		$M8$	-11.715	9.9173	-0.13350	0.85973
		$M7$	-11.818	9.7449	-0.14334	0.86536
		$M6$	-12.046	9.6221	-0.15518	0.87236
S_{31}	+1	$M9$	3.8017	1.9930	-1.0897	1.3266
		$M8$	4.2003	2.0120	-1.1815	1.3292
		$M7$	4.7214	2.0350	-1.3090	1.3365
		$M6$	5.4998	2.0668	-1.5227	1.3574
P_{31}	+1	$M9$	9.5578	2.5488		
		$M8$	10.339	2.5549		
		$M7$	11.250	2.5620		
		$M6$	12.370	2.5704		
P_{13}	+1	$M9$	3.6208	1.8244	1.5209	3.2380
		$M8$	3.5755	1.8022	1.4249	3.0757
		$M7$	3.5051	1.7801	1.3111	2.9082
		$M6$	3.3855	1.7492	1.1932	2.7126
P_{33}	-1	$M9$	0.74876	1.7551	1.2295	4.9512
		$M8$	0.80133	1.7535	1.2212	4.8276
		$M7$	0.86060	1.7519	1.2126	4.7019
		$M6$	0.93047	1.7501	1.2041	4.5665

Table 5.5: Parameters of fits to the s - and p -wave πN phase shifts (other than P_{11}) for each of the four models ($M9$, $M8$, $M7$, and $M6$) for the dressed Dyson nucleon propagator $g(E)$ used in the coupled πN equations of Equation 5.19. The parameters refer to the form factors of Equation 5.35. The s -wave strengths are in fm⁻¹, for p -waves S_2 is dimensionless and S_1 is in fm⁻¹.

Chapter 6

Numerical results

6.1 Co-authorship statement

This chapter is adapted from a manuscript, soon to be written and submitted to a peer-reviewed journal. The reference for the manuscript is:

Wray, J. L., Blankleider, B., & Khvinikidze, A. N, (2021). Convolution approach to πNN . II. Numerical solution. (to be submitted to *Physical Review C* upon completion)

The thesis author is listed as the first author in this manuscript. The relevant sections of this chapter that this manuscript is referred to is: the whole chapter including elements from Chapter 4 and Chapter 5.

The numerical design and solution of the convolution model whose theory is developed in Chapter 3, was done almost exclusively by the thesis author, and constitutes the content of Chapters 4, 5, and 6 of the thesis. The journal article is an account of this work and the author order reflects the relative contribution to this part of the research. The manuscript is as yet unwritten, but it is planned that the thesis author will be writing the majority of the paper.

6.2 Introduction

Now that we have discussed the method for solving our 4-dimensional (4D) scattering equations and developed numerical techniques, we present the numerical results of the 4-dimensional πNN convolution equations. We perform a numerical calculation of Equations 3.163, representing the processes of πd elastic scattering, $pp \rightarrow \pi^+ d$ scattering and NN scattering. From this numerical calculation, we calculate observables associated with each process with a particular interest in the $pp \rightarrow \pi^+ d$ scattering cross sections and the T_{20} polarisation observable for πd elastic scattering. We are interested in these particular observables as the πNN convolution equations are the first πNN equations to include full dressing of the nucleons, while the inadequacy of the “Unitary $NN - \pi NN$ ” model in reproducing these observables has long been attributed to the underdressing of nucleons in this model. While our primary goal would be to see if the πNN convolution equations are able to overcome the limitations of the “Unitary $NN - \pi NN$ ” model, the computational intensity of our numerical calculations limits our ability to achieve this goal. However, we are still able to

make some preliminary observations about the potential of the πNN convolution equations.

With our calculation of the 4-dimensional πNN convolution equations, our goals are as follows:

1. Compare the observables calculated using the πNN convolution equations with those obtained using the equations of the “Unitary $NN - \pi NN$ ” model, to determine the effect of consistent dressing.
2. Compare the observables calculated using the πNN convolution equations with experimental data, to determine whether the convolution equations provide a better prediction of experiments in comparison to the equations of the “Unitary $NN - \pi NN$ ” model.
3. Investigate the viability of the spline interpolation method as a method for solving 4-dimensional scattering equations with moving singularities in the kernel of the integral equations.

While we provide the numerical results to the πNN convolution equations, solving these 4-dimensional equations has turned out to be a computationally intensive task. As a result, it has only been viable to include just one coupled channel when performing our numerical calculations.

6.3 Numerical 4-dimensional πNN convolution equations

We will now explicitly express the equations we solve and their functional form. Solving these 4D equations using spline interpolation requires many interpolation points (or knots) to obtain numerical stability. The need for many interpolation points, in combination with many quadrature points needed to converge the z'' and p'' integrals, demands significant computational power. For this reason, we calculate our 4D results with only one coupled channel. This means that, in our numerical calculations, we only include one intermediate channel in our scattering equations.

For $NN \rightarrow \pi d$ scattering ($pp \rightarrow \pi^+ d$ scattering), we couple our equations only to the P_{33} channel ($N\Delta$ channel) with the lowest relative orbital angular momentum value L . By coupling only to the P_{33} channel, only $N\Delta$ states are allowed in the intermediate states i.e.

$NN \rightarrow N\Delta \rightarrow N\Delta \rightarrow \dots \rightarrow N\Delta \rightarrow \pi d$. When calculating results for πd scattering, we also couple only to the P_{33} channel with the lowest L value. The coupling to P_{33} is chosen as this channel is dominant due to the $\Delta(1232)$ resonance. In a separate calculation, we also calculate results for πd elastic scattering with coupling only to NN with the lowest orbital angular momentum value L . This will allow us to include the diagram referenced by Jennings [42], shown in Figure 1.6, who suggested that the inclusion of this diagram will improve the reproducibility of the T_{20} polarisation observable. We calculate results for elastic NN scattering without coupling to any other channel. In a separate calculation, we also calculate results for NN scattering coupled only the P_{33} channel with the lowest orbital angular momentum value L .

Here, we detail the numerical form of our equations describing πd elastic scattering, as equivalent numerical equations and diagrammatic representations can be obtained for $NN \rightarrow \pi d$ scattering and NN scattering, by following the same conventions. In the following numerical scattering equations that we present, we omit partial wave indices and antisymmetry labels to save on notation.

The fully on-shell partial wave πd t -matrix (coupled only to the P_{33} channel) is given as

$$\begin{aligned}
 X_{dd}(E) = & \left(-\frac{1}{2\pi i}\right) \int_{-\infty}^{\infty} dz'' \int_0^{\infty} dp'' (p'')^2 Z_{d\Delta}(z'', p''; E) g\left(z'' - \frac{p''^2}{2m_N}\right) \\
 & \times \tau_{\Delta}\left(E - z'' - \frac{p''^2}{2(m_N + m_{\pi})}\right) X_{\Delta d}(z'', p''; E).
 \end{aligned} \tag{6.1}$$

To distinguish between the fully on-shell, half off-shell and fully off-shell quantities, fully on-shell quantities will only be a function of E , half off-shell quantities will be a function of energy and one 4-momentum (E, z, p) and fully off-shell quantities will be a function of energy and two 4-momenta (E, z', p', z, p) . This numerical equation is represented diagrammatically in Figure 6.1.

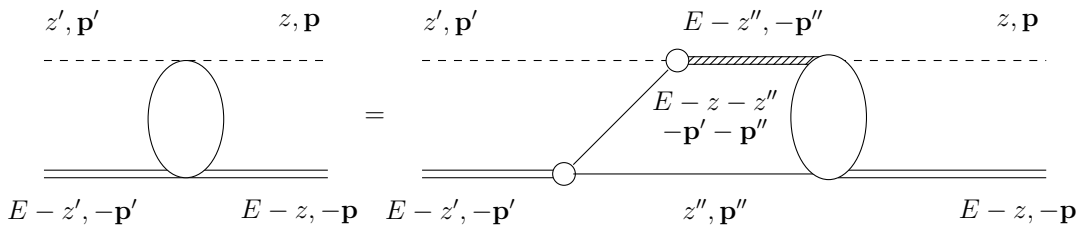


Figure 6.1: The πd elastic scattering amplitude where $N\Delta$ is the only coupled channel.

To calculate the full πd scattering t -matrix, we will first have to calculate the half

off-shell $N\Delta \rightarrow \pi d$ t -matrix $X_{\Delta d}(z'', p''; E)$, which is given by

$$\begin{aligned}
 X_{\Delta d}(z'', p''; E) &= Z_{\Delta d}(z'', p''; E) + \left(-\frac{1}{2\pi i}\right) \int_{-\infty}^{\infty} dz''' \int_0^{\infty} dp''' (p''')^2 Z_{\Delta\Delta}(z'', p'', z''', p'''; E) \\
 &\quad \times g\left(z''' - \frac{p'''^2}{2m_N}\right) \tau_{\Delta}\left(E - z''' - \frac{p'''^2}{2(m_N + m_{\pi})}\right) X_{\Delta d}(z''', p'''; E).
 \end{aligned}
 \tag{6.2}$$

This numerical equation is represented diagrammatically in Figure 6.2.

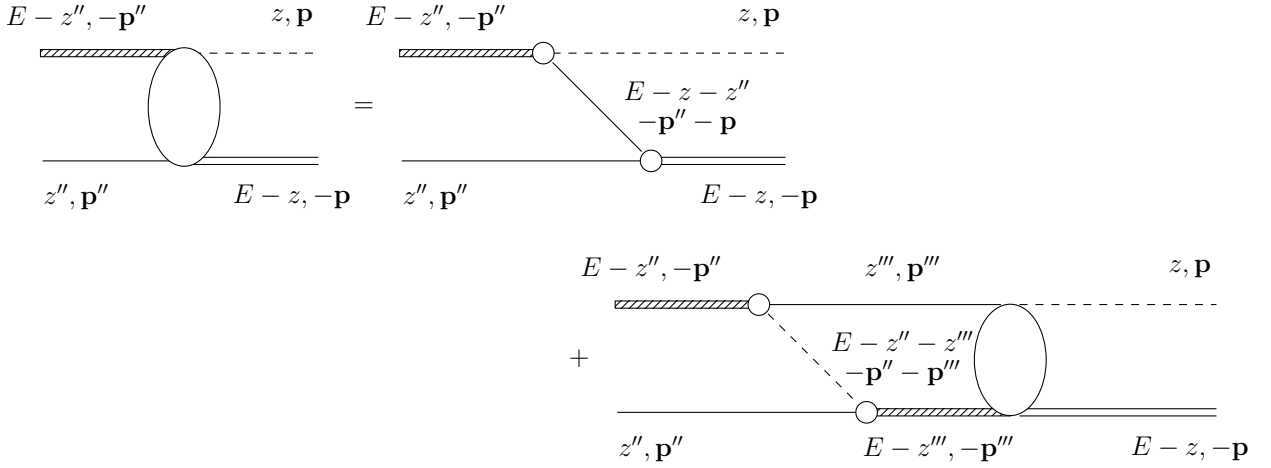


Figure 6.2: The $N\Delta \rightarrow \pi d$ scattering amplitude where $N\Delta$ is the only coupled channel. This amplitude is used in order to calculate the πd elastic scattering amplitude.

Now, when we couple our πd elastic scattering equations to the NN channel, the fully on-shell 4D $\pi d \rightarrow \pi d$ t -matrix is given as

$$\begin{aligned}
 X_{dd}(E) &= \left(-\frac{1}{2\pi i}\right) \int_{-\infty}^{\infty} dz'' \int_0^{\infty} dp'' (p'')^2 Z_{dN}(z'', p''; E) g\left(z'' - \frac{p''^2}{2m_N}\right) \\
 &\quad \times g\left(E - z'' - \frac{p''^2}{2m_N}\right) X_{Nd}(z'', p''; E),
 \end{aligned}
 \tag{6.3}$$

which is given diagrammatically in Figure 6.3.

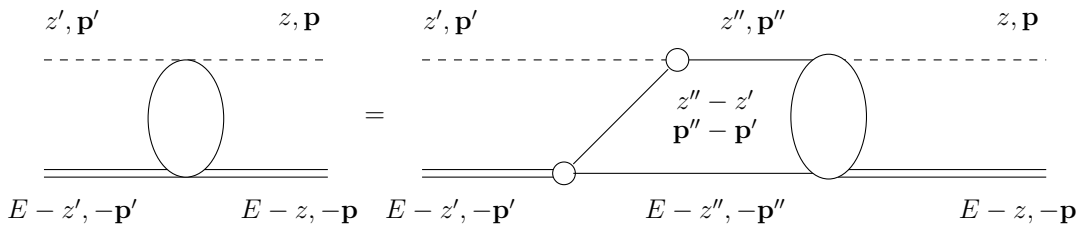


Figure 6.3: The πd elastic scattering amplitude where NN is the only coupled channel.

The half off-shell $NN \rightarrow \pi d$ t -matrix $X_{Nd}(z'', p''; E)$, is given by

$$\begin{aligned}
 X_{Nd}(z'', p''; E) &= Z_{Nd}(z'', p''; E) + \left(-\frac{1}{2\pi i}\right) \int_{-\infty}^{\infty} dz''' \int_0^{\infty} dp''' (p''')^2 Z_{NN}(z'', p'', z''', p'''; E) \\
 &\quad \times g\left(z''' - \frac{p'''^2}{2m_N}\right) g\left(E - z''' - \frac{p'''^2}{2m_N}\right) X_{Nd}(z''', p'''; E).
 \end{aligned}
 \tag{6.4}$$

This numerical equation is represented diagrammatically in Figure 6.4.

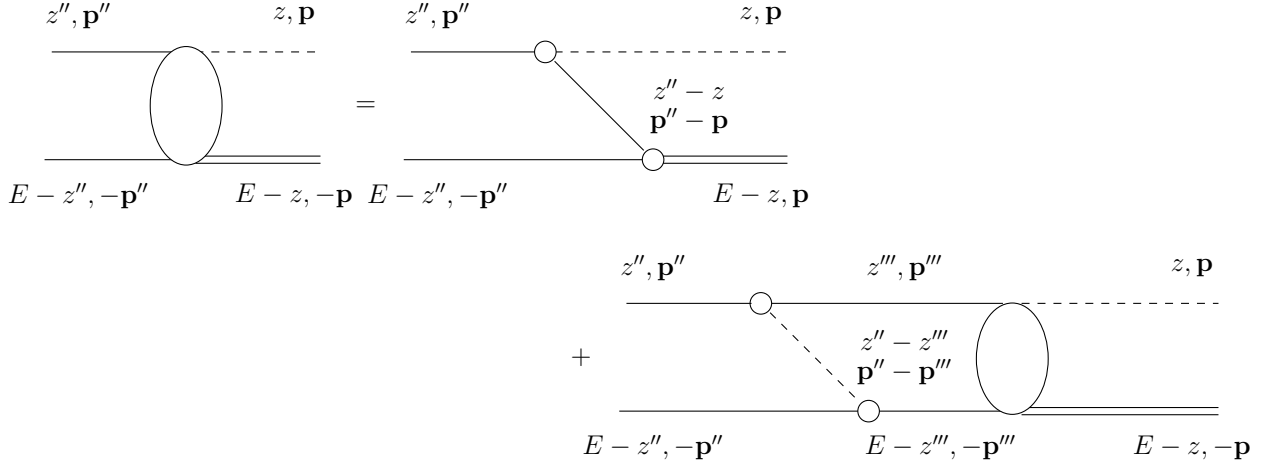


Figure 6.4: The $NN \rightarrow \pi d$ scattering amplitude where NN is the only coupled channel. This amplitude is used in order to calculate the πd elastic scattering amplitude.

6.3.1 4-dimensional Z -diagram

One of the key components in the numerical calculation of the πNN convolution equations is the calculation of the Z -diagrams (Born terms) in Equation 3.164. These Z -diagrams give rise to a difficult computational task as the presence of the fully dressed propagators $D_{0\alpha}$ and G_0 drastically increases computation time. We find that our fully dressed Z -diagrams obtained from time-ordered perturbation theory (TOPT) are, surprisingly, easier to calculate than their corresponding diagram in the πNN convolution equations. The numerical Z -diagram we use in our calculation of the 4-dimensional πNN convolution equations are given by the rules for constructing fully dressed Z -diagrams given in Chapter 2, with “chopped” nucleon legs. The only difference is that, if the exchanged particle in the Z -diagram is a nucleon, we use an undressed nucleon propagator rather than a dressed one-nucleon propagator. As discussed in the previous chapter, we do not include NN two-body input that incorporates nucleon dressing in our calculations and therefore, there is no need to dress the exchange nucleon in the Z -diagrams.

The Z -diagrams in Figures 6.1-6.4 are numerically the same as Equation 4.6, but acquires an extra dimension. After partial wave decomposition, as detailed in Chapter 4, the general 4-dimensional Z -diagram, with our “prime” notation, is given by

$$Z_{K',K}^{JT}(z', p', z, p; E) = \sum_{l',l,L} p^{l'} p^l \Gamma_{k',k}^L(z', p', z, p; E) \sum_{a=0}^{l'} \sum_{b=0}^l A_{K',K}^{L,a,b} \left(\frac{p'}{p} \right)^{a-b} \quad (6.5)$$

where

$$\Gamma_{k',k}^L(z', p', z, p; E) = \frac{1}{2} \int_{-1}^1 \frac{q'^{-l'} h_{k'}(q') h_k(q) q^{-l}}{D(x, z', p', z, p; E)} P_L(x) dx. \quad (6.6)$$

The other quantities are similarly defined in the previous chapters, except for the denominator function which is given below. When the Z -diagram involves an NN channel, the form factor h_k becomes the dressed vertex function f , thus acquires an energy dependence. The denominator function also acquires an extra dimension and is now given explicitly by:

1. For $N\Delta \rightarrow N\Delta$ Z -diagrams

$$D(x, z', p', z, p; E) = E^+ - z' - z - \sqrt{m_\pi^2 + p'^2 + p^2 + 2p'p x} \quad (6.7a)$$

2. For $N\Delta \rightarrow \pi d$ Z -diagrams

$$D(x, z', p', z, p; E) = E^+ - z' - z - \frac{p'^2 + p^2 + 2p'p x}{2m_N} - m_N \quad (6.7b)$$

3. For $NN \rightarrow \pi d$ Z -diagrams

$$D(x, z', p', z, p; E) = z^+ - z' - \frac{p'^2 + p^2 - 2p'p x}{2m_N} - m_N \quad (6.7c)$$

4. For $\pi d \rightarrow NN$ Z -diagrams

$$D(x, z', p', z, p; E) = z'^+ - z - \frac{p'^2 + p^2 - 2p'p x}{2m_N} - m_N \quad (6.7d)$$

5. For $NN \rightarrow N\Delta$ Z -diagrams

$$D(x, z', p', z, p; E) = z'^+ - z - \sqrt{m_\pi^2 + p'^2 + p^2 - 2p'p x} \quad (6.7e)$$

For $NN \rightarrow NN$ Z -diagrams, we must include both time-orderings of one-pion exchange (OPE). Therefore, we have one Z -diagram with the denominator $D(x, z', p', z, p; E) = z'^+ - z - \sqrt{m_\pi^2 + p'^2 + p^2 - 2p'p x}$ (negative slope Z -diagram) and the other Z -diagram

with the denominator $D(x, z', p', z, p; E) = z^+ - z' - \sqrt{m_\pi^2 + p'^2 + p^2 - 2p'p x}$ (positive slope Z -diagram).

When the Z -diagram corresponds to pion exchange, we calculate the x integral using the same method as described in Chapter 4 where we expose the pole in the x integral by manipulating the square roots and use a pole subtraction. When the Z -diagram corresponds to nucleon exchange, we must use a slightly different rearrangement as the denominator does not contain a square root like pion exchange. For nucleon exchange, the Γ function in the Z -diagram has the form

$$\frac{f(x)}{b + i\epsilon - \frac{p'^2 + p^2 \pm 2p'px}{2m_N} - m_N} \quad (6.8)$$

where b is either $z' - z$, $z - z'$ or $E - z - z'$ depending on the specific Z -diagram. Now with some algebra

$$\begin{aligned} \frac{f(x)}{b + i\epsilon - \frac{p'^2 + p^2 \pm 2p'px}{2m_N} - m_N} &= \frac{2m_N f(x)}{2m_N(b - m_N) + 2m_N i\epsilon - (p'^2 + p^2 \pm 2p'px)} \\ &= \frac{2m_N f(x)}{\frac{2m_N(b - m_N) - p'^2 - p^2}{\pm 2p'p} + \frac{2m_N \epsilon}{\pm 2p'p} i - x} \\ &= \frac{h(x)}{x_0 + i\epsilon' - x} \end{aligned} \quad (6.9)$$

where

$$\begin{aligned} h(x) &= 2m_N f(x), \\ x_0 &= \frac{2m_N(b - m_N) - p'^2 - p^2}{\pm 2p'p}, \\ \epsilon' &= \frac{2m_N \epsilon}{\pm 2p'p}. \end{aligned} \quad (6.10)$$

Now we can use the same pole subtraction method specified in Chapter 4 to calculate the integral.

6.3.2 Solving the scattering equations using splines

To solve our 4D scattering equations, we use the spline interpolation method developed in the previous chapter and apply it to our other scattering equations, not just NN . To illustrate this, we detail the application of spline interpolation to solving the 4D πd elastic scattering equation of Equation 6.1.

Firstly, we need to solve Equation 6.2, in which we would approximate the solution as a sum over spline functions that interpolate each dimension. However, because of the

inhomogeneous term of the equation, the solution will have singularities, which makes it difficult to perform the spline interpolation as the solution is not a smooth continuous curve. We overcome this problem by using the suggestion by Carbonell and Karmanov [74] (which we denote as the Carbonell-Karmanov (CK) factorisation) and factor out the inhomogeneous term from the solution

$$X_{\Delta d}(z, p; E) = Z_{\Delta d}(z, p; E)\chi(z, p; E)W_{\Delta d}(z, p; E) \quad (6.11)$$

where W should be smooth without any singularities and χ is a scalar function used to aid the convergence of the solution. Now, instead of using splines to approximate the full solution X , we will use them to approximate the function W as it is smooth, so there should be no problem using splines. Applying our factorisation on Equation 6.2

$$\begin{aligned} W_{\Delta d}(z'', p''; E) &= \frac{1}{\chi(z'', p''; E)} \\ &+ \left(-\frac{1}{2\pi i}\right) \frac{1}{Z_{\Delta d}(z'', p''; E)\chi(z'', p''; E)} \int_{-\infty}^{\infty} dz''' \int_0^{\infty} dp''' (p''')^2 Z_{\Delta\Delta}(z'', p'', z''', p'''; E) \\ &\quad \times g\left(z''' - \frac{p'''^2}{2m_N}\right) \tau_{\Delta}\left(E - z''' - \frac{p'''^2}{2(m_N + m_{\pi})}\right) \\ &\quad \times Z_{\Delta d}(z''', p'''; E)\chi(z''', p'''; E)W_{\Delta d}(z''', p'''; E). \end{aligned} \quad (6.12)$$

Notice that there is now an extra Z -diagram and χ function in the kernel of this equation as a result of the CK factorisation. Now, approximating the function $W_{\Delta d}$ using the splines, rather than the full solution $X_{\Delta d}$, our spline interpolation becomes

$$W_{\Delta d}(z, p; E) = \sum_{i'j'} a_{i'j'} S_{i'}(p) S_{j'}(z). \quad (6.13)$$

Inserting this sum into Equation 6.12, we obtain

$$\begin{aligned} \sum_{i'j'} a_{i'j'} S_{i'}(p'') S_{j'}(z'') &= \frac{1}{\chi(z'', p''; E)} \\ &+ \sum_{i'j'} a_{i'j'} \left(-\frac{1}{2\pi i}\right) \frac{1}{Z_{\Delta d}(z'', p''; E)\chi(z'', p''; E)} \int_{-\infty}^{\infty} dz''' \int_0^{\infty} dp''' (p''')^2 Z_{\Delta\Delta}(z'', p'', z''', p'''; E) \\ &\quad \times g\left(z''' - \frac{p'''^2}{2m_N}\right) \tau_{\Delta}\left(E - z''' - \frac{p'''^2}{2(m_N + m_{\pi})}\right) \\ &\quad \times Z_{\Delta d}(z''', p'''; E)\chi(z''', p'''; E) S_{i'}(p''') S_{j'}(z'''). \end{aligned} \quad (6.14)$$

We now calculate the equation at the collocation points where $\{\bar{p}_i\}$ are the p collocation points and $\{\bar{z}_j\}$ are the z collocation points. With condensed summation notation, the

equation becomes

$$U_{ij'j'} a_{i'j'} = \chi_{ij} + K_{ij'j'} a_{i'j'} \quad (6.15)$$

where

$$U_{ij'j'} = S_{i'}(\bar{p}_i) S_{j'}(\bar{z}_j), \quad (6.16a)$$

$$\chi_{ij} = \frac{1}{\chi(\bar{z}_j, \bar{p}_i; E)}, \quad (6.16b)$$

$$\begin{aligned} K_{ij'j'} = & \left(-\frac{1}{2\pi i} \right) \frac{1}{Z_{\Delta d}(\bar{z}_j, \bar{p}_i; E) \chi(\bar{z}_j, \bar{p}_i; E)} \\ & \int_{-\infty}^{\infty} dz''' \int_0^{\infty} dp''' (p''')^2 Z_{\Delta\Delta}(\bar{z}_j, \bar{p}_i, z''', p'''; E) g \left(z''' - \frac{p'''^2}{2m_N} \right) \tau_{\Delta} \left(E - z''' - \frac{p'''^2}{2(m_N + m_{\pi})} \right) \\ & \times Z_{\Delta d}(z''', p'''; E) \chi(z''', p'''; E) S_{i'}(p''') S_{j'}(z'''). \end{aligned} \quad (6.16c)$$

and we want to solve for the coefficients $a_{i'j'}$. This can be represented as the matrix equation

$$\mathbf{U} \cdot \mathbf{a} = \boldsymbol{\chi} + \mathbf{K} \cdot \mathbf{a}. \quad (6.17)$$

This equation allows us to solve for the unknown coefficients $a_{i'j'}$, which will allow us to calculate the $\pi d t$ -matrix. Using the same spline approximation as before and inserting this into Equation 6.1, we obtain

$$\begin{aligned} X_{dd}(E) = & \sum_{i'j'} a_{i'j'} \left(-\frac{1}{2\pi i} \right) \int_{-\infty}^{\infty} dz'' \int_0^{\infty} dp'' (p'')^2 Z_{d\Delta}(z'', p''; E) g \left(z'' - \frac{p''^2}{2m_N} \right) \\ & \times \tau_{\Delta} \left(E - z'' - \frac{p''^2}{2(m_N + m_{\pi})} \right) Z_{\Delta d}(z'', p''; E) \chi(z'', p''; E) S_{i'}(p'') S_{j'}(z''). \end{aligned} \quad (6.18)$$

Again, with condensed summation notation, this equation becomes

$$X_{dd}(E) = K_{0,i'j'} a_{i'j'} = \mathbf{K}_0 \cdot \mathbf{a} \quad (6.19)$$

where

$$\begin{aligned} K_{0,i'j'} = & \left(-\frac{1}{2\pi i} \right) \int_{-\infty}^{\infty} dz'' \int_0^{\infty} dp'' (p'')^2 Z_{d\Delta}(z'', p''; E) g \left(z'' - \frac{p''^2}{2m_N} \right) \\ & \times \tau_{\Delta} \left(E - z'' - \frac{p''^2}{2(m_N + m_{\pi})} \right) Z_{\Delta d}(z'', p''; E) \chi(z'', p''; E) S_{i'}(p'') S_{j'}(z''). \end{aligned} \quad (6.20)$$

Therefore, $\pi d t$ -matrix has been calculated using the spline interpolation method. The same expression can subsequently be obtained for the 4D $NN \rightarrow \pi d$ and 4D NN scattering equations.

6.3.3 Singularities in the z'' integral

We have discussed in the previous chapter about possible singularities in the z'' integral, however, this was only applicable to NN scattering. We have continued our investigation of singularities in the z'' integral and extended it to the scattering processes other than NN . We present a “general recipe” for singularities in the z'' integral that we have found in our investigation, that we used in our calculations of the πNN convolution equations. Be aware that this “general recipe” is purely based on the singularities that we were able to find in our investigation. In general, it is very difficult to accurately predict singularities in the z'' integral as there are many different factors contributing to the calculation.

Our “general recipe” for singularities in the z'' integral is:

1. A square-root type singularity for the logarithmic singularity that comes from each Z -diagram. When we say “square-root type” singularity, we refer to the value of z'' , in which there are no longer logarithmic singularities in the p'' integral i.e. the z'' value corresponding to the on-set of the logarithmic singularities. This z'' singularity can be found by solving the equation used to determine the logarithmic singularities with its first derivative. The term “square-root type” singularity is used in cubic spline literature and we will continue to use the term here
2. Interaction between the pole singularities and the logarithmic singularities that comes from each Z -diagram. These singularities can be determined by solving for the value of z'' for which the pole singularity and logarithmic singularity occurs for the same value of p''
3. Interaction between the logarithmic singularities of separate Z -diagrams (this is the result of the CK factorisation method, as the Z -diagram corresponding to the inhomogeneous term enters the kernel)
4. The value of z'' for which the p'' singularities are below the minimum value of p'' . Usually this would be where $p'' = 0$, but because we are using splines, the p'' interval is $[p_{min}, p_{max}]$. The minimum value of p'' corresponds to the first knot, which is not exactly equal to zero for reasons to do with the construction of the Z -diagram. However, if the minimum value of p'' was $p'' = 0$, this singularity would not exist. These singularities can be determined by setting p'' to the first p knot in the singularity

equation i.e. we would solve the following equation for z''

$$E - z' - z'' - \sqrt{m_\pi^2 + p'^2 + p_{min}^2 \pm 2p'p_{min}} = 0 \quad (6.21)$$

to find these singularities due to the p'' logarithmic singularities and we would solve

$$z'' - \frac{p_{min}^2}{2m_N} - m_N = 0 \quad (6.22)$$

to determine the singularity due to the nucleon pole. Here, p_{min} is the first (or 0th) knots in our set of knots $\{p_i\}$

As noted in the previous section, the square-root type singularities tend to be the major singularities as it is essential for numerical accuracy of the z'' integral that these singularities are handled. The singularities corresponding to the interaction of singularities of the p'' integral are considered to be minor singularities. For the best result from numerically integrating the z'' integral, it is best to include all the singularities listed above.

6.3.4 Numerical details

We briefly detail the specific numerical details used to calculate our 4D scattering amplitudes, before we present the results for our calculations.

Knots and collocation points

For the p knots, we choose $p_{min} = 0.1$ and $p_{max} = 16$. We discussed in the previous chapter that we cannot choose $p_{min} = 0$ as, due to the CK factorisation, the kernel of the integral equation has $1/Z$ where Z is a Z -diagram and this results in a division by zero. In general, we find that the integral becomes more difficult to evaluate as $p_{min} \rightarrow 0$, so we choose $p_{min} = 0.1$ so that it is close enough to zero without the issues mention previously. The solution of our equations should tend towards 0 as $p \rightarrow \infty$, so we choose $p_{max} = 16$, as this p_{max} should be a more than sufficient truncation of the semi-infinite p interval. A good test of an appropriate p_{max} is to run a few calculations with a small number of knots (to reduce the computational intensity), while increasing p_{max} and having the same knot density (knot density = $(p_{max} - p_{min})/N$ where N is the number of knots). Using similar logic, for the z knots, we choose $z_{min} = -15$ and $z_{max} = 15$ for NN scattering coupled to the P_{33} channel and we use $z_{min} = 0$ and $z_{max} = 15$ for all other processes. To construct the knots for p and z , we divide the full interval by the number of knots used in the calculation

and place a knot at each division point (thereby, splitting the full interval into N equal subintervals) and place a knot at start and end of the full interval.

For collocation points, we use 2 Gaussian quadrature points in each subinterval that we define before. This is essential for the accuracy of the calculation [173].

χ function

We have detailed previously that as part of the CK factorisation, we include the function χ as a smooth scalar function to improve the convergence of our spline interpolation method. In general, the solution of Lippmann-Schwinger type equations (or Fredholm integral equations of the second kind), tend to have a similar structure as the inhomogeneous term of the equation. This is why the CK factorisation is necessary and should theoretically remove the singularities from the solution. In the CK factorisation, the new inhomogeneous term becomes $1/\chi$, so theoretically one should pick a χ that has the properties one desires in the solution of the integral equation (such as tending towards zero as $p \rightarrow \infty, z \rightarrow \pm\infty$). As a result, we suggest the following χ

$$\chi(z, p; E) = \frac{1}{pe^{-p}ze^{-|z|}} \quad (6.23)$$

as the function $f(x) = xe^{-x}$ has this property that we desire. However, in actual numerical calculations, we find no added benefit of using any χ in comparison to using $\chi = 1$. Therefore, in our calculation, we just choose $\chi = 1$ for simplicity. This should also improve computational time.

Quadrature points

We know that the logarithmic singularities in the p'' integral are given by finding the roots of the denominator of Z -diagram's Γ function for $x = \pm 1$. After finding the logarithmic singularities, we calculate the p'' integral using the change of variable method mentioned in Chapter 4 and the Gauss-log quadrature points in [90]. We also need to take into account the complex pole in the P_{33} t -matrix. Find the complex pole m_Δ (around 1232 MeV) and solve the equation $E - z - p^2/(2(m_N + m_\pi)) - \text{Re}(m_\Delta) = 0$ for p . We then treat this value of p as if it were a logarithmic singularity. We have found this offers the best numerical accuracy of the p integral, while also being easy to implement into our calculation code. In each interval defined in the change of variable method, we use 32 quadrature points.

The singularities in the z'' interval are described in the previous section. We split the interval in which we are integrating at the singularities in the interval and use 32 Gaussian quadrature points in each sub-interval.

6.4 NN phase shifts

For elastic scattering, the partial wave scattering matrix S (simply referred to as the S matrix) is given as

$$S = I - 2i\mu p_0 T \quad (6.24)$$

where μ is the reduced mass, p_0 is the on-shell momentum and T is the partial wave t -matrix. For coupled waves, S and T are 2×2 matrices. For NN scattering, the reduced mass is $\mu = m_N^2/(m_N + m_N) = m_N/2$, so the S matrix becomes

$$S = I - im_N p_0 X_{NN}. \quad (6.25)$$

Since the scattering equation satisfies two-body unitarity, the S matrix satisfies the following relation:

$$S^\dagger S = I. \quad (6.26)$$

For uncoupled partial waves, the $NN \rightarrow NN$ S matrix can be expressed as

$$S = e^{2i\delta} \quad (6.27)$$

where δ is the partial wave phase shift, which is real below pion production threshold. For coupled partial waves it is usual to use the Stapp parametrisation [174] of the S matrix

$$S_{l's',ls}^{jt}(E) = \begin{pmatrix} e^{i\delta_{j-1}} & 0 \\ 0 & e^{i\delta_{j+1}} \end{pmatrix} \begin{pmatrix} \cos 2\epsilon_j & i \sin 2\epsilon_j \\ i \sin 2\epsilon_j & \cos 2\epsilon_j \end{pmatrix} \begin{pmatrix} e^{i\delta_{j-1}} & 0 \\ 0 & e^{i\delta_{j+1}} \end{pmatrix} \quad (6.28)$$

where ϵ_j is known as the mixing parameter.

While we are primarily interested in how our equations describe πd elastic scattering and $pp \rightarrow \pi^+ d$ scattering, our three-body equations also include a description of NN scattering. However, we do not expect our three-body equations to accurately reproduce NN phase shifts as we couple our equations to only one partial wave channel.

During our calculation of the 4D NN scattering amplitudes, we can use some numerical checks to confirm the results of our calculation. Firstly, the NN phase shifts will be real

values below pion production threshold (in the lab frame, the pion production threshold is $E_{lab} = 284.639$ MeV). Another numerical check is that the t -matrix for coupled channels should also be a symmetric 2×2 matrix (the off-diagonal elements of the matrix should be equal).

Results

As explained previously, we do not expect accurate reproduction of the phase shifts, regardless of whether dressing has been included. As the inclusion of Dyson-dressed πN input greatly increases computation time, we investigated whether there is a significant difference between the NN phase shifts with Dyson-dressed πN input and with undressed πN inputs. We find that there is not a significant difference between the two results. As a result, a comparison of 3-dimensional (3D) phase shifts and 4D phase shifts with Dyson-dressed πN inputs should provide an indication of the effect of the consistent nucleon dressing introduced by the convolutions. We would expect to see a similar result if we included Dyson-dressing into our equations for πd elastic scattering and $pp \rightarrow \pi^+ d$ scattering, despite not performing such a calculation due to the lack of a proper dressed NN input.

In Figure 6.5, we plot the 4D NN phase shifts coupled only to the NN channel for different partial waves and Dyson-dressed πN input corresponding to our $M7$ model. For comparison, we compare our results to the fits of experimental data by Workman et al. [175] and use their SW16 solution. This data was obtained from the SAID partial wave analysis database [176]. We note that including this Dyson-dressing into our computer code substantially increases the computation time, on top of the length of time it takes to calculate the 4-dimensional convolution equations using spline interpolation. We have reduced the computation time by using the Wick rotation method described by Levine et al. [54] for particles of equal mass, which we have compared with the phase shifts calculated using spline interpolation and find that the two methods agree. One can see in Figure 6.5 that the 4D phase shifts have a similar curvature to the fitted solution. One can see that there is a discrepancy towards $T_p = 0$ in the plot of the 1S_0 phase shifts between both calculated NN phase shifts and the fitted solution data. We have investigated this discrepancy by examining a 3D calculation of the NN phase shifts, as we are able to include more partial waves and coupled channels without the computational intensity. By investigating the inclusion of many partial waves and different coupled channels in the 3D calculation, we attribute this discrepancy to the missing P_{33} channel. There is a significant difference between the 4D

phase shifts and the SW16 solution in the lower partial waves (i.e. 3P_0 , 1S_0 , 3P_1 and 1D_2) at higher energies, however, they tend to agree more closely at very low energies, particularly 3P_0 . Comparing the 3D and 4D phase shifts, we see that the dressing makes a notable contribution to the lower partial waves. In particular, 3P_0 , 3P_1 and 1D_2 are significantly closer to the SW16 solution, especially for lower energies. For the higher partial waves, such as 3F_3 , 3H_5 and 1I_6 , the addition of dressing makes a noticeable difference for high energies.

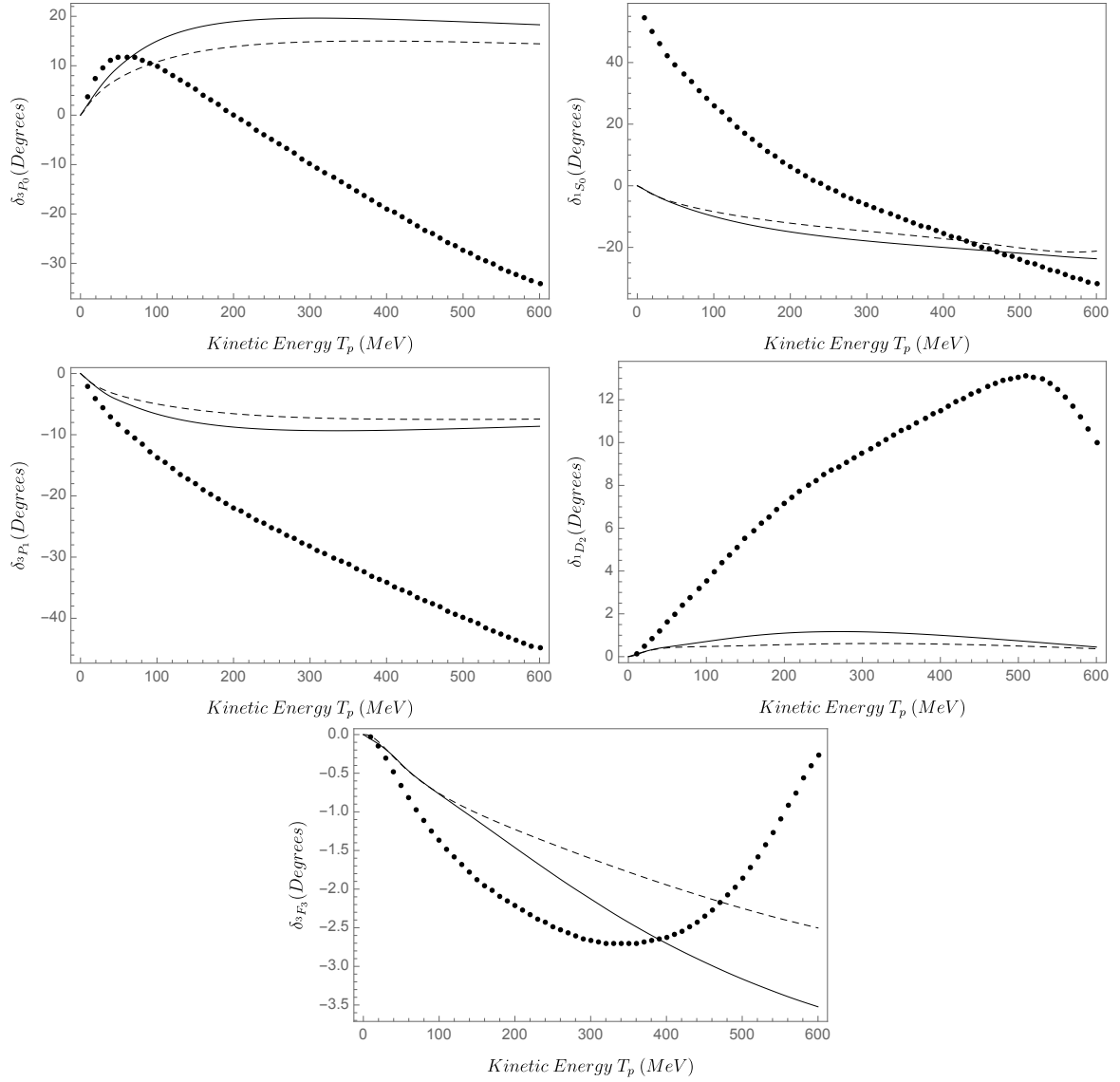


Figure 6.5: Comparison of the 4D NN phase shifts coupled to the NN channel with Dyson-dressing for different partial waves, calculated using the Wick rotation method of Levine et al. [54], compared with the 3D NN phase shifts, calculated using contour rotation. The dots represent the SW16 solution [175] obtained using the SAID database [176].

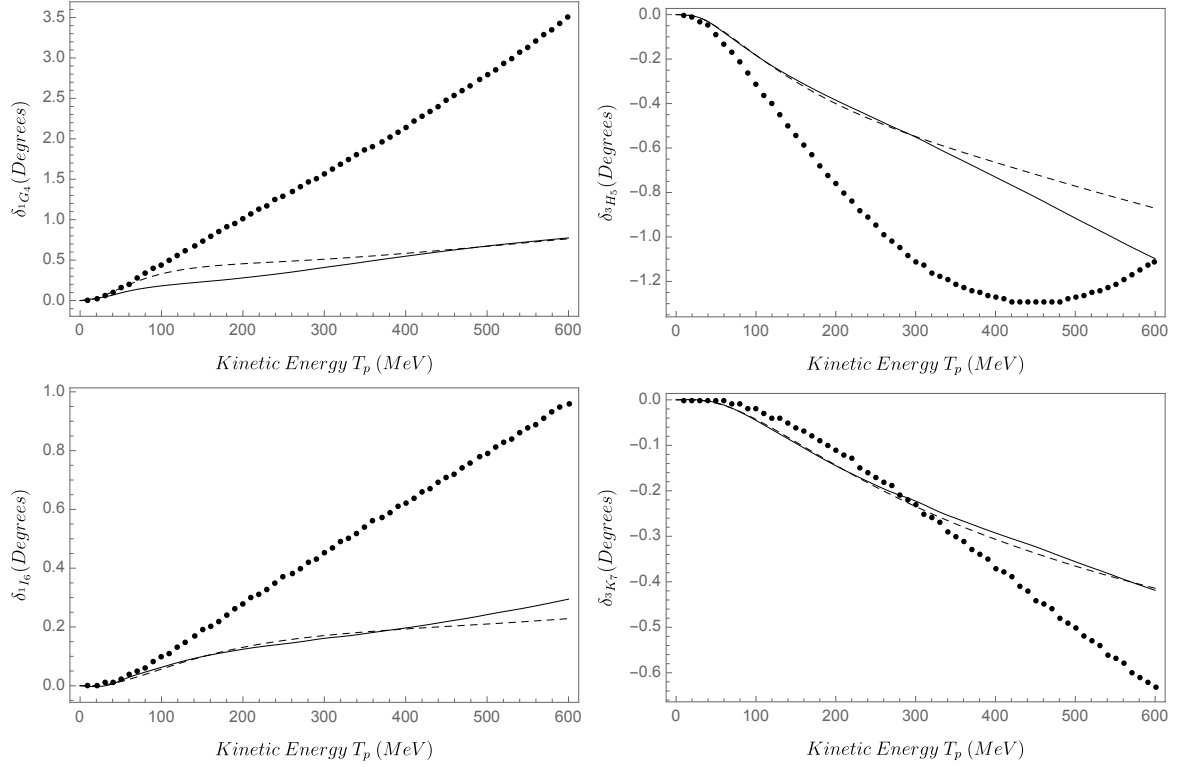


Figure 6.5: (cont.) Comparison of the 4D NN phase shifts coupled to the NN channel with Dyson-dressing for different partial waves, calculated using the Wick rotation method of Levine et al. [54], compared with the 3D NN phase shifts, calculated using contour rotation. The dots represent the SW16 solution [175] obtained using the SAID database [176].

Because of the drastic increase in computation time with the addition of Dyson-dressing, we only present results for one partial wave with 16 spline knots when we calculate 4D NN phase shifts coupled to the P_{33} channel. We calculate the 4D 3P_1 phase shifts with Dyson-dressed πN inputs in Figure 6.6 and compare it to the 3D NN phase shifts when coupled to the P_{33} . We see a similar trend as in Figure 6.5 when coupled only to the NN channel, in which the consistent dressing pushes the phase shifts towards the SW16 solution and is able to more accurately reproduce the data at very low energies. We also notice that the 3D phase shifts deflect towards 0 *degrees* and away from the experimental data at higher energies, while the 4D phase shifts do not exhibit this property.

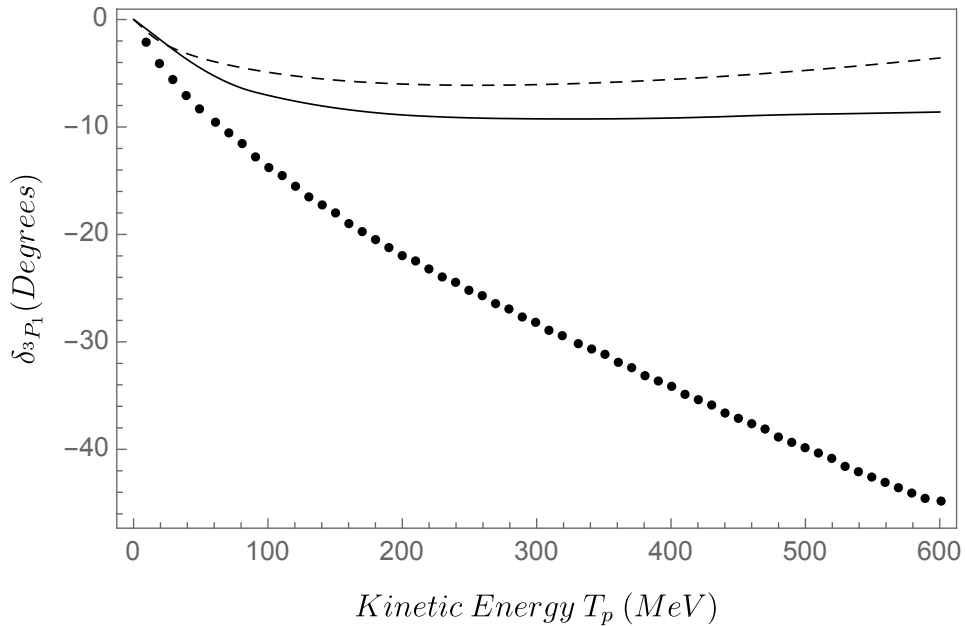


Figure 6.6: Comparison of the 4D 3P_1 NN phase shifts coupled to the P_{33} channel with Dyson-dressing, calculated using the spline interpolation method using 16 knots for p and z ($N_p = N_z = 16$), compared to the 3D NN phase shifts, calculated with contour rotation. The solid curve represents the phase shift with our 4D phase shifts with our $M7$ Dyson-dressing model, while the dashed curve represents the 3D phase shifts. The dots represent the SW16 solution [175] obtained using the SAID database [176].

6.5 $\pi d \rightarrow \pi d$ observables

In this section, we calculate the observables for πd elastic scattering for unpolarised states and a polarised final state deuteron. It is possible to calculate the observables corresponding to polarised deuteron in the final and initial state using the procedure outlined by Blankleider and Afnan [177], however, we restrict our investigation to observables with a polarised final state deuteron as we are particularly interested in the T_{20} observable calculated from a polarised final state deuteron state.

Most experimental data for πd elastic scattering is given for the reaction $\pi^+ d \rightarrow \pi^+ d$. There is a Coulomb interaction between the charged pion and the deuteron, which can be included in our calculation of the differential scattering cross using the methods of [22, 178]. However, the Coulomb effect should be mostly neglectable in comparison to the contribution of the strong interaction, except at scattering angles close to zero. In our calculations, we do not include the Coulomb effect.

As mentioned before, we only calculate results with one coupled channel, due to the computational intensity of our 4-dimensional equations. However, we do calculate fully coupled results for the 3-dimensional scattering equations using all the channels listed in Appendix G, in order to give a prediction of the 4-dimensional scattering equation results if we were to include full coupling rather than just coupling to one channel. By comparing the 3-dimensional results with many partial waves and all coupled channels with the 3-dimensional results containing only one coupled channel, we can explore the effect of including many partial waves and all coupled channels, to obtain an idea of what one might expect the 4-dimensional results would look like.

A good numerical check of our calculation for πd elastic scattering is that the off-diagonal elements of the t -matrix ($l = 0, l' = 2$ and $l = 2, l' = 0$ contributions) should be equal.

6.5.1 S -wave scattering length

For πd elastic scattering, we usually consider the scattering amplitude $f_{L_f L_i}^J$ which is given as

$$f_{L_f L_i}^J = -\pi \mu_d(q_0) T_{dd} \quad (6.29)$$

where

$$\mu_d(q_0) = \frac{(q_0^2 + m_\pi^2)^{1/2} m_d}{(q_0^2 + m_\pi^2)^{1/2} + m_d} \quad (6.30)$$

where m_d is the mass of the deuteron. The physical πd t -matrix T_{dd} is related to the numerical t -matrix X_{dd} through normalisation of the deuteron wave-function for separable potentials. Here, q_0 is the on-shell pion-deuteron momentum, which is calculated by solving the equation:

$$E - (q_0^2 + m_\pi^2)^{1/2} - \frac{q_0^2}{2m_d} - m_d = 0. \quad (6.31)$$

The S -wave πd scattering amplitude $f_{\pi d}^S$ is given by

$$f_{\pi d}^S = \frac{e^{i\delta_0} \sin \delta_0}{q_0} \quad (6.32)$$

which, as the on-shell pion-deuteron momentum goes to zero, approaches the S -wave πd scattering length $a_{\pi d}$

$$f_{\pi d}^S \sim a_{\pi d} \quad \text{as} \quad q_0 \rightarrow 0. \quad (6.33)$$

There has been recent interest in studying πd scattering lengths as one can determine the πN S -wave isoscalar (a^+) and isovector (a^-) scattering lengths [179, 180], which are given as a linear combination of the S_{11} and S_{31} πN scattering lengths. These πN scattering lengths are of current interest as a confirmation of recent effective field theories, as well as tests of symmetries in QCD [181]. As such, there has been recent experimental interest in pionic atoms, such as pionic hydrogen [182] and pionic deuterium [183] for the study of scattering lengths. Strong interactions in the Standard Model includes a description of isospin violation, which according to Weinberg [184] can be tested by investigating πN scattering lengths.

The most generally accepted value of the πd S -wave scattering length comes from Hauser et al. [185] which is

$$a_{\pi d} = -0.0261(\pm 0.0005) + i0.0063(\pm 0.0007)m_\pi^{-1} \quad (6.34)$$

with a more recent measurement being provided by Strauch et al. [183]

$$a_{\pi d} = -0.02499 \pm 0.00033 + i0.00622_{-0.26}^{+0.12} m_\pi^{-1}. \quad (6.35)$$

Without dressing and including all partial waves and couplings of Appendix G included, we calculate the S -wave scattering length for the Unitary equations using contour rotation. Our result is

$$a_{\pi d} = -0.0288503 + 0.00124728i m_\pi^{-1}. \quad (6.36)$$

This result is already in good agreement with the experimental scattering lengths above. Despite not being within the uncertainty values, the real part of scattering length is in excellent agreement with the experimental results, whereas the imaginary is approximately twice the value of our calculated result.

Calculating the 4D πd scattering length tends to be more difficult than calculating the 3D scattering length, due to the singularity structure of the 4D Z -diagram as $E_{lab} \rightarrow 0$. If we are coupling only to P_{33} , consider the $\pi d \rightarrow N\Delta$ Z -diagram, given in Figure 6.7

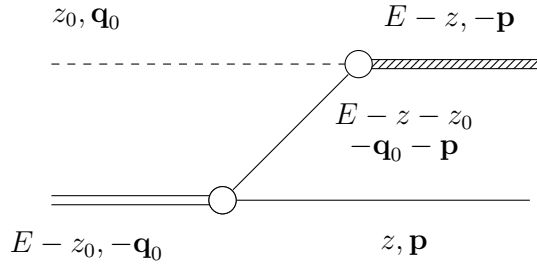


Figure 6.7: The half off-shell $\pi d \rightarrow N\Delta$ Z -diagram.

The integrand of the x integral in this Z -diagram has the denominator

$$E^+ - z_0 - z - \frac{q_0^2 + p^2 + 2q_0 p x}{2m_N} - m_N \quad (6.37)$$

where E is the centre of mass energy and $z_0 = (q_0 + m_\pi^2)^{1/2}$. Now, as $q_0 \rightarrow 0$ when $E_{lab} \rightarrow 0$, the x dependence in the denominator vanishes and the denominator becomes

$$E^+ - z_0 - z - \frac{p^2}{2m_N} - m_N. \quad (6.38)$$

So the x integral in the Z -diagram can be calculated without a pole subtraction as previously specified, however, there is now a pole in the p integral which can be found by solving Equation 6.38. So now we have to deal with two poles, one coming from the dressed one-nucleon propagator and the other coming from the Z -diagram itself. This is not such a big issue, as the two poles should not exist at the same time, given that the nucleon pole exists when $z > m_N = 4.7581$ and the pole from the Z -diagram exists when $z < E - z_0 - m_N = 4.7469$. So there is no value of z for which both poles exist at the same time and we can use our conventional methods of pole subtraction to calculate the integral.

The more alarming issue is that due to the CK factorisation, there are two Z -diagrams in the half off-shell kernel which both have this pole, which results in a double pole (pole of order two). In Appendix F, we detail a method for handling this double pole using modified

quadrature points constructed by Kolm and Rokhlin [93], while providing a re-derivation of their quadrature points due to an error in the original publication. We can also use a modification of the suggestion by Carley [186] and calculate the integral using a subtraction method. One can check that the pole subtraction method for an integral on a finite interval with a double pole is given by

$$\begin{aligned}
 \int_a^b \frac{f(t)}{(x-t+i\epsilon)^2} dt &= \int_a^b \frac{f(t) - f(x) + f'(x)(x-t)}{(x-t)^2} dt \\
 &\quad + f(x) \int_a^b \frac{1}{(x-t)^2} dt - f'(x) \int_a^b \frac{1}{x-t} dt \\
 &= \int_a^b \frac{f(t) - f(x) + f'(x)(x-t)}{(x-t)^2} dt \\
 &\quad + f(x) \left(\frac{1}{x-b} - \frac{1}{x-a} \right) - f'(x) (\log(x-a) - \log(x-b)).
 \end{aligned} \tag{6.39}$$

While we do present two methods to overcome this double pole due to the CK factorisation, in practice we find these processes to be a difficult numerical task. As an alternative, we calculate the 4D πd scattering amplitude using our spline interpolation method at energies near $E_{lab} = 0$ and extrapolate the results to determine the S -wave scattering length.

E_{lab} (MeV)	$N_p = N_z = 16$	$N_p = N_z = 24$	$N_p = N_z = 32$
1	$0.000911094 - 7.3686 \times 10^{-6}i$	$0.000923448 + 2.49209 \times 10^{-6}i$	$0.000925901 - 5.69164 \times 10^{-6}i$
2	$0.000833089 - 6.10674 \times 10^{-6}i$	$0.000837432 - 6.54377 \times 10^{-7}i$	$0.000850326 - 9.56478 \times 10^{-6}i$
3	$0.000762563 - 3.56948 \times 10^{-6}i$	$0.000788488 + 6.69259 \times 10^{-6}i$	$0.000780933 - 0.0000103081i$
4	$0.000703435 - 2.24347 \times 10^{-6}i$	$0.000656963 - 0.0000864888i$	$0.000721251 - 8.78417 \times 10^{-6}i$
5	$0.000651034 - 2.01173 \times 10^{-6}i$	$0.000645531 - 5.36741 \times 10^{-6}i$	$0.00066678 - 8.16304 \times 10^{-6}i$
Extrapolated	$0.000967175 - 8.6331 \times 10^{-6}i$	$0.000991264 + 0.0000138008i$	$0.000983233 - 7.25369 \times 10^{-6}i$
$a_{\pi d} (m_\pi^{-1})$	$0.000672953 - 6.00685 \times 10^{-6}i$	$0.000689714 + 9.60252 \times 10^{-6}i$	$0.000684126 - 5.04706 \times 10^{-6}i$

Table 6.1: Results of the πd extrapolation to determine the S -wave πd scattering length calculated using the spline interpolation method for different numbers of p and z spline knots, N_p and N_z respectively. These results include the extrapolated amplitude for $E_{lab} = 0$ calculated using a linear data fit and the corresponding S -wave scattering length for the respective knot number. The amplitudes are given in units of fm^{-1} , while the scattering length $a_{\pi d}$ is given in units of m_π^{-1} .

If we examine the results of Table 6.1 and compare the amplitudes for the different number of spline knots, we see that we have good convergence of the splines, particularly as the amplitudes are quite small themselves. This is excluding the imaginary part of the

amplitudes, which is neglectable and may be oscillating due to “numerical noise,” such as not enough Gaussian quadrature points to converge the amplitudes to an accuracy of 10^{-6} . It is particularly impressive to obtain this degree of convergence in a πd amplitude, as the entire πd amplitude relies on the accuracy of the spline interpolation method, due to the fact that there is no inhomogeneous first-order term that contributes to the amplitude. One would also expect that as $E_{lab} \rightarrow 0$, then the p and z integrals become more difficult to evaluate as the logarithmic singularities in the kernel of the equations gradually become closer together. This might be a testament to the change of variable method we use to calculate the p integral, which essentially stretches the integration interval and would push the logarithmic singularities further away from each other, allowing the integral to be more easily calculated.

Without dressing and only coupled to the P_{33} channel, the 3D S -wave scattering length is $0.000687359 - 1.96619 \times 10^{-9}i m_{\pi}^{-1}$. If we compare this value to the results of Table 6.1, one can see that results are quite similar, which may indicate that the effect of dressing at low energies may be small. This comparison would indicate that the 4D calculation with full coupling and all partial waves would give a similar result to our 3D results presented in Equation 6.36, however, the contribution of consistent dressing may be greater if we were to couple our equations to the other channels such as NN .

6.5.2 Scattering cross section

The differential scattering cross section is given by

$$\frac{d\sigma}{d\Omega}(\pi d \rightarrow \pi d) = \frac{1}{3} \sum_L \sum_{\substack{L_f, L_i \\ L'_f, L'_i}} \sum_{JJ'} \hat{L}_f \hat{L}_i \hat{L}'_f \hat{L}'_i (\hat{J} \hat{J}' \hat{L})^2 \begin{pmatrix} L_i & L'_i & L \\ 0 & 0 & 0 \end{pmatrix} \begin{pmatrix} L_f & L'_f & L \\ 0 & 0 & 0 \end{pmatrix} \begin{Bmatrix} J & J' & L \\ L'_i & L_i & 1 \end{Bmatrix} \begin{Bmatrix} J & J' & L \\ L'_f & L_f & 1 \end{Bmatrix} f_{L_f L_i}^J f_{L'_f L'_i}^{J*} P_L(\cos \theta) \quad (6.40)$$

where P_L is the Legendre polynomial of order L and $f_{L_f L_i}^J$ are the partial wave amplitudes given by Equation 6.29 [178]. The elastic and total scattering cross sections can be calculated using

$$\sigma_{\text{el}} = \frac{4}{3} \pi \sum_{\substack{L_i L_f \\ J}} (2J + 1) |f_{L_f L_i}^J|^2, \quad (6.41)$$

$$\sigma_{\text{tot}} = \frac{4\pi}{3k} \sum_L (2J + 1) |f_{LL}^J|^2. \quad (6.42)$$

In Table 6.2, we index the partial wave $\pi d \rightarrow \pi d$ amplitudes that we calculate, by assigning a label to each amplitude and state the values of L' , L and J^π for each amplitude. We recall that we calculate separate results for our πd equations when coupled to the P_{33} channel and when our equations are coupled to the NN channel. When we coupled our equations to the NN channel only, we see that for some values of J^π there are no NN channels, so there will be πd amplitudes that are equal to zero in our results.

$f_{L'L}^J$	L'	L	J^π
1	1	1	0^+
2	0	0	1^-
3	0	2	1^-
4	2	2	1^-
5	1	1	1^+
6	2	2	2^-
7	1	1	2^+
8	1	3	2^+
9	3	3	2^+
10	2	2	3^-
11	2	4	3^-
12	4	4	3^-
13	3	3	3^+
14	4	4	4^-
15	3	3	4^+
16	4	4	5^-
17	3	5	4^+
18	5	5	4^+
19	4	6	5^-
20	6	6	5^-
21	5	5	5^+
22	6	6	6^-
23	5	5	6^+
24	5	7	6^+
25	7	7	6^+
26	6	6	7^-
27	6	8	7^-
28	8	8	7^-
29	7	7	7^+

Table 6.2: The partial wave channels considered in the calculation of πd scattering, in which we consider the same channels as Blankleider [178].

Results

Comparing the πd amplitudes when coupled to the P_{33} channel in Table 6.3, it seems that these amplitudes show decent convergence with respect to the number of spline knots. Though, the 24 knot amplitude tends to be dissimilar to the other knot amplitudes, which can also be seen in Figure 6.8 as the 24 knot differential cross section is quite different from the other knot cross sections. It is understood that approximations using splines tend to have an oscillatory convergence rather than monotonic convergence, which might be what these results indicate. We expect to see this oscillation continue when we compare subsequent results of the spline interpolation method. The amplitudes corresponding to higher J^π values also demonstrate less convergence with respect to the number of knots. This may be because the amplitudes for higher J^π values are significantly smaller than the amplitudes for lower J^π values, so convergence to a certain degree of accuracy is more difficult. It may also be that the amount of quadrature points is not sufficient to obtain accurate amplitudes when the amplitudes are so small.

$f_{L'L}^J$	J^π	$N_p = N_z = 16$	$N_p = N_z = 24$	$N_p = N_z = 32$
1	0^+	$0.0703378 + 0.0353787i$	$0.0880965 + 0.0368853i$	$0.0699699 + 0.0430382i$
2	1^-	$0.0242919 + 0.022262i$	$0.034581 + 0.0298201i$	$0.0323945 + 0.0269061i$
3	1^-	$0.0161016 + 0.0142354i$	$0.0146456 + 0.0131041i$	$0.0171475 + 0.0152682i$
4	1^-	$0.00934522 + 0.00807751i$	$0.00878834 + 0.00788704i$	$0.0100211 + 0.00834243i$
5	1^+	$0.115105 + 0.0812473i$	$0.112574 + 0.08301i$	$0.109428 + 0.0831255i$
6	2^-	$0.0318256 + 0.0217924i$	$0.0322715 + 0.02379i$	$0.0317824 + 0.0228841i$
7	2^+	$0.279476 + 0.295451i$	$0.292993 + 0.300808i$	$0.325917 + 0.297074i$
8	2^+	$-0.00381991 - 0.00976864i$	$-0.00686136 - 0.00561729i$	$-0.00845083 - 0.00889393i$
9	2^+	$0.000492191 + 0.000731081i$	$0.000514627 + 0.000380899i$	$0.000638729 + 0.000658836i$
10	3^-	$0.0999778 + 0.0791449i$	$0.0766122 + 0.088906i$	$0.0991982 + 0.0821599i$
11	3^-	$-0.00298241 - 0.00216326i$	$-0.00241378 - 0.00264355i$	$-0.00251177 - 0.00233414i$
12	3^-	$0.000138193 + 0.000126512i$	$0.000125289 + 0.00010754i$	$0.0000858394 + 0.000110164i$
13	3^+	$0.00688968 + 0.00572318i$	$0.0074061 + 0.0052256i$	$0.00747385 + 0.00586564i$
14	4^-	$0.00201836 + 0.0018664i$	$0.0015342 + 0.00152044i$	$0.00212713 + 0.00164115i$
15	4^+	$0.0354388 + 0.0229207i$	$0.0274218 + 0.026857i$	$0.0286946 + 0.0207052i$
16	5^-	$0.00978766 + 0.00437859i$	$0.00973628 + 0.00563732i$	$0.00737586 + 0.00671715i$
17	4^+	$-0.00106873 - 0.00171062i$	$-0.000623899 - 0.000633385i$	$-0.00068926 - 0.000626805i$
18	4^+	$0.0000490762 + 0.00005981i$	$0.0000269838 + 0.0000348341i$	$0.000016719 + 0.0000207514i$
19	5^-	$-0.000141056 - 0.000133697i$	$-0.000154072 - 0.000192413i$	$-0.000124489 - 0.000160862i$
20	5^-	$3.13457 \times 10^{-6} + 7.09162 \times 10^{-6}i$	$2.22905 \times 10^{-6} + 0.0000110905i$	$-2.43377 \times 10^{-6} + 0.0000130584i$
21	5^+	$0.000239023 + 0.000135896i$	$0.000438378 + 0.00085439i$	$0.000625103 + 0.000419687i$
22	6^-	$0.0000676568 - 0.000726753i$	$0.000100426 + 0.0000439709i$	$0.0000969336 + 0.000247073i$
23	6^+	$-0.00555732 + 0.00282856i$	$-0.0000138326 + 0.00145672i$	$0.00231244 + 0.00258703i$
24	6^+	$-0.0000653513 - 0.000121492i$	$-0.0000412388 - 0.000031335i$	$1.51326 \times 10^{-6} - 0.0000345944i$
25	6^+	$-1.99515 \times 10^{-7} + 4.62629 \times 10^{-6}i$	$2.53895 \times 10^{-6} + 6.96504 \times 10^{-7}i$	$1.25692 \times 10^{-6} - 4.61597 \times 10^{-7}i$
26	7^-	$0.000893976 - 0.0000970802i$	$-0.000584324 - 0.000373124i$	$0.000193451 - 0.00002102i$
27	7^-	$-0.00021358 + 0.0000182866i$	$-7.5152 \times 10^{-6} - 0.0000205169i$	$-0.0000347223 - 0.0000402964i$
28	7^-	$-0.0000183426 - 0.000020772i$	$3.22497 \times 10^{-7} + 8.34259 \times 10^{-8}i$	$5.34916 \times 10^{-6} - 0.0000129373i$
29	7^+	$-0.000283474 + 0.0000114585i$	$0.0000231676 - 0.0000188949i$	$0.000161902 + 0.000199575i$

Table 6.3: 4D elastic πd scattering amplitudes when coupled to the P_{33} channel calculated using the spline interpolation method for different numbers of p and z spline knots, N_p and N_z respectively. The lab energy of the incident pion is equal to 140 MeV.

If we look at the differential cross sections for different spline knots in Figure 6.8, we can see that the curves are quite similar, indicating that the amplitudes already exhibit a good level of convergence, as we initially observed. The only major deviation is the minimum around $\theta_{cm} = 90$ degrees, where the 32 knot cross section has a higher minimum point. In Figure 6.9, we present a comparison of the 3D and 4D πd differential cross sections with the experimental data. The differential cross section with dressing is quite similar to the cross section without same-time dressing, indicating that the effect of consistent same-time dressing does not have a significant contribution to the πd different cross section with coupled

only to P_{33} . Both differential cross sections overlap at lower angles, then start to slightly diverge at higher angles. Again, it would be best to have results with a larger amount of spline knots, to confirm the accuracy of this differential cross section. We can also see that both the 3D and 4D cross sections are able to reproduce the experimental cross sections fairly well, in particularly the results are superb from $\theta_{cm} = 40$ degrees to $\theta_{cm} = 70$ degrees.

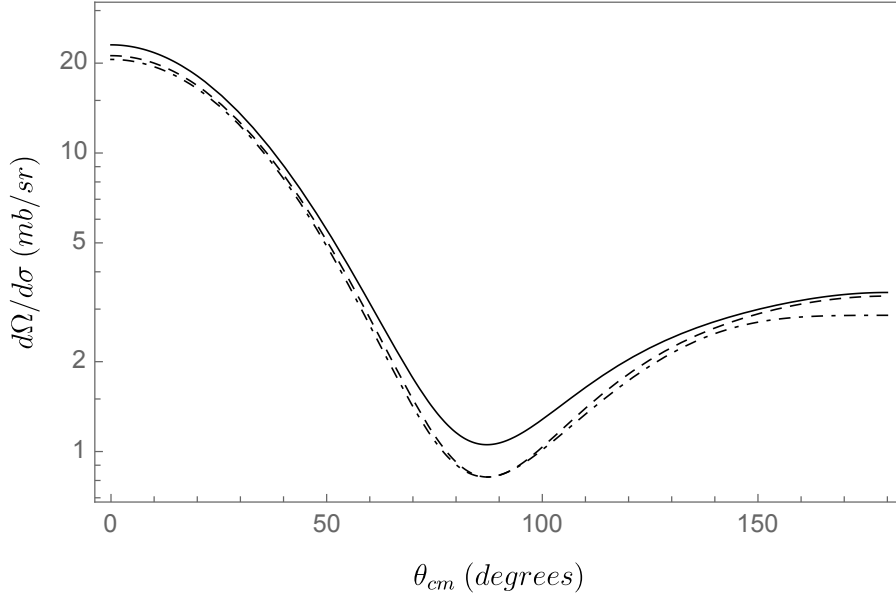


Figure 6.8: Comparison of the 4D πd differential cross section when coupled to the P_{33} channel with the lab energy of the incident pion equal to 140 MeV. The three curves in this graph each represent a different number of spline knots used in the calculation: the dot-dashed curve represents 16 knots, the dashed curve represents 24 knots and the solid curve represents 32 knots.

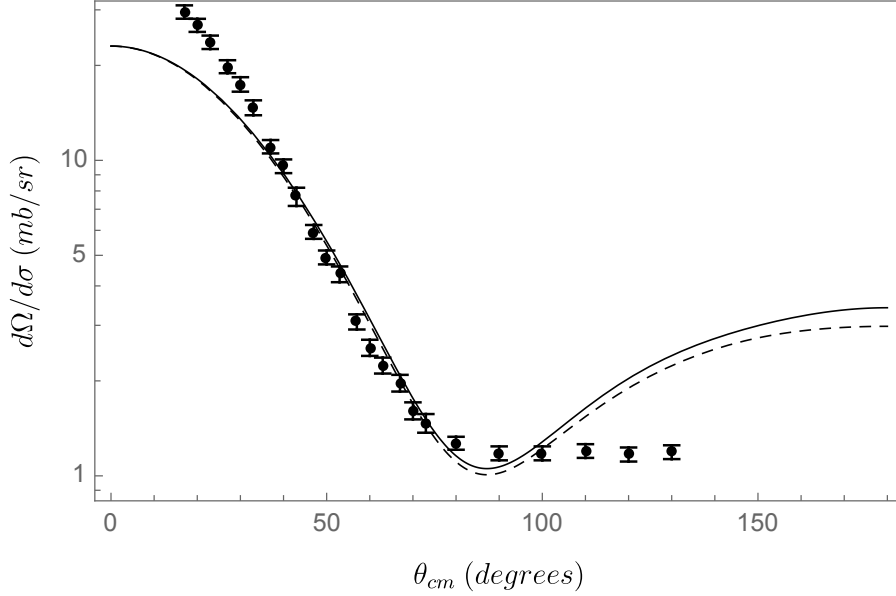


Figure 6.9: Comparison of the 3D πd and 4D πd ($N_p = N_z = 32$) differential cross section when coupled to the P_{33} channel with the lab energy of the incident pion equal to 140 MeV, also compared with the experimental data points provided by Gabathuler et al. [187]. The solid curve represents the 4D differential cross section, while the dashed curve represents the 3D differential cross section.

If we turn our attention to the results of πd scattering when the equations are coupled to the NN channel, we see that the 4D amplitudes in Table 6.4 have decent convergence with respect to the spline knots. However, this convergence tends to become worse as the value for J^π increases, particular when $J^\pi = 3^+$ we begin to see a decline in convergence of the amplitudes. From our previous results for the 4D πd scattering amplitudes, we do not expect excellent convergence for this number of spline knots, which is also evident from these results. The lack of convergence in the higher J^π values may not have a significant effect on the observables as Figure 6.10 shows that the differential cross section for different numbers of spline knots is quite similar. Comparing the NN coupled 4D πd differential cross section to the experimental data and the 3D cross section in Figure 6.11, we see that both cross sections are significantly smaller than the experimental cross section. We would not expect an accurate reproduction of the differential cross section, as these results are only coupled to the NN channel, however, we do see a significant difference between the 3D and 4D cross sections, which suggested the contribution of consistent dressing is more significant when we coupled our equations to the NN channel.

$f_{L'L}^J$	J^π	$N_p = N_z = 16$	$N_p = N_z = 24$	$N_p = N_z = 32$
1	0^+	$-0.349444 - 0.124758i$	$-0.338941 - 0.12523i$	$-0.343877 - 0.129752i$
2	1^-	$-0.0524484 - 0.00853924i$	$-0.0710012 - 0.0246773i$	$-0.0456308 - 0.0193147i$
3	1^-	$-0.0392496 - 0.0144713i$	$-0.0324809 - 0.0120805i$	$-0.0331899 - 0.0113803i$
4	1^-	$-0.0222812 - 0.00823246i$	$-0.0189179 - 0.00695923i$	$-0.0191067 - 0.00674675i$
5	1^+	0	0	0
6	2^-	$-0.0493888 - 0.018336i$	$-0.0515573 - 0.0190166i$	$-0.051241 - 0.0193418i$
7	2^+	$-0.021057 + 0.0130252i$	$-0.00916982 - 0.00255334i$	$-0.0108524 - 0.00175822i$
8	2^+	$0.00997128 + 0.00447703i$	$0.00957425 + 0.00339182i$	$0.00974292 + 0.00340803i$
9	2^+	$-0.0116696 - 0.00604436i$	$-0.010824 - 0.00429911i$	$-0.0113917 - 0.0046737i$
10	3^-	$0.000639151 - 0.00160377i$	$0.000414727 - 0.00039288i$	$-0.00293574 - 0.00143929i$
11	3^-	$0.00485675 - 0.00339194i$	$-0.000971641 - 0.000851919i$	$-0.00127236 - 0.00272045i$
12	3^-	$0.00505723 - 0.00495975i$	$-0.0014293 - 0.000926761i$	$-0.00202302 - 0.00269229i$
13	3^+	0	0	0
14	4^-	$-0.00255986 - 0.000867961i$	$-0.00362847 - 0.00146849i$	$-0.00304665 - 0.00104296i$
15	4^+	$-0.000161003 - 0.000291577i$	$-0.000379692 + 0.000353997i$	$-0.00105564 - 0.0000961879i$
16	5^-	$7.2344 \times 10^{-6} + 1.05151 \times 10^{-6}i$	$1.63729 \times 10^{-6} + 0.000300338i$	$-0.0000328837 + 0.000161622i$
17	4^+	$0.0000303582 - 0.0000581496i$	$0.000897096 + 0.000293644i$	$0.000996101 + 0.000173711i$
18	4^+	$0.0000103629 + 0.000110879i$	$-0.00101286 - 0.000367735i$	$-0.00106912 - 0.000296538i$
19	5^-	$-0.0000141965 + 0.0000397467i$	$-0.000064138 + 0.000211293i$	$-0.000127916 - 0.0000391972i$
20	5^-	$-0.0000123674 + 0.0000358142i$	$-0.0000936847 + 0.000150553i$	$-0.000131892 - 0.0000623894i$
21	5^+	0	0	0
22	6^-	$-0.0000583385 - 0.000132893i$	$-0.000322076 - 0.000123056i$	$-0.000303506 - 0.000145356i$
23	6^+	$-0.0000149595 - 0.0000441658i$	$-0.0000476734 - 0.0000967574i$	$-0.000126962 - 0.000179949i$
24	6^+	$1.86977 \times 10^{-6} + 0.0000510366i$	$-0.000319394 + 0.0000694768i$	$0.0000936657 + 0.000140969i$
25	6^+	$0.0000303315 - 0.0000665235i$	$0.0000714907 + 0.0000958909i$	$-0.0000711239 - 0.000101474i$
26	7^-	$0.0000174282 - 9.3329 \times 10^{-6}i$	$0.0000616101 + 0.0000453491i$	$0.000114012 - 0.000174147i$
27	7^-	$0.0000264184 - 0.0000130679i$	$-0.0000112335 + 0.000102362i$	$0.0000291877 - 0.0000736024i$
28	7^-	$0.000027628 - 0.0000290564i$	$0.0000294317 + 2.54616 \times 10^{-6}i$	$-0.0000194489 - 0.00014709i$
29	7^+	0	0	0

Table 6.4: 4D elastic πd scattering amplitudes when coupled to the NN channel calculated using the spline interpolation method for different numbers of p and z spline knots, N_p and N_z respectively. The lab energy of the incident pion is equal to 140 MeV.

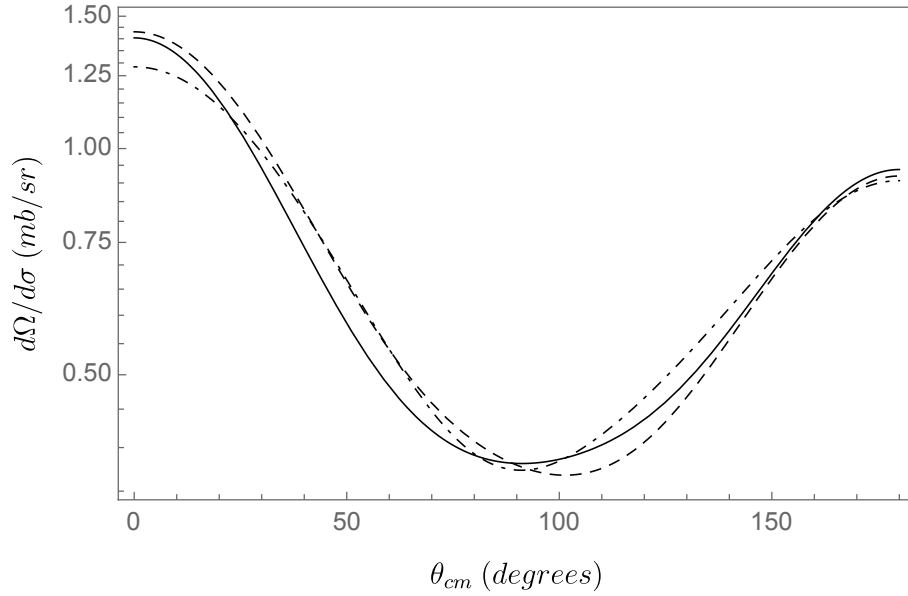


Figure 6.10: Comparison of the 4D πd differential cross section when coupled to the NN channel with the lab energy of the incident pion equal to 140 MeV. The three curves in this graph each represent a different number of spline knots used in the calculation: the dot-dashed curve represents 16 knots, the dashed curve represents 24 knots and the solid curve represents 32 knots.

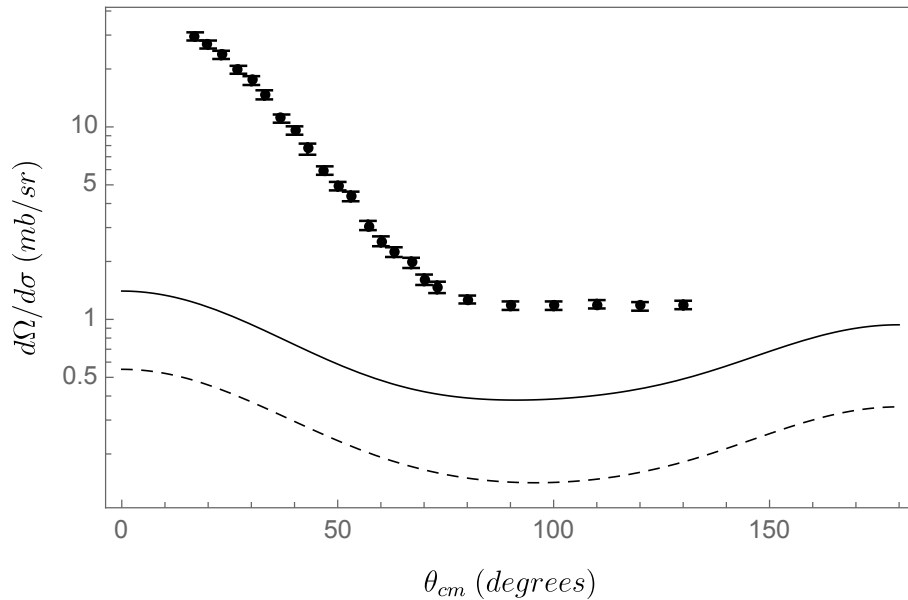


Figure 6.11: Comparison of the 3D πd and 4D πd ($N_p = N_z = 32$) differential cross section when coupled to the NN channel with the lab energy of the incident pion equal to 140 MeV, also compared with the experimental data points provided by Gabathuler et al. [187]. The solid curve represents the 4D differential cross section, while the dashed curve represents the 3D differential cross section.

We suggest that the 4D πd differential cross section would be able to more faithfully reproduce the experimental data if full coupling to the other channels was included by analysing the results of Figure 6.12, as opposed to only coupling to the P_{33} channel. In particular, the full coupling is able to better reproduce the differential cross section at angles closer to zero and at higher angles above 100 *degrees*. As the 3D and 4D differential cross sections are very similar in Figure 6.9, we would expect the 4D differential cross section with full coupling to be very similar to the curve shown in Figure 6.12.

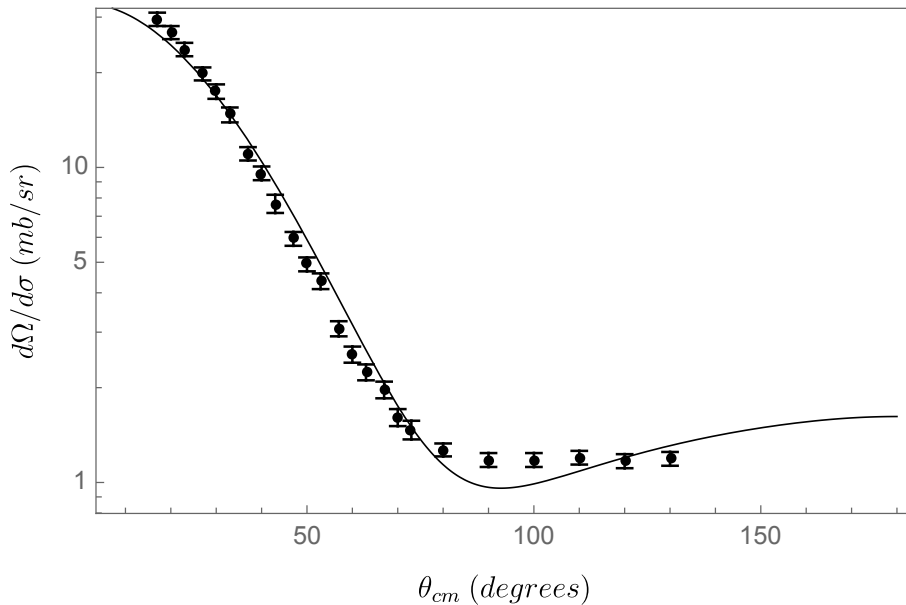


Figure 6.12: The 3D πd differential cross section with full coupling for the lab energy of the incident pion equal to 140 MeV, also compared with the experimental data points provided by Gabathuler et al. [187].

Table 6.5 lists the calculated values for the total cross section for the Unitary equations and the 4D equations for different spline knots. We see that the 4D cross sections are not numerically stable with respect to the knots, due to the variation for the results, despite being within the values for 111-120 mb. This suggests that we have not obtained adequate convergence with the number of spline knots used and more knots are needed to obtain a stable answer. Due to this variation, it is difficult to directly compare the 4D results to the 3D results, but it seems that both results agree to a certain extent. This would suggest that the addition of consistent same-time dressing do not have a significant effect on πd elastic scattering when coupled to the P_{33} , as we have seen with the differential cross section. Pedroni et al. [188] provide the experimental value for the total πd cross section. At a lab energy of 133.9 MeV, the experimental total πd cross section is 162.4 ± 1.8 mb when they

used a 20 cm target and at lab energy of 135.7 MeV, the experimental total πd cross section is 168.6 ± 1.1 mb when they used a 10 cm target. By analysing the results of the total cross section in Table 6.5, we can see that when the equations are only coupled to P_{33} , the total cross section is unable to be reproduced accurately. However, we also see that the 3D cross section with full coupling is, in fact, able to accurately reproduce the total scattering cross section, which suggests that it is simply the lack of more coupled channels that is preventing our 4D results from agreeing with the experimental value.

σ	$3D_{FC}$	$3D_{P_{33}}$	$N_p = N_z = 16$	$N_p = N_z = 24$	$N_p = N_z = 32$
σ_{el}	51.4336	47.8044	43.4895	45.1365	49.4721
σ_{tot}	169.094	115.384	111.704	118.372	114.967

Table 6.5: The total and elastic πd scattering cross section for lab energy of the incident pion equal to 140 MeV, comparing the result from the Unitary equations and the results from the 4D equations for a different number of spline knots. The results from the 3D scattering equation with full coupling are also presented (we denote $3D_{FC}$ as the results with full couplings and $3D_{P_{33}}$ as the results with coupling only to P_{33}).

6.5.3 Tensor observables

We now look at the observables that can be determined when the final state deuteron's spin is observed. We are looking at the scattering process

$$\pi d \rightarrow \pi \vec{d}. \quad (6.43)$$

In general, for the scattering of spin-0 particles off spin-1 particles, one can define four independent observables: one vector observable (vector analysing power) iT_{11} and three tensor observables (tensor analysing powers), T_{21} , T_{22} and T_{20} . We have previously discussed that the observable T_{20} cannot be accurately reproduced in πNN models such as the “Unitary $NN - \pi NN$ ” model. It was suggested by Jennings [41] that this is due to a lack of $\pi d \rightarrow \pi d$ diagrams that contained two pions in flight at the same time, which are neglected in the “Unitary $NN - \pi NN$ ” model. These four independent observables can be calculated using the centre of mass πd spin amplitudes of Kubodera et al. [189] given by

$$F_{\nu'\nu} = 4\pi \sum_{JL'L} Y_{L'0}^*(\hat{k}') Y_{LM}(\hat{k}) \langle L'01\nu' | J\nu' \rangle \langle LM1\nu | J\nu \rangle f_{L'L}^J \quad (6.44)$$

where $M = \nu' - \nu$. The four independent polarisation observables can be calculated using

$$iT_{11} = -\sqrt{6} \text{Im}(F_{01}F_{-11}^* + F_{11}F_{01}^* + F_{10}F_{00}^*)/\Sigma, \quad (6.45)$$

$$T_{20} = \sqrt{2}(|F_{-11}|^2 + |F_{10}|^2 + |F_{11}|^2 - |F_{00}|^2 - 2|F_{01}|^2)/\Sigma, \quad (6.46)$$

$$T_{21} = \sqrt{6} \text{Re}(F_{10}F_{00}^* + F_{11}F_{01}^* - F_{-11}F_{01}^*)/\Sigma, \quad (6.47)$$

$$T_{22} = \sqrt{3}(2\text{Re}F_{11}F_{-11}^* - |F_{10}|^2)/\Sigma, \quad (6.48)$$

where

$$\Sigma = \sum_{\nu'\nu} |F_{\nu'\nu}|^2 = 3 \frac{d\sigma}{d\Omega}. \quad (6.49)$$

The same πd spin amplitudes and expressions for the polarisation observables are derived by Blankleider [178]. Using Equation 6.49, we can also calculate the differential cross section of the unpolarised scattering process. This provides a good numerical check of the calculation of the differential cross section using Equation 6.40.

The four independent observables can be used to calculate subsequent polarisation observables. Following the definitions in Ottermann et al. [190]

$$\tau_{22} = \sqrt{\frac{1}{6}} T_{20} + T_{22}, \quad (6.50)$$

$$\tau_{21} = T_{21} + \frac{1}{2} \tau_{22} = T_{21} + \frac{1}{2} \sqrt{\frac{1}{6}} T_{20} + \frac{1}{2} T_{22}. \quad (6.51)$$

It is common to see to use lowercase and uppercase letters interchangeably to represent these polarisation observables in literature. We want to be clear about the observables that we are calculating. We follow the convention of Ottermann et al. [190] to define that uppercase T are used to represent scattering where the target's spin is observed and lowercase t are used to represent scattering where the recoiled particle's spin is observed. These observables are in the centre of mass frame unless otherwise stated that they are in the laboratory frame of reference. Grein and Locher [191] also define the relationship between the lab and centre of mass quantities, and because of time reversal invariance the following relationships between the observables can be determined:

$$iT_{11}^{\text{lab}} = iT_{11} = it_{11} \quad (6.52)$$

and

$$T_{2j}^{\text{lab}} = T_{2j} = (-1)^j t_{2j}. \quad (6.53)$$

So in general, the lab, centre of mass and the uppercase/lowercase observables are equal, up to a phase. The exception is the t_{2j}^{lab} observables, in which one can derive the following expression:

$$t_{20}^{\text{lab}} = \frac{3 \cos^2 \theta_R - 1}{2} T_{20} + \sqrt{6} \sin \theta_R \cos \theta_R T_{21} + \sqrt{\frac{3}{2}} \sin^2 \theta_R T_{22}, \quad (6.54)$$

$$t_{21}^{\text{lab}} = \sqrt{\frac{3}{2}} \sin \theta_R \cos \theta_R T_{20} + (1 - 2 \cos^2 \theta_R) T_{21} - \sin \theta_R \cos \theta_R T_{22}, \quad (6.55)$$

$$t_{22}^{\text{lab}} = \frac{1}{2} \sqrt{\frac{3}{2}} \sin^2 \theta_R T_{20} - \sin \theta_R \cos \theta_R T_{21} + \frac{1 + \cos^2 \theta_R}{2} T_{22}. \quad (6.56)$$

where θ_R is deuteron recoil angle in the lab frame. In our analysis, we only present the results for t_{20}^{lab} from our t_{2j}^{lab} observables, due to the lack of data for the other t_{2j}^{lab} observables and most literature being more commonly interested in t_{20}^{lab} .

Results

Comparing the πd polarisation observables when coupled to the P_{33} channel for a different number of spline knots in Figure 6.13, we see that the observables all essentially overlap with the exception of iT_{11} . This supports the claim that these amplitudes exhibit sufficient convergence with respect to the spline knots. Figure 6.13 also shows that iT_{11} is very sensitive to the accuracy of the πd amplitudes and we need many more spline knots to obtain a decent result for this observable, which is evident by the very dissimilar curves for iT_{11} .

The curves of the polarisation observables representing the 3D and 4D calculations in Figure 6.14 all essentially overlap, except for iT_{11} . This indicates that the nucleon dressing causes a minimal effect on the πd polarisation observables when coupled to P_{33} . Again the exception is the iT_{11} observable, in which we cannot make any conclusive remarks regarding the effect of consistent dressing as we are not convinced that sufficient convergence has been achieved for the πd amplitudes. A calculation with more spline knots should be performed to determine the effect on this observable.

Now turning our attention to the polarisation observables when our πd equations are coupled to the NN channel. In Figure 6.15, we compare the 4D polarisation observables for a different number of spline knots, where we can see that there is numerical instability in our results. This is opposed to the results of Figure 6.13 when we coupled our πd equations to the P_{33} channel, as the polarisation observables show much better numerical stability with respect to the spline knots. It may be that it is more difficult to obtain numerical stability for processes that involve pion creation and annihilation. Nevertheless, much more knots are required to obtain convergence of the πd amplitudes when we coupled to the NN channel. Comparing the 4D polarisation observables to experimental data in Figure 6.16, we see that coupling to the NN channel has more of an effect on the polarisation observables than coupling to the P_{33} channel. If we examine the T_{20} observables particularly, we see that the 4D result passes through three experimental uncertainty bars, as opposed to the 3D result which only passes through two uncertainty bars. As coupling to NN allows us to include the diagram described by Jennings [42], our results indicate that the addition of this diagram does, indeed, allow for a more faithful reproduction of the T_{20} observable. However, it seems evident from Figure 6.15 that our results have a high degree of numerical instability, so it is difficult to make definite remarks regarding the 4D polarisation observables.

The plots in Figure 6.17 show the polarisation observables for 3D with full coupling.

These plots should give us an indication of how the 4D results would differ if we included full coupling. We can see in Figure 6.17 that the iT_{11} observable can be much better reproduced, in comparison to the experimental, when the equations include full coupling. Thus, one would expect the 4D results with full coupling to agree with the experimental data closer in Figure 6.14, however as we have just discussed, it is difficult to make conclusive claims due to the numerical instability we see in the 4D iT_{11} observable. Looking at the other observables in 6.17, it seems that the inclusion of full coupling has a detrimental effect on the observables to more accurately reproduce the experimental data. While most of the observables for coupling to P_{33} and NN tend through some of the experimental uncertainty bars, the observables for the full coupling tend away from the experimental data. Particularly, we can see that T_{20} avoids the data completely, which supports the claims of inability to be reproduced in the literature (we will not mention the discrepancies for T_{21} and T_{22} , due to the lack of experimental data). It might be that the effect of neglecting diagrams with more than one pion has a more prevalent effect when more partial waves and all coupled channels are included. As we have seen in Figure 6.14, the difference between the 3D and 4D observables is quite minimal (with the exception of iT_{11}), so by analysing the results of full coupling, we expect the 4D results with full coupling with not be able to more accurately reproduce the experimental data.

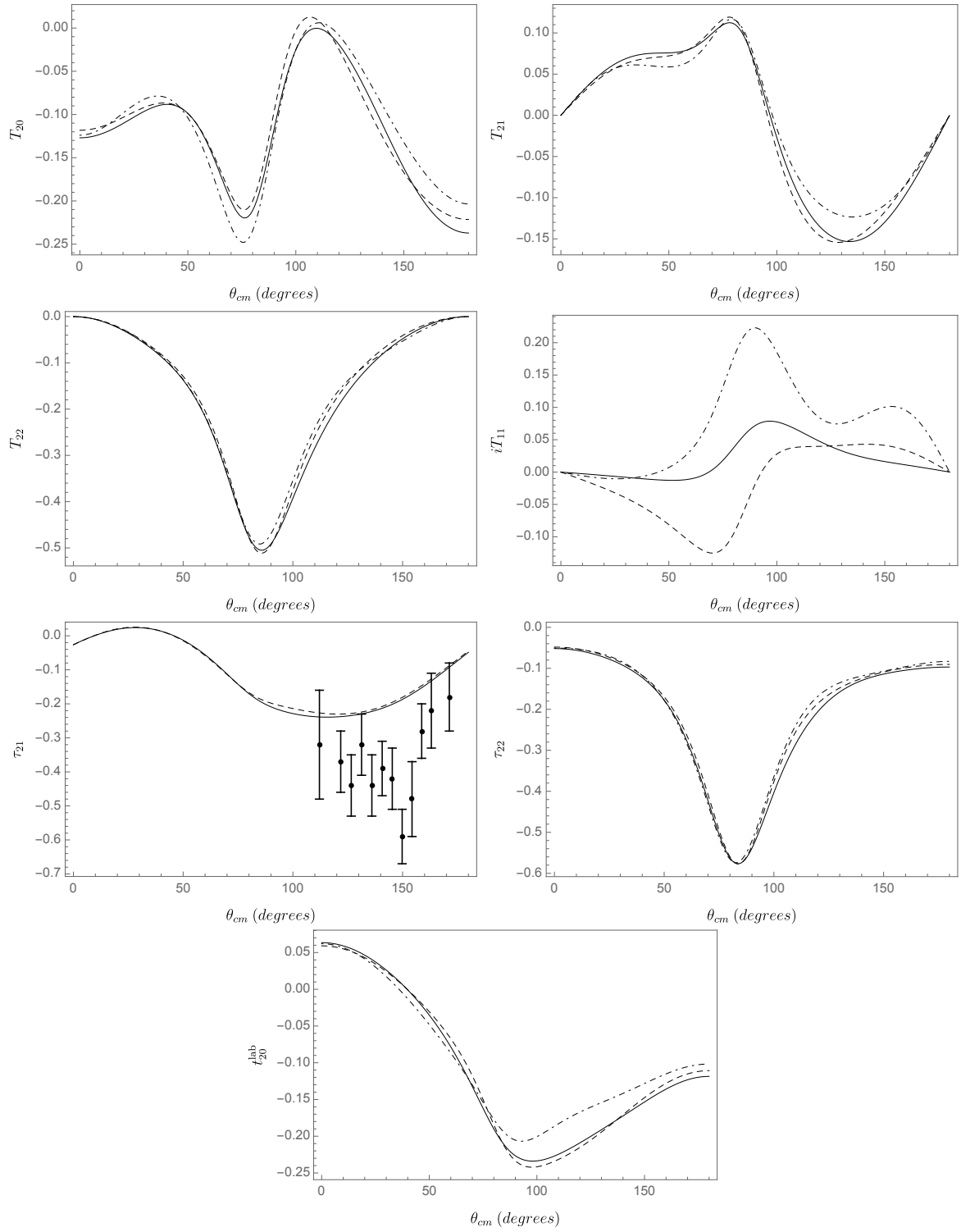


Figure 6.13: Comparison of the 4D πd polarisation observables when coupled to the P_{33} channel with the lab energy of the incident pion equal to 140 MeV. The three curves in this graph each represent a different number of spline knots used in the calculation: the dot-dashed curves represent 16 knots, the dashed curves represent 24 knots and the solid curves represent 32 knots.

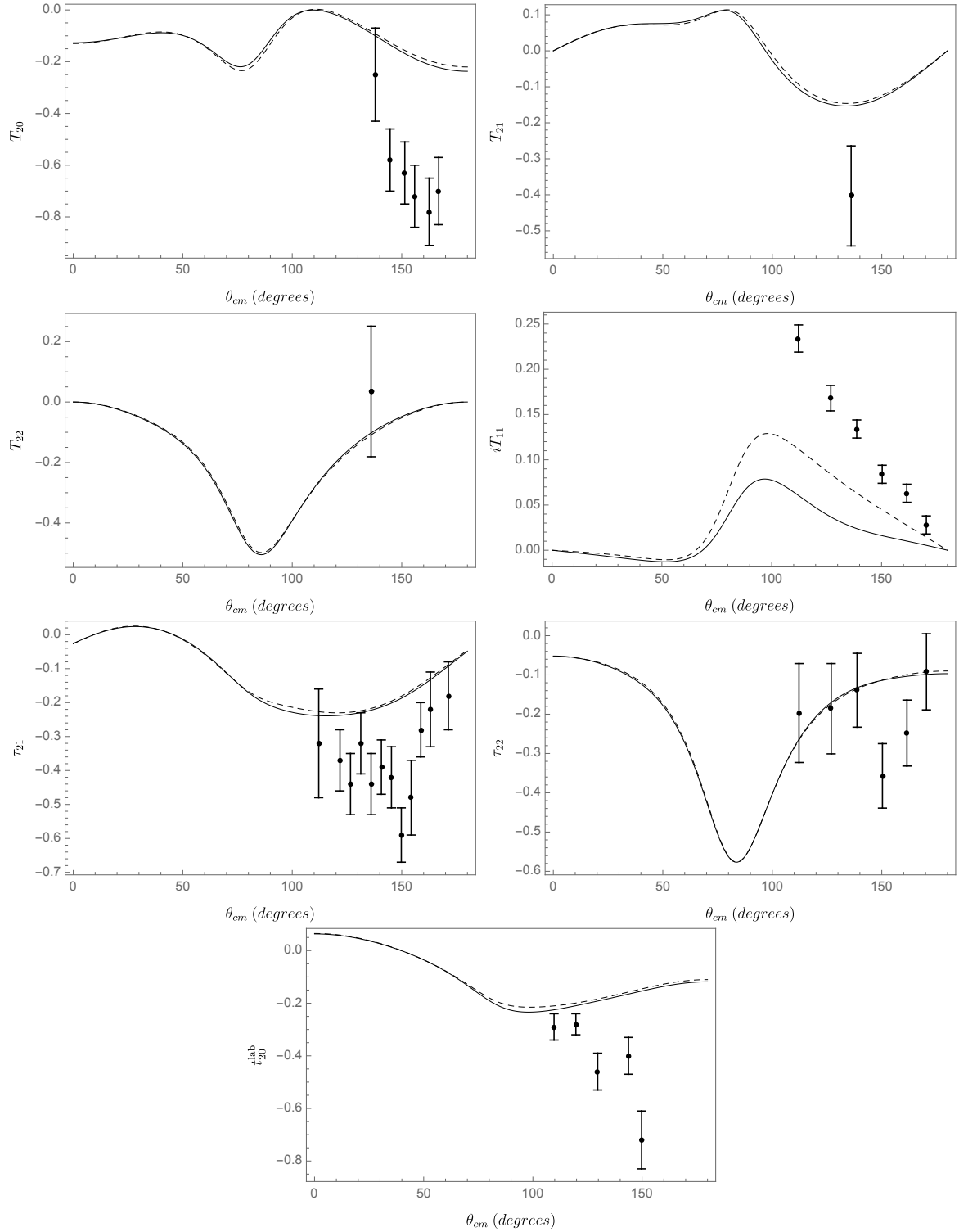


Figure 6.14: Comparison of the 3D πd and 4D πd ($N_p = N_z = 32$) polarisation observables when coupled to the P_{33} channel with the lab energy of the incident pion equal to 140 MeV, also compared with experimental data points (T_{20} and τ_{21} from [192], T_{21} and T_{22} from [193], iT_{11} and τ_{22} from [190] and t_{20}^{lab} from [194]). The solid curves represent the 4D polarisation observables, while the dashed curves represent the 3D polarisation observables.

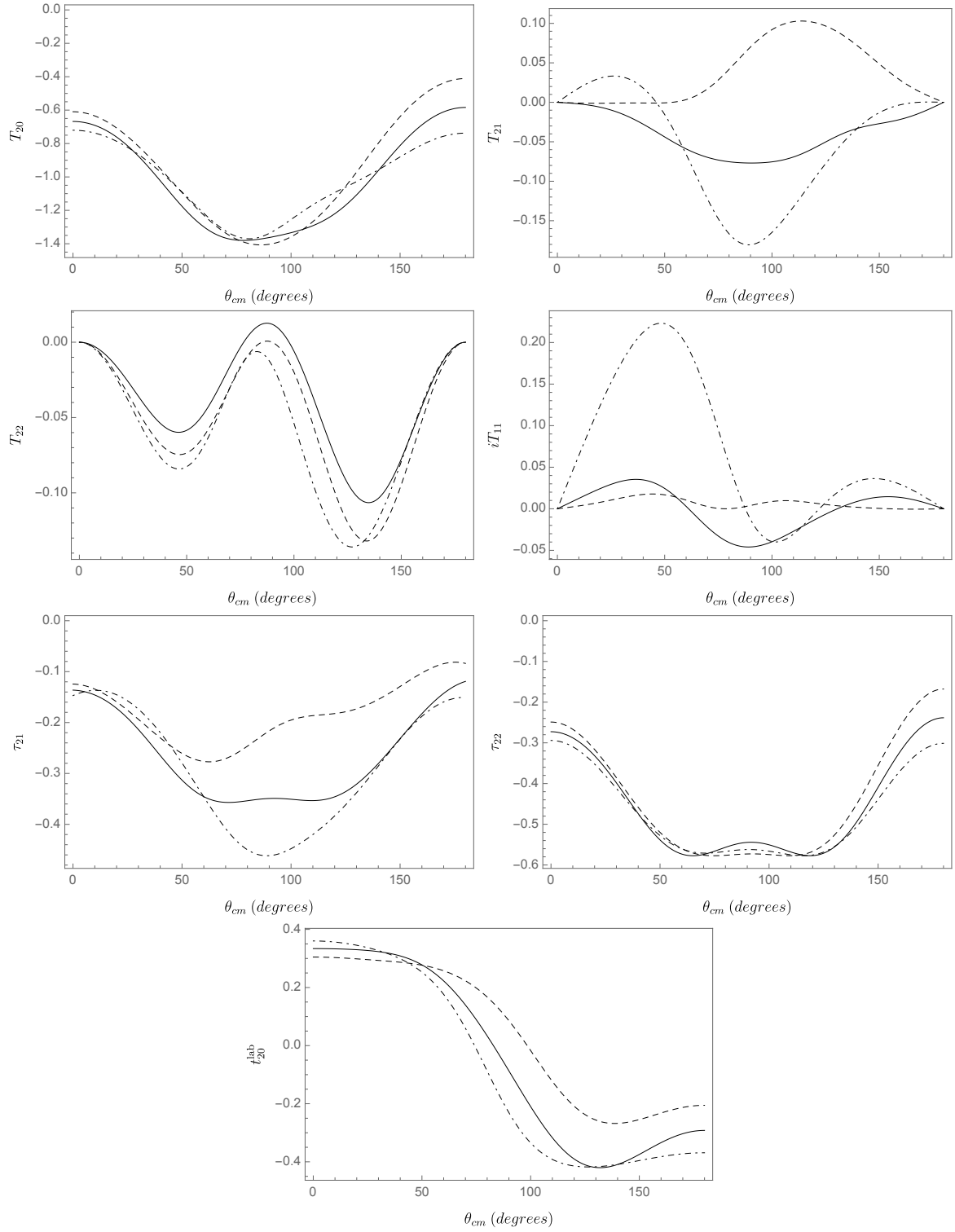


Figure 6.15: Comparison of the 4D πd polarisation observables when coupled to the NN channel with the lab energy of the incident pion equal to 140 MeV. The three curves in this graph each represent a different number of spline knots used in the calculation: the dot-dashed curves represent 16 knots, the dashed curves represent 24 knots and the solid curves represent 32 knots.

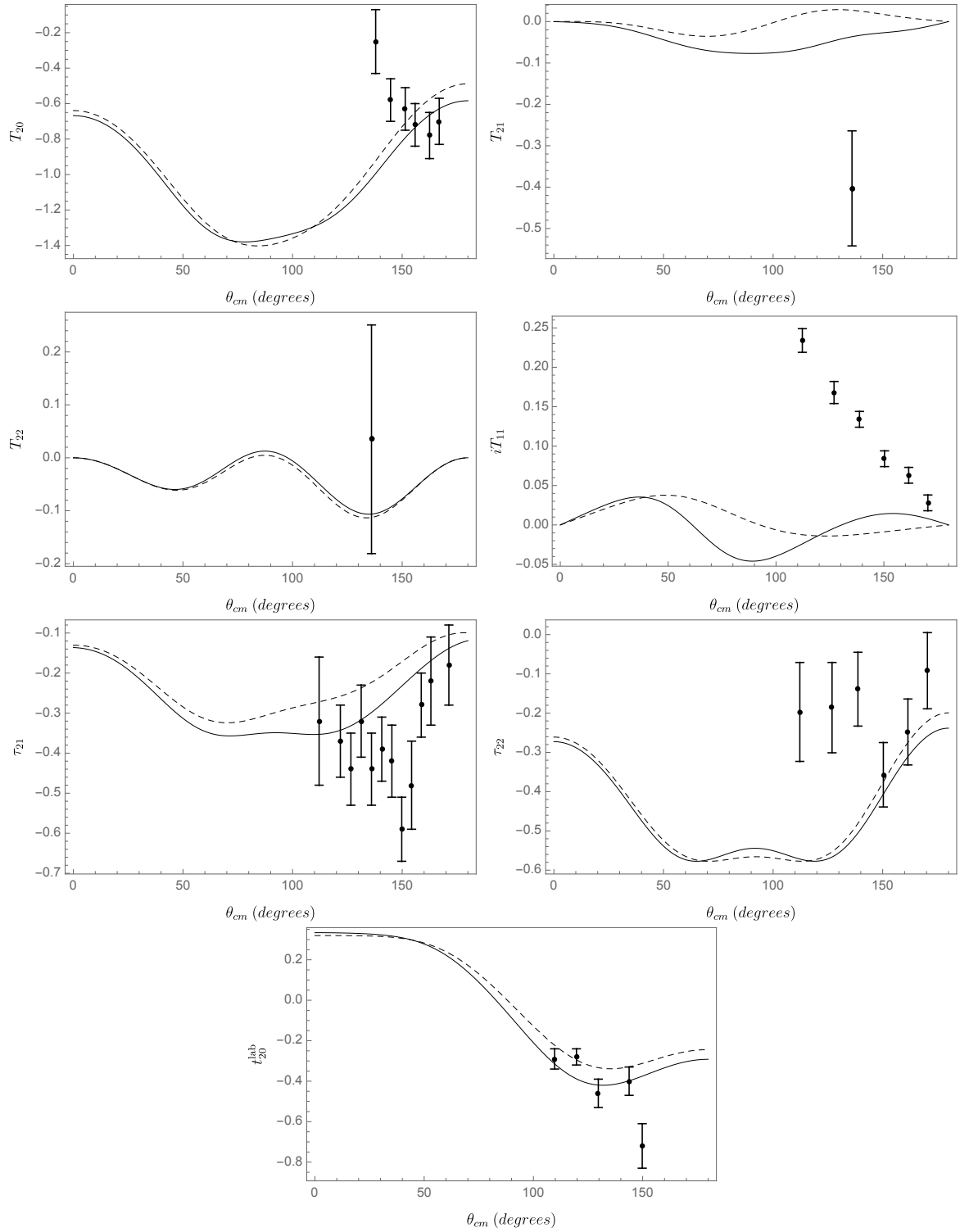


Figure 6.16: Comparison of the 3D πd and 4D πd ($N_p = N_z = 32$) polarisation observables when coupled to the NN channel with the lab energy of the incident pion equal to 140 MeV, also compared with experimental data points (T_{20} and τ_{21} from [192], T_{21} and T_{22} from [193], iT_{11} and τ_{22} from [190] and t_{20}^{lab} from [194]). The solid curves represent the 4D polarisation observables, while the dashed curves represent the 3D polarisation observables.

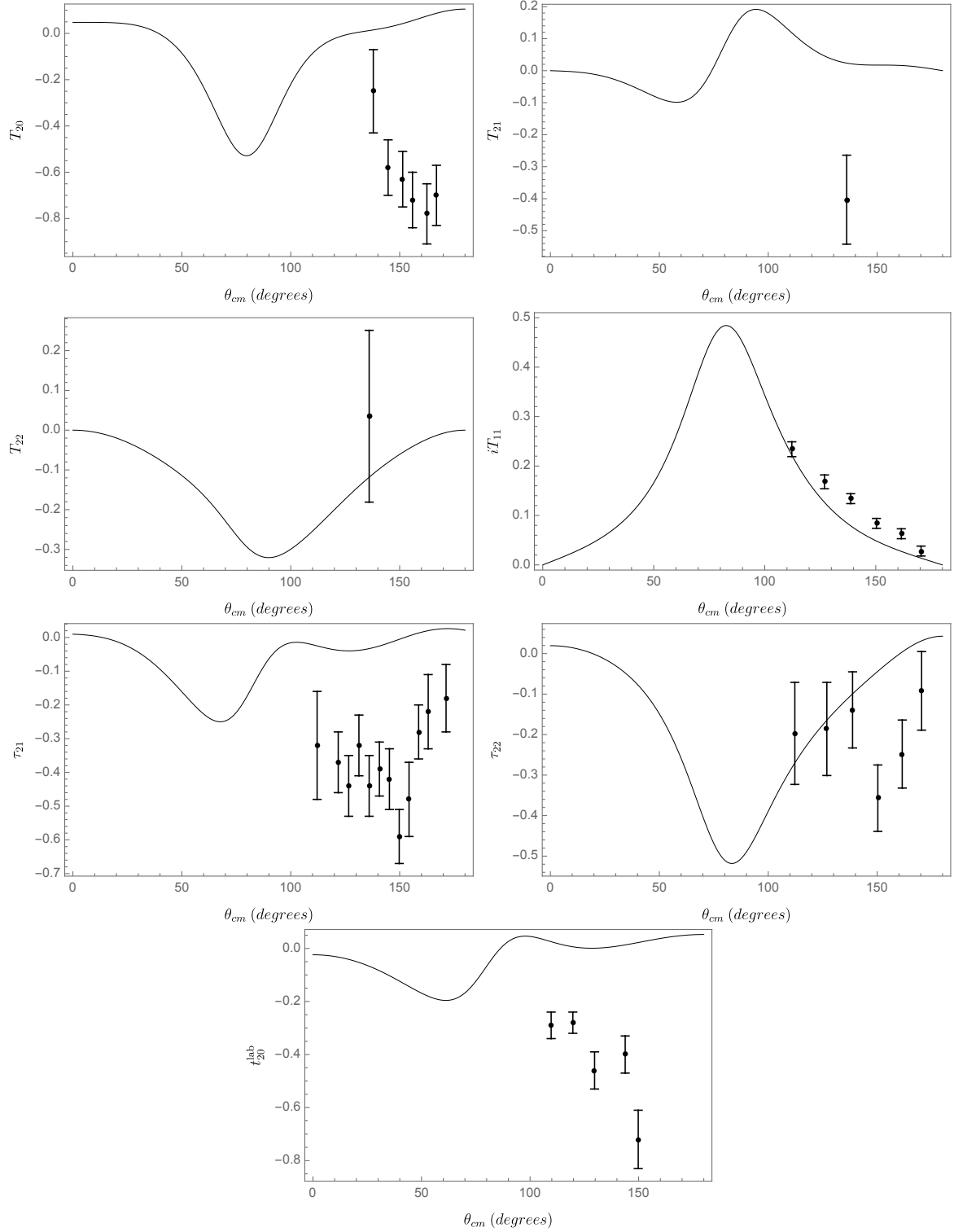


Figure 6.17: The 3D πd polarisation observables with full coupling for the lab energy of the incident pion equal to 140 MeV, also compared with experimental data points (T_{20} and τ_{21} from [192], T_{21} and T_{22} from [193], iT_{11} and τ_{22} from [190] and t_{20}^{lab} from [194]).

6.6 Pion production ($pp \rightarrow \pi^+d$ observables)

In this section, we calculate the observables for pion production from the scattering of two nucleons, i.e. the reaction $NN \rightarrow \pi d$. Generally in the literature, observables are determined for the reaction $pp \rightarrow \pi^+d$, however, we have discussed that similarly to πd elastic scattering, the Coulomb effect should be minimal in comparison to the effect of the strong interaction. As a result, we will tend to neglect the charge of the pion. Similar to the πd observables, we calculate the $pp \rightarrow \pi d$ observables using the 3-dimensional scattering equations and the 4-dimensional scattering equations that we have obtained using convolution integrals. We also calculate the results for 3-dimensional scattering equations with full coupling, in order to determine how our 4-dimensional results would differ if we were to include all the partial wave and couplings.

The unpolarised differential cross section for $pp \rightarrow \pi d$ is given by [178]

$$\frac{d\sigma}{d\Omega_{\text{unpol}}} (pp \rightarrow \pi d) = (2\pi)^4 \frac{k_f}{k_i} \mu_i(k_i) \mu_f(k_f) |M_{fi}|_{\text{unpol}}^2 \quad (6.57)$$

where

$$|M_{fi}|_{\text{unpol}}^2 = \frac{1}{(4\pi)^2} \sum_L B_L P_L(\cos \theta) \quad (6.58)$$

with

$$B_L = \frac{1}{(2s_1 + 1)(2s_2 + 1)} \sum_{S_f S_i} \sum_{L_f L_i L'_f L'_i} \sum_{J J'} (-1)^{S_f - S_i} \hat{L}_f \hat{L}_i \hat{L}'_f \hat{L}'_i (\hat{J} \hat{J}' \hat{L})^2 \quad (6.59)$$

$$\begin{pmatrix} L_i & L'_i & L \\ 0 & 0 & 0 \end{pmatrix} \begin{pmatrix} L_f & L'_f & L \\ 0 & 0 & 0 \end{pmatrix} \begin{Bmatrix} J & J' & L \\ L'_i & L_i & S_i \end{Bmatrix} \begin{Bmatrix} J & J' & L \\ L'_f & L_f & S_f \end{Bmatrix}$$

$$X_{L_f S_f L_i S_i}^{JT} X_{L'_f S'_f L'_i S'_i}^{J'T*}$$

Here, k_i is the initial on-shell momentum (the on-shell NN momentum) and k_f is the final on-shell momentum (the on-shell πd momentum). The reduced masses μ_i and μ_f are given as

$$\mu_i(k_i) = \frac{(k_i^2 + m_N^2)^{1/2} (k_i^2 + m_N^2)^{1/2}}{(k_i^2 + m_N^2)^{1/2} + (k_i^2 + m_N^2)^{1/2}}; \quad \mu_f(k_f) = \frac{(k_f^2 + m_\pi^2)^{1/2} (k_f^2 + m_d^2)^{1/2}}{(k_f^2 + m_\pi^2)^{1/2} + (k_f^2 + m_d^2)^{1/2}}. \quad (6.60)$$

We are particularly interested in this differential cross section, as it has been commonly suggested in the literature that the differential cross section for $pp \rightarrow \pi d$ calculated the “Unitary $NN - \pi NN$ ” model is significantly smaller compared to experiments. This was said

to be because there was an inconsistency with renormalisation in the “Unitary $NN - \pi NN$ ” model due to neglecting diagrams with more than one pion in flight at a time, which lead to the πNN coupling constant being significantly smaller than the experimental value. This renormalisation problem has been theoretically overcome through our use of convolution integrals, which allows us to sum all time-ordered perturbation diagrams, including diagrams that were previously neglected.

We also calculate the polarisation observables when both protons are polarised ($\vec{p}\vec{p} \rightarrow \pi d$). Following the procedure of Blankleider and Afnan [177], if we denote the polarisation of the beam by $\mathbf{P}^{(a)}$ and the polarisation of the target by $\mathbf{P}^{(b)}$, then the differential cross section for the reaction $\vec{p}\vec{p} \rightarrow \pi d$ in terms of partial cross sections σ_{ij} is given by

$$\frac{d\sigma}{d\Omega} = \sigma_{00} + \sum_{i=1}^3 P_i^{(a)} \sigma_{i0} + \sum_{j=1}^3 P_j^{(b)} \sigma_{0j} + \sum_{i,j=1}^3 P_i^{(a)} P_j^{(b)} \sigma_{ij} \quad (6.61)$$

where σ_{00} is the spin-averaged cross section, which is equivalent to the unpolarised differential cross section defined before. Being able to calculate the differential cross section in multiple ways provides a good numerical check. Equation 6.61 leads to the usual definition of the correlation tensor A_{ij}

$$A_{ij} = \frac{\sigma_{ij}}{\sigma_{00}}. \quad (6.62)$$

There are 16 possible A_{ij} (including the trivial $A_{00} = 1$), but because of parity invariance, only eight are non-zero. In addition, as the two polarised particles are identical, the number of independent correlations reduces to six ($A_{00} = \sigma_{00}, A_{y0}, A_{zx}, A_{xx}, A_{yy}$ and A_{zz}). The expressions for these six independent correlations are given in Blankleider and Afnan [177] for the choice of coordinate frame having the z axis along the beam direction.

Similarly to πd elastic scattering, we list and assign a label to each $pp \rightarrow \pi d$ amplitude in Table 6.6.

a_I	J^π	Pion wave	L_f (πd)	S_f (πd)	L_i (pp)	S_i (pp)	pp state
a_0	0^+	p	1	1	0	0	1S_0
a_1	1^-	s	0	1	1	1	3P_1
a_2	2^+	p	1	1	2	0	1D_2
a_3	1^-	d	2	1	1	1	3P_1
a_4	2^-	d	2	1	1	1	3P_2
a_5	2^-	d	2	1	3	1	3F_2
a_6	3^-	d	2	1	3	1	3F_3
a_7	2^+	f	3	1	2	0	1D_2
a_8	4^+	f	3	1	4	0	1G_4
a_9	3^-	g	4	1	3	1	3F_3
a_{10}	4^-	g	4	1	3	1	3F_4
a_{11}	4^-	g	4	1	5	1	3H_4
a_{12}	5^-	g	4	1	5	1	3H_5
a_{13}	4^+	h	5	1	4	0	1G_4
a_{14}	6^+	h	5	1	6	0	1I_6

Table 6.6: The partial wave channels considered in the calculation of pion production, in which we consider the same channels as Blankleider [178].

Results

Looking at the amplitudes in Table 6.7 and comparing the results for a different number of spline knots, we can see that these amplitudes show relatively good convergence. This is with the exception of the second amplitude for $J^\pi = 2^+$, which has unexpectedly terrible convergence with respect to the spline knots. We notice that for J^π values with multiple deuteron states except for $J^\pi = 1^-$ ($J^\pi = 2^+, 3^-, 4^+$), the convergence of the second amplitude tends to show poor convergence, with the worse offender being $J^\pi = 2^+$. We have investigated why the second amplitude of $J^\pi = 2^+$, in particular, has poor convergence and has not found any conclusive evidence or justification for this observation. There are no A coefficients for the corresponding half off-shell $N\Delta \leftrightarrow \pi d$ Z -diagram for the larger L value 3S_1 channel, so one might expect that this may contribute to the lack of convergence. This would be because the second amplitude would be dependent purely on the 3D_1 state, which may not be as dominant as the 3S_1 and may cause numerical instability in the calculations. As such, one could calculate the $pp \rightarrow \pi d$ amplitudes using a 3S_1 deuteron potential, similar to the potential by Mongan [134, 135]. However, it is not entirely clear whether this is the definite cause of the poor convergence. One would hope that this poor convergence in the second amplitude does not cause many issues to the observables, as it is not as large as some of the other amplitudes in Table 6.7, but this is to be determined.

a_I	J^π	$N_p = N_z = 16$	$N_p = N_z = 24$	$N_p = N_z = 32$
0	0^+	$-0.00502389 + 0.000192979i$	$-0.00502861 + 0.000166469i$	$-0.00503407 + 0.000150901i$
1	1^-	$-0.00285001 + 0.00107868i$	$-0.00283846 + 0.00106023i$	$-0.00284458 + 0.00106043i$
2	2^+	$-0.0230487 - 0.0165657i$	$-0.024932 - 0.0178315i$	$-0.026161 - 0.0171651i$
3	1^-	$0.000756171 + 0.000580918i$	$0.000751178 + 0.000585263i$	$0.000750864 + 0.000589203i$
4	2^-	$-0.000398274 + 0.0000316655i$	$-0.000402727 - 2.26507 \times 10^{-6}i$	$-0.000405418 - 9.90466 \times 10^{-6}i$
5	2^-	$-0.00264307 - 0.000397686i$	$-0.00262748 - 0.000401962i$	$-0.00264804 - 0.000399326i$
6	3^-	$0.00774937 + 0.00177407i$	$0.00768678 + 0.00182931i$	$0.00774077 + 0.00180424i$
7	2^+	$0.000808073 - 0.0000794356i$	$-0.000268574 - 0.000216726i$	$-0.00161075 - 0.00116797i$
8	4^+	$-0.00155936 - 0.000205007i$	$-0.00152656 - 0.000206277i$	$-0.00154662 - 0.000206835i$
9	3^-	$-0.000130079 - 0.0000318553i$	$-0.000130248 - 0.0000675877i$	$-0.00011812 - 0.0000397418i$
10	4^-	$-0.000139424 - 1.07945 \times 10^{-6}i$	$-0.000140325 - 4.67164 \times 10^{-6}i$	$-0.000140984 - 1.19775 \times 10^{-6}i$
11	4^-	$-0.0000971984 - 7.88704 \times 10^{-6}i$	$-0.0000966732 - 7.88521 \times 10^{-6}i$	$-0.0000966518 - 7.83165 \times 10^{-6}i$
12	5^-	$0.000412301 + 0.0000408623i$	$0.000418195 + 0.0000411949i$	$0.000418656 + 0.0000413198i$
13	4^+	$0.0000366134 + 3.51005 \times 10^{-7}i$	$0.000030066 + 9.06293 \times 10^{-6}i$	$0.0000347493 + 2.25112 \times 10^{-6}i$
14	6^+	$-0.0000666239 - 7.7292 \times 10^{-6}i$	$-0.0000876814 - 5.71702 \times 10^{-6}i$	$-0.0000878971 - 6.13754 \times 10^{-6}i$

Table 6.7: 4D $pp \rightarrow \pi d$ scattering amplitudes calculated using the spline interpolation method for different numbers of p and z spline knots, N_p and N_z respectively. The lab energy of the incident proton equal is to 560 MeV.

In Figure 6.18, we plot the 4D $pp \rightarrow \pi d$ differential cross section for different number of spline knots. We note that the 32 knot curve in Figure 6.18 has a noticeable concave shape, whereas the cross sections corresponding to the 16 and 24 knots amplitudes have all had a linear shape. This may be due to the unstable second amplitude of $J^\pi = 2^+$ that we commented on earlier.

We plot the 3D and 4D differential cross section in Figure 6.19 with the experimental data and see that the addition of consistent same-time nucleon dressing and consistent renormalisation as a result of the convolution integral allows the differential cross section to be more faithfully reproduced. This support the findings in the literature that the renormalisation inconsistency found in the “Unitary $NN - \pi NN$ ” model is the reason for the noticeably small theoretical cross sections for $pp \rightarrow \pi d$. This is further supported by the fact that, despite not showing absolute numerical stability, all the 4D differential cross sections in Figure 6.18 are all larger than the 3D cross section shown in Figure 6.19.

The addition of full coupling to the scattering equation also significantly reproduces the differential cross section with respect to the experimental data, as one can see in Figure 6.20. This implies that a 4D calculation with full coupling would increase the differential cross sections shown in Figure 6.18 and could possibly reproduce the cross section quite accurately. One could verify that by taking a ratio of the 3D cross section in Figure 6.19

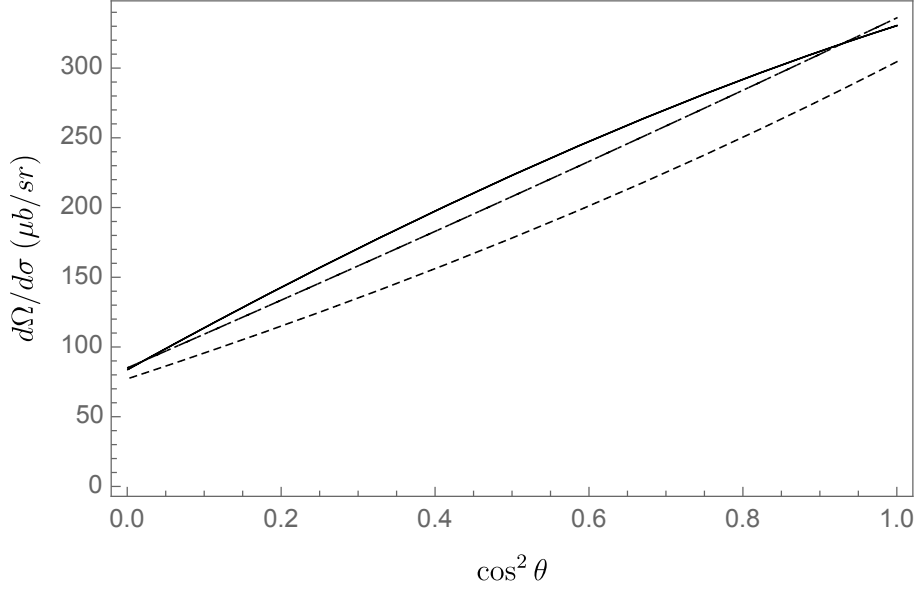


Figure 6.18: Comparison of the 4D $pp \rightarrow \pi d$ differential cross section with the lab energy of the incident proton equal to 560 MeV. The three curves in this graph each represent a different number of spline knots used in the calculation: the dot-dashed curve represents 16 knots, the dashed curve represents 24 knots and the solid curve represents 32 knots.

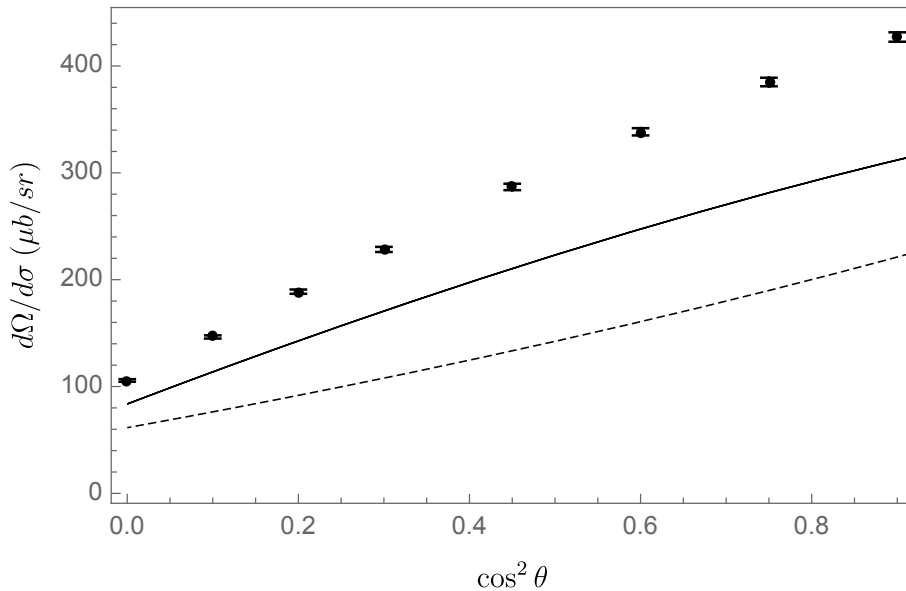


Figure 6.19: Comparison of the 3D and 4D ($N_p = N_z = 32$) $pp \rightarrow \pi d$ differential cross section with the lab energy of the incident proton equal to 560 MeV, also compared with the experimental data points provided by Hoftiezer et al. [195]. The solid curve represents the 4D differential cross section, while the dashed curve represents the 3D differential cross section.

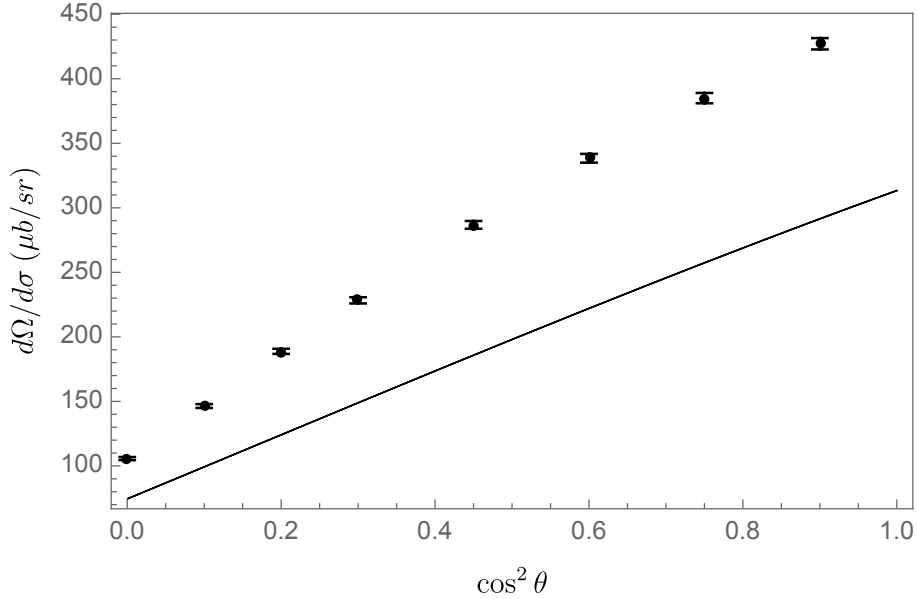


Figure 6.20: The 3D differential cross section with full coupling for the lab energy of the incident proton equal to 560 MeV, also compared with the experimental data points provided by Hoftiezer et al. [195].

with the 3D cross section that includes full coupling shown in 6.20 and multiplying the 4D cross sections in Figure 6.18 by this ratio.

Finally, we look at the polarisation observables for $pp \rightarrow \pi d$. Comparing the 4D observables with a different amount of spline knots in Figure 6.21 we see that there is minimal difference in the A_{zx} and the A_{y0} observable. Comparing these observables with their 3D counterpart and the experimental data in Figure 6.22, we see that our calculations are able to reproduce the data well. If we look at the 3D calculation with full coupling in Figure 6.23, one would expect that the addition of more coupled channels might provide the 4D observables with a more definite structure and push the results more towards the experimental data. The more concerning results are the A_{xx} , A_{yy} and A_{zz} observable. In particular, the curve corresponding to 32 knots is of the opposite curvature, in comparison to the 16 and 24 knot curves. This is similar to what we saw for the differential cross section, which had an unexpected concave shape. This concern is also emphasised when we look at the data in Figure 6.22, which has the opposite curvature than the calculated 4D observable. We also notice that the 3D observables without full coupling have the correct shape, so we are confident to stay the 32 knot result of the 4D calculation has major numerical instability and is not accurate. We suspect the second amplitude $J^\pi = 2^+$ again, due to its poor convergence.

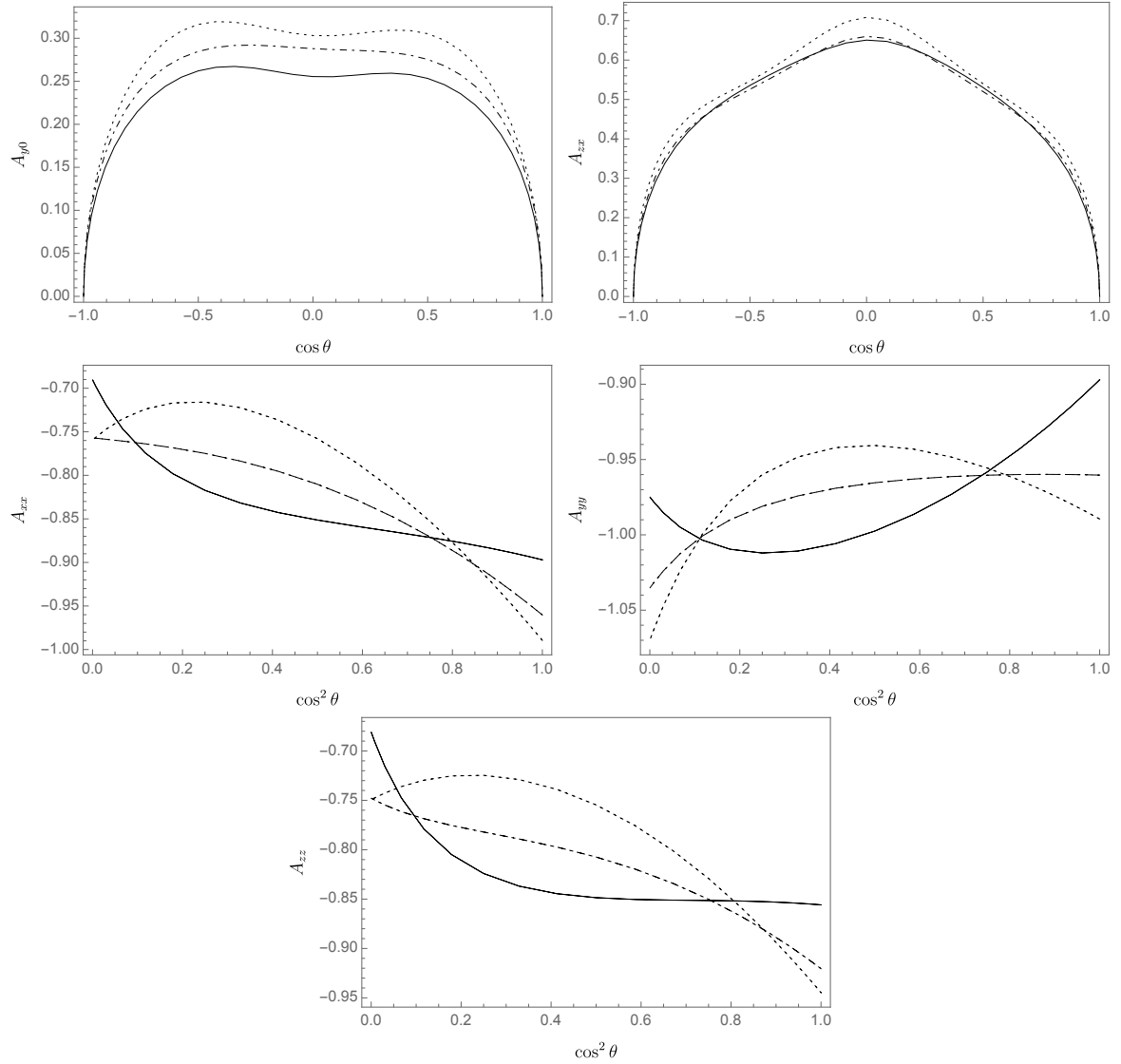


Figure 6.21: Comparison of the 4D $pp \rightarrow \pi d$ polarisation observables with the lab energy of the incident proton equal to 560 MeV. The three curves in this graph each represent a different number of spline knots used in the calculation: the dot-dashed curve represents 16 knots, the dashed curve represents 24 knots and the solid curve represents 32 knots.

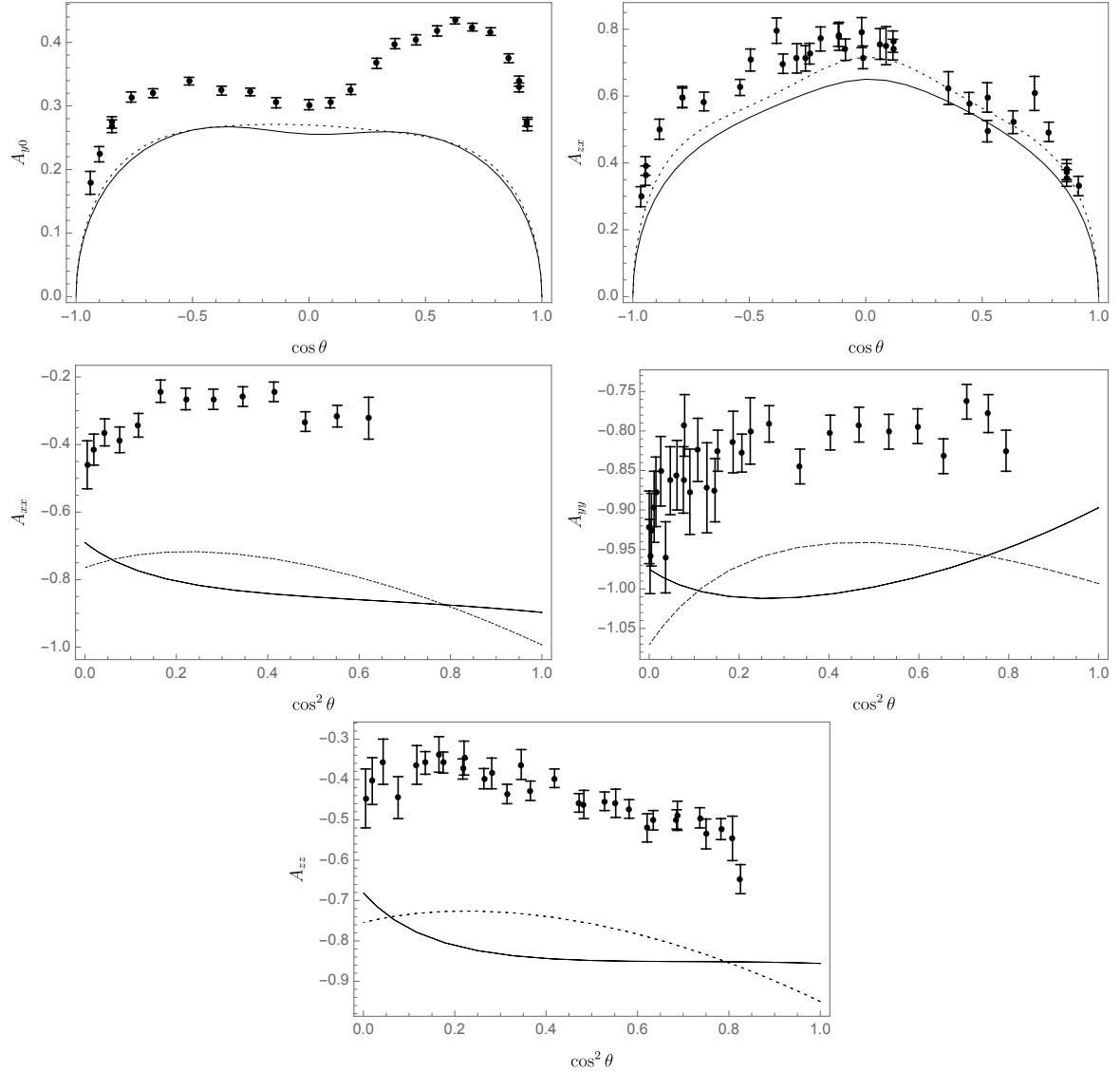


Figure 6.22: Comparison of the 3D and 4D ($N_p = N_z = 32$) polarisation observables with the lab energy of the incident proton equal to 560 MeV, also compared with the experimental data points (A_{y0} from [196], A_{xx} , A_{yy} and A_{zz} from [197, 198] and A_{zx} from Hoftiezer et al. [199]). The solid curve represents the 4D observable, while the dashed curve represents the 3D observable.

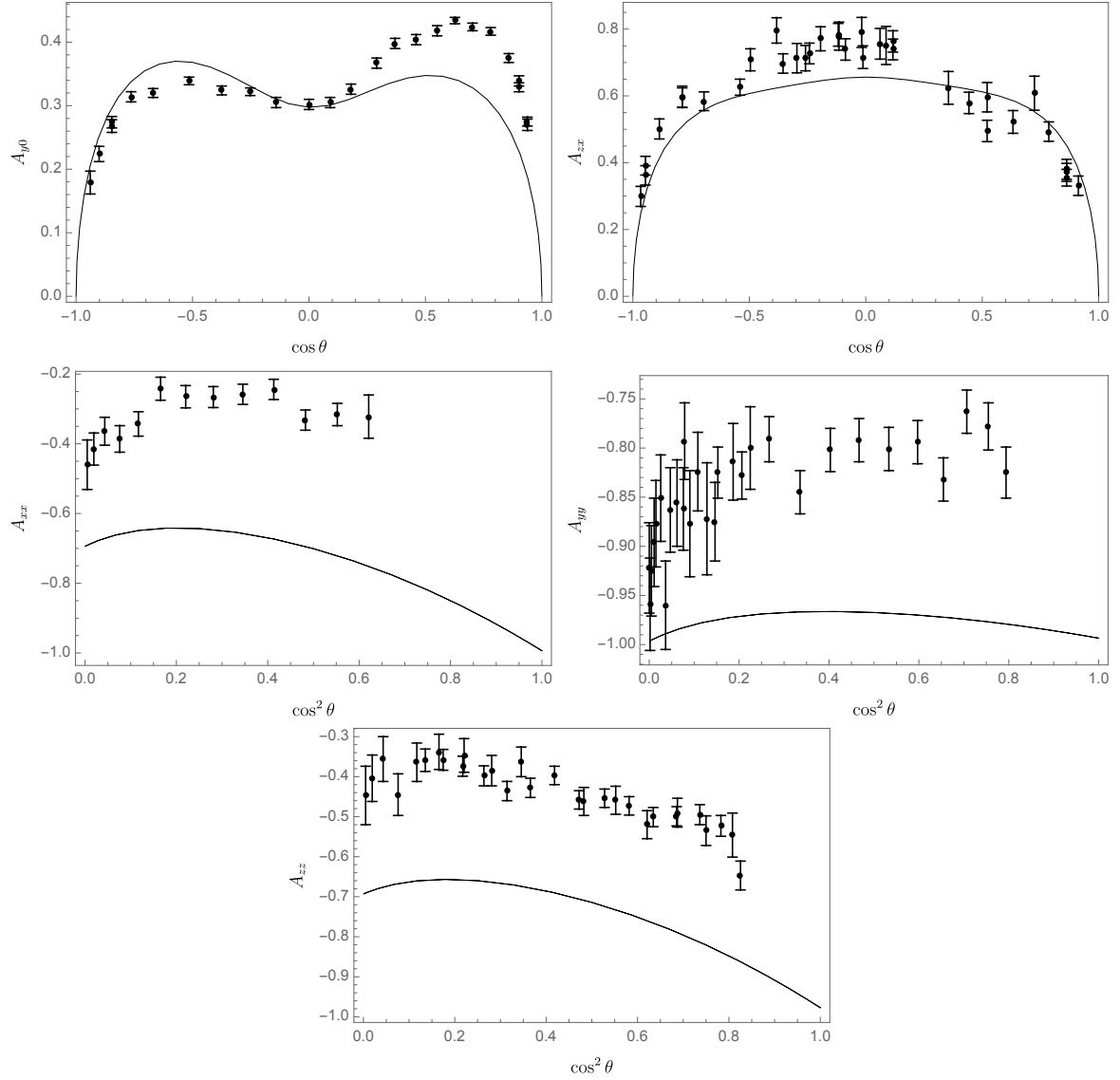


Figure 6.23: The 3D $pp \rightarrow \pi d$ polarisation observables with full coupling for the lab energy of the incident proton equal to 560 MeV, also compared with the experimental data points (A_{y0} from [196], A_{xx} , A_{yy} and A_{zz} from [197, 198] and A_{zx} from Hoftiezer et al. [199]).

Chapter 7

Conclusions

The overall goal of this thesis was to develop the convolution approach to the πNN system, and determine whether its property of a consistent formulation of nucleon wavefunction renormalisation, can resolve the inadequacies of previous few-body descriptions of the coupled $NN - \pi NN$ system in describing experimental data. The convolution approach can successfully overcome the long-standing renormalisation problem due to inconsistent nucleon dressing in the “Unitary $NN - \pi NN$ ” model, and therefore it is a primary goal of this thesis to determine whether the convolution approach can improve the reproducibility of particular scattering observables, such as the $pp \rightarrow \pi^+d$ differential cross section and the T_{20} polarisation observable in πd elastic scattering. Using the convolution approach, we extend the approach of Kvinikhidze and Blankleider [49] to derive coupled $NN - \pi NN$ equations in two equivalent forms: (i) a 3-dimensional form that is expressed in a similar way to the equations of Afnan and Blankleider [33], but differing from these equations in that all nucleon propagators are fully dressed, as well as containing non-pair-like terms in the kernel and (ii) a 4-dimensional form, which involves only pair-like interactions.

To achieve our overall goal, we concentrated on the solution of the 4-dimensional form of our coupled $NN - \pi NN$ convolution equations, as it avoids the complications of including non-pair-like interactions. This, nevertheless, presented many interesting but demanding challenges, having to evaluate our integrals along the real axes in the presence of moving singularities. The difficulty of this task has required extraordinarily large computation times that have limited the number of partial waves and the number of coupled channels that can be included, as well as affecting the numerical stability of the numerical results due to the limitation of spline interpolation points.

After partial wave decomposition, 4-dimensional equations reduce to 2-dimensional equations, and the kernel of these 2-dimensional equations involve an integral over the intermediate momentum p'' and the intermediate energy-like variable z'' . The difficulty in solving these equations is due to the presence of moving singularities in these integral equations. The complex singularity structure of our 4-dimensional equations also restricts our ability to include more than one coupled channel at a time. To include all coupled channels, one must account for the numerous logarithmic singularities in the p'' integral for each Z -diagram given in Equation 6.5. Additionally, the solution of our 4-dimensional equations also contain singularities, which makes it difficult to interpolate using splines, as the solution is not smooth due to these singularities. As these singularities in the solution originate from the inhomogeneous term of our 4-dimensional equations, we factor out the inhomogeneous term

from the solution and perform the spline interpolation on the factorised solution. We refer to this factorisation process as Carbonell-Karmanov (CK) factorisation, as these authors suggested such a factorisation in [73, 74]. This CK factorisation also further complicates the singularity issue in the equation kernel, as the factorisation introduces the inhomogeneous term into the kernel's integral, thereby introducing additional singularities. Despite an increase in computational time, accounting for the singularities in the p'' integral is not an extremely difficult task. The difficulty is in handling the singularities in the z'' integral, as it is the interaction of the singularities in the p'' integral which gives rise to the singularities in the z'' integral. Because of all the Z -diagrams in fully coupled equations in addition to the Z -diagrams introduced as a result of CK factorisation, the task of accounting for each singularity in the z'' integral becomes extremely cumbersome and difficult to implement based on our “general recipe” for determining the location of singularities in the z'' integral discussed in Chapter 6. In essence, calculating the integrals of our 4-dimensional πNN convolution equations with coupling to all channels is not feasible, due to the copious amount of singularities in the integrals.

After obtaining solutions to our 4-dimensional πNN convolution equations, we find that the consistent dressing improves the reproducibility of the NN phase shifts, in comparison to the fitted solution of experimental data, when the equations are coupled to either to the NN or P_{33} channel. While we do not expect to accurately reproduce the NN phase shifts as we include only one-pion exchange and only one coupled channel, it is reassuring to observe that the consistent nucleon dressing has a positive effect on the phase shifts.

If we look at our results for πd elastic scattering, we find that our 4-dimensional πNN convolution equations do not have a significant contribution to the scattering observables when we couple our equations to the P_{33} channel. This may be unsurprising as the only additional nucleon dressing comes from the intermediate $N\Delta$ state, as the spectator nucleon is represented by a dressed propagator. More of a significant difference between the 3-dimensional and 4-dimensional results may be present if we were to dress the exchanged nucleon in the Z -diagrams which involve a πd state. We also calculate πd elastic scattering observables when our equations are coupled to the NN channel, which we do in order to include the diagram described by Jennings [42]. This diagram is shown in Figure 1.6. It was suggested by Jennings that the inclusion of this diagram was necessary for an accurate description of the T_{20} polarisation observable in πd elastic scattering. We find that the equations coupled to NN have much greater numerical instability than the equations coupled

to P_{33} and much more spline knots would be required to obtain adequate convergence of the equations coupled to NN . Though there tends to be a greater difference between the 3-dimensional and 4-dimensional πd observables when we coupled to NN , so this is a good indication that the nucleon dressing has some significance in the 4-dimensional equations. While our 4-dimensional results with the included Jennings diagram can slightly reproduce the T_{20} polarisation observable better than the 3-dimensional equations, the numerical instability of the 4-dimensional results prevents us from making a definitive conclusion from our calculated results.

The πNN convolution equations solve the long-standing renormalisation problem in the “Unitary $NN - \pi NN$ ” model, which we see in the calculation of the $pp \rightarrow \pi d$ differential scattering cross section. Moreover, our calculation for the 3-dimensional equations of the “Unitary $NN - \pi NN$ ” model with full coupling to other scattering channels and inclusion of many partial waves convinces us that a calculation of the 4-dimensional $pp \rightarrow \pi d$ differential cross section with full coupling would be able to reproduce the experimental cross section, in comparison to experimental data. However, the $pp \rightarrow \pi d$ polarisation observables tend not to be reproduced significantly better using the 4-dimensional πNN convolution equations. We expect this may be due to a lack of partial waves used in our calculations and the numerical instability that we have encountered due to the spline interpolation method, particularly in the second amplitude of $J^\pi = 2^+$ (a_7 amplitude of Table 6.6).

The solution to our 4-dimensional scattering equations are found using spline interpolation and one of our goals has been to determine whether a spline interpolation method is a viable numerical method for solving these equations. Ultimately, we conclude that the spline interpolation method may be a viable solution to these scattering equations, provided a large number of spline knots are used in the calculation, beyond what was possible in this investigation. We have had difficulty making definitive conclusions based on our calculated results for our 4-dimensional equations, as we are not convinced that we have obtained satisfactory numerical stability. It is also difficult to determine whether our results are converging with respect to the number of spline knots, as the splines tend to exhibit an oscillatory convergence rather than a linear convergence.

It is also uncertain whether the CK factorisation has effectively removed the singularities in the solution. If our solution were completely smooth, then we should have no issue obtaining a numerically stable solution with a relatively low number of knots. However, the lack of convergence in our 4-dimensional results leads us to believe this is not the case.

The CK factorisation relies on the idea that the singularities in the solution are the same as the singularities of the inhomogeneous term of the equation (let us call this term Z), so one should be able to eliminate the singularities in the solution by dividing the solution by Z . However, we make a remark in Chapter 4 that if we divide Z by a scalar function that possesses the same singularities as Z (which we call Z_l), the singularities are not entirely eliminated. This is why we are required to divide by Z in the CK factorisation to obtain a new inhomogeneous term that has no singularities, as the inhomogeneous term becomes 1. But in the CK factorisation, we divide the solution of the equation by Z , so the singularities in the solution cannot be fully eliminated. One can see this by simply plotting the function Z/Z_l . We can also use a simple Fredholm equation such as $f(x) = \log(x - 0.5) + \int_0^2 \log(y - 0.5)f(y)$ and plot the solution $f(x) = (0.5715 - 1.615i) + \log(x - 0.5)$ divided by the inhomogeneous term. We believe this is why we are not seeing adequate convergence of our 4-dimensional results and one still requires much more spline knots in order to obtain a numerically stable answer. Though, the “brute force” method of using many knots may achieve numerical stability, regardless of singularities in the solution. However, a tremendous amount of knots would be required to obtain numerical stability and a calculation with a tremendous amount of knots is far beyond our available computing resources. Our lack of convergence with respect to the number of knots also leads us to believe that there might be other singularities or discontinuities in the solution that are not due solely to the inhomogeneous term of our scattering equations.

Part of our goal of trying to obtain consistent dressing in our three-body πNN scattering equations is the inclusion of dressed two-body inputs for πN and NN . We calculate the dressed πN inputs using the Dyson-Schwinger equations and develop the numerical procedure to calculate these inputs. To construct NN input that incorporates dressed nucleons, we should take an accurate NN potential from the literature and perform a separable approximation to obtain dressed NN input. However, as all accurate NN potentials in the literature are constructed using undressed nucleon propagators, there is no viable method for creating a realistic separable NN potential that incorporates nucleon dressing. As a result, we use undressed NN input in the calculations of our 4-dimensional πNN convolution equations.

The inclusion of Dyson-dressed inputs drastically increases the computational time of the calculations, in addition to the already computationally intense process of solving 4-dimensional equations. For this reason, and due to the lack of a realistic separable NN

potential that incorporates nucleon dressing as described above, we only include Dyson-dressed inputs in calculations of 4-dimensional NN scattering. For calculations of πd elastic scattering and $pp \rightarrow \pi d$ scattering, we use undressed two-body inputs for both πN and NN . We suspect that the Dyson-dressed πN inputs should have a minimal effect on these results as we have compared calculations of NN elastic scattering with Dyson-dressed inputs and with undressed input, finding no significant difference between the two results. So, even though we demonstrate the importance of nucleon dressing in our two-body inputs and provide a theoretically complete and consistent model that includes all dressing contributions, there should be a minimal difference to using dressed or non-dressed two-body input in πNN equations. Though, further investigations into the inclusion of dressed two-body inputs in the πNN convolution equations should be explored, including the effect of including Dyson-dressed πN inputs in calculations of πd elastic scattering and $pp \rightarrow \pi d$ scattering.

The only approximation used in the derivation of the πNN convolution equations is the neglect of connected three-body forces (connected $\pi NN \rightarrow \pi NN$ irreducible diagrams). We investigate the validity of this approximation by calculating the NN one-pion and two-pion exchange amplitudes as formulated in the πNN convolution equations and compare these amplitudes to the NN one-pion and two-pion exchange amplitudes that can be calculated with all contributions using TOPT. We find that the effect of connected three-body forces on the NN one-pion exchange amplitudes to be minimal, with graphs of the amplitude with and without connected three-body forces essentially overlapping one another. The NN two-pion exchange amplitude has a more noticeable difference when we compare the amplitudes with and without connected three-body forces, however, the difference is still minimal and deviation only occurs at high energies, above the energies we use in the calculation of our three-body equations. Therefore, we expect that the neglect of connected three-body forces to have a minimal contribution to the πNN convolution equations.

Further work

As pointed out by Sauer et al. [38], any attempt to describe the many-nucleon problem in terms of interactions mediated by pions, while truncating the Hilbert space to states of at most one pion, will encounter a renormalisation problem whose severity grows exponentially with A , the number of nucleons. Such a problem is encountered, for example, in the formulation of the coupled $NNN - \pi NNN$ system by Canton and Cattapan [200]. The convolution approach developed in this thesis could be extended to overcome the renormal-

isation problem in Canton and Cattapan [200] where $A = 3$, and possibly to any value of A .

Afnan and Blankleider [201] have also derived a set of Faddeev-type equations, referred to as the $BB - \pi BB$ equations, allowing a generalisation of the previous “Unitary $NN - \pi NN$ ” model to include excited baryon states. The authors allow the nucleon and Δ particles to be treated on an equal footing, while also including the contribution of “backward going mesons,” which was also thought to be a possible mechanism, whose neglect is responsible for the small cross section in the $pp \rightarrow \pi^+ d$ reaction in the “Unitary $NN - \pi NN$ ” model. However, the renormalisation problem was seen to have a bigger effect in the $BB - \pi BB$ equations than it did on the $NN - \pi NN$ equations [31]. Convolution equations describing a πBB system would be a logical extension and could be used, for example, to investigate the possible formation of di-baryons [145]. As suggested by Wessler et al. [202] it may also be important to include heavy meson exchange.

One of the main issues with our numerical results from the 4-dimensional πNN convolution equations is that we are not convinced we have obtained numerically stable results with respect to the spline knots. With the ever increasing power of computers, it should, with time, be possible to calculate our equations with more spline knots to see if one can obtain results that are more numerically stable. One should calculate our equations with increasing intervals of spline knots, as this will give a good indication of whether the results are converging and one can determine the minimum number of knots needed for adequate convergence. One should also perform the calculations with more coupled channels. It may be possible that the effect of dressing is more prevalent in channels other than the $N\Delta$ (as we have seen when we coupled our πd equations to the NN channel), so one might see a more noticeable contribution to the scattering observables. From our calculations of the 3-dimensional scattering equations with full coupling to other channels, we do not expect that the 4-dimensional equations with full coupling would significantly change the scattering observable (particularly for πd elastic scattering), but it is difficult to know the full effect of dressing until a full calculation is performed. These suggestions rely on having sufficient computational power, which we have lacked during this investigation and has prevented this further work.

Despite the benefits and intellectual interest in solving 4-dimensional scattering equations, one should investigate the possibility of solving the 3-dimensional versions of the πNN convolution equations in Equation 3.123 as it may be possible to use contour rotation

rather than spline interpolation to solve the 3-dimensional equations. As done by Blankleider et al. [203], one can calculate the convolution integral in the amplitudes w_α using the dispersion relation of $g(E)$, then calculate the omega integral using Gaussian quadrature points. Using quadrature points and applying a separable approximation of the two-body input discretises the equations and allows the equations to be solved by matrix inversion. We have attempted to solve the 3-dimensional πNN convolution equations using this method, however the main issue is that Blankleider et al. [203] have a pure three-body problem and thus, only have disconnected Faddeev-like $\pi NN \rightarrow \pi NN$ amplitudes w_1 , w_2 and w_3 , which represent the interaction between two particles while the other spectates. In our work, we include $\pi NN \rightarrow \pi NN$ amplitudes w_4 and w_5 , which involve disconnected pair-like interactions, and therefore, are not of the same form as w_1 , w_2 , w_3 . Thus, it is not clear whether this approach of Blankleider et al. [203] can be applied to our equations and we would need to determine a method that incorporates the $\pi NN \rightarrow \pi NN$ amplitudes w_4 and w_5 .

It may be worth investigating the other forms of spline interpolation that could be applied to our equations and hopefully provide greater numerical stability. We have noted in the main text about the use of Chebyshev polynomials, which seem to have a very good reputation for fast convergence. These polynomials are easy to implement and should be a less intensive computational task. It was noted that the problem with using these polynomials is that they cannot be used for disconnected kernels, which we have in our equations due to the presence of singularities in the kernel. This is not a definite property of Chebyshev polynomial, merely an observation, and the more concerning issue would be that the Chebyshev polynomials oscillate highly as the order of the polynomial increases. This would make it much more difficult to evaluate the integrals as the order of the Chebyshev polynomials increase but could be overcome by using quadrature points for oscillatory integrals such as Filon-Clenshaw-Curtis quadratures [204].

The spline interpolation method has proved to be quite an intense computational task, without the guarantee of numerical stability. Therefore, it would be worth exploring more viable methods to solve our 4-dimensional scattering equations, especially if we want to include more coupled channels and partial waves. A possible method that has already been discussed is Wick rotation, which we use to calculate our NN scattering equation with Dyson-dressed inputs. This was possible as the method is described in detail by Levine et al. [54], however it is not clear how to use Wick rotation for our other scattering processes and coupled channels. In particular, it is unknown how to handle the nucleon pole crossing

the imaginary z axis for processes other than NN , as this is handled by an innovative factorisation method that is suitable only for the case of equal mass scattering.

On top of an investigation into better choices for spline functions, one could also investigate an alternative method to the CK factorisation to eliminate the singularities in the solution of our scattering equations, as the CK factorisation is not completely effective at eliminating the singularities in the solution. This would allow for better convergence of the amplitudes with respect to the spline knots, as the solution will be smooth.

References

-
- [1] L. D. Faddeev, Sov. Phys. JEPT **12**, 1014 (1961).
- [2] D. J. Gross and F. Wilczek, Phys. Rev. Lett. **30**, 1343 (1973).
- [3] H. D. Politzer, Phys. Rev. Lett. **30**, 1346 (1973).
- [4] G. Munster and M. Walzl, in *Zuoos Summer School on Phenomenology of Gauge Interactions* (2000) arXiv:hep-lat/0012005 .
- [5] A. Deur, S. J. Brodsky, and G. F. de Teramond, Nucl. Phys. **90**, 1 (2016), arXiv:1604.08082 [hep-ph] .
- [6] M. Luscher, Annales Henri Poincare **4**, S197 (2003), arXiv:hep-ph/0211220 .
- [7] W. Greiner, S. Schramm, E. Stein, and D. A. Bromley, *Quantum Chromodynamics* (Springer Berlin / Heidelberg, Berlin/Heidelberg, 2007).
- [8] K. G. Wilson, Phys. Rev. D **10**, 2445 (1974).
- [9] M. Carmen Bañuls and K. Cichy, Rep. Prog. Phys. **83**, 024401 (2020).
- [10] P. N. Bogoliubov, Ann. Inst. Henri Poincare **163** (1967).
- [11] A. Chodos, R. L. Jaffe, K. Johnson, C. B. Thorn, and V. F. Weisskopf, Phys. Rev. D **9**, 3471 (1974).
- [12] A. Chodos, R. L. Jaffe, K. Johnson, and C. B. Thorn, Phys. Rev. D **10**, 2599 (1974).
- [13] A. W. Thomas, Chiral symmetry and the bag model: A new starting point for nuclear physics, in *Advances in Nuclear Physics: Volume 13*, edited by J. W. Negele and E. Vogt (Springer US, Boston, MA, 1984) pp. 1–137.
- [14] A. Chodos and C. B. Thorn, Phys. Rev. D **12**, 2733 (1975).
- [15] F. Fernández and J. Segovia, Symmetry **13**, 252 (2021).
- [16] S. Theberge, A. W. Thomas, and G. A. Miller, Phys. Rev. D **22**, 2838 (1980), [Erratum: Phys.Rev.D 23, 2106 (1981)].
- [17] S. Weinberg, Phys. Lett. B **251**, 288 (1990).
- [18] S. Weinberg, Nucl. Phys. B **363**, 3 (1991).

-
- [19] E. Epelbaum, H. W. Hammer, and U. G. Meißner, Rev. Mod. Phys. **81**, 1773 (2009), arXiv:0811.1338 [nucl-th] .
- [20] F. Myhrer and D. S. Koltun, Phys. Lett. B **46**, 322 (1973).
- [21] D. S. Koltun and F. Myhrer, Z. Phys. A **283**, 397 (1977).
- [22] A. W. Thomas, Nucl. Phys. A **258**, 417 (1976).
- [23] M. Betz and T. S. H. Lee, Phys. Rev. C **23**, 375 (1981).
- [24] T. S. H. Lee and A. Matsuyama, Phys. Rev. C **32**, 516 (1985).
- [25] T. S. H. Lee and A. Matsuyama, Phys. Rev. C **32**, 1986 (1985).
- [26] V. S. Varma, Phys. Rev. **163**, 1682 (1967).
- [27] C. Lovelace, Phys. Rev. **135**, B1225 (1964).
- [28] A. W. Thomas and I. R. Afnan, Phys. Lett. B **45**, 437 (1973).
- [29] I. R. Afnan and A. W. Thomas, Phys. Rev. C **10**, 109 (1974).
- [30] H. Garcilazo and T. Mizutani, *πNN systems* (World Scientific, Singapore, 1990).
- [31] B. Blankleider, Nucl. Phys. A **543**, 163 (1992).
- [32] A. W. Thomas, *A study of the πNN system at low energy*, Thesis (1973).
- [33] I. R. Afnan and B. Blankleider, Phys. Rev. C **22**, 1638 (1980).
- [34] A. S. Rinat, Nucl. Phys. A **287**, 399 (1977).
- [35] Y. Avishai and T. Mizutani, Nucl. Phys. A **352**, 399 (1981).
- [36] Y. Avishai and T. Mizutani, Nucl. Phys. A **326**, 352 (1979).
- [37] B. Blankleider and A. N. Kvinikhidze, in *6th International Symposium on Meson - Nucleon Physics and Structure of the Nucleon* (1995) arXiv:nucl-th/9508027 .
- [38] P. U. Sauer, M. Sawicki, and S. Furui, Prog. Theor. Phys **74**, 1290 (1985), <https://academic.oup.com/ptp/article-pdf/74/6/1290/5220322/74-6-1290.pdf> .

-
- [39] B. Blankleider and A. N. Kvinikhidze, *Few Body Syst. Suppl.* **7**, 294 (1994),
arXiv:nucl-th/9402011 .
- [40] I. R. Afnan and R. J. McLeod, *Phys. Rev. C* **31**, 1821 (1985).
- [41] B. K. Jennings, *Phys. Lett. B* **205**, 187 (1988).
- [42] B. K. Jennings and A. S. Rinat, *Nucl. Phys. A* **485**, 421 (1988).
- [43] T. Mizutani, C. Fayard, G. H. Lamot, and B. Saghai, *Phys. Rev. C* **40**, 2763 (1989).
- [44] A. T. Stelbovics and M. Stingl, *Nucl. Phys. A* **294**, 391 (1978).
- [45] M. Stingl and A. T. Stelbovics, *J. Phys. G: Nucl. Phys.* **4**, 1371 (1978).
- [46] M. Stingl and A. T. Stelbovics, *J. Phys. G: Nucl. Phys.* **4**, 1389 (1978).
- [47] I. R. Afnan and A. T. Stelbovics, *Phys. Rev. C* **23**, 1384 (1981).
- [48] A. N. Kvinikhidze and B. Blankleider, *Phys. Rev. C* **48**, 25 (1993).
- [49] A. N. Kvinikhidze and B. Blankleider, *Phys. Lett. B* **307**, 7 (1993).
- [50] E. E. Salpeter and H. A. Bethe, *Phys. Rev.* **84**, 1232 (1951).
- [51] G. C. Wick, *Phys. Rev.* **96**, 1124 (1954).
- [52] R. E. Cutkosky, *Phys. Rev.* **96**, 1135 (1954).
- [53] M. Levine, J. Tjon, and J. Wright, *Phys. Rev. Lett.* **16**, 962 (1966).
- [54] M. J. Levine, J. Wright, and J. A. Tjon, *Phys. Rev.* **154**, 1433 (1967).
- [55] J. Nuttall, *Phys. Lett.* **23**, 492 (1966).
- [56] H. M. Nieland and J. A. Tjon, *Phys. Lett. B* **27**, 309 (1968).
- [57] J. Fleischer and J. A. Tjon, *Nucl. Phys. B* **84**, 375 (1975).
- [58] J. Fleischer and J. A. Tjon, *Phys. Rev. D* **15**, 2537 (1977).
- [59] J. A. Tjon and E. E. van Faassen, *Phys. Lett. B* **120**, 39 (1983).
- [60] E. E. van Faassen and J. A. Tjon, *Phys. Rev. C* **28**, 2354 (1983).

-
- [61] E. E. van Faassen and J. A. Tjon, Phys. Rev. C **30**, 285 (1984).
- [62] E. E. van Faassen and J. A. Tjon, Phys. Rev. C **33**, 2105 (1986).
- [63] V. A. Karmanov, J. Carbonell, and M. Mangin-Brinet, Nucl. Phys. A **790**, 598c (2007), arXiv:hep-th/0610158 .
- [64] V. A. Karmanov, J. Carbonell, and M. Mangin-Brinet, Few Body Syst. **44**, 283 (2008), arXiv:0712.0971 [hep-ph] .
- [65] J. Carbonell, V. A. Karmanov, and M. Mangin-Brinet, Eur. Phys. J. A **39**, 53 (2009), arXiv:0809.3678 [hep-ph] .
- [66] J. Carbonell and V. A. Karmanov, PoS **LC2010**, 014 (2010), arXiv:1009.4522 [hep-ph] .
- [67] J. Carbonell and V. A. Karmanov, Eur. Phys. J. A **46**, 387 (2010), arXiv:1010.4640 [hep-ph] .
- [68] J. Carbonell and V. A. Karmanov, Few Body Syst. **49**, 205 (2011), arXiv:1012.0246 [hep-ph] .
- [69] J. Carbonell and V. A. Karmanov, Eur. Phys. J. A **27**, 11 (2006), arXiv:hep-th/0505262 .
- [70] V. A. Karmanov and J. Carbonell, PoS **Baldin-ISHEPP-XXI**, 027 (2012).
- [71] N. Nakanishi, Phys. Rev. **130**, 1230 (1963).
- [72] V. A. Karmanov and J. Carbonell, Few Body Syst. **54**, 1509 (2013), arXiv:1210.0925 [hep-ph] .
- [73] J. Carbonell and V. A. Karmanov, Phys. Lett. B **727**, 319 (2013).
- [74] J. Carbonell and V. A. Karmanov, Phys. Rev. D **90**, 056002 (2014).
- [75] J. Carbonell and V. A. Karmanov, EPJ Web Conf. **113**, 03012 (2016), arXiv:1605.01263 [hep-ph] .
- [76] J. Carbonell and V. A. Karmanov, Few Body Syst. **57**, 533 (2016), arXiv:1605.02807 [hep-ph] .

-
- [77] T. Frederico, G. Salmè, and M. Viviani, Phys. Rev. D **85**, 036009 (2012), arXiv:1112.5568 [hep-ph] .
- [78] T. Frederico, G. Salmè, and M. Viviani, Eur. Phys. J. C **75**, 398 (2015), arXiv:1504.01624 [hep-ph] .
- [79] A. A. Logunov and A. N. Tavkhelidze, Nuovo Cim. **29**, 380 (1963).
- [80] T. Mizutani and D. S. Koltun, Ann. Phys. **109**, 1 (1977).
- [81] B. Blankleider and I. R. Afnan, Phys. Rev. C **24**, 1572 (1981).
- [82] A. S. Rinat and Y. Starkand, Nucl. Phys. A **397**, 381 (1983).
- [83] R. J. McLeod and I. R. Afnan, Phys. Rev. C **32**, 222 (1985).
- [84] B. Blankleider, J. L. Wray, and A. N. Kvinikhidze, AIP Adv. **11**, 025204 (2021), arXiv:2010.11710 [nucl-th] .
- [85] E. O. Alt, P. Grassberger, and W. Sandhas, Nucl. Phys. B **2**, 167 (1967).
- [86] D. R. Phillips and I. R. Afnan, (1993), arXiv:nucl-th/9309020 .
- [87] M. Stingl and A. S. Rinat, Nucl. Phys. A **154**, 613 (1970).
- [88] R. J. Ord-Smith, Phys. Rev. **94**, 1227 (1954).
- [89] H. Liu, C. Elster, and W. Glöckle, Phys. Rev. C **72**, 054003 (2005).
- [90] K. Pachucki, M. Puchalski, and V. A. Yerokhin, Comput. Phys. Commun. **185**, 2913 (2014).
- [91] A. Matsuyama, Phys. Lett. B **152**, 42 (1985).
- [92] J. V. Noble, Comput. Sci. Eng. **2**, 92 (2000).
- [93] P. Kolm and V. Rokhlin, Comput. Math. App **41**, 327 (2001).
- [94] H. P. Noyes, Phys. Rev. Lett. **15**, 538 (1965).
- [95] K. L. Kowalski, Phys. Rev. Lett. **15**, 798 (1965).
- [96] A. D. Lahiff, *Covariant formulation of pion-nucleon scattering*, Thesis (1999).

-
- [97] A. D. Lahiff and I. R. Afnan, Phys. Rev. C **60**, 024608 (1999).
- [98] F. Gross, Phys. Rev. **186**, 1448 (1969).
- [99] R. Blankenbecler and R. Sugar, Phys. Rev. **142**, 1051 (1966).
- [100] D. R. Phillips and S. J. Wallace, Phys. Rev. C **54**, 507 (1996), arXiv:nucl-th/9603008 .
- [101] D. R. Phillips, in *Workshop on Electron Nucleus Scattering* (1998) arXiv:nucl-th/9811007 .
- [102] D. R. Phillips, S. J. Wallace, and N. K. Devine, (1999), arXiv:nucl-th/9906086 .
- [103] D. R. Phillips, S. J. Wallace, and N. K. Devine, Phys. Rev. C **72**, 014006 (2005), arXiv:nucl-th/0411092 .
- [104] A. N. Kvinikhidze and B. Blankleider, Phys. Rev. D **68**, 025021 (2003), arXiv:hep-th/0303038 .
- [105] A. N. Kvinikhidze and B. Blankleider, Phys. Rev. C **72**, 054001 (2005), arXiv:nucl-th/0502084 .
- [106] A. N. Kvinikhidze, B. Blankleider, E. Epelbaum, C. Hanhart, and M. P. Valderrama, Phys. Rev. C **80**, 044004 (2009), arXiv:0904.4128 [nucl-th] .
- [107] A. Matsuyama, T. Sato, and T. S. H. Lee, Phys. Rept. **439**, 193 (2007), arXiv:nucl-th/0608051 .
- [108] N. M. Larson and J. H. Hetherington, Phys. Rev. C **9**, 699 (1974).
- [109] A. Deltuva, K. Chmielewski, and P. U. Sauer, Phys. Rev. C **67**, 034001 (2003).
- [110] J. P. Boyd, *Chebyshev and Fourier Spectral Methods* (2000).
- [111] Y. Liu, Math. Com. Mod. **50**, 465 (2009).
- [112] A. Alaylioglu, D. Eyre, M. Brannigan, and J. P. Svenne, J. Comput. Phys. **62**, 383 (1986).
- [113] A. J. Huizing and B. L. G. Bakker, J. Comput. Phys. **90**, 200 (1990).

-
- [114] W. Glöckle, G. Hasberg, and A. R. Neghabian, *Z. Phys. A* **305**, 217 (1982).
- [115] D. Huber, H. Witala, A. Nogga, W. Gloeckle, and H. Kamada, *Few Body Syst.* **22**, 107 (1997), arXiv:nucl-th/9611021 .
- [116] J. Carbonell and V. A. Karmanov, *Few-Body Syst.* **57**, 533 (2016).
- [117] G. L. Payne, in *Models and Methods in Few-Body Physics*, edited by L. S. Ferreira, A. C. Fonseca, and L. Streit (Springer Berlin Heidelberg) pp. 64–99.
- [118] R. Machleidt, K. Holinde, and C. Elster, *Phys. Rep.* **149**, 1 (1987).
- [119] R. Machleidt, *Phys. Rev. C* **63**, 024001 (2001), arXiv:nucl-th/0006014 .
- [120] R. B. Wiringa, R. A. Smith, and T. L. Ainsworth, *Phys. Rev. C* **29**, 1207 (1984).
- [121] R. B. Wiringa, V. G. J. Stoks, and R. Schiavilla, *Phys. Rev. C* **51**, 38 (1995), arXiv:nucl-th/9408016 .
- [122] V. G. J. Stoks, R. A. M. Klomp, M. C. M. Rentmeester, and J. J. de Swart, *Phys. Rev. C* **48**, 792 (1993).
- [123] V. G. J. Stoks, R. A. M. Klomp, C. P. F. Terheggen, and J. J. de Swart, *Phys. Rev. C* **49**, 2950 (1994), arXiv:nucl-th/9406039 .
- [124] W. N. Cottingham, M. Lacombe, B. Loiseau, J. M. Richard, and R. V. Mau, *Phys. Rev. D* **8**, 800 (1973).
- [125] M. Lacombe, B. Loiseau, J. M. Richard, R. V. Mau, J. Côté, P. Pirès, and R. de Tournell, *Phys. Rev. C* **21**, 861 (1980).
- [126] R. V. Reid, *Ann. Phys.* **50**, 411 (1968).
- [127] J. Haidenbauer and W. Plessas, *Phys. Rev. C* **30**, 1822 (1984).
- [128] J. Haidenbauer and W. Plessas, *Phys. Rev. C* **32**, 1424 (1985).
- [129] J. Haidenbauer, Y. Koike, and W. Plessas, *Phys. Rev. C* **33**, 439 (1986).
- [130] M. Baldo, L. S. Ferreira, L. Streit, and T. Vertse, *Phys. Rev. C* **33**, 1587 (1986).
- [131] M. Baldo and L. S. Ferreira, *Phys. Rev. C* **41**, 2298 (1990).

-
- [132] D. R. Entem, F. Fernandez, and A. Valcarce, *J. Phys. G* **27**, 1537 (2001).
- [133] S. C. Bhatt, J. S. Levinger, and E. Harms, *Phys. Lett. B* **40**, 23 (1972).
- [134] T. R. Mongan, *Phys. Rev.* **175**, 1260 (1968).
- [135] T. R. Mongan, *Phys. Rev.* **178**, 1597 (1969).
- [136] T. Mizutani, C. Fayard, G. H. Lamot, and R. S. Nahabetian, *Phys. Rev. C* **24**, 2633 (1981).
- [137] M. G. Piepho and G. E. Walker, *Phys. Rev. C* **9**, 1352 (1974).
- [138] W. R. Gibbs, A. T. Hess, and W. B. Kaufmann, *Phys. Rev. C* **13**, 1982 (1976).
- [139] H. Garcilazo, *Phys. Rev. C* **21**, 2094 (1980).
- [140] F. Di Marzio and K. Amos, *Phys. Rev. C* **31**, 561 (1985), [Erratum: *Phys.Rev.C* **32**, 1106–1106 (1985)].
- [141] T. Y. Saito and I. R. Afnan, *Phys. Rev. C* **50**, 2756 (1994), arXiv:nucl-th/9308011 .
- [142] T. Y. Saito and I. R. Afnan, *Few Body Syst.* **18**, 101 (1995), arXiv:nucl-th/9412004 .
- [143] S. Nozawa, B. Blankleider, and T. S. H. Lee, *Nucl. Phys. A* **513**, 459 (1990).
- [144] E. M. Darwish and R. S. Alamry, *J. Taibah Univ. Sci.* **4**, 46 (2010).
- [145] A. Gal and H. Garcilazo, *Phys. Rev. Lett.* **111**, 172301 (2013), arXiv:1308.2112 [nucl-th] .
- [146] A. Gal and H. Garcilazo, *Nucl. Phys. A* **928**, 73 (2014), arXiv:1402.3171 [nucl-th] .
- [147] J. Frohlich, K. Schwarz, and H. F. K. Zingl, *Phys. Rev. C* **27**, 265 (1983).
- [148] J. Frohlich, K. Schwarz, L. Streit, and H. F. K. Zingl, *Phys. Rev. C* **25**, 2591 (1982).
- [149] H. Garcilazo and L. Mathelitsch, *Phys. Lett. B* **205**, 199 (1988).
- [150] L. Mathelitsch and H. Garcilazo, *Phys. Rev. C* **32**, 1635 (1985).
- [151] D. J. Ernst, C. M. Shakin, and R. M. Thaler, *Phys. Rev. C* **10**, 2176 (1974).
- [152] S. K. Adhikari, *Phys. Rev. C* **10**, 1623 (1974).

-
- [153] D. J. Ernst, C. M. Shakin, R. M. Thaler, and D. L. Weiss, *Phys. Rev. C* **8**, 2056 (1973).
- [154] R. J. McLeod and D. J. Ernst, *Phys. Rev. C* **18**, 1060 (1978).
- [155] S. K. Adhikari and I. H. Sloan, *Phys. Rev. C* **11**, 1133 (1975).
- [156] S. C. Pieper, *Phys. Rev. C* **9**, 883 (1974).
- [157] D. J. Ernst, C. M. Shakin, and R. M. Thaler, *Phys. Rev. C* **8**, 46 (1973).
- [158] D. J. Ernst and R. J. McLeod, *AIP Conf. Proc.* **54**, 71 (1979).
- [159] R. J. McLeod, *Phys. Rev. C* **29**, 1098 (1984).
- [160] R. L. Workman, M. W. Paris, W. J. Briscoe, and I. I. Strakovsky, *Phys. Rev. C* **86**, 015202 (2012).
- [161] T. D. Cohen, *Phys. Rev. D* **34**, 2187 (1986).
- [162] F. Gross and Y. Surya, *Phys. Rev. C* **47**, 703 (1993).
- [163] C. Schütz, J. W. Durso, K. Holinde, and J. Speth, *Phys. Rev. C* **49**, 2671 (1994).
- [164] T. Sato and T. S. H. Lee, *Phys. Rev. C* **54**, 2660 (1996).
- [165] R. Böckmann, C. Hanhart, O. Krehl, S. Krewald, and J. Speth, *Phys. Rev. C* **60**, 055212 (1999).
- [166] V. Pascalutsa and J. A. Tjon, *Phys. Rev. C* **61**, 054003 (2000).
- [167] I. R. Afnan and A. D. Lahiff, *Eur. Phys. J. A* **18**, 301 (2003).
- [168] M. Oettel and A. W. Thomas, *Phys. Rev. C* **66**, 065207 (2002).
- [169] H. Kamano, S. X. Nakamura, T. S. H. Lee, and T. Sato, *Phys. Rev. C* **88**, 035209 (2013).
- [170] D. Rönchen, M. Döring, F. Huang, H. Haberzettl, J. Haidenbauer, C. Hanhart, S. Krewald, U. G. Meißner, and K. Nakayama, *Eur. Phys. J. A* **49**, 44 (2013).
- [171] T. Skawronski, B. Blankleider, and A. N. Kvinikhidze, *Phys. Rev. C* **99**, 034001 (2019).

- [172] T. Meissner, Phys. Rev. C **52**, 3386 (1995).
- [173] J. Carbonell, private communication.
- [174] H. P. Stapp, T. J. Ypsilantis, and N. Metropolis, Phys. Rev. **105**, 302 (1957).
- [175] R. L. Workman, W. J. Briscoe, and I. I. Strakovsky, Phys. Rev. C **94**, 065203 (2016), arXiv:1609.01741 [nucl-th] .
- [176] SAID database, <https://gwdac.phys.gwu.edu/>.
- [177] B. Blankleider and I. R. Afnan, Phys. Rev. C **31**, 1380 (1985).
- [178] B. Blankleider, *A unitary approach to the coupling between the NN and πNN channels*, Thesis (1980).
- [179] U. G. Meißner, U. Raha, and A. Rusetsky, Phys. Lett. B **639**, 478 (2006).
- [180] U. G. Meißner, U. Raha, and A. Rusetsky, Eur. Phys. J. C **45**, 545 (2006).
- [181] S. R. Beane, V. Bernard, E. Epelbaum, U.-G. Meißner, and D. R. Phillips, Nucl. Phys. A **720**, 399 (2003).
- [182] D. Gotta, F. Amaro, D. Anagnostopoulos, A. Buhler, D. Covita, H. Gorke, A. Gruber, M. Hennebach, A. Hirtl, P. Indelicato, T. Ishiwatari, E.-O. Le Bigot, J. Marton, M. Nikipelov, J. dos Santos, S. Schlessler, P. Schmid, L. Simons, T. Strauch, M. Trassinelli, J. Veloso, and J. Zmeskal, Phys. Proc. **17**, 69 (2011).
- [183] T. Strauch, F. D. Amaro, D. F. Anagnostopoulos, P. Bühler, D. S. Covita, H. Gorke, D. Gotta, A. Gruber, A. Hirtl, P. Indelicato, E. O. Le Bigot, M. Nikipelov, J. M. F. dos Santos, P. Schmid, S. Schlessler, L. M. Simons, M. Trassinelli, J. F. C. A. Veloso, and J. Zmeskal, Eur. Phys. J. A **47**, 88 (2011).
- [184] S. Weinberg, Trans. New York Acad. Sci. **38**, 185 (1977).
- [185] P. Hauser, K. Kirch, L. M. Simons, G. Borchert, D. Gotta, T. Siems, P. El-Khoury, P. Indelicato, M. Augsburger, D. Chatellard, J. P. Egger, and D. F. Anagnostopoulos, Phys. Rev. C **58**, R1869 (1998).
- [186] M. Carley, SIAM J. Sci. Comput. **29**, 1207 (2007).

- [187] K. Gabathuler, J. Domingo, P. Gram, W. Hirt, G. Jones, P. Schwaller, J. Zichy, J. Bolger, Q. Ingram, J. P. Albanese, and J. Arvieux, *Nucl. Phys. A* **350**, 253 (1980).
- [188] E. Pedroni, K. Gabathuler, J. J. Domingo, W. Hirt, P. Schwaller, J. Arvieux, C. H. Q. Ingram, P. Gretillat, J. Piffaretti, N. W. Tanner, and C. Wilkin, *Nucl. Phys. A* **300**, 321 (1978).
- [189] K. Kubodera, M. P. Locher, F. Myhrer, and A. W. Thomas, *J. Phys. G: Nucl. Phys.* **6**, 171 (1980).
- [190] C. R. Ottermann, E. T. Boschitz, H. Garcilazo, W. Gyles, W. List, R. Tacik, M. Wessler, S. Mango, B. van den Brandt, J. A. Konter, and E. L. Mathie, *Phys. Rev. C* **38**, 2310 (1988).
- [191] W. Grein and M. P. Locher, *J. Phys. G: Nucl. Phys.* **7**, 1355 (1981).
- [192] G. R. Smith, D. R. Gill, D. Healey, D. Ottewell, G. D. Wait, P. Walden, R. R. Johnson, G. Jones, R. Olszewski, F. M. Rozon, R. Rui, M. E. Sevier, R. P. Trelle, E. L. Mathie, G. Lolos, S. I. H. Naqvi, V. Pafilis, N. R. Stevenson, R. B. Schubank, W. Gyles, C. R. Ottermann, and G. S. Kyle, *Phys. Rev. C* **38**, 251 (1988).
- [193] G. Suft, W. Kretschmer, E. Boschitz, R. Meier, B. Brinkmüller, B. van Den Brandt, P. Hautle, J. A. Konter, S. Mango, L. Mathelitsch, H. Garcilazo, and W. Gruebler, *Phys. Rev. C* **66**, 034003 (2002).
- [194] N. R. Stevenson, Y. M. Shin, K. Itoh, G. Retzlaff, D. R. Gill, D. F. Ottewell, G. D. Wait, T. E. Drake, D. Frekers, R. B. Schubank, and G. J. Lolos, *Phys. Rev. C* **39**, 1488 (1989).
- [195] J. Hoftiezer, C. Weddigen, P. Chatelain, B. Favier, F. Foroughi, C. Nussbaum, J. Piffaretti, S. Jaccard, and P. Walden, *Nucl. Phys. A* **402**, 429 (1983).
- [196] J. Hoftiezer, C. Weddigen, P. Chatelain, B. Favier, F. Foroughi, J. Piffaretti, S. Jaccard, and P. Walden, *Nucl. Phys. A* **412**, 286 (1984).
- [197] E. Aprile-Giboni, J. Bystricky, J. Deregél, P. H. Drompt, C. Eisenegger, J. M. Fontaine, E. Heer, R. Hess, S. Jaccard, F. Lehar, W. R. Leo, S. Mango, S. Morenzoni, Y. Onel, F. Perrot, D. Rapin, J. Vrzal, and J. Yonnet, *Nucl. Phys. A* **431**, 637 (1984).

-
- [198] E. Aprile-Giboni, G. Cantale, E. Heer, R. Hess, C. Lechanoine-Leluc, W. R. Leo, Y. Onel, and D. Rapin, Nucl. Phys. A **415**, 391 (1984).
- [199] J. Hoftiezer, G. S. Mutchler, C. Weddigen, J. A. Konter, S. Mango, A. Berdoz, B. Favier, and F. Foroughi, Nucl. Phys. A **412**, 273 (1984).
- [200] L. Canton and G. Cattapan, Phys. Rev. C **50**, 2761 (1994), arXiv:nucl-th/9312016 .
- [201] I. R. Afnan and B. Blankleider, Phys. Rev. C **32**, 2006 (1985).
- [202] M. Wessler, E. Boschitz, B. Brinkmüller, J. Bühler, H. Garcilazo, W. Gyles, W. List, R. Meier, S. Ritt, R. Tacik, J. A. Konter, D. Gill, S. Mango, D. Renker, B. van den Brandt, G. Wait, V. A. Efimovych, A. I. Kovalev, A. N. Prokofiev, W. Thiel, and B. Blankleider, Phys. Rev. C **51**, 2575 (1995).
- [203] B. Blankleider, S. S. Kumar, and A. N. Kvinikhidze, (2020), arXiv:2001.04401 [nucl-th] .
- [204] V. Domínguez, J. Comput. Appl. Math. **261**, 299 (2014).
- [205] N. Clisby, *The Dressed One and Two Pion Exchange NN Potentials*, Thesis (1997).
- [206] I. R. Afnan and B. F. Gibson, Few-Body Syst. **54**, 2303 (2013).
- [207] D. R. Phillips, *The coupled-channels problem in field theory: the NN – π NN system*, Thesis (1995).

Chapter A

Pion-nucleon theory

A.1 Pion-nucleon model

The pion-nucleon model we consider involves only pion and nucleon degrees of freedom, and is defined by the Hamiltonian

$$H = H_0 + H_I = H_0^N + H_0^\pi + H_I \quad (\text{A.1})$$

where

$$H_0^N = \int (E_p + m_0) a_N^\dagger(\mathbf{p}) a_N(\mathbf{p}) d\mathbf{p} \quad (\text{A.2})$$

$$H_0^\pi = \int \omega_k a_\pi^\dagger(\mathbf{k}) a_\pi(\mathbf{k}) d\mathbf{k} \quad (\text{A.3})$$

$$H_I = \int J_N(\mathbf{k}) a_\pi^\dagger(\mathbf{k}) d\mathbf{k} + \int J_N^\dagger(\mathbf{k}) a_\pi(\mathbf{k}) d\mathbf{k} \quad (\text{A.4})$$

$$J_N(\mathbf{k}) = \int \delta(\mathbf{p} + \mathbf{k} - \mathbf{p}') \frac{1}{\sqrt{\omega_k}} F_0(\mathbf{p}, \mathbf{p}') a_N^\dagger(\mathbf{p}) a_N(\mathbf{p}') d\mathbf{p} d\mathbf{p}' \quad (\text{A.5})$$

where the a^\dagger and a states are creation and destruction operators act upon a Hilbert space of multi-pion and nucleon states; in particular,

$$|\mathbf{p}\rangle \equiv a_N^\dagger(\mathbf{p})|0\rangle, \quad |\mathbf{k}\rangle \equiv a_\pi^\dagger(\mathbf{k})|0\rangle \quad (\text{A.6})$$

represent states of a bare nucleon of momentum \mathbf{p} and a pion of momentum \mathbf{k} . Note that the bare and dressed vacua are identical in this model. We use semi-relativistic kinematics, non-relativistic kinematics for the nucleons and relativistic kinematics for the pion. So that

$$E_p = \frac{\mathbf{p}^2}{2m}, \quad \omega_k = (\mathbf{k}^2 + m_\pi^2)^{1/2} \quad (\text{A.7})$$

We note the commutation relations

$$[a_\pi(\mathbf{k}), a_\pi^\dagger(\mathbf{k}')] = \delta(\mathbf{k} - \mathbf{k}') \quad (\text{A.8})$$

$$[a_\pi(\mathbf{k}), a_\pi(\mathbf{k}')] = 0 \quad (\text{A.9})$$

$$\{a_N(\mathbf{p}), a_N^\dagger(\mathbf{p}')\} = \delta(\mathbf{p} - \mathbf{p}') \quad (\text{A.10})$$

$$\{a_N(\mathbf{p}), a_N(\mathbf{p}')\} = 0 \quad (\text{A.11})$$

With these commutator relations, we find that H_0^N acting on a nucleon state with momentum \mathbf{p}

$$\begin{aligned} H_0^N |\mathbf{p}\rangle &\equiv \int d\mathbf{p}' (E_{p'} + m_0) a_N^\dagger(\mathbf{p}') a_N(\mathbf{p}') a_N^\dagger(\mathbf{p}) |0\rangle \\ &= \int d\mathbf{p}' (E_{p'} + m_0) a_N^\dagger(\mathbf{p}') \{a_N(\mathbf{p}') a_N^\dagger(\mathbf{p})\} |0\rangle \\ &= (E_p + m_0) |\mathbf{p}\rangle \end{aligned} \quad (\text{A.12})$$

as expected. Using these commutator relations, we can also find new commutator relations, which become useful later on.

$$[a_\pi(\mathbf{k}), H_0^\pi] = \int \omega'_k [a_\pi(\mathbf{k}), a_\pi^\dagger(\mathbf{k}')] a_\pi(\mathbf{k}') d\mathbf{k}' = \omega_k a_\pi(\mathbf{k}) \quad (\text{A.13})$$

Likewise

$$\begin{aligned} [a_\pi^\dagger(\mathbf{k}), H_0^\pi] &= \int \omega_{k'} [a_\pi^\dagger(\mathbf{k}), a_\pi^\dagger(\mathbf{k}') a_\pi(\mathbf{k}')] d\mathbf{k}' \\ &= \int \omega_{k'} ([a_\pi^\dagger(\mathbf{k}), a_\pi^\dagger(\mathbf{k}')] a_\pi(\mathbf{k}') + a_\pi^\dagger(\mathbf{k}') [a_\pi^\dagger(\mathbf{k}), a_\pi(\mathbf{k}')]) d\mathbf{k}' \\ &= \int \omega_{k'} a_\pi^\dagger(\mathbf{k}') [a_\pi^\dagger(\mathbf{k}), a_\pi(\mathbf{k}')] d\mathbf{k}' \\ &= - \int \omega_{k'} a_\pi^\dagger(\mathbf{k}') [a_\pi(\mathbf{k}'), a_\pi^\dagger(\mathbf{k})] d\mathbf{k}' \\ &= -\omega_k a_\pi^\dagger(\mathbf{k}) \end{aligned} \quad (\text{A.14})$$

Therefore, we obtain the commutator relation

$$[a_\pi^\dagger(\mathbf{k}), H_0^\pi] = -\omega_k a_\pi^\dagger(\mathbf{k}) \quad (\text{A.15})$$

Similarly,

$$\begin{aligned} [a_\pi(\mathbf{k}), H_I^\pi] &= \int J_N(\mathbf{k}') [a_\pi(\mathbf{k}), a_\pi^\dagger(\mathbf{k}')] d\mathbf{k}' + \int J_N^\dagger(\mathbf{k}') [a_\pi^\dagger(\mathbf{k}), a_\pi^\dagger(\mathbf{k}')] d\mathbf{k}' \\ &= \int J_N(\mathbf{k}') \delta(\mathbf{k} - \mathbf{k}') d\mathbf{k}' = J_N(\mathbf{k}) \end{aligned} \quad (\text{A.16})$$

We can do this as a_N, a_N^\dagger and a_π, a_π^\dagger act on different Hilbert spaces, so they commute. Therefore, we have

$$[a_\pi(\mathbf{k}), H_I^\pi] = J_N(\mathbf{k}) \quad (\text{A.17})$$

A.2 The πN t -matrix

Consider the system of one nucleon and one pion. The πN t -matrix is the connected part of the full πN Green's function

$$\langle \mathbf{k}', \mathbf{p}' | t_{\pi N}(E) | \mathbf{k}, \mathbf{p} \rangle = \langle \mathbf{k}', \mathbf{p}' | \frac{1}{E^+ - H} | \mathbf{k}, \mathbf{p} \rangle_c \quad (\text{A.18})$$

where the disconnected part of the full t -matrix is equal to the dressed pion-nucleon propagator

$$\langle \mathbf{k}', \mathbf{p}' | g_{\pi N}(E) | \mathbf{k}, \mathbf{p} \rangle = \langle \mathbf{k}', \mathbf{p}' | \frac{1}{E^+ - H} | \mathbf{k}, \mathbf{p} \rangle_d \quad (\text{A.19})$$

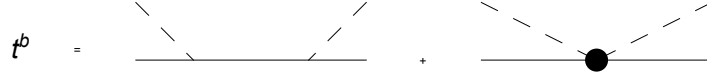


Figure A.1: The πN t represented diagrammatically as its pole and non-pole parts.

The full πN t -matrix can be written in terms of nucleon pole and non-pole parts, shown diagrammatically as

which corresponds to the equation

$$t_{\pi N}(E) = f(E)g(E)\bar{f}(E) + t^b(E) \quad (\text{A.20})$$

where $t^b(E)$ is the background term, given in terms of the integral equation:

$$t^b(E) = v^b(E) + v^b(E)g_{\pi N}(E)t^b(E) \quad (\text{A.21})$$

where $v^b(E)$ represents the sum of all one-particle irreducible graphs for πN scattering and $g_{\pi N}(E)$ is the fully dressed pion-nucleon propagator.

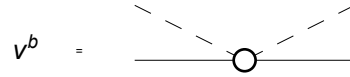


Figure A.2: Diagram for v^b representing the sum of all one-particle irreducible πN graphs.

A.3 The dressed pion-nucleon vertex

The dressed pion-nucleon vertex is given diagrammatically below and a perturbation expansion, beginning with the bare vertex f_0

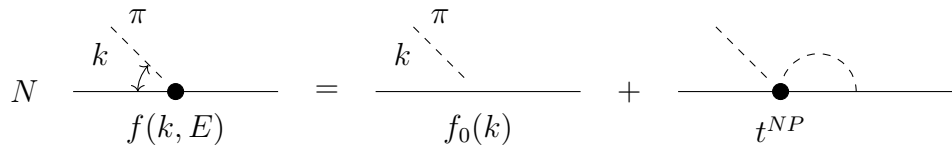


Figure A.3: Diagram representation of the dressed vertex function $f(k, E)$, shown as a finite sum of Figure

With all the propagators, we can see that

$$g_{\pi N}fg = g_{\pi N}f_0g + g_{\pi N}v^bg_{\pi N}f_0g + g_{\pi N}v^bg_{\pi N}v^bg_{\pi N}f_0g + \dots \quad (\text{A.22})$$

and with the final/initial propagators removed

$$f = f_0 + v^b g_{\pi N} f_0 + v^b g_{\pi N} v^b g_{\pi N} f_0 + \dots \quad (\text{A.23})$$

and since we know that the background term t^b is given by

$$t^b(E) = v^b(E) + v^b(E)g_{\pi N}(E)v^b(E) + v^b(E)g_{\pi N}(E)v^b(E)g_{\pi N}v^b(E) + \dots \quad (\text{A.24})$$

we can express the dressed pion-nucleon vertex as

$$f(k, E) = f_0(k) + t^b(E)g_{\pi N}f_0(k) \quad (\text{A.25})$$

where k is the momentum of the pion.

Now, the dressing amplitude is given diagrammatically by

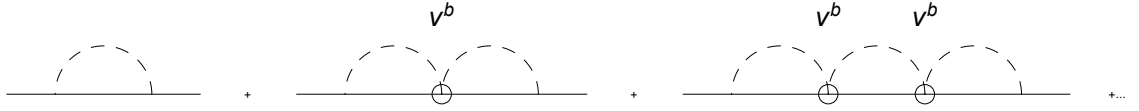


Figure A.4: Iteration of v^b .

But, if a cut is made in the middle of the first bubble of each diagram, one obtains

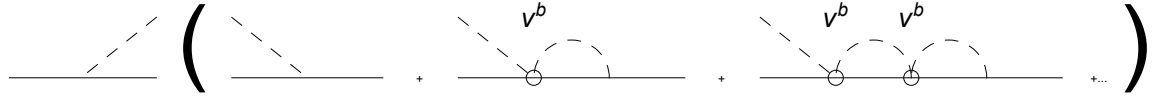


Figure A.5: Diagram showing how a cut in the bubble of the iterated v^b can lead to factorising a f_0 term.

where the first diagram corresponds to the bare pion-nucleon vertex f_0 (technically \bar{f}_0 , but this is equal to f_0) and the bracketed terms correspond to the dressed vertex f . So this becomes

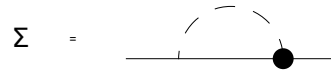


Figure A.6: Diagrammatic representation of the dressing amplitude $\Sigma(E)$.

which is given by the matrix element

$$\Sigma(E) = \langle f_0 | g_{\pi N}(E) | f(E) \rangle \quad (\text{A.26})$$

Chapter B

Theory of one nucleon

B.1 The dressed one-nucleon propagator

With this model defined, we can define the undressed and dressed one-nucleon propagators such that

$$\delta(\mathbf{p} - \mathbf{p}')g_0(E, \mathbf{p}) = \langle \mathbf{p}' | \frac{1}{E^+ - H_0} | \mathbf{p} \rangle \quad (\text{B.1})$$

$$\delta(\mathbf{p} - \mathbf{p}')g(E, \mathbf{p}) = \langle \mathbf{p}' | \frac{1}{E^+ - H} | \mathbf{p} \rangle \quad (\text{B.2})$$

where, as we have just shown, the bra and ket nucleon states are eigenstates of H_0 . Note that, H_0 contains the Hamiltonian for both nucleon and pion. However, after during a perturbation theory expanding about H_0^π , all terms with this Hamiltonian would be equal to zero as it would be acting on a nucleon state.

After perturbation theory, the dressed one-nucleon propagator is given as the following iteration

$$g(E) = g_0(E) + g_0(E)\Sigma(E)g(E) \quad (\text{B.3})$$

where $\Sigma(E)$ is the dressing amplitude. This equation is given diagrammatically as This

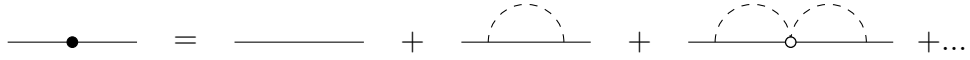


Figure B.1: The dressing of a single nucleon, shown as a perturbation expansion of diagrams, where the dashed lines represent the propagation of pions and the solid lines represent the propagation of the nucleon.

equation can be rearranged to give

$$g(E)^{-1} = g_0(E)^{-1} - \Sigma(E) = E^+ - H_0 - \Sigma(E) \quad (\text{B.4})$$

Therefore, we obtain an expression for the dressed one-nucleon propagator

$$g(E) = \frac{1}{E^+ - H_0 - \Sigma(E)} \quad (\text{B.5})$$

B.2 Calculating the dressed one-nucleon propagator

In bra-ket notation, we have

$$\Sigma(E) = \langle f_0 | g_{\pi N} | f(E) \rangle \quad (\text{B.6})$$

$$|f(E)\rangle = |f_0\rangle + t^b(E) g_{\pi N}(E) |f_0\rangle \quad (\text{B.7})$$

$$t_{\pi N}(E) = |f(E)\rangle + t^b(E) g_{\pi N}(E) |f_0\rangle \quad (\text{B.8})$$

We now introduce separable potentials for $v^b(E)$, and for numerical calculations, we shall take a P_{11} interaction using $NN-\pi NN$ calculation of Afnan and McLeod [40]. In particular, we use their $M1$ interaction which is specified by the equations

$$v^b(q', q) = h(q') \lambda h(q) \quad (\text{B.9})$$

where $\lambda = -1$. In bra-ket notation

$$v^b(q', q) = \langle q' | v^b | q \rangle = \langle q' | h \rangle \lambda \langle h | q \rangle v^b = |h\rangle \lambda \langle h| \quad (\text{B.10})$$

Putting this in our equation for the non-pole part of $t^b(E)$

$$\begin{aligned} t^b(E) &= v^b(E) + v^b(E) g_{\pi N}(E) v^b(E) + v^b(E) g_{\pi N}(E) v^b(E) g_{\pi N}(E) v^b(E) + \dots \\ &= |h\rangle \lambda \langle h| + |h\rangle \lambda \langle h | g_{\pi N}(E) | h \rangle \lambda \langle h| + |h\rangle \lambda \langle h | g_{\pi N}(E) | h \rangle \lambda \langle h | g_{\pi N}(E) | h \rangle \lambda \langle h| + \dots \\ &= |h\rangle (\lambda + \lambda \langle h | g_{\pi N}(E) | h \rangle \lambda + \lambda \langle h | g_{\pi N}(E) | h \rangle \lambda \langle h | g_{\pi N}(E) | h \rangle \lambda + \dots) \langle h| \\ &= |h\rangle (\lambda + \lambda \langle h | g_{\pi N}(E) | h \rangle + \lambda^2 \langle h | g_{\pi N}(E) | h \rangle^2 + \dots) \langle h| \end{aligned} \quad (\text{B.11})$$

Now, one can see the middle term(s) form a power series

$$\begin{aligned} &\lambda + \lambda \langle h | g_{\pi N}(E) | h \rangle + \lambda^2 \langle h | g_{\pi N}(E) | h \rangle^2 + \dots + \dots \\ &= \lambda \frac{1}{1 - \lambda \langle h | g_{\pi N}(E) | h \rangle} = \lambda \frac{\lambda^{-1}}{\lambda^{-1} 1 - \lambda \langle h | g_{\pi N}(E) | h \rangle} = \frac{1}{\lambda^{-1} - \langle h | g_{\pi N}(E) | h \rangle} = \tau(E) \end{aligned} \quad (\text{B.12})$$

So, the non-pole part becomes

$$t^b(E) = |h\rangle \tau(E) \langle h| \quad (\text{B.13})$$

where

$$\tau(E) = \frac{1}{\lambda^{-1} - \langle h | g_{\pi N}(E) | h \rangle} \quad (\text{B.14})$$

Here, we are using the free pion-nucleon propagator

$$g_{\pi N}(E, \mathbf{p}) = \frac{1}{E^+ - E_N(\mathbf{p}) - \omega_k} \quad (\text{B.15})$$

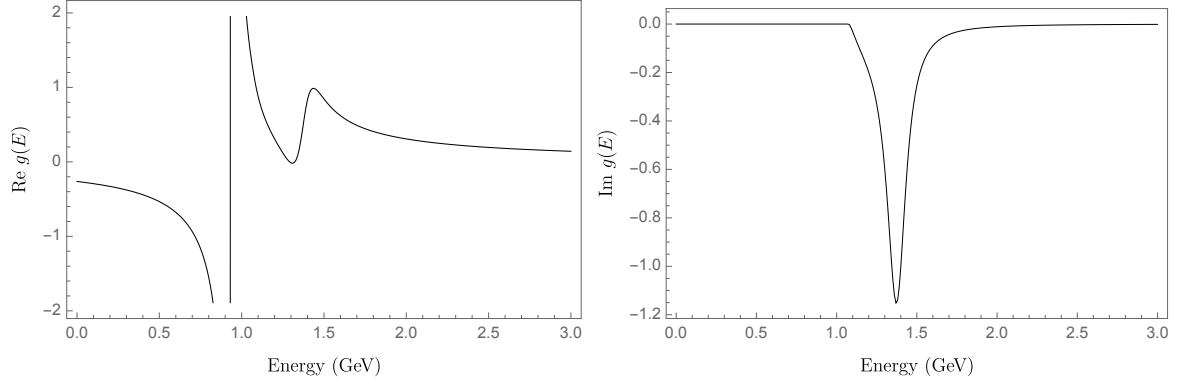


Figure B.2: Real and imaginary parts of the dressed one-nucleon propagator $g(E)$.

B.3 Analytical Structure of $g(E)$

The analytical structure of the dressed one-nucleon propagator $g(E)$ is implied directly from its definition. The dressed one-nucleon propagator must have a pole at the physical nucleon mass m where $E = m + i\epsilon$ and it must also have a cut along the positive real axis due to the momentum integration required in $\Sigma(E)$, resulting in unitary cuts for multi-pion production, as shown in Figure B.3. Consider an arbitrary function argument z to be inside the contour. Cauchy's Residue Theorem can then be used to obtain the following expression

$$\int_C \frac{g(\omega)}{z^+ - \omega} d\omega = 2\pi i \frac{Z}{z^+ - m} - 2\pi i g(z) \quad (\text{B.16})$$

as the integral in the contour C has a pole at $\omega = z + i\epsilon$. Now, taking the integration around the contour C , we obtain

$$\int_C \frac{g(\omega)}{z^+ - \omega} d\omega = \int_{-\infty}^{m+m_\pi} \frac{g(\omega^-)}{z^+ - \omega} d\omega + \int_{m+m_\pi}^{\infty} \frac{g(\omega^+)}{z^+ - \omega} d\omega = \int_{m+m_\pi}^{\infty} \frac{g(\omega^+) - g(\omega^-)}{z^+ - \omega} d\omega \quad (\text{B.17})$$

Across the cut, the imaginary part of $g(z)$ changes sign. Therefore

$$g(\omega^+) - g(\omega^-) = g(\omega^+) - g^*(\omega^+) = 2i \text{Im } g(\omega^+) \quad (\text{B.18})$$

Hence,

$$\int_C \frac{g(\omega)}{z^+ - \omega} d\omega = 2i \int_{m+m_\pi}^{\infty} \frac{\text{Im } g(\omega^+)}{z^+ - \omega} d\omega \quad (\text{B.19})$$

Now, by equating Equations B.16 and B.19, an expression for $g(E)$ is obtained

$$g(E) = \frac{Z}{E^+ - m} - \frac{1}{\pi} \int_{m_N+m_\pi}^{\infty} d\omega \frac{\text{Im } g(\omega)}{E^+ - \omega} \quad (\text{B.20})$$

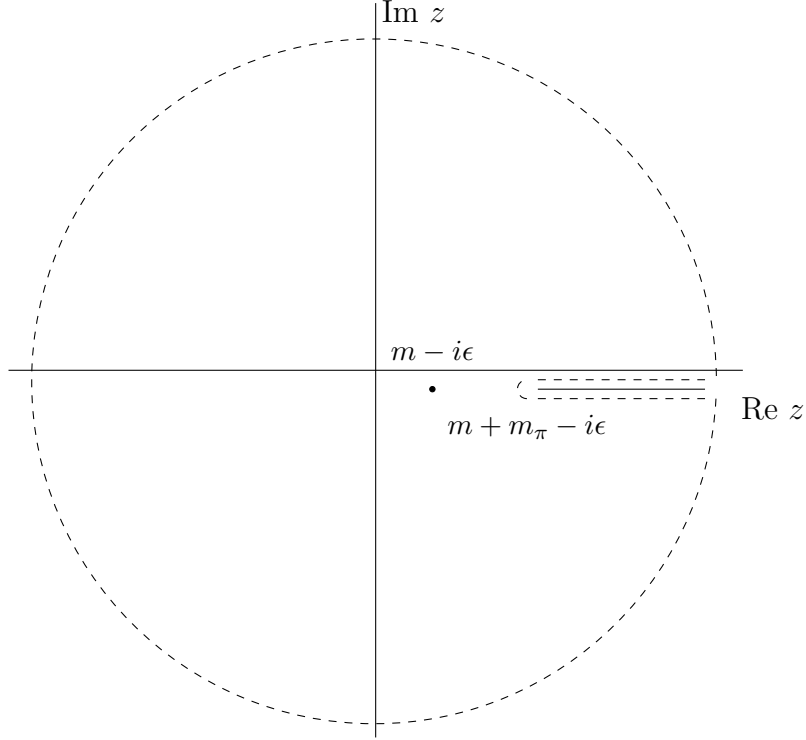


Figure B.3: The contour enclosing the pole at $m + i\epsilon$ and that forms around the branch cut beginning at $m + m_\pi - i\epsilon$ present in the dressed one-nucleon propagator.

Thus, assuming that the dressed one-nucleon propagator has no other poles or discontinuities in the complex E plane, one can display the analytic structure of $g(E)$ by exposing the pole at the physical nucleon mass m and one-pion unitary cut, as given by Equation B.20 [205].

Knowing this analytical structure of $g(E)$, we can also find the value of the bare mass m_0 as it cannot be determined experimentally. We know that $g(E)$ has a pole at the physical mass m . Hence,

$$m - m_0 - \Sigma(m) = 0 \quad (\text{B.21})$$

$$\longrightarrow m_0 = m - \Sigma(m) \quad (\text{B.22})$$

B.3.1 Calculating the dressed two-nucleon propagator

Galilean Invariance of the dressed one-nucleon propagator implies that

$$g(E, \mathbf{p}) = g\left(E - \frac{\mathbf{p}^2}{2m_N}, \mathbf{0}\right) \quad (\text{B.23})$$

which implies that for the dressed two-nucleon propagator

$$D_0(E, \mathbf{p}_1, \mathbf{p}_2) = D_0\left(E - \frac{\mathbf{p}_1^2}{2m_N} - \frac{\mathbf{p}_2^2}{2m_N}, \mathbf{0}, \mathbf{0}\right) \quad (\text{B.24})$$

From simplicity, we consider $\mathbf{p}_1 = \mathbf{p}_2 = \mathbf{0}$, so that $D_0(E, \mathbf{0}, \mathbf{0}) = D_0(E)$, without loss of generality. Hence, the following expression is obtained:

$$D_0(E) = \left(-\frac{1}{2\pi i} \right) \int_{-\infty}^{\infty} dz g(E-z)g(z) \quad (\text{B.25})$$

Using the dispersion relation of $g(E)$, one obtains:

$$D_0(E) = \left(-\frac{1}{2\pi i} \right) \int_{-\infty}^{\infty} dz \left(\frac{Z}{E^+ - z - m_N} - \frac{1}{\pi} \int_{m_N+m_\pi}^{\infty} d\omega_1 \frac{\text{Im } g(\omega_1)}{E^+ - z - \omega_1} \right) \left(\frac{Z}{z^+ - m_N} - \frac{1}{\pi} \int_{m_N+m_\pi}^{\infty} d\omega_2 \frac{\text{Im } g(\omega_2)}{z^+ - \omega_2} \right) \quad (\text{B.26})$$

Using Cauchy's Residue Theorem to evaluate the integrals by taking the residues at the poles that are enclosed in the contour in the lower half plane, we obtain

$$D_0(E) = \frac{Z^2}{E^+ - 2m_N} - \frac{2}{\pi} \int_{m_N+m_\pi}^{\infty} d\omega \frac{Z \text{Im } g(\omega)}{E^+ - m_N - \omega} + \frac{1}{\pi^2} \int_{m_N+m_\pi}^{\infty} d\omega_1 \int_{m_N+m_\pi}^{\infty} d\omega_2 \frac{\text{Im } g(\omega_1) \text{Im } g(\omega_2)}{E^+ - \omega_1 - \omega_2} \quad (\text{B.27})$$

For numerical calculations, the analytical structure of $g(E)$ is used to write this expression as:

$$D_0(E) = 2Zg(E - m_N) - \frac{Z^2}{E^+ - 2m_N} + \frac{1}{\pi} \int_{m_N+m_\pi}^{\infty} d\omega \left[\frac{Z}{E^+ - \omega - m_N} - g(E - \omega) \right] \text{Im } g(\omega) \quad (\text{B.28})$$

The input parameters required to numerically calculate the dressed one-nucleon propagator and hence, subsequently the dressed two-nucleon propagator is presented by Afnan and McLeod [40]. The authors provide such parameters as form factor functions and the model of πN elastic scattering used in this formulation. The multiple models presented by these authors has been previously used in calculations and has shown to be an effective model of πN elastic scattering. The author have obtained their constants and functions through comparison with experimental results, where we focus specifically on their $M1$ interaction, which is specified by the partial wave equations

$$v^b(q', q) = -h(q')h(q) \quad (\text{B.29a})$$

$$h(q) = \frac{c_1 q}{(q^2 + m_\pi^2)^{1/4}} \left[\frac{1}{q^2 + b_1^2} + \frac{c_2 q^4}{(q^2 + b_2^2)^3} \right] \quad (\text{B.29b})$$

$$f_0(q) = \frac{c_0}{(q^2 + m_\pi^2)^{1/4}} \frac{q}{q^2 + b_0^2} \quad (\text{B.29c})$$

where $c_0 = 1.0726$, $b_0 = 2.7703$, $c_1 = 0.3433$, $b_1 = 1.4422$, $c_2 = 7.4026$ and $b_2 = 2.1982$. Blankleider and Kvinikhidze [39, 48] have used this model in their previous numerical work. Here, we will also use this model in our subsequent numerical calculations. For comparison and in order to see the effect of full nucleon dressing, we consider other two-nucleon propagators. First, we consider the pole term of the dressed two-nucleon propagator, given by

$$G_{PT}(E) = \frac{Z^2}{E^+ - 2m_N} \quad (\text{B.30})$$

Next, we consider an approximation of the dressed two-nucleon propagator, by removing the integral from the derived expression. We denote this approximation by $G^\pi(E)$ which is given by

$$G^\pi(E) = 2Zg(E - m_N) - \frac{Z^2}{E^+ - 2m_N} \quad (\text{B.31})$$

Lastly, we consider the no dressing at the same time or different-time propagator $G_{DT}(E)$ given by

$$G_{DT}(E) = \frac{1}{E^+ - 2m_0 - 2\Sigma(E - m_N)} \quad (\text{B.32})$$

This different-time dressing propagator is an important propagator, as we will use it to calculate our three-body equations without same time dressing. This will allow us to determine the effect of same time consistent dressing on three-body equations in the main body. We plot each of the renormalised four propagators in Figure B.4. It should be noted that while we renormalised each of the four propagators by Z^2 to obtain unit residues, we should not do this for the different-time dressing propagator of Equation B.32. The residue is not Z^2 for the different-time dressing propagator, rather it is equal to $1/(1 + 2\Sigma'(m_N))$. However, we simply renormalise this propagator by Z^2 in Figure B.4 to be consistent with [48]. In future calculations with this propagator, we will use the correct residue in our renormalisation.

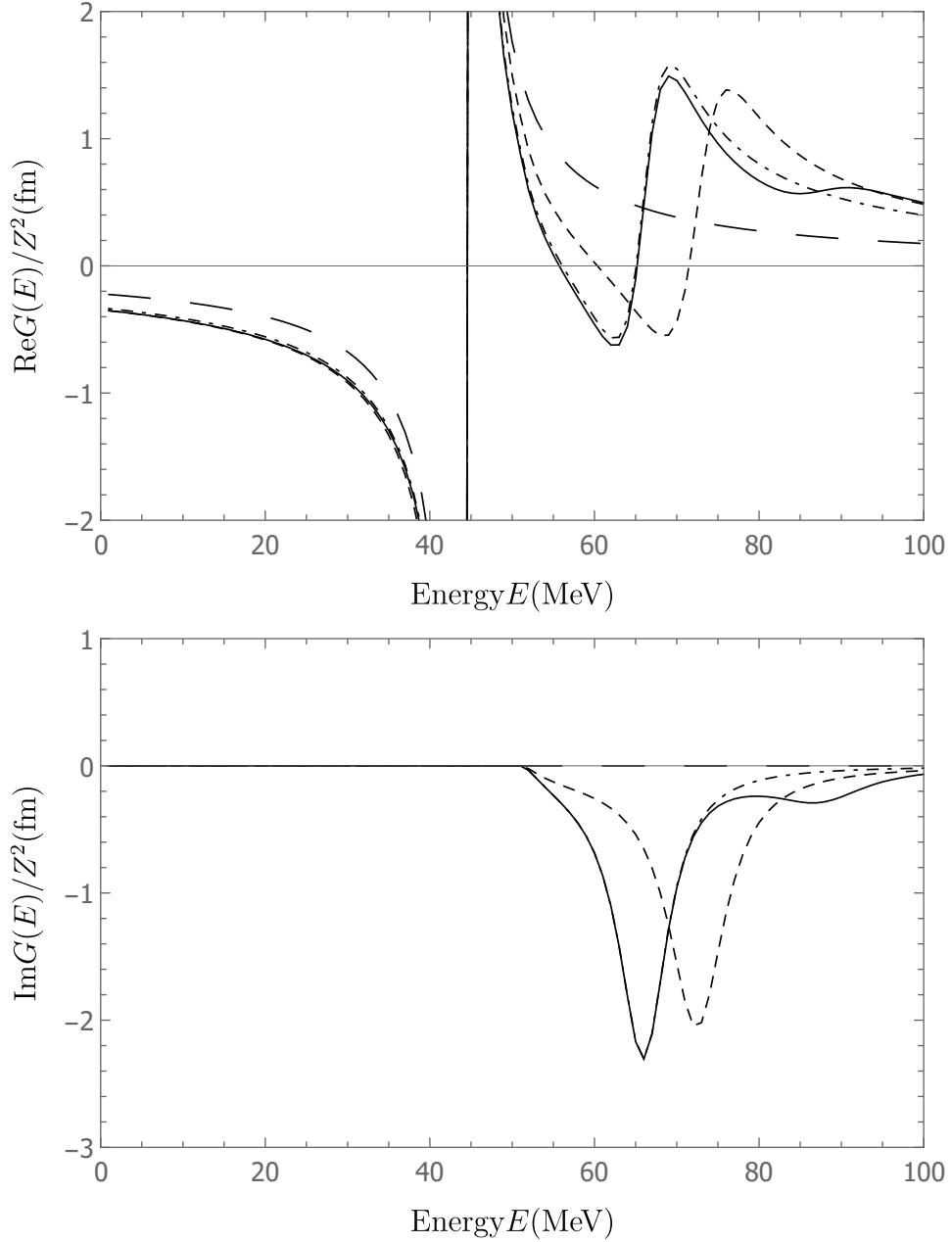


Figure B.4: Real and Imaginary parts of the dressed two-nucleon propagator and two-nucleon propagator approximations. The solid line represents the dressed two-nucleon propagator $D_0(E)$, the long dash represents $G_{PT}(E)$, dot dashed represents $G^\pi(E)$ and the short dashed line represents $G_{DT}(E)$. To be consistent with the results of Blankleider and Kvinikhidze [48], these graphs are normalised by a factor of Z^2 so that each propagator has a unit residue.

Chapter C

Theory of two nucleons

C.1 Time independent formulation

Given a Hamiltonian H , we want to solve the Schrödinger equation

$$H |\psi\rangle = E |\psi\rangle \quad (\text{C.1})$$

where the Hamiltonian is given as a sum of a free Hamiltonian H_0 and a scattering potential V given by

$$H = H_0 + V \quad (\text{C.2})$$

We can rewrite Equation C.1 into the following integral equation

$$\begin{aligned} (H_0 + V) |\psi\rangle &= E |\psi\rangle \\ \longrightarrow V |\psi\rangle &= (E - H_0) |\psi\rangle \end{aligned} \quad (\text{C.3})$$

Now say, we know the solution to the eigenvalue problem

$$H_0 |\phi\rangle = E |\phi\rangle \quad (\text{C.4})$$

where E is the eigenvalue for both the free and full Hamiltonian. We can write this equation into

$$(E - H_0) |\phi\rangle = 0 \quad (\text{C.5})$$

Now, the addition of Equations C.3 and C.5 gives

$$V |\psi\rangle + (E - H_0) |\phi\rangle = (E - H_0) |\psi\rangle \quad (\text{C.6})$$

and dividing through by $E - H_0$

$$|\psi\rangle = |\phi\rangle + \frac{1}{E - H_0} V |\psi\rangle \quad (\text{C.7})$$

However, the operator $(E - H_0)^{-1}$ is singular, as E is the eigenvalue of the operator H_0 . This can be fixed by adding a small imaginary number to E , which yields

$$|\psi^{(\pm)}\rangle = |\phi\rangle + \frac{1}{E \pm i\epsilon - H_0} V |\psi^{(\pm)}\rangle \quad (\text{C.8})$$

where $\epsilon > 0$ and $\epsilon \rightarrow 0$. This equation is known as the Lippmann – Schwinger equation. This equation contains, what is known as, the free Green's function or free Green's operator $G_0(E)$ and its hermitian operator $G_0^\dagger(E)$, defined as

$$G_0(E) = \frac{1}{E - H_0 + i\epsilon} = \frac{1}{E^+ - H_0} \quad (\text{C.9})$$

and

$$G_0^\dagger(E) = \frac{1}{E - H_0 - i\epsilon} \quad (\text{C.10})$$

So, the Lippmann-Schwinger equation can be written as

$$|\psi^{(+)}\rangle = |\phi\rangle + G_0(E)V|\psi^{(+)}\rangle \quad (\text{C.11})$$

We choose $|\psi^{(+)}\rangle$ as it obeys the correct boundary conditions for scattering. However, this is merely a convention, allowing us to be more precise with the physics and mathematics. This notation will be continued briefly for this section, but it is not entirely necessary for what we wish to achieve.

C.2 The t -matrix operator

Now, consider

$$V|\psi^{(+)}\rangle = T(E)|\phi\rangle \quad (\text{C.12})$$

where the operator $T(E)$ is referred to as the t -matrix operator. Putting this into Equation C.11, one obtains

$$|\psi^{(+)}\rangle = |\phi\rangle + G_0(E)T(E)|\phi\rangle \quad (\text{C.13})$$

Now, we have the ket $|\psi^{(+)}\rangle$ written as a linear combination of $|\phi\rangle$, which is an eigenket of the free Hamiltonian. Multiplying on the left by V

$$V|\psi^{(+)}\rangle = V|\phi\rangle + VG_0(E)T(E)|\phi\rangle \quad (\text{C.14})$$

$$\longrightarrow T(E)|\phi\rangle = V|\phi\rangle + VG_0(E)T(E)|\phi\rangle \quad (\text{C.15})$$

Hence, we have that the t -matrix operator $T(E)$ can be written as

$$T(E) = V + VG_0(E)T(E) \quad (\text{C.16})$$

Thus, this shows that $T(E)$ can be expanded in a perturbation series consisting of V and G_0

$$T(E) = V + VG_0(E)V + VG_0(E)VG_0(E)V + VG_0(E)VG_0(E)VG_0(E)V + \dots \quad (\text{C.17})$$

By taking Equation C.16 between initial and final momentum states, $|\mathbf{k}\rangle$ and $|\mathbf{k}'\rangle$ respectively, while also introducing the completeness relation or a complete set of momentum states

$$I = \int d\mathbf{k}'' |\mathbf{k}''\rangle \langle \mathbf{k}''| \quad (\text{C.18})$$

we can write the t -matrix operator as

$$\langle \mathbf{k}'| T(E) |\mathbf{k}\rangle = \langle \mathbf{k}'| V |\mathbf{k}\rangle + \int d\mathbf{k}'' \frac{\langle \mathbf{k}'| V |\mathbf{k}''\rangle \langle \mathbf{k}''| T(E) |\mathbf{k}\rangle}{E - H_0 + i\epsilon} \quad (\text{C.19})$$

We also recall the way we have defined $G_0(E)$ in Equation C.9. Hence, the matrix element becomes a function of energy E , and the initial and final momentum states, \mathbf{k} and \mathbf{k}' respectively. The function $T(\mathbf{k}', \mathbf{k}, E) = \langle \mathbf{k}'| T(E) |\mathbf{k}\rangle$ is known as the t -matrix. Therefore, the t -matrix can be expressed as

$$T(\mathbf{k}', \mathbf{k}, E) = V(\mathbf{k}', \mathbf{k}, E) + \int d\mathbf{k}'' \frac{V(\mathbf{k}', \mathbf{k}'', E) T(\mathbf{k}'', \mathbf{k}, E)}{E - H_0 + i\epsilon} \quad (\text{C.20})$$

C.3 Separable potential model of NN scattering

We assume that the potential V is a separable potential, meaning the potential V can be written as

$$V = |h\rangle \lambda \langle h| \quad (\text{C.21})$$

For uncoupled partial waves, the rank-1 separable potential operator (in 1D momentum space) is

$$V_{ls}^{jt} = |h\rangle \lambda \langle h| \quad (\text{C.22})$$

and a rank-2 is

$$V_{ls}^{jt} = |h_1\rangle \lambda_1 \langle h_1| + |h_2\rangle \lambda_2 \langle h_2| = (|h_1\rangle |h_2\rangle) \begin{pmatrix} \lambda_1 & 0 \\ 0 & \lambda_2 \end{pmatrix} \begin{pmatrix} \langle h_1| \\ \langle h_2| \end{pmatrix} \quad (\text{C.23})$$

For coupled partial waves, a separable potential operator is

$$V_{l's',ls}^{jt} = |h_{l's'}^{jt}\rangle \lambda_{l's',ls}^{jt} \langle h_{ls}^{jt}| \quad (\text{C.24})$$

where $\lambda_{l's',ls}^{jt}$ are adjustable “strength” parameters. The quantum numbers $l's'$ and ls can be considered as row and column indices of a 2×2 matrix, thus

$$\begin{pmatrix} V_{11} & V_{12} \\ V_{21} & V_{22} \end{pmatrix} = \begin{pmatrix} |h_1\rangle & 0 \\ 0 & |h_2\rangle \end{pmatrix} \begin{pmatrix} \lambda_{11} & \lambda_{12} \\ \lambda_{21} & \lambda_{22} \end{pmatrix} \begin{pmatrix} \langle h_1| & 0 \\ 0 & \langle h_2| \end{pmatrix} \quad (\text{C.25})$$

or

$$V = |h\rangle\lambda\langle h| \quad (\text{C.26})$$

where all quantities are square matrices with $|h\rangle$ and $\langle h|$ being diagonal. Using a separable potential allows us to calculate the t -matrix analytically

$$\begin{aligned} T(E) &= V + VG_0(E)T(E) = V + VG_0(E)V + VG_0(E)VG_0(E)V + \dots \\ &= |h\rangle\lambda\langle h| + |h\rangle\lambda\langle h|G_0(E)|h\rangle\lambda\langle h| + \dots \\ &= |h\rangle (\lambda + \lambda^2\langle h|G_0(E)|h\rangle + \dots) \langle h| \\ &= |h\rangle\tau(E)\langle h| \end{aligned} \quad (\text{C.27})$$

where

$$\tau(E) = [I - \lambda\langle h|G_0(E)|h\rangle]^{-1}\lambda \quad (\text{C.28})$$

The scattering S matrix is given by

$$S(E) = I - 2\pi ik_0\mu T(k_0, k_0) \quad (\text{C.29})$$

where k_0 is the on-shell two-nucleon momentum

$$E = \frac{k_0^2}{2m} \quad (\text{C.30})$$

and μ is the reduced mass

$$\mu = \frac{mm}{m+m} = \frac{m}{2} \quad (\text{C.31})$$

For uncoupled partial waves, one has that

$$S_{l_s}^{jt}(E) = e^{2i\delta_l} \quad (\text{C.32})$$

where δ_l are the phase shifts. For coupled partial waves it is usual to use the Stapp parametrisation of the S matrix

$$S_{l's',l_s}^{jt}(E) = \begin{pmatrix} e^{i\delta_{j-1}} & 0 \\ 0 & e^{i\delta_{j+1}} \end{pmatrix} \begin{pmatrix} \cos 2\epsilon_j & i \sin 2\epsilon_j \\ i \sin 2\epsilon_j & \cos 2\epsilon_j \end{pmatrix} \begin{pmatrix} e^{i\delta_{j-1}} & 0 \\ 0 & e^{i\delta_{j+1}} \end{pmatrix} \quad (\text{C.33})$$

where ϵ_j is known as the mixing parameter.

C.4 Separable potential model of the NN bound state

The bound state wave-function $|\psi_b\rangle$ is given by the equation

$$H|\psi_b\rangle = E_b|\psi_b\rangle \quad (\text{C.34})$$

where $E_b < 0$ is the bound state energy. It follows that

$$|\psi_b\rangle = G_0(E_b) V |\psi_b\rangle \quad (\text{C.35})$$

The NN system has only one bound state in the coupled ${}^3S_1 - {}^3D_1$ channel, which corresponds to the deuteron. Experimentally, the binding energy of the deuteron is $E_b = -2.225$ MeV. Our goal now is to calculate this binding energy. If we represent the potential as a separable potential

$$\begin{aligned} |\psi_b\rangle &= G_0(E_b) |h\rangle \lambda \langle h | \psi_b\rangle \\ \langle h | \psi_b\rangle &= \langle h | G_0(E_b) |h\rangle \lambda \langle h | \psi_b\rangle \\ [I - \langle h | G_0(E_b) |h\rangle \lambda] \langle h | \psi_b\rangle &= 0 \end{aligned} \quad (\text{C.36})$$

So, to solve for the binding energy, we can solve the following equation

$$\det [I - \langle h | G_0(E_b) |h\rangle \lambda] = 0 \quad (\text{C.37})$$

When doing calculation involving the deuteron, such as πd scattering, we require the normalisation constants F . We can calculate these normalisation constants using the bound state equation for ${}^3S_1 - {}^3D_1$. This equation is given as

$$|\psi_b\rangle = G_0(E_b) |h\rangle F \quad (\text{C.38})$$

where

$$F \equiv \lambda \langle h | \psi_b\rangle \quad (\text{C.39})$$

Here, F is a column vector of length 2.

The bound state is normalised such that

$$\langle \psi_b | \psi_b\rangle = 1 \quad (\text{C.40})$$

Therefore,

$$\langle \psi_b | \psi_b\rangle = F^\dagger \langle h | G_0(E_b)^2 |h\rangle F = 1 \quad (\text{C.41})$$

so that

$$\langle h_1 | G_0(E_b)^2 |h_1\rangle F_1^2 + \langle h_2 | G_0(E_b)^2 |h_2\rangle F_2^2 = 1 \quad (\text{C.42})$$

If we multiply our bound state equation on the left by $\lambda \langle h |$

$$\lambda \langle h | \psi_b\rangle = \lambda \langle h | G_0(E_b) |h\rangle F (I - \lambda \langle h | G_0(E_b) |h\rangle) F = 0 \quad (\text{C.43})$$

We now have two equations and two unknowns F_1 and F_2 , which we can solve simultaneously to find the normalisation constants.

C.4.1 Finding the binding energy and normalisation constants using Reid Soft Core UPA

The binding energy can be found by solving the following equation for E_b

$$\det [I - \langle h|G_0(E_b)|h\rangle\lambda] = 0 \quad (\text{C.44})$$

where

$$\langle h|G_0(E_b)|h\rangle = \begin{pmatrix} \langle h_0|G_0(E_b)|h_0\rangle & 0 \\ 0 & \langle h_2|G_0(E_b)|h_2\rangle \end{pmatrix} \quad (\text{C.45})$$

and

$$\langle h_0|G_0(E_b)|h_0\rangle = \int dk \frac{h_0(k)^2 k^2}{E_b - \frac{k^2}{2m} - 2m} \quad (\text{C.46})$$

Similarly for $\langle h_2|G_0(E_b)|h_2\rangle$. Here, E_b is in the centre of mass, so we will need to account for the rest masses. The form factor functions are defined in Chapter 5. For UPA, the λ matrix is given as

$$\lambda = \begin{pmatrix} -1 & -1 \\ -1 & -1 \end{pmatrix} \quad (\text{C.47})$$

We can calculate this integral using standard contour rotation methods and will result in a binding energy of $E_b = -2.21082$ MeV. To calculate the normalisation constants F , we solve the following equations simultaneously

$$\langle h_1|G_0(E_b)^2|h_1\rangle F_1^2 + \langle h_2|G_0(E_b)^2|h_2\rangle F_2^2 = 1 \quad (\text{C.48})$$

$$(I - \lambda \langle h|G_0(E_b)|h\rangle) F = 0 \quad (\text{C.49})$$

where

$$\langle h_0|G_0(E_b)^2|h_0\rangle = \int dk \frac{h_0(k)^2 k^2}{(E_b - \frac{k^2}{2m} - 2m)^2} \quad (\text{C.50})$$

By numerically solving these equations, we obtain

$$F_1 = 0.352715, F_2 = 0.352715 \quad (\text{C.51})$$

or

$$F_1 = -0.352715, F_2 = -0.352715 \quad (\text{C.52})$$

Chapter D

Dressed one-pion and two-exchange
for NN

D.1 Dressed one-pion exchange from perturbation theory

When considering $NN \rightarrow NN$, we have found that the first term in the perturbation theory gives us the dressed two-nucleon propagator as a convolution of dressed one-nucleon propagators. If we consider the next two terms in the perturbation theory, corresponding to a single H_I^π , these two terms become zero for $NN \rightarrow NN$, as annihilation operators for pion states will operate on two nucleon states in both cases. In this chapter, we are interested in the next terms in the perturbation theory, corresponding to two H_I^π , given as

$$\begin{aligned}
 & \langle \mathbf{p}'_1 \mathbf{p}'_2 | \frac{1}{E^+ - H_1 - H_2 - H_0^\pi} H_I^\pi(1) \frac{1}{E^+ - H_1 - H_2 - H_0^\pi} H_I^\pi(1) \frac{1}{E^+ - H_1 - H_2 - H_0^\pi} | \mathbf{p}_1 \mathbf{p}_2 \rangle \\
 & \langle \mathbf{p}'_1 \mathbf{p}'_2 | \frac{1}{E^+ - H_1 - H_2 - H_0^\pi} H_I^\pi(1) \frac{1}{E^+ - H_1 - H_2 - H_0^\pi} H_I^\pi(2) \frac{1}{E^+ - H_1 - H_2 - H_0^\pi} | \mathbf{p}_1 \mathbf{p}_2 \rangle \\
 & \langle \mathbf{p}'_1 \mathbf{p}'_2 | \frac{1}{E^+ - H_1 - H_2 - H_0^\pi} H_I^\pi(2) \frac{1}{E^+ - H_1 - H_2 - H_0^\pi} H_I^\pi(1) \frac{1}{E^+ - H_1 - H_2 - H_0^\pi} | \mathbf{p}_1 \mathbf{p}_2 \rangle \\
 & \langle \mathbf{p}'_1 \mathbf{p}'_2 | \frac{1}{E^+ - H_1 - H_2 - H_0^\pi} H_I^\pi(2) \frac{1}{E^+ - H_1 - H_2 - H_0^\pi} H_I^\pi(2) \frac{1}{E^+ - H_1 - H_2 - H_0^\pi} | \mathbf{p}_1 \mathbf{p}_2 \rangle
 \end{aligned} \tag{D.1}$$

By inspection, we can determine the corresponding diagram for each of these terms. Consider term 1 and term 3, which corresponds to a pion being created by one nucleon and then absorbed by the same nucleon. These terms just corresponds to nucleon dressing, but this is already included as we considered each nucleon to be dressed by its own pion. Thus, these terms are of no interest and we now consider term 2 and 4. These terms correspond to the creation of a pion on one nucleon and absorption of that pion on the other nucleon. Therefore, these term correspond to one-pion exchange (OPE) for both time-orderings, which is shown diagrammatically in Figure D.1.



Figure D.1: Diagram representation of both time-ordering of one-pion exchange between two nucleons

Our goal now is to show the explicit calculation for OPE and we consider only the first time-ordering, whose Green's function we denote as G_{12}^{OPE} and corresponds to the following

term

$$G_{12}^{OPE} = \langle \mathbf{p}'_1 \mathbf{p}'_2 | \frac{1}{E^+ - H_1 - H_2 - H_0^\pi} H_I^\pi(1) \frac{1}{E^+ - H_1 - H_2 - H_0^\pi} H_I^\pi(2) \frac{1}{E^+ - H_1 - H_2 - H_0^\pi} | \mathbf{p}_1 \mathbf{p}_2 \rangle \quad (\text{D.2})$$

We choose to ignore the momentum conserving functions δ in order to space on notation. We now use the definitions of H_I^π to introduce the creation and annihilation operators for the exchange pion. For simplicity, we ignore the left hand side and the final and initial momentum states, as well as suppress the operator $1/(E^+ - H_1 - H_2 - H_0^\pi)$ and the integrals, just for now. So, expanding these terms gives

$$\begin{aligned} & a_\pi^\dagger(\mathbf{k}) J_{N_1}(\mathbf{k}) a_\pi^\dagger(\mathbf{k}') J_{N_2}(\mathbf{k}') + a_\pi^\dagger(\mathbf{k}) J_{N_1}(\mathbf{k}) J_{N_2}^\dagger(\mathbf{k}') a_\pi(\mathbf{k}') \\ & + J_{N_1}^\dagger(\mathbf{k}) a_\pi(\mathbf{k}) a_\pi^\dagger(\mathbf{k}') J_{N_2}(\mathbf{k}') + J_{N_1}^\dagger(\mathbf{k}) a_\pi(\mathbf{k}) J_{N_2}^\dagger(\mathbf{k}') a_\pi(\mathbf{k}') \end{aligned}$$

Again, we have pion annihilation operators acting on two-nucleon states and we can see that the only remaining term would correspond to term 3. Hence, using this 3rd term and returning the operator $1/(E^+ - H_1 - H_2 - H_0^\pi)$, as well as the integrals

$$G_{12}^{OPE} = \int d\mathbf{k} d\mathbf{k}' \langle \mathbf{p}'_1 \mathbf{p}'_2 | \frac{1}{E^+ - H_1 - H_2 - H_0^\pi} J_{N_1}^\dagger(\mathbf{k}) a_\pi(\mathbf{k}) \frac{1}{E^+ - H_1 - H_2 - H_0^\pi} \times a_\pi^\dagger(\mathbf{k}') J_{N_2}(\mathbf{k}') \frac{1}{E^+ - H_1 - H_2 - H_0^\pi} | \mathbf{p}_1 \mathbf{p}_2 \rangle \quad (\text{D.3})$$

Using the commutator relation between $a_\pi(\mathbf{k})$ and H_0^π , we move the $a_\pi(\mathbf{k})$ next to the $a_\pi^\dagger(\mathbf{k}')$ in an attempt to form a commutator relation between the creation and annihilation operator

$$G_{12}^{OPE} = \int d\mathbf{k} d\mathbf{k}' \langle \mathbf{p}'_1 \mathbf{p}'_2 | \frac{1}{E^+ - H_1 - H_2 - H_0^\pi} J_{N_1}^\dagger(\mathbf{k}) \frac{1}{E^+ - H_1 - H_2 - \omega_k} \times a_\pi(\mathbf{k}) a_\pi^\dagger(\mathbf{k}') J_{N_2}(\mathbf{k}') \frac{1}{E^+ - H_1 - H_2 - H_0^\pi} | \mathbf{p}_1 \mathbf{p}_2 \rangle \quad (\text{D.4})$$

A rearrangement of the commutator relation between $a_\pi(\mathbf{k})$ and $a_\pi^\dagger(\mathbf{k}')$ shows

$$a_\pi(\mathbf{k}) a_\pi^\dagger(\mathbf{k}') = \delta(\mathbf{k} - \mathbf{k}') - a_\pi^\dagger(\mathbf{k}') a_\pi(\mathbf{k}) \quad (\text{D.5})$$

for which, we could insert into the above equation and obtain two separate integrals, one containing the delta function and the other containing $a_\pi^\dagger(\mathbf{k}') a_\pi(\mathbf{k})$. However, the integral containing $a_\pi^\dagger(\mathbf{k}') a_\pi(\mathbf{k})$ would become zero as the final states do not contain any pions.

Leaving us with

$$G_{12}^{OPE} = \int d\mathbf{k} \langle \mathbf{p}'_1 \mathbf{p}'_2 | \frac{1}{E^+ - H_1 - H_2 - H_0^\pi} J_{N_1}^\dagger(\mathbf{k}) \frac{1}{E^+ - H_1 - H_2 - H_0^\pi} \times J_{N_2}(\mathbf{k}) \frac{1}{E^+ - H_1 - H_2 - H_0^\pi} | \mathbf{p}_1 \mathbf{p}_2 \rangle \quad (\text{D.6})$$

We can then separate the H_1 and H_2 contributions by introducing two convolution integrals

$$G_{12}^{OPE} = \left(-\frac{1}{2\pi i} \right)^2 \int d\mathbf{k} dz' dz \langle \mathbf{p}'_1 \mathbf{p}'_2 | \frac{1}{z'^+ - H_1} J_{N_1}^\dagger(\mathbf{k}) \frac{1}{z^+ - H_1} \frac{1}{z'^+ - z - \omega_k} \frac{1}{E^+ - z' - H_2} J_{N_2}(\mathbf{k}) \frac{1}{E^+ - z - H_2} | \mathbf{p}_1 \mathbf{p}_2 \rangle \quad (\text{D.7})$$

Now, both Hamiltonians for each nucleon are represented by individual terms. This allows us to take the matrix elements using the momentum states of nucleon 1 and nucleon 2 individually. Therefore,

$$G_{12}^{OPE} = \left(-\frac{1}{2\pi i} \right)^2 \int d\mathbf{k} dz' dz \langle \mathbf{p}'_1 | \frac{1}{z'^+ - H_1} J_{N_1}^\dagger(\mathbf{k}) \frac{1}{z^+ - H_1} | \mathbf{p}_1 \rangle \frac{1}{z'^+ - z - \omega_k} \langle \mathbf{p}'_2 | \frac{1}{E^+ - z' - H_2} J_{N_2}(\mathbf{k}) \frac{1}{E^+ - z - H_2} | \mathbf{p}_2 \rangle \quad (\text{D.8})$$

The matrix elements define the two-energy dependent vertices $f(\mathbf{p}', \mathbf{p}, z', z)$ where

$$\delta(\mathbf{p}' + \mathbf{k} - \mathbf{p}) g(z', \mathbf{p}') f(\mathbf{p}', \mathbf{p}, z', z) g(z, \mathbf{p}) = \langle \mathbf{p}' | \frac{1}{z'^+ - H} J_N(\mathbf{k}) \frac{1}{z^+ - H} | \mathbf{p} \rangle \quad (\text{D.9})$$

Now, using the definition of the dressed one-nucleon propagator and without the momentum-conserving functions, we obtain

$$G_{12}^{OPE} = \left(-\frac{1}{2\pi i} \right)^2 \int dz dz' g(z', \mathbf{p}') \bar{f}(\mathbf{p}'_1, \mathbf{p}_1, z', z) g(z, \mathbf{p}_1) \frac{1}{z'^+ - z - \omega_k} g(E - z', \mathbf{p}'_2) f(\mathbf{p}'_2, \mathbf{p}_2, E - z', E - z) g(E - z, \mathbf{p}_2) \quad (\text{D.10})$$

From this convolution approach, we obtain two-energy vertices, which differ from the usual one-energy vertices we obtain in “old-fashioned” perturbation theory. So, we seek to relate the matrix element to that of a usual one-energy vertex, thus require

$$\langle \mathbf{k} \mathbf{p}' | \frac{1}{z^+ - H} | \mathbf{p} \rangle \quad (\text{D.11})$$

to be obtained from Equation D.9. For this, we need a $a_\pi(\mathbf{k})$, which will act to the left. We can write

$$\begin{aligned} \langle \mathbf{p}' | \frac{1}{z'^+ - H} J_N(\mathbf{k}) \frac{1}{z^+ - H} | \mathbf{p} \rangle \\ = \langle \mathbf{k} \mathbf{p}' | \frac{1}{z^+ - H} | \mathbf{p} \rangle + \langle \mathbf{p}' | \frac{1}{z'^+ - H} (J_N(\mathbf{k}) - (z'^+ - H)) \frac{1}{z^+ - H} | \mathbf{p} \rangle \end{aligned} \quad (\text{D.12})$$

We can simplify this last term, using the commutator relations we found in Chapter 2

$$\begin{aligned}
 & \langle \mathbf{p}' | \frac{1}{z'^+ - H} (J_N(\mathbf{k}) - (z'^+ - H) a_\pi(\mathbf{k})) \frac{1}{z^+ - H} | \mathbf{p} \rangle \\
 &= \langle \mathbf{p}' | \frac{1}{z'^+ - H} (a_\pi(\mathbf{k}) H_I^\pi + (-z'^+ + H - H_I^\pi) a_\pi(\mathbf{k})) \frac{1}{z^+ - H} | \mathbf{p} \rangle \\
 &= \langle \mathbf{p}' | \frac{1}{z'^+ - H} (a_\pi(\mathbf{k}) H_I^\pi + (-z'^+ + H_0^N + H_0^\pi) a_\pi(\mathbf{k})) \frac{1}{z^+ - H} | \mathbf{p} \rangle \\
 &= \langle \mathbf{p}' | \frac{1}{z'^+ - H} a_\pi(\mathbf{k}) (H_I^\pi - z'^+ + H_0^N + H_0^\pi - \omega_k) \frac{1}{z^+ - H} | \mathbf{p} \rangle \\
 &= \langle \mathbf{p}' | \frac{1}{z'^+ - H} a_\pi(\mathbf{k}) (H - z'^+ - \omega_k) \frac{1}{z^+ - H} | \mathbf{p} \rangle \\
 &= (z - z' - \omega_k) \langle \mathbf{p}' | \frac{1}{z'^+ - H} a_\pi(\mathbf{k}) \frac{1}{z^+ - H} | \mathbf{p} \rangle
 \end{aligned} \tag{D.13}$$

Therefore, we obtain

$$\begin{aligned}
 & \langle \mathbf{p}' | \frac{1}{z'^+ - H} J_N(\mathbf{k}) \frac{1}{z^+ - H} | \mathbf{p} \rangle \\
 &= \langle \mathbf{k} \mathbf{p}' | \frac{1}{z^+ - H} | \mathbf{p} \rangle + (z - z' - \omega_k) \langle \mathbf{p}' | \frac{1}{z'^+ - H} a_\pi(\mathbf{k}) \frac{1}{z^+ - H} | \mathbf{p} \rangle
 \end{aligned} \tag{D.14}$$

This shows that the two-energy vertex is equal to the usual one-energy vertex when initial and final energies are equal, namely $z = z' + \omega_k$. We are, thus, motivated to approximate the two-energy vertex by the one-energy vertex $f(\mathbf{p}', \mathbf{p}, z', z) \approx f(\mathbf{p}', \mathbf{p}, z)$, which is exact when $z = z' + \omega_k$. Thus, we obtain our Green's function with one-energy vertices

$$\begin{aligned}
 G_{12}^{OPE} &= \left(-\frac{1}{2\pi i} \right)^2 \int dz dz' g(z', \mathbf{p}'_1) \bar{f}(\mathbf{p}'_1, \mathbf{p}_1, z') g(z, \mathbf{p}_1) \frac{1}{z'^+ - z - \omega_k} \\
 & \quad g(E - z', \mathbf{p}'_2) f(\mathbf{p}'_2, \mathbf{p}_2, E - z) g(E - z, \mathbf{p}_2)
 \end{aligned} \tag{D.15}$$

Therefore, we obtain the Green's function for one-pion exchange between two nucleons, which defines this new type of connected diagram in Figure D.2 [39]. The dressed one-pion exchange potential V_{12}^{OPE} can therefore be calculated in the usually way of ‘‘chopping off’’ the external legs of the Green's function

$$V_{12}^{OPE} = D_0^{-1} G_{12}^{OPE} D_0^{-1} \tag{D.16}$$

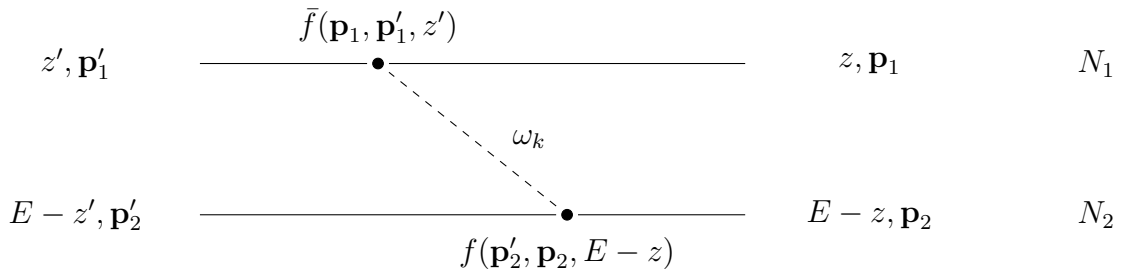


Figure D.2: Diagram representation of the one-pion exchange between two nucleons

We can take this one step further by including Galilean invariance and obtain a more calculable form. Using Galilean invariance on the dressed one-nucleon propagators

$$g(E, \mathbf{p}) = g\left(E - \frac{\mathbf{p}^2}{2m}, \mathbf{0}\right) = g(E - E_p) \quad (\text{D.17})$$

where $E_p = \frac{\mathbf{p}^2}{2m}$ and m is the mass of the nucleon. Using Galilean invariance, and assuming $m_\pi \ll m$

$$f(\mathbf{p}', \mathbf{p}, E) \approx f\left(\mathbf{p}' - \mathbf{p}, \mathbf{0}, E - \frac{\mathbf{p}^2}{2m}\right) = f(\mathbf{k}, E - E_p) \quad (\text{D.18})$$

Therefore,

$$G_{12}^{OPE} = \left(-\frac{1}{2\pi i}\right)^2 \int dz dz' g(z' - E_{p_1}) \bar{f}(\mathbf{k}, z' - E_{p_1}) g(z - E_{p_1}) \frac{1}{z'^+ - z - \omega_k} \\ g(E - z' - E_{p_2}) f(\mathbf{k}, E - z - E_{p_2}) g(E - z - E_{p_2}) \quad (\text{D.19})$$

D.2 Full derivation of the analytical form for dressed two-pion exchange

We concern ourselves primarily with how to perform the z'' integral. For simplicity, we focus only on terms that contain z'' and ignore everything else, which can easily be added back in later. This leaves us with

$$\left(-\frac{1}{2\pi i}\right) \int_0^\infty dp'' (p'')^2 \int_{-\infty}^\infty dz'' \\ \frac{f(k, m) f(k, E - z'' - E_{p''})}{E/2 + i\epsilon - z'' - \omega_k} g(z'' - E_{p''}) g(E - z'' - E_{p''}) \frac{f(k', z'' - E_{p''}) f(k', m)}{z'' + i\epsilon - E/2 - \omega_{k'}} \quad (\text{D.20})$$

Notice that $f(k, m)$ and $f(k', m)$ do not contain z'' , so we take them out of the z'' integral

$$\left(-\frac{1}{2\pi i}\right) \int_0^\infty dp'' (p'')^2 f(k, m) f(k', m) \int_{-\infty}^\infty dz'' \\ \frac{f(k, E - z'' - E_{p''})}{E/2 + i\epsilon - z'' - \omega_k} g(z'' - E_{p''}) g(E - z'' - E_{p''}) \frac{f(k', z'' - E_{p''})}{z'' + i\epsilon - E/2 - \omega_{k'}} \quad (\text{D.21})$$

We now perform the z'' integral using Cauchy's Residue Theorem by taking the residues of the poles. We choose to take the residue of the poles below the real z'' axis. As can be seen from the above equation, there are 3 possible poles below the real z'' axis; one due to the nucleon propagator, one due to the dressed vertex function and the last one due to the pion

propagator. To expose the poles in the nucleon propagator and dressed vertex, we use the analytical structure of both functions. We use a reduced form to save on notation and also choose the $+i\epsilon$ for convenience to our calculation, as they need not equal. Our analytical structure in reduced form becomes

$$\begin{aligned} f(k, E) &= f_0(k) + \frac{X(\omega_1)}{E + 3i\epsilon - \omega_1} \\ g(E) &= \frac{Z}{E + 2i\epsilon - m} + \frac{Y(\omega_2)}{E + 2i\epsilon - \omega_2} \end{aligned} \quad (\text{D.22})$$

Putting these equation into our integral for the functions that contain the poles and expanding

$$\begin{aligned} &\left(-\frac{1}{2\pi i}\right) \int_0^\infty dp'' (p'')^2 f(k, m) f(k', m) \int_{-\infty}^\infty dz'' \\ &\frac{Z f(k, E - E_{p''} - z'') f_0(k') g(E - E_{p''} - z'')}{(-E_{p''} + 2i\epsilon - m + z'')(E/2 + i\epsilon - z'' - \omega_k)(-E/2 + i\epsilon + z'' - \omega_{k'})} + \\ &\frac{Z f(k, E - E_{p''} - z'') g(E - E_{p''} - z'') X(\omega_1)}{(-E_{p''} + 2i\epsilon - m + z'')(-E_{p''} + 3i\epsilon + z'' - \omega_1)(E/2 + i\epsilon - z'' - \omega_k)(-E/2 + i\epsilon + z'' - \omega_{k'})} \\ &+ \frac{f(k, E - E_{p''} - z'') f_0(k') g(E - E_{p''} - z'') Y(\omega_2)}{(-E_{p''} + 2i\epsilon + z'' - \omega_2)(E/2 + i\epsilon - z'' - \omega_k)(-E/2 + i\epsilon + z'' - \omega_{k'})} + \\ &\frac{f(k, E - E_{p''} - z'') g(E - E_{p''} - z'') X(\omega_1) Y(\omega_2)}{(-E_{p''} + 3i\epsilon + z'' - \omega_1)(-E_{p''} + 2i\epsilon + z'' - \omega_2)(E/2 + i\epsilon - z'' - \omega_k)(-E/2 + i\epsilon + z'' - \omega_{k'})} \end{aligned} \quad (\text{D.23})$$

Now, we focus on each term individually and see that each term either has 2 or 3 poles below the real z'' axis. The z'' integral thus, becomes a sum of residues.

Term 1

$$\begin{aligned} &\left(-\frac{1}{2\pi i}\right) \int_0^\infty dp'' (p'')^2 f(k, m) f(k', m) \int_{-\infty}^\infty dz'' \\ &\frac{Z f(k, E - E_{p''} - z'') f_0(k') g(E - E_{p''} - z'')}{(-E_{p''} + 2i\epsilon - m + z'')(E/2 + i\epsilon - z'' - \omega_k)(-E/2 + i\epsilon + z'' - \omega_{k'})} \\ &= \int_0^\infty dp'' (p'')^2 f(k, m) f(k', m) \\ &\frac{Z f(k, E - 2E_{p''} + 2i\epsilon - m) f_0(k') g(E - 2E_{p''} + 2i\epsilon - m)}{(E/2 - E_{p''} + 3i\epsilon - m - \omega_k)(-E/2 + E_{p''} - i\epsilon + m - \omega_{k'})} \\ &+ \frac{Z f(k, E/2 - E_{p''} + i\epsilon - \omega_{k'}) f_0(k') g(E/2 - E_{p''} + i\epsilon - \omega_{k'})}{(2i\epsilon - \omega_k - \omega_{k'})(E/2 - E_{p''} + i\epsilon - m + \omega_{k'})} \end{aligned} \quad (\text{D.24})$$

Term 2

$$\begin{aligned}
 & \left(-\frac{1}{2\pi i} \right) \int_0^\infty dp'' (p'')^2 f(k, m) f(k', m) \int_{-\infty}^\infty dz'' \\
 & \frac{Z f(k, E - E_{p''} - z'') g(E - E_{p''} - z'') X(\omega_1)}{(-E_{p''} + 2i\epsilon - m + z'') (-E_{p''} + 3i\epsilon + z'' - \omega_1) (E/2 + i\epsilon - z'' - \omega_k) (-E/2 + i\epsilon + z'' - \omega_{k'})} \\
 & = \int_0^\infty dp'' (p'')^2 f(k, m) f(k', m) \\
 & \frac{Z f(k, E - 2E_{p''} + 2i\epsilon - m) g(E - 2E_{p''} + 2i\epsilon - m) X(\omega_1)}{(i\epsilon + m - \omega_1) (E/2 - E_{p''} + 3i\epsilon - m - \omega_k) (-E/2 + E_{p''} - i\epsilon + m - \omega_{k'})} \\
 & + \frac{Z f(k, E - 2E_{p''} + 3i\epsilon - \omega_1) g(E - 2E_{p''} + 3i\epsilon - \omega_1) X(\omega_1)}{(-i\epsilon - m + \omega_1) (E/2 - E_{p''} + 4i\epsilon - \omega_1 - \omega_k) (-E/2 + E_{p''} - 2i\epsilon + \omega_1 - \omega_{k'})} \\
 & + \frac{Z f(k, E/2 - E_{p''} + i\epsilon - \omega_{k'}) g(E/2 - E_{p''} + i\epsilon - \omega_{k'}) X(\omega_1)}{(2i\epsilon - \omega_k - \omega_{k'}) (E/2 - E_{p''} + i\epsilon - m + \omega_{k'}) (E/2 - E_{p''} + 2i\epsilon - \omega_1 + \omega_{k'})}
 \end{aligned} \tag{D.25}$$

Term 3

$$\begin{aligned}
 & \left(-\frac{1}{2\pi i} \right) \int_0^\infty dp'' (p'')^2 f(k, m) f(k', m) \int_{-\infty}^\infty dz'' \\
 & \frac{f(k, E - E_{p''} - z'') f_0(k') g(E - E_{p''} - z'') Y(\omega_2)}{(-E_{p''} + 2i\epsilon + z'' - \omega_2) (E/2 + i\epsilon - z'' - \omega_k) (-E/2 + i\epsilon + z'' - \omega_{k'})} \\
 & = \int_0^\infty dp'' (p'')^2 f(k, m) f(k', m) \\
 & \frac{f(k, E - 2E_{p''} + 2i\epsilon - \omega_2) f_0(k') g(E - 2E_{p''} + 2i\epsilon - \omega_2) Y(\omega_2)}{(E/2 - E_{p''} + 3i\epsilon - \omega_2 - \omega_k) (-E/2 + E_{p''} - i\epsilon + \omega_2 - \omega_{k'})} \\
 & + \frac{f(k, E/2 - E_{p''} + i\epsilon - \omega_{k'}) f_0(k') g(E/2 - E_{p''} + i\epsilon - \omega_{k'}) Y(\omega_2)}{(2i\epsilon - \omega_k - \omega_{k'}) (E/2 - E_{p''} + i\epsilon - \omega_2 + \omega_{k'})}
 \end{aligned} \tag{D.26}$$

Term 4

$$\begin{aligned}
 & \left(-\frac{1}{2\pi i} \right) \int_0^\infty dp'' (p'')^2 f(k, m) f(k', m) \int_{-\infty}^\infty dz'' \\
 & \frac{f(k, E - E_{p''} - z'') g(E - E_{p''} - z'') X(\omega_1) Y(\omega_2)}{(-E_{p''} + 3i\epsilon + z'' - \omega_1) (-E_{p''} + 2i\epsilon + z'' - \omega_2) (E/2 + i\epsilon - z'' - \omega_k) (-E/2 + i\epsilon + z'' - \omega_{k'})} \\
 & = \int_0^\infty dp'' (p'')^2 f(k, m) f(k', m) \\
 & \frac{f(k, E - 2E_{p''} + 3i\epsilon - \omega_1) g(E - 2E_{p''} + 3i\epsilon - \omega_1) X(\omega_1) Y(\omega_2)}{(-i\epsilon + \omega_1 - \omega_2) (E/2 - E_{p''} + 4i\epsilon - \omega_1 - \omega_k) (-E/2 + E_{p''} - 2i\epsilon + \omega_1 - \omega_{k'})} \\
 & + \frac{f(k, E - 2E_{p''} + 2i\epsilon - \omega_2) g(E - 2E_{p''} + 2i\epsilon - \omega_2) X(\omega_1) Y(\omega_2)}{(i\epsilon - \omega_1 + \omega_2) (E/2 - E_{p''} + 3i\epsilon - \omega_2 - \omega_k) (-E/2 + E_{p''} - i\epsilon + \omega_2 - \omega_{k'})} \\
 & + \frac{f(k, E/2 - E_{p''} + i\epsilon - \omega_{k'}) g(E/2 - E_{p''} + i\epsilon - \omega_{k'}) X(\omega_1) Y(\omega_2)}{(2i\epsilon - \omega_k - \omega_{k'}) (E/2 - E_{p''} + 2i\epsilon - \omega_1 + \omega_{k'}) (E/2 - E_{p''} + i\epsilon - \omega_2 + \omega_{k'})}
 \end{aligned} \tag{D.27}$$

We now, want to reduce the amount of terms we have by combining terms and using our analytical structure of $g(E)$ and $f(k, E)$.

Factorisation (1)

We group all terms which have $2i\epsilon - \omega_k - \omega_{k'}$ in the denominator

$$\begin{aligned}
 & \int_0^\infty dp'' (p'')^2 f(k, m) f(k', m) \\
 & \frac{Z f(k, E/2 - E_{p''} + i\epsilon - \omega_{k'}) f_0(k') g(E/2 - E_{p''} + i\epsilon - \omega_{k'})}{(2i\epsilon - \omega_k - \omega_{k'}) (E/2 - E_{p''} + i\epsilon - m + \omega_{k'})} \\
 & + \frac{Z f(k, E/2 - E_{p''} + i\epsilon - \omega_{k'}) g(E/2 - E_{p''} + i\epsilon - \omega_{k'}) X(\omega_1)}{(2i\epsilon - \omega_k - \omega_{k'}) (E/2 - E_{p''} + i\epsilon - m + \omega_{k'}) (E/2 - E_{p''} + 2i\epsilon - \omega_1 + \omega_{k'})} \\
 & + \frac{f(k, E/2 - E_{p''} + i\epsilon - \omega_{k'}) f_0(k') g(E/2 - E_{p''} + i\epsilon - \omega_{k'}) Y(\omega_2)}{(2i\epsilon - \omega_k - \omega_{k'}) (E/2 - E_{p''} + i\epsilon - \omega_2 + \omega_{k'})} \\
 & + \frac{f(k, E/2 - E_{p''} + i\epsilon - \omega_{k'}) g(E/2 - E_{p''} + i\epsilon - \omega_{k'}) X(\omega_1) Y(\omega_2)}{(2i\epsilon - \omega_k - \omega_{k'}) (E/2 - E_{p''} + 2i\epsilon - \omega_1 + \omega_{k'}) (E/2 - E_{p''} + i\epsilon - \omega_2 + \omega_{k'})} \\
 & = \int_0^\infty dp'' (p'')^2 f(k, m) f(k', m) \\
 & \frac{f(k, E/2 - E_{p''} + i\epsilon - \omega_{k'}) g(E/2 - E_{p''} + i\epsilon - \omega_{k'})}{2i\epsilon - \omega_k - \omega_{k'}} \\
 & \left(\frac{Z f_0(k')}{(E/2 - E_{p''} + i\epsilon - m + \omega_{k'})} + \frac{ZX(\omega_1)}{(E/2 - E_{p''} + i\epsilon - m + \omega_{k'}) (E/2 - E_{p''} + 2i\epsilon - \omega_1 + \omega_{k'})} \right) \\
 & + \frac{f_0(k') Y(\omega_2)}{(E/2 - E_{p''} + i\epsilon - \omega_2 + \omega_{k'})} + \frac{X(\omega_1) Y(\omega_2)}{(E/2 - E_{p''} + 2i\epsilon - \omega_1 + \omega_{k'}) (E/2 - E_{p''} + i\epsilon - \omega_2 + \omega_{k'})} \\
 & = \int_0^\infty dp'' (p'')^2 f(k, m) f(k', m) \\
 & \frac{f(k, E/2 - E_{p''} + i\epsilon - \omega_{k'}) g(E/2 - E_{p''} + i\epsilon - \omega_{k'})}{2i\epsilon - \omega_k - \omega_{k'}} \\
 & \left(\frac{Z}{E/2 - E_{p''} + i\epsilon - m + \omega_{k'}} + \frac{Y(\omega_2)}{E/2 - E_{p''} + i\epsilon - \omega_2 + \omega_{k'}} \right) \\
 & \left(f_0(k') + \frac{X(\omega_1)}{E/2 - E_{p''} + 2i\epsilon - \omega_1 + \omega_{k'}} \right) \\
 & = \int_0^\infty dp'' (p'')^2 f(k, m) f(k', m) \\
 & \frac{f(k, E/2 - E_{p''} + i\epsilon - \omega_{k'}) g(E/2 - E_{p''} + i\epsilon - \omega_{k'})}{2i\epsilon - \omega_k - \omega_{k'}} g(E/2 - E_{p''} + \omega_{k'}) f(k', E/2 - E_{p''} + \omega_{k'})
 \end{aligned} \tag{D.28}$$

Factorisation (2)

We group all terms which have $(E/2 - E_{p''} + 3i\epsilon - m - \omega_k)(-E/2 + E_{p''} - i\epsilon + m - \omega_{k'})$ in the denominator

$$\begin{aligned}
 & \int_0^\infty dp'' (p'')^2 f(k, m) f(k', m) \\
 & \frac{Z f(k, E - 2E_{p''} + 2i\epsilon - m) f_0(k') g(E - 2E_{p''} + 2i\epsilon - m)}{(E/2 - E_{p''} + 3i\epsilon - m - \omega_k)(-E/2 + E_{p''} - i\epsilon + m - \omega_{k'})} \\
 & + \frac{Z f(k, E - 2E_{p''} + 2i\epsilon - m) g(E - 2E_{p''} + 2i\epsilon - m) X(\omega_1)}{(i\epsilon + m - \omega_1)(E/2 - E_{p''} + 3i\epsilon - m - \omega_k)(-E/2 + E_{p''} - i\epsilon + m - \omega_{k'})} \\
 & = \int_0^\infty dp'' (p'')^2 f(k, m) f(k', m) \\
 & \frac{Z f(k, E - 2E_{p''} + 2i\epsilon - m) g(E - 2E_{p''} + 2i\epsilon - m)}{(E/2 - E_{p''} + 3i\epsilon - m - \omega_k)(-E/2 + E_{p''} - i\epsilon + m - \omega_{k'})} \left(f_0(k') + \frac{X(\omega_1)}{i\epsilon + m - \omega_1} \right) \\
 & = \int_0^\infty dp'' (p'')^2 f(k, m) f(k', m) \\
 & \frac{Z f(k, E - 2E_{p''} + 2i\epsilon - m) g(E - 2E_{p''} + 2i\epsilon - m)}{(E/2 - E_{p''} + 3i\epsilon - m - \omega_k)(-E/2 + E_{p''} - i\epsilon + m - \omega_{k'})} f(k', m)
 \end{aligned} \tag{D.29}$$

Factorisation (3)

We group all terms which have $(E/2 - E_{p''} + 4i\epsilon - \omega_1 - \omega_k)(-E/2 + E_{p''} - 2i\epsilon + \omega_1 - \omega_{k'})$ in the denominator

$$\begin{aligned}
 & \int_0^\infty dp'' (p'')^2 f(k, m) f(k', m) \\
 & \frac{Z f(k, E - 2E_{p''} + 3i\epsilon - \omega_1) g(E - 2E_{p''} + 3i\epsilon - \omega_1) X(\omega_1)}{(-i\epsilon - m + \omega_1)(E/2 - E_{p''} + 4i\epsilon - \omega_1 - \omega_k)(-E/2 + E_{p''} - 2i\epsilon + \omega_1 - \omega_{k'})} \\
 & + \frac{f(k, E - 2E_{p''} + 3i\epsilon - \omega_1) g(E - 2E_{p''} + 3i\epsilon - \omega_1) X(\omega_1) Y(\omega_2)}{(-i\epsilon + \omega_1 - \omega_2)(E/2 - E_{p''} + 4i\epsilon - \omega_1 - \omega_k)(-E/2 + E_{p''} - 2i\epsilon + \omega_1 - \omega_{k'})} \\
 & = \int_0^\infty dp'' (p'')^2 f(k, m) f(k', m) \\
 & \frac{f(k, E - 2E_{p''} + 3i\epsilon - \omega_1) g(E - 2E_{p''} + 3i\epsilon - \omega_1) X(\omega_1)}{(E/2 - E_{p''} + 4i\epsilon - \omega_1 - \omega_k)(-E/2 + E_{p''} - 2i\epsilon + \omega_1 - \omega_{k'})} \\
 & \left(\frac{Z}{-i\epsilon - m + \omega_1} + \frac{Y(\omega_2)}{-i\epsilon + \omega_1 - \omega_2} \right) \\
 & = \int_0^\infty dp'' (p'')^2 f(k, m) f(k', m) \\
 & \frac{f(k, E - 2E_{p''} + 3i\epsilon - \omega_1) g(E - 2E_{p''} + 3i\epsilon - \omega_1) X(\omega_1)}{(E/2 - E_{p''} + 4i\epsilon - \omega_1 - \omega_k)(-E/2 + E_{p''} - 2i\epsilon + \omega_1 - \omega_{k'})} g^*(\omega_1)
 \end{aligned} \tag{D.30}$$

Factorisation (4)

We group all terms which have $(E/2 - E_{p''} + 3i\epsilon - \omega_2 - \omega_k) (-E/2 + E_{p''} - i\epsilon + \omega_2 - \omega_{k'})$ in the denominator

$$\begin{aligned}
 & \int_0^\infty dp'' (p'')^2 f(k, m) f(k', m) \\
 & \frac{f(k, E - 2E_{p''} + 2i\epsilon - \omega_2) f_0(k') g(E - 2E_{p''} + 2i\epsilon - \omega_2) Y(\omega_2)}{(E/2 - E_{p''} + 3i\epsilon - \omega_2 - \omega_k) (-E/2 + E_{p''} - i\epsilon + \omega_2 - \omega_{k'})} \\
 & + \frac{f(k, E - 2E_{p''} + 2i\epsilon - \omega_2) g(E - 2E_{p''} + 2i\epsilon - \omega_2) X(\omega_1) Y(\omega_2)}{(i\epsilon - \omega_1 + \omega_2) (E/2 - E_{p''} + 3i\epsilon - \omega_2 - \omega_k) (-E/2 + E_{p''} - i\epsilon + \omega_2 - \omega_{k'})} \\
 & = \int_0^\infty dp'' (p'')^2 f(k, m) f(k', m) \\
 & \frac{f(k, E - 2E_{p''} + 2i\epsilon - \omega_2) g(E - 2E_{p''} + 2i\epsilon - \omega_2) Y(\omega_2)}{(E/2 - E_{p''} + 3i\epsilon - \omega_2 - \omega_k) (-E/2 + E_{p''} - i\epsilon + \omega_2 - \omega_{k'})} \left(f_0(k') + \frac{X(\omega_1)}{i\epsilon - \omega_1 + \omega_2} \right) \\
 & = \int_0^\infty dp'' (p'')^2 f(k, m) f(k', m) \\
 & \frac{f(k, E - 2E_{p''} + 2i\epsilon - \omega_2) g(E - 2E_{p''} + 2i\epsilon - \omega_2) Y(\omega_2)}{(E/2 - E_{p''} + 3i\epsilon - \omega_2 - \omega_k) (-E/2 + E_{p''} - i\epsilon + \omega_2 - \omega_{k'})} f(k', \omega_2)
 \end{aligned} \tag{D.31}$$

Final expression

Therefore, our final expression consists of four terms in our p'' integral

$$\begin{aligned}
 & \int_0^\infty dp'' (p'')^2 f(k, m) f(k', m) \\
 & \frac{f(k, E/2 - E_{p''} + i\epsilon - \omega_{k'}) g(E/2 - E_{p''} + i\epsilon - \omega_{k'})}{2i\epsilon - \omega_k - \omega_{k'}} \\
 & \quad \times g(E/2 - E_{p''} + \omega_{k'}) f(k', E/2 - E_{p''} + \omega_{k'}) \\
 & + \frac{Z f(k, E - 2E_{p''} + 2i\epsilon - m) g(E - 2E_{p''} + 2i\epsilon - m)}{(E/2 - E_{p''} + 3i\epsilon - m - \omega_k) (-E/2 + E_{p''} - i\epsilon + m - \omega_{k'})} f(k', m) \\
 & + \frac{f(k, E - 2E_{p''} + 3i\epsilon - \omega_1) g(E - 2E_{p''} + 3i\epsilon - \omega_1) X(\omega_1)}{(E/2 - E_{p''} + 4i\epsilon - \omega_1 - \omega_k) (-E/2 + E_{p''} - 2i\epsilon + \omega_1 - \omega_{k'})} g^*(\omega_1) \\
 & + \frac{f(k, E - 2E_{p''} + 2i\epsilon - \omega_2) g(E - 2E_{p''} + 2i\epsilon - \omega_2) Y(\omega_2)}{(E/2 - E_{p''} + 3i\epsilon - \omega_2 - \omega_k) (-E/2 + E_{p''} - i\epsilon + \omega_2 - \omega_{k'})} f(k', \omega_2)
 \end{aligned} \tag{D.32}$$

Chapter E

Unitary $NN - \pi NN$ equations

E.1 Numerical Unitary $NN - \pi NN$ equations

One of our goals in the numerical calculation of the 4-dimensional πNN convolution equations is to determine the effect of consistent nucleon dressing. We also want to determine whether the 4-dimensional πNN convolution equations are able to better reproduce experimental data in comparison to equations without nucleon dressing. In order to make these comparisons, we will use the Afnan and Blankleider equations [33], which we will refer to as the 3D πNN equations or simply as the 3D equations.

For scattering processes with an initial NN state, the antisymmetrised partial wave 3D πNN equations with separable potentials are:

$$\begin{aligned}
 X_{K'_N, K_N}^{JT}(p', p; E) &= Z_{K'_N, K_N}^{JT}(p', p; E) \\
 &+ \sum_{K''_N} \int dp'' p''^2 Z_{K'_N, K''_N}^{JT}(p', p''; E) \frac{1}{2} \tau_{K''_N}(e_{N, p''}) X_{K''_N, K_N}^{JT}(p'', p; E) \\
 &+ \sum_{K''_d} \int dp'' p''^2 Z_{K'_N, K''_d}^{JT}(p', p''; E) \tau_{K''_d}(e_{d, p''}) X_{K''_d, K_N}^{JT}(p'', p; E) \\
 &+ \sum_{K''_\Delta} \int dp'' p''^2 Z_{K'_N, K''_\Delta}^{JT}(p', p''; E) \tau_{K''_\Delta}(e_{\Delta, p''}) X_{K''_\Delta, K_N}^{JT}(p'', p; E),
 \end{aligned} \tag{E.1}$$

$$\begin{aligned}
 X_{K'_\Delta, K_N}^{JT}(p', p; E) &= Z_{K'_\Delta, K_N}^{JT}(p', p; E) \\
 &+ \sum_{K''_N} \int dp'' p''^2 Z_{K'_\Delta, K''_N}^{JT}(p', p''; E) \frac{1}{2} \tau_{K''_N}(e_{N, p''}) X_{K''_N, K_N}^{JT}(p'', p; E) \\
 &+ \sum_{K''_d} \int dp'' p''^2 Z_{K'_\Delta, K''_d}^{JT}(p', p''; E) \tau_{K''_d}(e_{d, p''}) X_{K''_d, K_N}^{JT}(p'', p; E) \\
 &+ \sum_{K''_\Delta} \int dp'' p''^2 Z_{K'_\Delta, K''_\Delta}^{JT}(p', p''; E) \tau_{K''_\Delta}(e_{\Delta, p''}) X_{K''_\Delta, K_N}^{JT}(p'', p; E),
 \end{aligned} \tag{E.2}$$

$$\begin{aligned}
 X_{K'_d, K_N}^{JT}(p', p; E) &= Z_{K'_d, K_N}^{JT}(p', p; E) \\
 &+ \sum_{K''_N} \int dp'' p''^2 Z_{K'_d, K''_N}^{JT}(p', p''; E) \frac{1}{2} \tau_{K''_N}(e_{N, p''}) X_{K''_N, K_N}^{JT}(p'', p; E) \\
 &+ \sum_{K''_\Delta} \int dp'' p''^2 Z_{K'_d, K''_\Delta}^{JT}(p', p''; E) \tau_{K''_\Delta}(e_{\Delta, p''}) X_{K''_\Delta, K_N}^{JT}(p'', p; E).
 \end{aligned} \tag{E.3}$$

For scattering processes with a initial πd state, the 3D πNN equations are given as

$$\begin{aligned}
 X_{K'_d, K_d}^{JT}(p', p; E) &= \sum_{K''_N} \int dp'' p''^2 Z_{K'_d, K''_N}^{JT}(p', p''; E) \frac{1}{2} \tau_{K''_N}(e_{N, p''}) X_{K''_N, K_d}^{JT}(p'', p; E) \\
 &+ \sum_{K''_\Delta} \int dp'' p''^2 Z_{K'_d, K''_\Delta}^{JT}(p', p''; E) \tau_{K''_\Delta}(e_{\Delta, p''}) X_{K''_\Delta, K_d}^{JT}(p'', p; E),
 \end{aligned} \tag{E.4}$$

$$\begin{aligned}
 X_{K'_\Delta, K_d}^{JT}(p', p; E) &= Z_{K'_\Delta, K_d}^{JT}(p', p; E) \\
 &+ \sum_{K''_N} \int dp'' p''^2 Z_{K'_\Delta, K''_N}^{JT}(p', p''; E) \frac{1}{2} \tau_{K''_N}(e_{N,p''}) X_{K''_N, K_d}^{JT}(p'', p; E) \\
 &+ \sum_{K''_d} \int dp'' p''^2 Z_{K'_\Delta, K''_d}^{JT}(p', p''; E) \tau_{K''_d}(e_{d,p''}) X_{K''_d, K_d}^{JT}(p'', p; E) \\
 &+ \sum_{K''_\Delta} \int dp'' p''^2 Z_{K'_\Delta, K''_\Delta}^{JT}(p', p''; E) \tau_{K''_\Delta}(e_{\Delta,p''}) X_{K''_\Delta, K_d}^{JT}(p'', p; E),
 \end{aligned} \tag{E.5}$$

$$\begin{aligned}
 X_{K'_N, K_d}^{JT}(p', p; E) &= Z_{K'_N, K_d}^{JT}(p', p; E) \\
 &+ \sum_{K''_N} \int dp'' p''^2 Z_{K'_N, K''_N}^{JT}(p', p''; E) \frac{1}{2} \tau_{K''_N}(e_{N,p''}) X_{K''_N, K_d}^{JT}(p'', p; E) \\
 &+ \sum_{K''_d} \int dp'' p''^2 Z_{K'_N, K''_d}^{JT}(p', p''; E) \tau_{K''_d}(e_{d,p''}) X_{K''_d, K_d}^{JT}(p'', p; E) \\
 &+ \sum_{K''_\Delta} \int dp'' p''^2 Z_{K'_N, K''_\Delta}^{JT}(p', p''; E) \tau_{K''_\Delta}(e_{\Delta,p''}) X_{K''_\Delta, K_d}^{JT}(p'', p; E),
 \end{aligned} \tag{E.6}$$

where τ_{K_N} is the different-time dressing propagator in [48] with the proper renormalisation. The energy inputs into the τ functions are given as

$$e_{N,p} = E - \frac{p^2}{m_N}, \tag{E.7a}$$

$$e_{\Delta,p} = E - \frac{p^2}{2m_N} - \frac{p^2}{2(m_N + m_\pi)} - m_N, \tag{E.7b}$$

$$e_{d,p} = E - (p^2 + m_\pi^2)^{1/2} - \frac{p^2}{4m_N}. \tag{E.7c}$$

It should be clear that these equations are not the 3-dimensional πNN convolution equations of Equation 3.123, and the only nucleon dressing is present in the different-time dressing propagator.

E.1.1 3-dimensional Z -diagram

The 3-dimensional Z -diagram is similarly defined in Equation 4.6 in Chapter 4, where we modify the Γ function to be

$$\Gamma_{k',k}^L(p', p; E) = \frac{1}{2} \int_{-1}^1 \frac{q'^{-l} h_{k'}(q') h_k(q) q^{-l}}{D(x, p', p; E)} P_L(x) dx. \tag{E.8}$$

In this equation, $P_L(x)$ is the Legendre polynomial of order L , while $h_{k'}(q')$ is the form factor for the two-body channel k' corresponding to relative orbital angular momentum l' and equivalent for $h_k(q)$. When h_k corresponds to the dressed vertex function f e.g. the

nucleon channel, h_k has an energy dependence. To account for the momentum component, we use Galilean invariance of the dressed vertex and shift the energy by the energy of the spectator nucleon. As a result, the energy dependence is $E - \frac{p^2}{m_N} - m_N$, where p is either p' or p depending on which channel is the nucleon channel. The function $D(x, p', p; E)$ we refer to as the denominator function and is dependent on the initial and final state described by the Z -diagram:

1. *Initial $\neq \pi d$ and final $\neq \pi d$*

$$D(x, p', p; E) = E^+ - \frac{p'^2}{2m_N} - \frac{p^2}{2m_N} - 2m_N - \sqrt{m_\pi^2 + p'^2 + p^2 + 2p'p x} \quad (\text{E.9})$$

2. *Initial = πd and final $\neq \pi d$*

$$D(x, p', p; E) = E^+ - \frac{p'^2}{2m_N} - (p^2 + m_\pi^2)^{1/2} - 2m_N - \sqrt{m_\pi^2 + p'^2 + p^2 + 2p'p x} \quad (\text{E.10})$$

3. *Initial $\neq \pi d$ and final = πd*

$$D(x, p', p; E) = E^+ - (p'^2 + m_\pi^2)^{1/2} - \frac{p^2}{2m_N} - 2m_N - \frac{p'^2 + p^2 + 2p'p x}{2m_N} \quad (\text{E.11})$$

We use contour rotation to calculate the scattering amplitudes and as a result, we can calculate the x integral of the 3D Z -diagram directly as the pole in the x integral is avoided due to the contour rotation.

E.2 Antisymmetry

Let us discuss the antisymmetry of the πNN equations. The formalism of antisymmetry for the 3D πNN equations is equivalent to the πNN convolution equations, despite us describing the antisymmetry using the 3D equations.

The formula given by Afnan and Thomas [29] gives

$$\langle (\beta\gamma)\alpha | G_0(E) | (\gamma\alpha)\beta \rangle \quad (\text{E.12})$$

which has assumed cyclic ordering where α, β and γ are a cyclic permutation of 1, 2 and 3. We adopt the scheme where we want the pion to coupled first in the πN system and for nucleon 1 to be coupled first in the NN system. We also would the quasiparticle to be coupled first. In the πNN system, there are 9 possible Z -diagrams

1. $Z_{dd} = 0$

2. $Z_{\Delta d} = \langle (\pi N_2)N_1 | G_0(E) | (N_1 N_2)\pi \rangle$
3. $Z_{Nd} = \langle (\pi N_2)N_1 | G_0(E) | (N_1 N_2)\pi \rangle$
4. $Z_{d\Delta} = \langle (N_1 N_2)\pi | G_0(E) | (\pi N_2)N_1 \rangle$
5. $Z_{\Delta\Delta} = \langle (\pi N_1)N_2 | G_0(E) | (\pi N_2)N_1 \rangle$
6. $Z_{N\Delta} = \langle (\pi N_2)N_1 | G_0(E) | (\pi N_1)N_2 \rangle$
7. $Z_{dN} = \langle (N_1 N_2)\pi | G_0(E) | (\pi N_2)N_1 \rangle$
8. $Z_{\Delta N} = \langle (\pi N_2)N_1 | G_0(E) | (\pi N_1)N_2 \rangle$
9. $Z_{NN} = \langle (\pi N_2)N_1 | G_0(E) | (\pi N_1)N_2 \rangle$

These amplitudes should not have a cyclic ordering if we were to label α as the first spectator, β as the second spectator and γ as the exchange particle. We also use the labelling convention $N_1 = 1, N_2 = 2$ and $\pi = 3$. Thus we must introduce a phase to obtain cyclic ordering. For example, consider the 2nd Z -diagram, where $\alpha = 1, \beta = 3$ and $\gamma = 2$. This would correspond to $\langle (32)1 | G_0(E) | (12)3 \rangle = \langle (\beta\gamma)\alpha | G_0(E) | (\alpha\gamma)\beta \rangle$. To obtain the cyclic ordering consistent with Afnan and Thomas, we need to introduce a phase which with swap α with γ in the ket on the right-hand side $\langle (32)1 | G_0(E) | (12)3 \rangle = \langle (\beta\gamma)\alpha | G_0(E) | (\alpha\gamma)\beta \rangle = (\text{phase } \alpha \leftrightarrow \gamma) \langle (\beta\gamma)\alpha | G_0(E) | (\gamma\alpha)\beta \rangle$. Therefore, the phases for the remaining Z -diagrams are as follows

2.
$$\begin{aligned} Z_{\Delta d} &= \langle (32)1 | G_0(E) | (12)3 \rangle = \langle (\beta\gamma)\alpha | G_0(E) | (\alpha\gamma)\beta \rangle \\ &= (\text{phase } \alpha \leftrightarrow \gamma) \langle (\beta\gamma)\alpha | G_0(E) | (\gamma\alpha)\beta \rangle \end{aligned}$$
3.
$$\begin{aligned} Z_{Nd} &= \langle (32)1 | G_0(E) | (12)3 \rangle = \langle (\beta\gamma)\alpha | G_0(E) | (\alpha\gamma)\beta \rangle \\ &= (\text{phase } \alpha \leftrightarrow \gamma) \langle (\beta\gamma)\alpha | G_0(E) | (\gamma\alpha)\beta \rangle \end{aligned}$$
4.
$$\begin{aligned} Z_{d\Delta} &= \langle (12)3 | G_0(E) | (32)1 \rangle = \langle (\beta\gamma)\alpha | G_0(E) | (\alpha\gamma)\beta \rangle \\ &= (\text{phase } \alpha \leftrightarrow \gamma) \langle (\beta\gamma)\alpha | G_0(E) | (\gamma\alpha)\beta \rangle \end{aligned}$$
5.
$$\begin{aligned} Z_{\Delta\Delta} &= \langle (32)1 | G_0(E) | (31)2 \rangle = \langle (\gamma\beta)\alpha | G_0(E) | (\gamma\alpha)\beta \rangle \\ &= (\text{phase } \beta \leftrightarrow \gamma) \langle (\beta\gamma)\alpha | G_0(E) | (\gamma\alpha)\beta \rangle \end{aligned}$$
6.
$$\begin{aligned} Z_{N\Delta} &= \langle (32)1 | G_0(E) | (31)2 \rangle = \langle (\gamma\beta)\alpha | G_0(E) | (\gamma\alpha)\beta \rangle \\ &= (\text{phase } \beta \leftrightarrow \gamma) \langle (\beta\gamma)\alpha | G_0(E) | (\gamma\alpha)\beta \rangle \end{aligned}$$

7. $Z_{dN} = \langle (12)3 | G_0(E) | (32)1 \rangle = \langle (\beta\gamma)\alpha | G_0(E) | (\alpha\gamma)\beta \rangle$
 $= (\text{phase } \alpha \leftrightarrow \gamma) \langle (\beta\gamma)\alpha | G_0(E) | (\gamma\alpha)\beta \rangle$
8. $Z_{\Delta N} = \langle (32)1 | G_0(E) | (31)2 \rangle = \langle (\gamma\beta)\alpha | G_0(E) | (\gamma\alpha)\beta \rangle$
 $= (\text{phase } \beta \leftrightarrow \gamma) \langle (\beta\gamma)\alpha | G_0(E) | (\gamma\alpha)\beta \rangle$
9. $Z_{NN} = \langle (32)1 | G_0(E) | (31)2 \rangle = \langle (\gamma\beta)\alpha | G_0(E) | (\gamma\alpha)\beta \rangle$
 $= (\text{phase } \beta \leftrightarrow \gamma) \langle (\beta\gamma)\alpha | G_0(E) | (\gamma\alpha)\beta \rangle$

One can see that when the amplitude contains a πd state, then the phase involves the switching of $\alpha \leftrightarrow \gamma$, otherwise the phase involves the switching of $\beta \leftrightarrow \gamma$. Therefore we must introduce the phase,

$$\begin{aligned} \text{phase} &= (-1)^{l_\beta + s_\gamma + s_\alpha - s_\beta + \tau_\gamma + \tau_\alpha - t_\beta} \quad \text{if the amplitude involves } \pi d, \\ \text{phase} &= (-1)^{l_\alpha + s_\gamma + s_\beta - s_\alpha + \tau_\gamma + \tau_\beta - t_\alpha} \quad \text{otherwise.} \end{aligned} \quad (\text{E.13})$$

We can now discuss antisymmetry, in which we follow the antisymmetry procedure of Blankleider [178]. We represent the wave-function of the two-body state as Ψ , while $\chi(\mathbf{p})$ is the plane wave of the appropriate spectator particle. We also denote $\chi_N(\sigma, \sigma'; \mathbf{p})$ as the two nucleon plane wave with nucleon 1 having internal quantum numbers and momentum given by (σ, \mathbf{p}) and with nucleon 2 similarly specified by $(\sigma', -\mathbf{p})$. Therefore, with explicit particle labelling we write the states for πd , $N\Delta$ and NN as

$$|\Psi_d(12), \chi_\pi(\mathbf{p})\rangle, \quad (\text{E.14a})$$

$$|\Psi_{\Delta_j}(j3), \chi_{N_i}(\mathbf{p})\rangle, \quad (\text{E.14b})$$

$$|\chi_N(\sigma, \sigma'; \mathbf{p})\rangle. \quad (\text{E.14c})$$

Now, if we introduce separable potentials for the two-body interactions, we can write our antisymmetric states in terms of the two-body form factors h as the form factors are directly proportional to the wave-function. We must also consider the form factor $f(i)$, which will give us our πNN vertex

$$|f(1)\rangle = f(1) |\chi_N(\sigma, \sigma'; \mathbf{p})\rangle = |f_{N_1}^\sigma, \chi_{N_2}(\sigma', -\mathbf{p})\rangle, \quad (\text{E.15a})$$

$$|f(2)\rangle = f(2) |\chi_N(\sigma, \sigma'; \mathbf{p})\rangle = |f_{N_2}^{\sigma'}, \chi_{N_1}(\sigma, \mathbf{p})\rangle. \quad (\text{E.15b})$$

We now define our antisymmetric states. First, defining the NN antisymmetric state as

$$|\chi_N\rangle^{\text{AS}} \equiv \frac{1}{\sqrt{2}} (|\chi_N(\sigma, \sigma'; \mathbf{p})\rangle - |\chi_N(\sigma', \sigma; -\mathbf{p})\rangle). \quad (\text{E.16})$$

The antisymmetric states that we explicitly use to calculate our antisymmetric Z -diagrams are

$$|h_d\pi\rangle^{\text{AS}} \equiv |h_d(12), \chi_\pi(\mathbf{p})\rangle, \quad (\text{E.17a})$$

$$|h_\Delta N\rangle^{\text{AS}} \equiv \frac{1}{\sqrt{2}} (|h_{\Delta_2}(23), \chi_{N_1}(\mathbf{p})\rangle - |h_{\Delta_1}(13), \chi_{N_2}(\mathbf{p})\rangle), \quad (\text{E.17b})$$

$$\begin{aligned} |f(1)\rangle^{\text{AS}} &\equiv f(1) |\chi_N\rangle^{\text{AS}} = \frac{1}{\sqrt{2}} (f(1) |\chi_N(\sigma, \sigma'; \mathbf{p})\rangle - f(1) |\chi_N(\sigma', \sigma; -\mathbf{p})\rangle) \\ &= \frac{1}{\sqrt{2}} \left(|f_{N_1}^\sigma, \chi_{N_2}(\sigma', -\mathbf{p})\rangle - |f_{N_1}^{\sigma'}, \chi_{N_2}(\sigma, \mathbf{p})\rangle \right), \end{aligned} \quad (\text{E.17c})$$

$$\begin{aligned} |f(2)\rangle^{\text{AS}} &\equiv f(2) |\chi_N\rangle^{\text{AS}} = \frac{1}{\sqrt{2}} (f(2) |\chi_N(\sigma, \sigma'; \mathbf{p})\rangle - f(2) |\chi_N(\sigma', \sigma; -\mathbf{p})\rangle) \\ &= \frac{1}{\sqrt{2}} \left(|f_{N_2}^{\sigma'}, \chi_{N_1}(\sigma, \mathbf{p})\rangle - |f_{N_2}^\sigma, \chi_{N_1}(\sigma', -\mathbf{p})\rangle \right). \end{aligned} \quad (\text{E.17d})$$

We now define the antisymmetric Z -diagrams

$$Z_{Nd}^{\text{AS}} = \sum_i^{\text{AS}} \langle f(i) | G_0(E) | h_d\pi \rangle^{\text{AS}}, \quad (\text{E.18a})$$

$$Z_{N\Delta}^{\text{AS}} = \sum_i^{\text{AS}} \langle f(i) | G_0(E) | h_\Delta N \rangle^{\text{AS}}, \quad (\text{E.18b})$$

$$Z_{\Delta d}^{\text{AS}} = {}^{\text{AS}} \langle h_\Delta N | G_0(E) | h_d\pi \rangle^{\text{AS}}, \quad (\text{E.18c})$$

$$Z_{\Delta\Delta}^{\text{AS}} = {}^{\text{AS}} \langle h_\Delta N | G_0(E) | h_\Delta N \rangle^{\text{AS}}, \quad (\text{E.18d})$$

$$Z_{NN}^{\text{AS}} = \sum_{ij}^{\text{AS}} \langle f(i) | G_0(E) | f(j) \rangle^{\text{AS}}, \quad (\text{E.18e})$$

with the reverse processes similarly defined. Now we can use our definition of the antisymmetric states in these Z -diagrams. For example, for Z_{Nd}^{AS}

$$\begin{aligned} Z_{Nd}^{\text{AS}} &= \sum_i^{\text{AS}} \langle f(i) | G_0(E) | h_d\pi \rangle^{\text{AS}} \\ &= \frac{1}{\sqrt{2}} \left(\langle f_{N_1}^\sigma, \chi_{N_2}(\sigma', -\mathbf{p}') | G_0(E) | h_d(12), \chi_\pi(\mathbf{p}) \rangle - \langle f_{N_1}^{\sigma'}, \chi_{N_2}(\sigma, \mathbf{p}') | G_0(E) | h_d(12), \chi_\pi(\mathbf{p}) \rangle \right) \\ &\quad + \langle f_{N_2}^{\sigma'}, \chi_{N_1}(\sigma, \mathbf{p}') | G_0(E) | h_d(12), \chi_\pi(\mathbf{p}) \rangle - \langle f_{N_2}^\sigma, \chi_{N_1}(\sigma', -\mathbf{p}') | G_0(E) | h_d(12), \chi_\pi(\mathbf{p}) \rangle. \end{aligned} \quad (\text{E.19})$$

Our goal is to now represent Z_{Nd}^{AS} in terms of one of these 4 matrix elements. We want Z_{Nd}^{AS} to be in terms of the Z -diagram with the specific ordering that was discussed earlier. This means we would want Z_{Nd}^{AS} to be represented in terms of $\langle f_{N_2}^{\sigma'}, \chi_{N_1}(\sigma, \mathbf{p}') | G_0(E) | h_d(12), \chi_\pi(\mathbf{p}) \rangle$. By interchanging the nucleon labels and applying the antisymmetry property of the deuteron of

the 1st and 2nd matrix element

$$\begin{aligned}
 & Z_{Nd}^{\text{AS}} \\
 &= \frac{1}{\sqrt{2}} \left(\langle f_{N_2}^\sigma, \chi_{N_1}(\sigma', -\mathbf{p}') | G_0(E) | h_d(21), \chi_\pi(\mathbf{p}) \rangle - \langle f_{N_2}^{\sigma'}, \chi_{N_1}(\sigma, \mathbf{p}') | G_0(E) | h_d(21), \chi_\pi(\mathbf{p}) \rangle \right) \\
 &\quad + \langle f_{N_2}^{\sigma'}, \chi_{N_1}(\sigma, \mathbf{p}') | G_0(E) | h_d(12), \chi_\pi(\mathbf{p}) \rangle - \langle f_{N_2}^\sigma, \chi_{N_1}(\sigma', -\mathbf{p}') | G_0(E) | h_d(12), \chi_\pi(\mathbf{p}) \rangle \\
 &= \frac{1}{\sqrt{2}} \left(- \langle f_{N_2}^\sigma, \chi_{N_1}(\sigma', -\mathbf{p}') | G_0(E) | h_d(12), \chi_\pi(\mathbf{p}) \rangle + \langle f_{N_2}^{\sigma'}, \chi_{N_1}(\sigma, \mathbf{p}') | G_0(E) | h_d(12), \chi_\pi(\mathbf{p}) \rangle \right) \\
 &\quad + \langle f_{N_2}^{\sigma'}, \chi_{N_1}(\sigma, \mathbf{p}') | G_0(E) | h_d(12), \chi_\pi(\mathbf{p}) \rangle - \langle f_{N_2}^\sigma, \chi_{N_1}(\sigma', -\mathbf{p}') | G_0(E) | h_d(12), \chi_\pi(\mathbf{p}) \rangle \\
 &= \sqrt{2} \left(\langle f_{N_2}^{\sigma'}, \chi_{N_1}(\sigma, \mathbf{p}') | G_0(E) | h_d(12), \chi_\pi(\mathbf{p}) \rangle - \langle f_{N_2}^\sigma, \chi_{N_1}(\sigma', -\mathbf{p}') | G_0(E) | h_d(12), \chi_\pi(\mathbf{p}) \rangle \right). \tag{E.20}
 \end{aligned}$$

Now the only difference between the two matrix elements is the momenta and quantum numbers for the NN state. We can interchange the momenta of the two nucleons by introducing a factor of $(-1)^L$, while introducing a factor of $(-1)^{S-s_1-s_2}$ for the spin quantum numbers and $(-1)^{T-t_1-t_2}$ for the isospin quantum numbers. But, since the two nucleons are identical, they obviously have identical spin and isospin quantum numbers. As the spin and isospin of a nucleon is $1/2$, the sum of s_1, s_2, t_1 and t_2 will result in -2 , which will contribute a factor of $(-1)^{-2} = 1$ to the overall factor. Therefore, the interchange of the momenta and quantum numbers is done by introducing a factor of $(-1)^{L+S+T}$. Thus

$$\begin{aligned}
 & \langle f_{N_2}^\sigma, \chi_{N_1}(\sigma', -\mathbf{p}') | G_0(E) | h_d(12), \chi_\pi(\mathbf{p}) \rangle \\
 &= (-1)^{L+S+T} \langle f_{N_2}^{\sigma'}, \chi_{N_1}(\sigma, \mathbf{p}') | G_0(E) | h_d(12), \chi_\pi(\mathbf{p}) \rangle. \tag{E.21}
 \end{aligned}$$

However, $(-1)^{L+S+T} = -1$ as the nucleons obey Fermi-Dirac statistics and must be anti-symmetric. Therefore, Z_{Nd}^{AS} acquires a factor of $2\sqrt{2}$. Following the same procedure for the remaining Z -diagrams,

$$Z_{Nd}^{\text{AS}} = 2\sqrt{2} \langle f_{N_2}^{\sigma'}, \chi_{N_1}(\sigma, \mathbf{p}') | G_0(E) | h_d(12), \chi_\pi(\mathbf{p}) \rangle, \tag{E.22a}$$

$$Z_{N\Delta}^{\text{AS}} = -2 \langle f_{N_2}^{\sigma'}, \chi_{N_1}(\sigma, \mathbf{p}') | G_0(E) | h_{\Delta_1}(13), \chi_{N_2}(\mathbf{p}) \rangle, \tag{E.22b}$$

$$Z_{\Delta d}^{\text{AS}} = \sqrt{2} \langle h_{\Delta_2}(23) \chi_{N_1}(\mathbf{p}') | G_0(E) | h_d(12) \chi_\pi(\mathbf{p}) \rangle, \tag{E.22c}$$

$$Z_{\Delta\Delta}^{\text{AS}} = - \langle h_{\Delta_2}(23) \chi_{N_1}(\mathbf{p}') | G_0(E) | h_{\Delta_1}(13) \chi_{N_2}(\mathbf{p}) \rangle, \tag{E.22d}$$

$$Z_{NN}^{\text{AS}} = -4 \langle f_{N_2}^{\sigma'}, \chi_{N_1}(\sigma, \mathbf{p}') | G_0(E) | f_{N_1}^\sigma, \chi_{N_2}(\sigma', \mathbf{p}) \rangle. \tag{E.22e}$$

Equivalent expressions and factors can be derived for the reverse processes, e.g. the Z -diagram Z_{dN}^{AS} will acquire a factor of $2\sqrt{2}$.

These antisymmetry factors are equivalent for both the 3-dimensional or 4-dimensional equations, except for the case of NN scattering. In the 4-dimensional equations, the extra dimension forces us to include both time-orderings of NN . We find that in the 4-dimensional equations, each time-ordering of NN acquires an antisymmetry factor of -2 .

Now if we focus on NN scattering, regardless of whether the equations are 3-dimensional or 4-dimensional, the Lippmann-Schwinger equation has the form

$$T = Z + ZG_0T. \quad (\text{E.23})$$

For NN scattering, the completeness relation for antisymmetric NN states is

$$\frac{1}{2} |\chi_N\rangle^{\text{AS AS}} \langle \chi_N| = I \quad (\text{E.24})$$

which is easy to see by acting on the antisymmetric state $|\chi_N\rangle$. If we “sandwich” our Lippmann-Schwinger equation antisymmetric NN states and use the above completeness relation, we obtain

$$T^{\text{AS}} = Z^{\text{AS}} + \frac{1}{2} Z^{\text{AS}} G_0 T^{\text{AS}} \quad (\text{E.25})$$

where $T^{\text{AS}} = {}^{\text{AS}} \langle \chi_N | T | \chi_N \rangle^{\text{AS}}$ and Z^{AS} is the same as Z_{NN}^{AS} defined earlier. Now, only the original Lippmann-Schwinger equation satisfies unitarity whereas our new equation does not due to the extra factor of $\frac{1}{2}$. So we will need to find a way to convert our antisymmetrised equation to have the same form as the original Lippmann-Schwinger equation. If we multiply our antisymmetrised equation by $\frac{1}{2}$

$$\frac{1}{2} T^{\text{AS}} = \frac{1}{2} Z^{\text{AS}} + \frac{1}{2} Z^{\text{AS}} G_0 \frac{1}{2} T^{\text{AS}}. \quad (\text{E.26})$$

We can see that we obtain an equation that has the same form as the original Lippmann-Schwinger equation. Therefore, the true physical t -matrix is half of the antisymmetric t -matrix.

Chapter F

Various numerical methods

F.1 Unitary pole expansion (UPE) method

F.1.1 Application to 1S_0 UPA in momentum space

We now present the simplest UPE, the unitary pole approximation (UPA), for a 1S_0 and $^3S_1 - ^3D_1$ potential to illustrate the method. Conventionally, we would exploit the (real) pole of the potential to perform a UPA. However for 1S_0 , the pole resides on the second energy sheet and the use of which would require that we analytically continue our analysis onto the second energy sheet. So, we will take $E = 0$ for the 1S_0 channel rather than the anti-bound state pole [206].

If we want to do a UPA to the 1S_0 potential, then $N = 1$ and $l = l' = 0$. So the eigenvalue problem reduces to

$$|\phi\rangle = -\lambda K|\phi\rangle \quad (\text{F.1})$$

Now using the expression for the form factors $|\chi\rangle$ in this eigenvalue problem

$$\begin{aligned} G_0^{1/2}|\chi\rangle &= -\lambda G_0^{1/2}V G_0^{1/2}G_0^{1/2}|\chi\rangle \\ |\chi\rangle &= -\lambda V G_0|\chi\rangle \end{aligned} \quad (\text{F.2})$$

Our normalisation condition also becomes

$$\sum_l \langle \phi_l^m | \phi_l^{m'} \rangle = \delta_{mm'} \rightarrow \langle \phi | \phi \rangle = 1 \rightarrow \langle \chi | G_0 | \chi \rangle = 1 \quad (\text{F.3})$$

We want to follow the work of Afnan and Gibson [206] by having an analytic form for the form factors, so we assume that the form factors have the form

$$\langle k | \chi_l \rangle = \sum_j b_j^l g_l(k; \beta_j) \quad (\text{F.4})$$

where

$$g_l(k; \beta) = \frac{k^l}{(k^2 + \beta^2)^{(l+2)/2}} \quad (\text{F.5})$$

For our application to the 1S_0 potential, $l = 0$ so this reduces to

$$\langle k | \chi \rangle = \sum_j b_j g(k; \beta_j) = \sum_j b_j g_j(k) \quad (\text{F.6})$$

where

$$g(k; \beta) = \frac{1}{(k^2 + \beta^2)} \quad (\text{F.7})$$

Solving the eigenvalue problem

Now, we convert the eigenvalue problem into a numerical form

$$\begin{aligned}
 \langle k|\chi\rangle &= -\lambda\langle k|VG_0|\chi\rangle \\
 \langle k|\chi\rangle &= -\lambda\int dk'(k')^2\langle k|VG_0|k'\rangle\langle k'|\chi\rangle \\
 \langle k|\chi\rangle &= -\lambda\int dk'(k')^2\langle k|V|k'\rangle G_0(k')\langle k'|\chi\rangle \\
 \chi(k) &= -\lambda\int dk'(k')^2V(k,k')G_0(k')\chi(k')
 \end{aligned} \tag{F.8}$$

Now we can use our analytic expression for the form factors in the eigenvalue problem and solve for the constants b_j and the eigenvalue λ . We can do this in two ways:

1. A collocation method, where we calculate the eigenvalue problem at different values of k (the set of k values is called collocation points $\{k_i\}$). The number of values of k we choose must equal the number of b_j as we require a square matrix

$$\begin{aligned}
 g_j(k)b_j &= -\lambda\left(\int dk'(k')^2V(k,k')G_0(k')g_j(k')\right)b_j \\
 g_j(k_i)b_j &= -\lambda\left(\int dk'(k')^2V(k_i,k')G_0(k')g_j(k')\right)b_j
 \end{aligned} \tag{F.9}$$

This gives use the generalised eigenvalue problem

$$\mathbf{G}\mathbf{b} = -\lambda\mathbf{V}\mathbf{b} \tag{F.10}$$

where the matrices in the above eigenvalue problem are

$$[\mathbf{G}]_{ij} = g_j(k_i) \tag{F.11}$$

$$[\mathbf{V}]_{ij} = \int dk'(k')^2V(k_i,k')G_0(k')g_j(k') \tag{F.12}$$

2. Follow the method for Afnan and Gibson by multiplying the left side by $g_i(k)$ and integrating over k

$$\begin{aligned}
 g_j(k)b_j &= -\lambda\left(\int dk'(k')^2V(k,k')G_0(k')g_j(k')\right)b_j \\
 g_i(k)g_j(k)b_j &= -\lambda g_i(k)\left(\int dk'(k')^2V(k,k')G_0(k')g_j(k')\right)b_j \\
 \int dk k^2 g_i(k)g_j(k)b_j &= -\lambda\left(\int dk k^2 g_i(k)\left(\int dk'(k')^2V(k,k')G_0(k')g_j(k')\right)\right)b_j
 \end{aligned} \tag{F.13}$$

which gives us the same generalised eigenvalue problem as for the collocation method, where the matrices are

$$[\mathbf{G}]_{ij} = \int dk k^2 g_i(k) g_j(k) \quad (\text{F.14})$$

$$[\mathbf{V}]_{ij} = \left(\int dk k^2 g_i(k) \left(\int dk' (k')^2 V(k, k') G_0(k') g_j(k') \right) \right) \quad (\text{F.15})$$

The matrix \mathbf{G} can be calculated analytically

$$\int_0^\infty \frac{1}{k^2 + \beta_i^2} \frac{1}{k^2 + \beta_j^2} k^2 dk = \frac{\pi}{2(\beta_i + \beta_j)} \quad (\text{F.16})$$

Once we find the constants b_j , we can use the normalisation condition to normalise these constants. The strength matrix becomes

$$C = A^{-1} B A^{-1} = B \quad (\text{F.17})$$

as $A = \langle \phi | \phi \rangle = 1$ by our normalisation condition. We can show that B is given as

$$B = \langle \phi | K | \phi \rangle = \lambda^{-1} \langle \phi | \lambda K | \phi \rangle = -\lambda^{-1} \langle \phi | \phi \rangle = -\lambda^{-1} \quad (\text{F.18})$$

F.1.2 Application to ${}^3S_1 - {}^3D_1$ UPA in momentum space

If we were to calculate a UPA for the ${}^3S_1 - {}^3D_1$ potential, we would still have no m index (as we are only doing a UPA), but l' and l take on the values 0 and 2. So the eigenvalue problem is

$$|\chi_l\rangle = -\lambda \sum_{l'} V_{l'l} G_0 |\chi_{l'}\rangle \quad (\text{F.19})$$

with the normalisation condition

$$\sum_l \langle \phi_l | \phi_l \rangle = 1 \quad (\text{F.20})$$

Again, we want an analytic form for the form factors, so we assume that the form factors have the form

$$\langle k | \chi_l \rangle = \sum_j b_j^l g_l(k; \beta_j) \quad (\text{F.21})$$

where

$$g_l(k; \beta) = \frac{k^l}{(k^2 + \beta^2)^{(l+2)/2}} \quad (\text{F.22})$$

Solving the eigenvalue problem

We convert the eigenvalue problem into a numerical form

$$\begin{aligned}
 \langle k | \chi_l \rangle &= -\lambda \sum_{l'} \langle k | V_{ll'} G_0 | \chi_{l'} \rangle \\
 \langle k | \chi_l \rangle &= -\lambda \sum_{l'} \int dk' \langle k | V_{ll'} | k' \rangle \langle k' | G_0 | \chi_{l'} \rangle \\
 \chi_l(k) &= -\lambda \sum_{l'} \int dk' V_{ll'}(k, k') G_0(k') \chi_{l'}(k')
 \end{aligned} \tag{F.23}$$

Using the method of collocation

$$\begin{aligned}
 b_j^l g_l(k, \beta_j) &= -\lambda \sum_{l'} \int dk' V_{ll'}(k, k') G_0(k') b_j^{l'} g_{l'}(k', \beta_j) \\
 b_j^l g_l(\beta_i, \beta_j) &= -\lambda \sum_{l'} \int dk' V_{ll'}(\beta_i, k') G_0(k') b_j^{l'} g_{l'}(k', \beta_j)
 \end{aligned} \tag{F.24}$$

This will give us the generalised eigenvalue problem

$$\begin{pmatrix} G_{l=0} & 0 \\ 0 & G_{l=2} \end{pmatrix} \begin{pmatrix} b_0 \\ b_2 \end{pmatrix} = -\lambda \begin{pmatrix} V_{00} & V_{02} \\ V_{20} & V_{22} \end{pmatrix} \begin{pmatrix} b_0 \\ b_2 \end{pmatrix} \tag{F.25}$$

and in more condensed notation

$$\mathbf{G}\mathbf{b} = -\lambda\mathbf{V}\mathbf{b} \tag{F.26}$$

If we were to follow the method of Afnan and Gibson by multiplying the left side by $g_i(k)$ and integrating over k

$$\begin{aligned}
 b_j^l g_l(k, \beta_j) &= -\lambda \sum_{l'} \int dk' V_{ll'}(k, k') G_0(k') b_j^{l'} g_{l'}(k', \beta_j) \\
 b_j^l \int dk k^2 g_l(k, \beta_i) g_l(k, \beta_j) &= -\lambda \sum_{l'} \left(\int dk k^2 g_l(k, \beta_i) \left(\int dk' V_{ll'}(k, k') G_0(k') g_{l'}(k', \beta_j) \right) \right) b_j^{l'}
 \end{aligned} \tag{F.27}$$

which will give us the same generalised eigenvalue problem as the collocation method.

Normalisation

Recall the normalisation condition

$$\begin{aligned}
 \sum_l \langle \phi_l | \phi_l \rangle &= 1 \\
 \sum_l \langle \chi_l | G_0 | \chi_l \rangle &= 1
 \end{aligned} \tag{F.28}$$

Let us assume that the original coefficients b will not satisfy the above normalisation condition. We introduce a normalisation constant N such that

$$N^2 \sum_l \sum_{ij} b_i^l b_j^l \int dk k^2 g_l(k, \beta_i) G_0(k) g_l(k, \beta_j) = 1 \quad (\text{F.29})$$

We can introduce new coefficients c given by

$$c_i^l = b_i^l N \quad (\text{F.30})$$

that will satisfy the normalisation condition. The normalisation constant is given as

$$N = 1 / \sqrt{\sum_l \sum_{ij} b_i^l b_j^l \int dk k^2 g_l(k, \beta_i) G_0(k) g_l(k, \beta_j)} \quad (\text{F.31})$$

Calculating the coefficients

For ${}^3S_1 - {}^3D_1$, the strength parameters are given as

$$\mathbf{C}_{W'}(N) = \mathbf{A}_l^{-1} \mathbf{B}_{W'} \mathbf{A}_l^{-1} \quad (\text{F.32})$$

in terms of the $N \times N$ matrices \mathbf{A}_l and $\mathbf{B}_{W'}$

$$\begin{aligned} \mathbf{A}_l &= \langle \phi_l | \phi_l \rangle = \langle \chi_l | G_0 | \chi_l \rangle \\ \mathbf{A}_l &= \int dk k^2 \langle \chi_l | k \rangle G_0(k) \langle k | \chi_l \rangle \\ &= \sum_{ij} b_i^l b_j^l \int dk k^2 g_l(k, \beta_i) G_0(k) g_l(k, \beta_j) \end{aligned} \quad (\text{F.33})$$

Notice that because of the normalisation condition

$$\sum_l \mathbf{A}_l = 1 \quad (\text{F.34})$$

and

$$\begin{aligned} \mathbf{B}_{W'} &= \langle \phi_l | K_{W'} | \phi_{l'} \rangle = \langle \chi_l | G_0 V_{W'} G_0 | \chi_{l'} \rangle \\ \mathbf{B}_{W'} &= \sum_{ij} b_i^l b_j^{l'} \int dk dk' k^2 (k')^2 g_l(k, \beta_i) G_0(k) V_{W'}(k, k') G_0(k') g_{l'}(k, \beta_j) \end{aligned} \quad (\text{F.35})$$

F.2 Handling a double pole

Firstly, let us consider our integral with the double pole

$$\int_0^\infty \frac{f(p)}{(p-a+i\epsilon)^2} dp \quad (\text{F.36})$$

where a is the pole ($0 < a < \infty$). This integral is equal to the following limit

$$\lim_{\eta \rightarrow 0} \int_0^{\infty} \frac{f(p)}{(p - (a + \eta) + i\epsilon)(p - a + i\epsilon)} dp \quad (\text{F.37})$$

where η is some arbitrarily small parameter. Separating this integral into separate terms

$$\lim_{\eta \rightarrow 0} \frac{1}{\eta} \left(\int_0^{\infty} \frac{f(p)}{p - (a + \eta) + i\epsilon} dp - \int_0^{\infty} \frac{f(p)}{p - a + i\epsilon} dp \right) \quad (\text{F.38})$$

Now using the Sokhotski–Plemelj theorem to handle the $+i\epsilon$ in the denominator

$$\lim_{\eta \rightarrow 0} \frac{1}{\eta} \left(P \int_0^{\infty} \frac{f(p)}{p - (a + \eta)} dp - P \int_0^{\infty} \frac{f(p)}{p - a} dp \right) - i\pi \lim_{\eta \rightarrow 0} \left(\frac{f(a + \eta) - f(a)}{\eta} \right) \quad (\text{F.39})$$

One can see that the second term is the derivative of $f(p)$ at the point $p = a$. Now using the definition of the principal value integral

$$\begin{aligned} \lim_{\eta \rightarrow 0} \lim_{\epsilon \rightarrow 0} \frac{1}{\eta} \left(\int_0^{a+\eta-\epsilon} \frac{f(p)}{p - (a + \eta)} dp + \int_{a+\eta+\epsilon}^{\infty} \frac{f(p)}{p - (a + \eta)} dp \right. \\ \left. - \int_0^{a-\epsilon} \frac{f(p)}{p - a} dp - \int_{a+\epsilon}^{\infty} \frac{f(p)}{p - a} dp \right) - i\pi f'(a) \end{aligned} \quad (\text{F.40})$$

We note that the ϵ is different from the ϵ used in the original integral, but it is not so important to distinguish the difference between these parameters. We split the first two integrals, so we have integrals with the same limits as the last two integrals

$$\begin{aligned} \lim_{\eta \rightarrow 0} \lim_{\epsilon \rightarrow 0} \frac{1}{\eta} \left(\int_0^{a-\epsilon} \frac{f(p)}{p - (a + \eta)} dp + \int_{a-\epsilon}^{a+\eta-\epsilon} \frac{f(p)}{p - (a + \eta)} dp + \int_{a+\epsilon}^{\infty} \frac{f(p)}{p - (a + \eta)} dp \right. \\ \left. - \int_{a+\eta}^{a+\eta+\epsilon} \frac{f(p)}{p - (a + \eta)} dp - \int_0^{a-\epsilon} \frac{f(p)}{p - a} dp - \int_{a+\epsilon}^{\infty} \frac{f(p)}{p - a} dp \right) - i\pi f'(a) \end{aligned} \quad (\text{F.41})$$

Splitting the integrals this way is true for any $\eta > 0$ and $\epsilon > 0$ regardless if $\eta > \epsilon$ or vice versa. Now combining the integrals with the same limits

$$\begin{aligned} \lim_{\eta \rightarrow 0} \lim_{\epsilon \rightarrow 0} \left(\int_0^{a-\epsilon} \frac{f(p)}{(p - (a + \eta))(p - a)} dp + \int_{a+\epsilon}^{\infty} \frac{f(p)}{(p - (a + \eta))(p - a)} dp \right. \\ \left. - \frac{1}{\eta} \int_{a+\eta}^{a+\eta+\epsilon} \frac{f(p)}{p - (a + \eta)} dp + \frac{1}{\eta} \int_{a-\epsilon}^{a+\eta-\epsilon} \frac{f(p)}{p - (a + \eta)} dp \right) - i\pi f'(a) \end{aligned} \quad (\text{F.42})$$

Now because η is arbitrarily small, the last two integrals can be calculated using an Riemann sum. We choice an upper Riemann sum, which gives us

$$\begin{aligned} \lim_{\eta \rightarrow 0} \lim_{\epsilon \rightarrow 0} \left(\int_0^{a-\epsilon} \frac{f(p)}{(p - (a + \eta))(p - a)} dp + \int_{a+\epsilon}^{\infty} \frac{f(p)}{(p - (a + \eta))(p - a)} dp \right. \\ \left. - \frac{1}{\eta} \frac{f(a + \eta + \epsilon)}{a + \eta + \epsilon - (a + \eta)} \eta + \frac{1}{\eta} \frac{f(a + \eta - \epsilon)}{a + \eta - \epsilon - (a + \eta)} \eta \right) - i\pi f'(a) \end{aligned} \quad (\text{F.43})$$

We can now take the limit as $\eta \rightarrow 0$

$$\lim_{\epsilon \rightarrow 0} \left(\int_0^{a-\epsilon} \frac{f(p)}{(p-a)^2} dp + \int_{a+\epsilon}^{\infty} \frac{f(p)}{(p-a)^2} dp - \frac{2f(a)}{\epsilon} \right) - i\pi f'(a) \quad (\text{F.44})$$

The remaining limit is the definition of a finite part integral. Therefore, our original integral is given by

$$\int_0^{\infty} \frac{f(p)}{(p-a+i\epsilon)^2} dp = \text{f.p.} \int_0^{\infty} \frac{f(p)}{(p-a)^2} dp - i\pi f'(a) \quad (\text{F.45})$$

where f.p. corresponds to the finite part integral.

F.2.1 The quadratures of Kolm and Rokhlin

So calculating our integral with a double pole comes down to calculating the finite part integral, as the derivative of the function without the pole can be calculated numerically using a finite difference method. We have discussed in Chapter 4 that there exists modified quadrature points by Kolm and Rokhlin [93] which can be used to handle a pole of order two. However, the expression for the modified quadrature points presented by Kolm and Rokhlin has a slight error in it as calculating this expression does not lead to the quadrature point given in Table 1 of their paper. So we need to re-derive the expression to understand the error.

Kolm and Rokhlin give the following quadrature rule in Theorem 3.1

$$\int_{-1}^1 \omega(x)\phi(x)dx \approx \sum_{n=1}^N \tilde{\omega}_n \phi(x_n) \quad (\text{F.46})$$

where the modified weights are given by

$$\tilde{\omega}_n = \omega_n \sum_{j=0}^{N-1} \left(\frac{2j+1}{2} P_j(x_n) \left(\int_{-1}^1 \omega(x) P_j(x) dx \right) \right) \quad (\text{F.47})$$

where $P_n(x)$ is a Legendre polynomial. In this case, the weight function is $\omega(x) = \frac{1}{(y-x)^2}$ where y is the double pole and $-1 < y < 1$. In Theorem 2.7, the authors give the following expression

$$\text{f.p.} \int_{-1}^1 \frac{P_n(x)}{(y-x)^2} dx = \text{p.v.} \int_{-1}^1 \frac{P'_n(x)}{x-y} dx + \frac{1}{y-1} - \frac{(-1)^n}{y+1} \quad (\text{F.48})$$

where f.p. denotes a finite part integral and p.v. denotes a Cauchy principal value integral.

Inserting this expression into Equation F.47

$$\begin{aligned}
 \tilde{\omega}_n &= \omega_n \sum_{j=0}^{N-1} \left(\frac{2j+1}{2} P_j(x_n) \left(\text{p.v.} \int_{-1}^1 \frac{P_j'(x)}{x-y} dx + \frac{1}{y-1} - \frac{(-1)^j}{y+1} \right) \right) \\
 &= \omega_n \sum_{j=0}^{N-1} \left(\frac{2j+1}{2} P_j(x_n) \left(\text{p.v.} \int_{-1}^1 \frac{P_j'(x)}{x-y} dx \right) \right) \\
 &\quad + \omega_n \sum_{j=0}^{N-1} \left(\frac{2j+1}{2} P_j(x_n) \left(\frac{1}{y-1} - \frac{(-1)^j}{y+1} \right) \right)
 \end{aligned} \tag{F.49}$$

We could leave this expression as it is and calculate the modified weights, however this can be a computationally intense task due to the principal value integral. The expression will also break down for larger values of j if the principal value integral is not calculated precisely. Let us focus on the term that contains the principal value integral and try to reduce the expression to a more computationally friendly expression. From Theorem 2.4 of [93], a polynomial defined on $[-1, 1]$ can be represented by the formula

$$p(x) = \sum_{n=0}^{N'-1} a_n P_n(x) \tag{F.50}$$

where N' is some natural number, which we distinguish from the number of quadrature points N . The derivative of this polynomial can also be represented by

$$p'(x) = \sum_{l=0}^{N'-2} b_l P_l(x) \tag{F.51}$$

where the coefficient b_l is given by the expression

$$b_l = (2l+1) \sum_{k=l}^{\lfloor \frac{N'+l-3}{2} \rfloor} a_{2k+1-l}, \quad n = 0, 1, \dots, N'-2 \tag{F.52}$$

and $\lfloor \frac{N'+l-3}{2} \rfloor$ denotes the integer part of $\frac{N'+l-3}{2}$. Now, if we were to let the polynomial $p(x)$ be equal to the Legendre polynomial $P_j(x)$, we can see that the coefficient a_n becomes a Kronecker delta, specifically $a_n = \delta_{nj}$. By combining our formulas, we can obtain an expression for the Legendre polynomial derivative

$$P_j'(x) = \sum_{l=0}^{N'-2} (2l+1) \sum_{k=l}^{\lfloor \frac{N'+l-3}{2} \rfloor} \delta_{2k+1-l,j} P_l(x) \tag{F.53}$$

If we return to our term containing the Legendre polynomial derivative and insert the above

expression

$$\begin{aligned}
 & \omega_n \sum_{j=0}^{N-1} \left(\frac{2j+1}{2} P_j(x_n) \left(\text{p.v.} \int_{-1}^1 \frac{P_j'(x)}{x-y} dx \right) \right) \\
 &= \omega_n \sum_{j=0}^{N-1} \sum_{l=0}^{N'-2} \sum_{k=l}^{\lfloor \frac{N'+l-3}{2} \rfloor} \left(\frac{2j+1}{2} P_j(x_n) (2l+1) \delta_{2k+1-l,j} \int_{-1}^1 \frac{P_l(x)}{x-y} dx \right)
 \end{aligned} \tag{F.54}$$

By Theorem 2.6 of [93]

$$\int_{-1}^1 \frac{P_j(x)}{y-x} dx = 2Q_j(y) \tag{F.55}$$

where $Q_n(x)$ is a Legendre polynomial of the second kind. The principal value integral in Equation F.54 reduces to

$$\begin{aligned}
 & \omega_n \sum_{j=0}^{N-1} \left(\frac{2j+1}{2} P_j(x_n) \left(\text{p.v.} \int_{-1}^1 \frac{P_j'(x)}{x-y} dx \right) \right) \\
 &= -\omega_n \sum_{j=0}^{N-1} \sum_{l=0}^{N'-2} \sum_{k=l}^{\lfloor \frac{N'+l-3}{2} \rfloor} (2j+1) P_j(x_n) (2l+1) \delta_{2k+1-l,j} Q_l(y)
 \end{aligned} \tag{F.56}$$

Now by performing the sum over j with the Kronecker delta, we obtain

$$\begin{aligned}
 & \omega_n \sum_{j=0}^{N-1} \left(\frac{2j+1}{2} P_j(x_n) \left(\text{p.v.} \int_{-1}^1 \frac{P_j'(x)}{x-y} dx \right) \right) \\
 &= -\omega_n \sum_{l=0}^{N'-2} \sum_{k=l}^{\lfloor \frac{N'+l-3}{2} \rfloor} (4k+3-2l) P_{2k+1-l}(x_n) (2l+1) Q_l(y)
 \end{aligned} \tag{F.57}$$

For consistency with Kolm and Rokhlin, let us change the index l in our expression to the index j

$$\begin{aligned}
 & \omega_n \sum_{j=0}^{N-1} \left(\frac{2j+1}{2} P_j(x_n) \left(\text{p.v.} \int_{-1}^1 \frac{P_j'(x)}{x-y} dx \right) \right) \\
 &= -\omega_n \sum_{j=0}^{N'-2} \sum_{k=j}^{\lfloor \frac{N'+j-3}{2} \rfloor} (4k+3-2j) P_{2k+1-j}(x_n) (2j+1) Q_j(y)
 \end{aligned} \tag{F.58}$$

This expression looks like the same expression presented by Kolm and Rokhlin, however there are some important differences. Firstly, the natural number N' is not the same as the number of quadrature points N as N' comes from our representation of the Legendre polynomials in Equations F.50 and F.51. Notice that Equations F.50 and F.51 is true for any integer N' , so if we let $N' = N + 1$, this will always allow us to ensure these equations

are always satisfied in our expression for the modified weights. Secondly, we point out the use of the index n in the term $4k + 3 - 2n$ and the Legendre polynomial P_{2k+1-n} . The index n is used to denote the specific quadrature point/quadrature weight and is not the correct index in this expression as seen from our derived expression. Our final expression for the modified quadrature weights is

$$\begin{aligned} \tilde{\omega}_n = \omega_n \left(- \sum_{j=0}^{N-1} \sum_{k=j}^{\lfloor \frac{N+j-2}{2} \rfloor} (4k + 3 - 2j) P_{2k+1-j}(x_n) (2j + 1) Q_j(y) \right. \\ \left. + \sum_{j=0}^{N-1} \frac{2j + 1}{2} P_j(x_n) \left(\frac{1}{y - 1} - \frac{(-1)^j}{y + 1} \right) \right) \end{aligned} \quad (\text{F.59})$$

These quadrature are only defined on the interval $[-1, 1]$, so we will need a transformation from $[-1, 1]$ to a finite interval $[a, b]$. We can use the transformation

$$\tilde{x} = \frac{b - a}{2}(x - 1) + b \quad (\text{F.60})$$

Now, if we consider the integral

$$\int_a^b \frac{1}{(\tilde{y} - \tilde{x})^2} f(\tilde{x}) d\tilde{x} \quad (\text{F.61})$$

and apply our transformation

$$\begin{aligned} \int_{-1}^1 \frac{1}{\left(\frac{b-a}{2}(y-x)\right)^2} f\left(\frac{b-a}{2}(x-1)+b\right) \frac{b-a}{2} dx \\ = \int_{-1}^1 \left(\frac{2}{b-a}\right)^2 \frac{1}{(y-x)^2} \bar{f}(x) \frac{b-a}{2} dx \\ = \int_{-1}^1 \left(\frac{2}{b-a}\right) \frac{1}{(y-x)^2} \bar{f}(x) dx \\ \approx \left(\frac{2}{b-a}\right) \sum_{n=1}^N \tilde{\omega}_n \bar{f}(x_n) \end{aligned} \quad (\text{F.62})$$

Therefore, due to our transformation from $[-1, 1]$ to a finite interval $[a, b]$, the integral acquires a factor of $\frac{2}{b-a}$, which we accomodate by absorbing this factor into the quadrature weights.

F.3 Solving the NN scattering equations using Wick rotation

To perform a Wick rotation for our 4D NN scattering equation, we will need to perform a change of the z variables: $z \rightarrow z + E/2$

$$\begin{aligned}
 X_{NN}(E) &= Z_{NN}(E) + \left(-\frac{1}{2\pi i}\right) \int_{-\infty}^{\infty} dz'' \int_0^{\infty} dp'' (p'')^2 Z_{0,NN}(z'' + E/2, p''; E) \\
 &\quad \times g\left(E/2 + z'' - \frac{p''^2}{2m_N}\right) g\left(E/2 - z'' - \frac{p''^2}{2m_N}\right) X_{0,NN}(z'' + E/2, p''; E)
 \end{aligned} \tag{F.63}$$

The reason for this change of variable is two-fold:

1. Our equation becomes equivalent to the Bethe-Salpeter equation considered by Levine et al., so we can simply apply their method to our convolution equation
2. The change of variables is necessary to avoid the logarithmic cuts present in $Z_{0,NN}$, which would interfere with the Wick rotation

The only issue from this change of variable is that we now have “pinching” of the nucleon poles at $z'' = 0$ when $p'' = p_0$. However since our problem is now equivalent to Levine et al., the “pinching” can be handled using the same factorisation technique of the half off-shell t -matrix

$$X_{0,NN}(z, p; E) = f(z, p) X_{NN}(E) \tag{F.64}$$

Inserting this factorisation in Equation F.63 and solving the equation for the fully on-shell amplitude $X_{NN}(E)$, we obtain an expression for $X_{NN}(E)$ in terms of the function $f(z, p)$

$$X_{NN}(E) = \frac{Z_{NN}(E)}{1 - I_{NN}} \tag{F.65}$$

where

$$\begin{aligned}
 I_{NN} &= \left(-\frac{1}{2\pi i}\right) \int_{-\infty}^{\infty} dz'' \int_0^{\infty} dp'' (p'')^2 Z_{0,NN}(z'' + E/2, p''; E) \\
 &\quad \times g\left(E/2 + z'' - \frac{p''^2}{2m_N}\right) g\left(E/2 - z'' - \frac{p''^2}{2m_N}\right) f(z'', p'')
 \end{aligned} \tag{F.66}$$

With this expression for $X_{NN}(E)$, we can determine an expression for the function $f(z, p)$

$$\begin{aligned}
 f(z, p) &= \frac{Z_{0,NN}(z, p; E)}{Z_{NN}(E)} \\
 &\quad + \left(-\frac{1}{2\pi i}\right) \int_{-\infty}^{\infty} dz' \int_0^{\infty} dp' (p')^2 g\left(E/2 + z' - \frac{p'^2}{2m_N}\right) g\left(E/2 - z' - \frac{p'^2}{2m_N}\right) \\
 &\quad \times Z_f(z, p, z', p'; E)
 \end{aligned} \tag{F.67}$$

where

$$Z_f(z, p, z', p'; E) = Z_{NN}(z + E/2, p, z' + E/2, p'; E) - \frac{Z_{0,NN}(z + E/2, p; E)Z_{0,NN}(z' + E/2, p'; E)}{Z_{NN}(E)} \quad (\text{F.68})$$

One can see that when the “pinching” of the nucleon poles occur (when $z' = 0, p' = p_0$), the term Z_f is equal to zero, allowing the Wick rotation to be performed.

Now we perform the Wick rotation on Equation F.67 by closing the contour around the first and third quadrants of the complex z' plane and analytically continuing the interval of integration to the imaginary z' axis. The z variable will undergo the transform $z \rightarrow iz$ and we will need to include the residue of both nucleon poles. Both nucleon pole only exist within the contour when $p' < p_0$, so the p' integral of the residue terms will only be on the interval $[0, p_0]$. Performing the Wick rotation and adding the residues of each nucleon pole, we obtain

$$\begin{aligned} f(iz, p) &= \frac{Z_{0,NN}(iz, p; E)}{Z_{NN}(E)} \\ &+ i \left(-\frac{1}{2\pi i} \right) \int_{-\infty}^{\infty} dz' \int_0^{\infty} dp' (p')^2 g \left(E/2 + iz' - \frac{p'^2}{2m_N} \right) g \left(E/2 - iz' - \frac{p'^2}{2m_N} \right) \\ &\quad \times Z_f(iz, p, iz', p'; E) \\ &+ \int_0^{p_0} dp' (p')^2 g \left(E - \frac{p'^2}{m_N} - m_N \right) Z_f \left(iz, p, \frac{p'^2}{2m_N} + m_N - E/2, p'; E \right) \\ &+ \int_0^{p_0} dp' (p')^2 g \left(E - \frac{p'^2}{m_N} - m_N \right) Z_f \left(iz, p, E/2 - \frac{p'^2}{2m_N} - m_N, p'; E \right) \end{aligned} \quad (\text{F.69})$$

There is now an end-point pole in the residue terms at $p' = p_0$, which tends to be difficult to evaluate. However, the term Z_f is zero when $p' = p_0$, so we can evaluate the integrals of the residue term without any issues. This factorisation of the half-off shell t -matrix is a powerful numerical tool, as it has the benefit of handling the “pinching” of the poles and the end-point pole in the residue terms. We can now solve this equation for the function $f(iz, p)$ by discretising the z and p variables using quadrature points.

Once we obtain a solution of $f(iz, p)$, we will need to use Equation F.65 to determine the fully on-shell amplitude. However, the integral in the denominator of Equation F.65 suffers from the same “pinching” problem as earlier, so we will need to determine a method to handle this problem. We can add and subtract an integral term in order to introduce a term that will make I_{NN} zero at $z'' = 0, p'' = p_0$. The extra integral term is then calculated

explicitly. The term that is added is not unique, and we have two suggestions from the literature:

Phillips :

$$\left(-\frac{1}{2\pi i}\right) \int_{-\infty}^{\infty} dz'' \int_0^{\infty} dp'' (p'')^2 g\left(E/2 + iz' - \frac{p'^2}{2m_N}\right) g\left(E/2 - iz' - \frac{p'^2}{2m_N}\right) \quad (\text{F.70a})$$

Levine et al. :

$$\left(-\frac{1}{2\pi i}\right) \int_{-\infty}^{\infty} dz'' \int_0^{\infty} dp'' (p'')^2 g\left(E/2 + iz' - \frac{p'^2}{2m_N}\right) g\left(E/2 - iz' - \frac{p'^2}{2m_N}\right) \times \frac{Z_{0,NN}(z'' + E/2, p''; E)^2}{Z_{NN}(E)} \quad (\text{F.70b})$$

While the suggestion of Phillips [207] is similar to calculate explicitly, we find it is much more accurate to use the suggestion of Levine et al. The Levine et al. term corresponds to the fully dressed two-pion exchange amplitude that we calculated in Chapter 4 (with a division by $Z_{NN}(E)$), so there is no issue using the suggestion of Levine et al.

Chapter G

Three-body channels

We now list the possible three-body channels for a fixed total angular momentum J and parity π , which in combination we represent by J^π . To generate a finite amount of channel for each J^π , we have restricted the orbital angular momentum l and total angular momentum j of the interacting pair to a maximum value. In this case, l_{max} is 1 for a πN interacting pair and 2 for a NN interacting pair, while j_{max} is $\frac{3}{2}$ for a πN interacting pair and 2 for a NN interacting pair. For the notation used in the following tables, the lowercase letters (and \mathcal{S}) represent the angular momenta of the interacting pair (quasiparticle), while the uppercase letters represent the angular momenta of the interacting pair with the spectator. We use standard spectator notation for the partial wave label for the interacting pair: $^{2\mathcal{S}+1}l_j$ for NN , $l_{2t,2j}$ for πN and we denote the nucleon channel by NUC .

$J^\pi = 0^-$

Channel Number	Interacting Pair Partial Wave	t	l	S	j	S	L
1	1S_0	1	0	0	0	0	0
2	1P_1	0	1	0	1	1	1
3	3P_1	1	1	1	1	1	1
4	3D_2	0	2	1	2	2	2
5	1D_2	1	2	0	2	2	2
6	S_{11}	1/2	0	1/2	1/2	0	0
7	S_{31}	3/2	0	1/2	1/2	0	0
8	P_{11}	1/2	1	1/2	1/2	1	1
9	NUC	1/2	1	1/2	1/2	1	1
10	P_{13}	1/2	1	1/2	3/2	1	1
11	P_{31}	3/2	1	1/2	1/2	1	1
12	P_{33}	3/2	1	1/2	3/2	1	1

 $J^\pi = 0^+$

Channel Number	Interacting Pair Partial Wave	t	l	S	j	S	L
1	3P_0	1	1	1	0	0	0
2	3S_1	0	0	1	1	1	1
3	3D_1	0	2	1	1	1	1
4	3P_2	1	1	1	2	2	2
5	P_{11}	1/2	1	1/2	1/2	0	0
6	NUC	1/2	1	1/2	1/2	0	0
7	P_{31}	3/2	1	1/2	1/2	0	0
8	S_{11}	1/2	0	1/2	1/2	1	1
9	S_{31}	3/2	0	1/2	1/2	1	1
10	P_{13}	1/2	1	1/2	3/2	2	2
11	P_{33}	3/2	1	1/2	3/2	2	2

$J^\pi = 1^-$

Channel Number	Interacting Pair Partial Wave	t	l	S	j	S	L
1	3S_1	0	0	1	1	1	0
2	3D_1	0	2	1	1	1	0
3	3P_0	1	1	1	0	0	1
4	1P_1	0	1	0	1	1	1
5	3P_1	1	1	1	1	1	1
6	3P_2	1	1	1	2	2	1
7	3S_1	0	0	1	1	1	2
8	3D_1	0	2	1	1	1	2
9	3D_2	0	2	1	2	2	2
10	1D_2	1	2	0	2	2	2
11	3P_2	1	1	1	2	2	3
12	S_{11}	1/2	0	1/2	1/2	1	0
13	S_{31}	3/2	0	1/2	1/2	1	0
14	P_{11}	1/2	1	1/2	1/2	0	1
15	P_{31}	3/2	1	1/2	1/2	0	1
16	P_{11}	1/2	1	1/2	1/2	1	1
17	NUC	1/2	1	1/2	1/2	1	1
18	P_{13}	1/2	1	1/2	3/2	1	1
19	P_{31}	3/2	1	1/2	1/2	1	1
20	P_{33}	3/2	1	1/2	3/2	1	1
21	P_{13}	1/2	1	1/2	3/2	2	1
22	P_{33}	3/2	1	1/2	3/2	2	1
23	S_{11}	1/2	0	1/2	1/2	1	2
24	S_{31}	3/2	0	1/2	1/2	1	2
25	P_{13}	1/2	1	1/2	3/2	2	3
26	P_{33}	3/2	1	1/2	3/2	2	3

$J^\pi = 1^+$

Channel Number	Interacting Pair Partial Wave	t	l	S	j	S	L
1	1P_1	0	1	0	1	1	0
2	3P_1	1	1	1	1	1	0
3	1S_0	1	0	0	0	0	1
4	3S_1	0	0	1	1	1	1
5	3D_1	0	2	1	1	1	1
6	3D_2	0	2	1	2	2	1
7	1D_2	1	2	0	2	2	1
8	1P_1	0	1	0	1	1	2
9	3P_1	1	1	1	1	1	2
10	3P_2	1	1	1	2	2	2
11	3D_2	0	2	1	2	2	3
12	1D_2	1	2	0	2	2	3
13	P_{11}	1/2	1	1/2	1/2	1	0
14	P_{13}	1/2	1	1/2	3/2	1	0
15	P_{31}	3/2	1	1/2	1/2	1	0
16	P_{33}	3/2	1	1/2	3/2	1	0
17	S_{11}	1/2	0	1/2	1/2	0	1
18	S_{31}	3/2	0	1/2	1/2	0	1
19	S_{11}	1/2	0	1/2	1/2	1	1
20	S_{31}	3/2	0	1/2	1/2	1	1
21	P_{11}	1/2	1	1/2	1/2	1	2
22	P_{13}	1/2	1	1/2	3/2	1	2
23	P_{31}	3/2	1	1/2	1/2	1	2
24	P_{33}	3/2	1	1/2	3/2	1	2
25	P_{13}	1/2	1	1/2	3/2	2	2
26	P_{33}	3/2	1	1/2	3/2	2	2

$J^\pi = 2^-$

Channel Number	Interacting Pair Partial Wave	t	l	S	j	S	L
1	3D_2	0	2	1	2	2	0
2	1D_2	1	2	0	2	2	0
3	1P_1	0	1	0	1	1	1
4	3P_1	1	1	1	1	1	1
5	3P_2	1	1	1	2	2	1
6	1S_0	1	0	0	0	0	2
7	3S_1	0	0	1	1	1	2
8	3D_1	0	2	1	1	1	2
9	3D_2	0	2	1	2	2	2
10	1D_2	1	2	0	2	2	2
11	1P_1	0	1	0	1	1	3
12	3P_1	1	1	1	1	1	3
13	3P_2	1	1	1	2	2	3
14	3D_2	0	2	1	2	2	4
15	1D_2	1	2	0	2	2	4
16	P_{11}	1/2	1	1/2	1/2	1	1
17	NUC	1/2	1	1/2	1/2	1	1
18	P_{13}	1/2	1	1/2	3/2	1	1
19	P_{31}	3/2	1	1/2	1/2	1	1
20	P_{33}	3/2	1	1/2	3/2	1	1
21	P_{13}	1/2	1	1/2	3/2	2	1
22	P_{33}	3/2	1	1/2	3/2	2	1
23	S_{11}	1/2	0	1/2	1/2	0	2
24	S_{31}	3/2	0	1/2	1/2	0	2
25	S_{11}	1/2	0	1/2	1/2	1	2
26	S_{31}	3/2	0	1/2	1/2	1	2
27	P_{11}	1/2	1	1/2	1/2	1	3
28	NUC	1/2	1	1/2	1/2	1	3
29	P_{13}	1/2	1	1/2	3/2	1	3
30	P_{31}	3/2	1	1/2	1/2	1	3
31	P_{33}	3/2	1	1/2	3/2	1	3
32	P_{13}	1/2	1	1/2	3/2	2	3
33	P_{33}	3/2	1	1/2	3/2	2	3

$J^\pi = 2^+$

Channel Number	Interacting Pair Partial Wave	t	l	\mathcal{S}	j	S	L
1	3P_2	1	1	1	2	2	0
2	3S_1	0	0	1	1	1	1
3	3D_1	0	2	1	1	1	1
4	3D_2	0	2	1	2	2	1
5	1D_2	1	2	0	2	2	1
6	3P_0	1	1	1	0	0	2
7	1P_1	0	1	0	1	1	2
8	3P_1	1	1	1	1	1	2
9	3P_2	1	1	1	2	2	2
10	3S_1	0	0	1	1	1	3
11	3D_1	0	2	1	1	1	3
12	3D_2	0	2	1	2	2	3
13	1D_2	1	2	0	2	2	3
14	3P_2	1	1	1	2	2	4
15	P_{13}	1/2	1	1/2	3/2	2	0
16	P_{33}	3/2	1	1/2	3/2	2	0
17	S_{11}	1/2	0	1/2	1/2	1	1
18	S_{31}	3/2	0	1/2	1/2	1	1
19	P_{11}	1/2	1	1/2	1/2	0	2
20	NUC	1/2	1	1/2	1/2	0	2
21	P_{31}	3/2	1	1/2	1/2	0	2
22	P_{11}	1/2	1	1/2	1/2	1	2
23	P_{13}	1/2	1	1/2	3/2	1	2
24	P_{31}	3/2	1	1/2	1/2	1	2
25	P_{33}	3/2	1	1/2	3/2	1	2
26	P_{13}	1/2	1	1/2	3/2	2	2
27	P_{33}	3/2	1	1/2	3/2	2	2
28	S_{11}	1/2	0	1/2	1/2	1	3
29	S_{31}	3/2	0	1/2	1/2	1	3
30	P_{13}	1/2	1	1/2	3/2	2	4
31	P_{33}	3/2	1	1/2	3/2	2	4

$J^\pi = 3^-$

Channel Number	Interacting Pair Partial Wave	t	l	\mathcal{S}	j	S	L
1	3P_2	1	1	1	2	2	1
2	3S_1	0	0	1	1	1	2
3	3D_1	0	2	1	1	1	2
4	3D_2	0	2	1	2	2	2
5	1D_2	1	2	0	2	2	2
6	3P_0	1	1	1	0	0	3
7	1P_1	0	1	0	1	1	3
8	3P_1	1	1	1	1	1	3
9	3P_2	1	1	1	2	2	3
10	3S_1	0	0	1	1	1	4
11	3D_1	0	2	1	1	1	4
12	3D_2	0	2	1	2	2	4
13	1D_2	1	2	0	2	2	4
14	3P_2	1	1	1	2	2	5
15	P_{13}	1/2	1	1/2	3/2	2	1
16	P_{33}	3/2	1	1/2	3/2	2	1
17	S_{11}	1/2	0	1/2	1/2	1	2
18	S_{31}	3/2	0	1/2	1/2	1	2
19	P_{11}	1/2	1	1/2	1/2	0	3
20	P_{31}	3/2	1	1/2	1/2	0	3
21	P_{11}	1/2	1	1/2	1/2	1	3
22	<i>NUC</i>	1/2	1	1/2	1/2	1	3
23	P_{13}	1/2	1	1/2	3/2	1	3
24	P_{31}	3/2	1	1/2	1/2	1	3
25	P_{33}	3/2	1	1/2	3/2	1	3
26	P_{13}	1/2	1	1/2	3/2	2	3
27	P_{33}	3/2	1	1/2	3/2	2	3
28	S_{11}	1/2	0	1/2	1/2	1	4
29	S_{31}	3/2	0	1/2	1/2	1	4
30	P_{13}	1/2	1	1/2	3/2	2	5
31	P_{33}	3/2	1	1/2	3/2	2	5

$J^\pi = 3^+$

Channel Number	Interacting Pair Partial Wave	t	l	\mathcal{S}	j	S	L
1	3D_2	0	2	1	2	2	1
2	1D_2	1	2	0	2	2	1
3	1P_1	0	1	0	1	1	2
4	3P_1	1	1	1	1	1	2
5	3P_2	1	1	1	2	2	2
6	1S_0	1	0	0	0	0	3
7	3S_1	0	0	1	1	1	3
8	3D_1	0	2	1	1	1	3
9	3D_2	0	2	1	2	2	3
10	1D_2	1	2	0	2	2	3
11	1P_1	0	1	0	1	1	4
12	3P_1	1	1	1	1	1	4
13	3P_2	1	1	1	2	2	4
14	3D_2	0	2	1	2	2	5
15	1D_2	1	2	0	2	2	5
16	P_{11}	1/2	1	1/2	1/2	1	2
17	P_{13}	1/2	1	1/2	3/2	1	2
18	P_{31}	3/2	1	1/2	1/2	1	2
19	P_{33}	3/2	1	1/2	3/2	1	2
20	P_{13}	1/2	1	1/2	3/2	2	2
21	P_{33}	3/2	1	1/2	3/2	2	2
22	S_{11}	1/2	0	1/2	1/2	0	3
23	S_{31}	3/2	0	1/2	1/2	0	3
24	S_{11}	1/2	0	1/2	1/2	1	3
25	S_{31}	3/2	0	1/2	1/2	1	3
26	P_{11}	1/2	1	1/2	1/2	1	4
27	P_{13}	1/2	1	1/2	3/2	1	4
28	P_{31}	3/2	1	1/2	1/2	1	4
29	P_{33}	3/2	1	1/2	3/2	1	4
30	P_{13}	1/2	1	1/2	3/2	2	4
31	P_{33}	3/2	1	1/2	3/2	2	4

$J^\pi = 4^-$

Channel Number	Interacting Pair Partial Wave	t	l	S	j	S	L
1	3D_2	0	2	1	2	2	2
2	1D_2	1	2	0	2	2	2
3	1P_1	0	1	0	1	1	3
4	3P_1	1	1	1	1	1	3
5	3P_2	1	1	1	2	2	3
6	1S_0	1	0	0	0	0	4
7	3S_1	0	0	1	1	1	4
8	3D_1	0	2	1	1	1	4
9	3D_2	0	2	1	2	2	4
10	1D_2	1	2	0	2	2	4
11	1P_1	0	1	0	1	1	5
12	3P_1	1	1	1	1	1	5
13	3P_2	1	1	1	2	2	5
14	3D_2	0	2	1	2	2	6
15	1D_2	1	2	0	2	2	6
16	P_{11}	1/2	1	1/2	1/2	1	3
17	NUC	1/2	1	1/2	1/2	1	3
18	P_{13}	1/2	1	1/2	3/2	1	3
19	P_{31}	3/2	1	1/2	1/2	1	3
20	P_{33}	3/2	1	1/2	3/2	1	3
21	P_{13}	1/2	1	1/2	3/2	2	3
22	P_{33}	3/2	1	1/2	3/2	2	3
23	S_{11}	1/2	0	1/2	1/2	0	4
24	S_{31}	3/2	0	1/2	1/2	0	4
25	S_{11}	1/2	0	1/2	1/2	1	4
26	S_{31}	3/2	0	1/2	1/2	1	4
27	P_{11}	1/2	1	1/2	1/2	1	5
28	NUC	1/2	1	1/2	1/2	1	5
29	P_{13}	1/2	1	1/2	3/2	1	5
30	P_{31}	3/2	1	1/2	1/2	1	5
31	P_{33}	3/2	1	1/2	3/2	1	5
32	P_{13}	1/2	1	1/2	3/2	2	5
33	P_{33}	3/2	1	1/2	3/2	2	5

$J^\pi = 4^+$

Channel Number	Interacting Pair Partial Wave	t	l	\mathcal{S}	j	S	L
1	3P_2	1	1	1	2	2	2
2	3S_1	0	0	1	1	1	3
3	3D_1	0	2	1	1	1	3
4	3D_2	0	2	1	2	2	3
5	1D_2	1	2	0	2	2	3
6	3P_0	1	1	1	0	0	4
7	1P_1	0	1	0	1	1	4
8	3P_1	1	1	1	1	1	4
9	3P_2	1	1	1	2	2	4
10	3S_1	0	0	1	1	1	5
11	3D_1	0	2	1	1	1	5
12	3D_2	0	2	1	2	2	5
13	1D_2	1	2	0	2	2	5
14	3P_2	1	1	1	2	2	6
15	P_{13}	1/2	1	1/2	3/2	2	2
16	P_{33}	3/2	1	1/2	3/2	2	2
17	S_{11}	1/2	0	1/2	1/2	1	3
18	S_{31}	3/2	0	1/2	1/2	1	3
19	P_{11}	1/2	1	1/2	1/2	0	4
20	NUC	1/2	1	1/2	1/2	0	4
21	P_{31}	3/2	1	1/2	1/2	0	4
22	P_{11}	1/2	1	1/2	1/2	1	4
23	P_{13}	1/2	1	1/2	3/2	1	4
24	P_{31}	3/2	1	1/2	1/2	1	4
25	P_{33}	3/2	1	1/2	3/2	1	4
26	P_{13}	1/2	1	1/2	3/2	2	4
27	P_{33}	3/2	1	1/2	3/2	2	4
28	S_{11}	1/2	0	1/2	1/2	1	5
29	S_{31}	3/2	0	1/2	1/2	1	5
30	P_{13}	1/2	1	1/2	3/2	2	6
31	P_{33}	3/2	1	1/2	3/2	2	6

$J^\pi = 5^-$

Channel Number	Interacting Pair Partial Wave	t	l	\mathcal{S}	j	S	L
1	3P_2	1	1	1	2	2	3
2	3S_1	0	0	1	1	1	4
3	3D_1	0	2	1	1	1	4
4	3D_2	0	2	1	2	2	4
5	1D_2	1	2	0	2	2	4
6	3P_0	1	1	1	0	0	5
7	1P_1	0	1	0	1	1	5
8	3P_1	1	1	1	1	1	5
9	3P_2	1	1	1	2	2	5
10	3S_1	0	0	1	1	1	6
11	3D_1	0	2	1	1	1	6
12	3D_2	0	2	1	2	2	6
13	1D_2	1	2	0	2	2	6
14	3P_2	1	1	1	2	2	7
15	P_{13}	1/2	1	1/2	3/2	2	3
16	P_{33}	3/2	1	1/2	3/2	2	3
17	S_{11}	1/2	0	1/2	1/2	1	4
18	S_{31}	3/2	0	1/2	1/2	1	4
19	P_{11}	1/2	1	1/2	1/2	0	5
20	P_{31}	3/2	1	1/2	1/2	0	5
21	P_{11}	1/2	1	1/2	1/2	1	5
22	<i>NUC</i>	1/2	1	1/2	1/2	1	5
23	P_{13}	1/2	1	1/2	3/2	1	5
24	P_{31}	3/2	1	1/2	1/2	1	5
25	P_{33}	3/2	1	1/2	3/2	1	5
26	P_{13}	1/2	1	1/2	3/2	2	5
27	P_{33}	3/2	1	1/2	3/2	2	5
28	S_{11}	1/2	0	1/2	1/2	1	6
29	S_{31}	3/2	0	1/2	1/2	1	6
30	P_{13}	1/2	1	1/2	3/2	2	7
31	P_{33}	3/2	1	1/2	3/2	2	7

$J^\pi = 5^+$

Channel Number	Interacting Pair Partial Wave	t	l	\mathcal{S}	j	S	L
1	3D_2	0	2	1	2	2	3
2	1D_2	1	2	0	2	2	3
3	1P_1	0	1	0	1	1	4
4	3P_1	1	1	1	1	1	4
5	3P_2	1	1	1	2	2	4
6	1S_0	1	0	0	0	0	5
7	3S_1	0	0	1	1	1	5
8	3D_1	0	2	1	1	1	5
9	3D_2	0	2	1	2	2	5
10	1D_2	1	2	0	2	2	5
11	1P_1	0	1	0	1	1	6
12	3P_1	1	1	1	1	1	6
13	3P_2	1	1	1	2	2	6
14	3D_2	0	2	1	2	2	7
15	1D_2	1	2	0	2	2	7
16	P_{11}	1/2	1	1/2	1/2	1	4
17	P_{13}	1/2	1	1/2	3/2	1	4
18	P_{31}	3/2	1	1/2	1/2	1	4
19	P_{33}	3/2	1	1/2	3/2	1	4
20	P_{13}	1/2	1	1/2	3/2	2	4
21	P_{33}	3/2	1	1/2	3/2	2	4
22	S_{11}	1/2	0	1/2	1/2	0	5
23	S_{31}	3/2	0	1/2	1/2	0	5
24	S_{11}	1/2	0	1/2	1/2	1	5
25	S_{31}	3/2	0	1/2	1/2	1	5
26	P_{11}	1/2	1	1/2	1/2	1	6
27	P_{13}	1/2	1	1/2	3/2	1	6
28	P_{31}	3/2	1	1/2	1/2	1	6
29	P_{33}	3/2	1	1/2	3/2	1	6
30	P_{13}	1/2	1	1/2	3/2	2	6
31	P_{33}	3/2	1	1/2	3/2	2	6

$J^\pi = 6^-$

Channel Number	Interacting Pair Partial Wave	t	l	S	j	S	L
1	3D_2	0	2	1	2	2	4
2	1D_2	1	2	0	2	2	4
3	1P_1	0	1	0	1	1	5
4	3P_1	1	1	1	1	1	5
5	3P_2	1	1	1	2	2	5
6	1S_0	1	0	0	0	0	6
7	3S_1	0	0	1	1	1	6
8	3D_1	0	2	1	1	1	6
9	3D_2	0	2	1	2	2	6
10	1D_2	1	2	0	2	2	6
11	1P_1	0	1	0	1	1	7
12	3P_1	1	1	1	1	1	7
13	3P_2	1	1	1	2	2	7
14	3D_2	0	2	1	2	2	8
15	1D_2	1	2	0	2	2	8
16	P_{11}	1/2	1	1/2	1/2	1	5
17	NUC	1/2	1	1/2	1/2	1	5
18	P_{13}	1/2	1	1/2	3/2	1	5
19	P_{31}	3/2	1	1/2	1/2	1	5
20	P_{33}	3/2	1	1/2	3/2	1	5
21	P_{13}	1/2	1	1/2	3/2	2	5
22	P_{33}	3/2	1	1/2	3/2	2	5
23	S_{11}	1/2	0	1/2	1/2	0	6
24	S_{31}	3/2	0	1/2	1/2	0	6
25	S_{11}	1/2	0	1/2	1/2	1	6
26	S_{31}	3/2	0	1/2	1/2	1	6
27	P_{11}	1/2	1	1/2	1/2	1	7
28	NUC	1/2	1	1/2	1/2	1	7
29	P_{13}	1/2	1	1/2	3/2	1	7
30	P_{31}	3/2	1	1/2	1/2	1	7
31	P_{33}	3/2	1	1/2	3/2	1	7
32	P_{13}	1/2	1	1/2	3/2	2	7
33	P_{33}	3/2	1	1/2	3/2	2	7

$J^\pi = 6^+$

Channel Number	Interacting Pair Partial Wave	t	l	\mathcal{S}	j	S	L
1	3P_2	1	1	1	2	2	4
2	3S_1	0	0	1	1	1	5
3	3D_1	0	2	1	1	1	5
4	3D_2	0	2	1	2	2	5
5	1D_2	1	2	0	2	2	5
6	3P_0	1	1	1	0	0	6
7	1P_1	0	1	0	1	1	6
8	3P_1	1	1	1	1	1	6
9	3P_2	1	1	1	2	2	6
10	3S_1	0	0	1	1	1	7
11	3D_1	0	2	1	1	1	7
12	3D_2	0	2	1	2	2	7
13	1D_2	1	2	0	2	2	7
14	3P_2	1	1	1	2	2	8
15	P_{13}	1/2	1	1/2	3/2	2	4
16	P_{33}	3/2	1	1/2	3/2	2	4
17	S_{11}	1/2	0	1/2	1/2	1	5
18	S_{31}	3/2	0	1/2	1/2	1	5
19	P_{11}	1/2	1	1/2	1/2	0	6
20	NUC	1/2	1	1/2	1/2	0	6
21	P_{31}	3/2	1	1/2	1/2	0	6
22	P_{11}	1/2	1	1/2	1/2	1	6
23	P_{13}	1/2	1	1/2	3/2	1	6
24	P_{31}	3/2	1	1/2	1/2	1	6
25	P_{33}	3/2	1	1/2	3/2	1	6
26	P_{13}	1/2	1	1/2	3/2	2	6
27	P_{33}	3/2	1	1/2	3/2	2	6
28	S_{11}	1/2	0	1/2	1/2	1	7
29	S_{31}	3/2	0	1/2	1/2	1	7
30	P_{13}	1/2	1	1/2	3/2	2	8
31	P_{33}	3/2	1	1/2	3/2	2	8

$J^\pi = 7^-$

Channel Number	Interacting Pair Partial Wave	t	l	\mathcal{S}	j	S	L
1	3P_2	1	1	1	2	2	5
2	3S_1	0	0	1	1	1	6
3	3D_1	0	2	1	1	1	6
4	3D_2	0	2	1	2	2	6
5	1D_2	1	2	0	2	2	6
6	3P_0	1	1	1	0	0	7
7	1P_1	0	1	0	1	1	7
8	3P_1	1	1	1	1	1	7
9	3P_2	1	1	1	2	2	7
10	3S_1	0	0	1	1	1	8
11	3D_1	0	2	1	1	1	8
12	3D_2	0	2	1	2	2	8
13	1D_2	1	2	0	2	2	8
14	3P_2	1	1	1	2	2	9
15	P_{13}	1/2	1	1/2	3/2	2	5
16	P_{33}	3/2	1	1/2	3/2	2	5
17	S_{11}	1/2	0	1/2	1/2	1	6
18	S_{31}	3/2	0	1/2	1/2	1	6
19	P_{11}	1/2	1	1/2	1/2	0	7
20	P_{31}	3/2	1	1/2	1/2	0	7
21	P_{11}	1/2	1	1/2	1/2	1	7
22	NUC	1/2	1	1/2	1/2	1	7
23	P_{13}	1/2	1	1/2	3/2	1	7
24	P_{31}	3/2	1	1/2	1/2	1	7
25	P_{33}	3/2	1	1/2	3/2	1	7
26	P_{13}	1/2	1	1/2	3/2	2	7
27	P_{33}	3/2	1	1/2	3/2	2	7
28	S_{11}	1/2	0	1/2	1/2	1	8
29	S_{31}	3/2	0	1/2	1/2	1	8
30	P_{13}	1/2	1	1/2	3/2	2	9
31	P_{33}	3/2	1	1/2	3/2	2	9

$J^\pi = 7^+$

Channel Number	Interacting Pair Partial Wave	t	l	\mathcal{S}	j	S	L
1	3D_2	0	2	1	2	2	5
2	1D_2	1	2	0	2	2	5
3	1P_1	0	1	0	1	1	6
4	3P_1	1	1	1	1	1	6
5	3P_2	1	1	1	2	2	6
6	1S_0	1	0	0	0	0	7
7	3S_1	0	0	1	1	1	7
8	3D_1	0	2	1	1	1	7
9	3D_2	0	2	1	2	2	7
10	1D_2	1	2	0	2	2	7
11	1P_1	0	1	0	1	1	8
12	3P_1	1	1	1	1	1	8
13	3P_2	1	1	1	2	2	8
14	3D_2	0	2	1	2	2	9
15	1D_2	1	2	0	2	2	9
16	P_{11}	1/2	1	1/2	1/2	1	6
17	P_{13}	1/2	1	1/2	3/2	1	6
18	P_{31}	3/2	1	1/2	1/2	1	6
19	P_{33}	3/2	1	1/2	3/2	1	6
20	P_{13}	1/2	1	1/2	3/2	2	6
21	P_{33}	3/2	1	1/2	3/2	2	6
22	S_{11}	1/2	0	1/2	1/2	0	7
23	S_{31}	3/2	0	1/2	1/2	0	7
24	S_{11}	1/2	0	1/2	1/2	1	7
25	S_{31}	3/2	0	1/2	1/2	1	7
26	P_{11}	1/2	1	1/2	1/2	1	8
27	P_{13}	1/2	1	1/2	3/2	1	8
28	P_{31}	3/2	1	1/2	1/2	1	8
29	P_{33}	3/2	1	1/2	3/2	1	8
30	P_{13}	1/2	1	1/2	3/2	2	8
31	P_{33}	3/2	1	1/2	3/2	2	8

Chapter H

Publications

1. Blankleider, B., Wray, J. L., & Khvinikidze, A. N, (2021). Dyson–Schwinger approach to pion–nucleon scattering using time-ordered perturbation theory. *AIP Advances*, 11(2), 1-11. [025204]. <https://doi.org/10.1063/5.0034753>
2. Blankleider, B., Khvinikidze, A. N., & Wray, J. L, (2021). Convolution approach to πNN . I. Theory. (to be submitted to *Physical Review C* upon completion)
3. Wray, J. L., Blankleider, B., & Khvinikidze, A. N, (2021). Convolution approach to πNN . II. Numerical solution. (to be submitted to *Physical Review C* upon completion)